

**PREPARATION AND CHARACTERIZATION OF RICE
STARCH BASED SOLID POLYMER ELECTROLYTES FOR
DYE-SENSITIZED SOLAR CELL APPLICATION**

MOHAMMAD HASSAN KHANMIRZAEI

**FACULTY OF SCIENCE
UNIVERSITY OF MALAYA
KUALA LUMPUR**

2015

**PREPARATION AND CHARACTERIZATION OF RICE
STARCH BASED SOLID POLYMER ELECTROLYTES
FOR DYE-SENSITIZED SOLAR CELL APPLICATION**

MOHAMMAD HASSAN KHANMIRZAEI

**THESIS SUBMITTED IN FULFILMENT OF THE
REQUIREMENT FOR THE DEGREE OF DOCTOR OF
PHILOSOPHY**

**DEPARTMENT OF PHYSICS
FACULTY OF SCIENCE
UNIVERSITY OF MALAYA
KUALA LUMPUR**

2015

UNIVERSITY OF MALAYA
ORIGINAL LITERARY WORK DECLARATION

Name of Candidate: Mohammad Hassan Khanmirzaei (I.C/Passport No: P95425641)

Registration/Matric No: SHC110076

Name of Degree: Doctor of Philosophy

Title of Project Paper/Research Report/Dissertation/Thesis (“this Work”):

PREPARATION AND CHARACTERIZATION OF RICE STARCH BASED SOLID
POLYMER ELECTROLYTES FOR DYE-SENSITIZED SOLAR CELL
APPLICATION

Field of Study: Experimental Physics

I do solemnly and sincerely declare that:

- (1) I am the sole author/writer of this Work;
- (2) This Work is original;
- (3) Any use of any work in which copyright exists was done by way of fair dealing and for permitted purposes and any excerpt or extract from, or reference to or reproduction of any copyright work has been disclosed expressly and sufficiently and the title of the Work and its authorship have been acknowledged in this Work;
- (4) I do not have any actual knowledge nor do I ought reasonably to know that the making of this work constitutes an infringement of any copyright work;
- (5) I hereby assign all and every rights in the copyright to this Work to the University of Malaya (“UM”), who henceforth shall be owner of the copyright in this Work and that any reproduction or use in any form or by any means whatsoever is prohibited without the written consent of UM having been first had and obtained;
- (6) I am fully aware that if in the course of making this Work I have infringed any copyright whether intentionally or otherwise, I may be subject to legal action or any other action as may be determined by UM.

Candidate’s Signature

Date:

Subscribed and solemnly declared before,

Witness’s Signature

Date:

Name: Dr. Ramesh T. Subramaniam

Designation: Professor and Supervisor

ABSTRACT

Biodegradable polymers have economic and environmental benefits due to cheap in cost and biodegradability. Utilizing environmental friendly polymers in polymer electrolytes and electronics field can be good replacement for some harmful existing materials and admirable category for green energy applications such as solar cells, specifically, dye sensitized solar cells, super capacitors, batteries, etc. Solid polymer electrolyte (SPE) systems based on rice starch as a biodegradable polymer, three iodide salts namely lithium iodide, ammonium iodide and sodium iodide, and two ionic liquids namely 1-methyl-3-propylimidazolium iodide (MPII) and 1-hexyl-3-methylimidazolium iodide (HMII) were studied for dielectric properties and solar cell applications in this research. Polymer electrolytes were prepared using solution cast technique. The ionic conductivity and temperature-dependent conductivity and dielectric behavior were analyzed in this work. The highest ionic conductivities were achieved in SPE systems after addition of ionic liquid. The solid polymer electrolytes were characterized for dielectric, structural and thermal properties using EIS, FTIR, XRD, TGA and DSC. In temperature-dependent study, all SPEs follow the Arrhenius thermal activated model. In structural study using FTIR and XRD, complexations between polymer, salt and ionic liquid were confirmed for all SPEs. Furthermore, Thermal studies using TGA and DSC thermograms demonstrated that decomposition temperature (T_{dc}) and glass transition temperature (T_g) for rice starch shift upon complexation with iodide salt and ionic liquid. Dye sensitized solar cells (DSSCs) were fabricated using SPE systems with highest ionic conductivities. TiO_2 paste was doctor-bladed on FTO substrate and sintered at 450 °C as photo-electrode. The photo-electrode was immersed in Ruthenium based dye (N719) for 24 hr. Platinum coated FTO was used as the counter electrode.

Solid polymer electrolytes were sandwiched between two photo and counter electrode with the configuration of Glass/FTO/TiO₂/N719-Dye/Solid polymer electrolyte/Pt/FTO/Glass. The fabricated DSSCs were analyzed for energy conversion using Sun simulator with white light illumination of 1000 (W m⁻²) defined as incident light power. The DSSCs show significant conversion energy efficiencies for solid biopolymer based solar cells as green energy source.

ABSTRAK

Biodegradasi polimer mempunyai keuntungan dari segi ekonomi dan alam sekitar disebabkan kos yang murah dan boleh biodegradasi. Dengan menggunakan polimer mesra alam sekitar dalam elektrolit polimer dan bidang elektronik, ia boleh menjadi pengganti yang baik untuk beberapa bahan berbahaya yang sedia ada untuk aplikasi tenaga hijau seperti sel-sel solar, khususnya, dye sel peka solar, super kapasitor, bateri, dll. Sistem elektrolit polimer pepejal (SPE) berasaskan kanji beras sebagai biodegradasi polimer, tiga garam iodida iaitu litium, ammonium iodida dan natrium iodida, dan dua cecair ionik iaitu 1-metil-3-propylimidazolium iodida (MPII) dan 1-hexyl-3-methylimidazolium iodida (HMII) dikaji untuk sifat dielektrik dan aplikasi sel solar dalam kajian ini. Sistem elektrolit polimer telah disediakan dengan menggunakan teknik penuang pelarut. Kekonduksian ionik dan kekonduksian berdasarkan kajian pergantungan suhu dan tingkah laku dielektrik dianalisis di dalam kajian ini. Selepas penambahan cecair ionik di dalam sistem SPE, kekonduksian ionik tertinggi telah dicapai. Elektrolit polimer pepejal telah dicirikan untuk dielektrik, struktur dan sifat terma dengan menggunakan EIS, FTIR, XRD, TGA dan DSC. Dalam kajian pergantungan suhu, semua SPEs mengikuti Arrhenius model haba diaktifkan. Dalam kajian struktur yang menggunakan FTIR dan XRD, kompleks antara polimer, garam dan cecair ionik telah disahkan untuk semua SPEs. Tambahan pula, kajian Thermal menggunakan TGA dan DSC thermograms menunjukkan bahawa suhu penguraian (T_{dc}) dan suhu peralihan kaca (T_g) kanji beras teranjak pada komposisi garam iodida dan cecair ionik. Dye sel solar peka (DSSCs) telah direka menggunakan sistem SPE dengan keberaliran ionik tertinggi. Pes TiO_2 diratakan pada FTO substrat melalui kaedah doctor-blade dan di bakar pada suhu $450\text{ }^\circ\text{C}$ sebagai foto-elektrod. Foto-elektrod direndam dalam pewarna berasaskan ruthenium (N719) selama 24 jam.

Platinum bersalut FTO telah digunakan sebagai elektrod kaunter. Elektrolit polimer pepejal telah diapit di antara dua foto-elektrod dan kaunter elektrod dengan konfigurasi Kaca/FTO/TiO₂ /N719-Dye/elektrolit polimer pepejal/Pt/FTO/Kaca. Rekaan DSSCs dianalisis untuk penukaran tenaga menggunakan simulasi cahaya matahari dengan pencahayaan cahaya putih 1000 (W m⁻²) ditakrifkan sebagai kuasa cahaya jatuh. DSSCs menunjukkan kecekapan penukaran tenaga yang ketara untuk biopolimer pepejal berasaskan sel-sel solar sebagai sumber tenaga hijau.

To My Beloved Parents
&
My Beloved Wife and Daughter

ACKNOWLEDGEMENTS

IN THE NAME OF ALLAH, THE MOST GRACIOUS, THE MOST MERCIFUL

I would like to express my heartily thanks and appreciation to all the people who assisted me to perform this work, specially my supervisors Prof. Dr. Ramesh T. Subramaniam and Dr. Ramesh Kais, for their kind attitude, patience and supports during my PhD study. Dr. Bandara is acknowledged for his assistance in electrode preparation and DSSC fabrication. I would like to thank to all my colleagues and staffs in CIUM center for their technical supports and assistance during my research. Especially for assistance of Eng. Ismail for his technical supports, Mr. Fareezwan for his assistance in DSSC fabrication, Miss Shanti and Miss Wendy for their guidance in polymer electrolyte preparation. In addition, I would like to thank Bright Sparks unit for their financial and research support. Finally, the staffs of infra lab in IPPP, UM are acknowledged for their support and services in STA and DSC characterizations.

In particular, I would like to thank my father, Abdol Ali Khanmirzaei, for his prayer for me, great supports and attention to my progress in academic stream; my mother, Azar Manzouri, for his prayer and concern for me, who kindly helps and encourages me; my beloved wife, Narjes Dehghany, for his great patience, sacrifice, unfading love, support and encourages; and my the only daughter, Asal, who her presence gives me positive energy to do more in my life. Thank you all, which gave me strong motivations.

TABLE OF CONTENTS

Abstract	iii
Abstrak	v
Dedication	vii
Acknowledgements	viii
Table of Contents	ix
List of Figures	xiii
List of Tables	xvii
List of Symbols and Abbreviations	xviii
List of Publications and papers presented	xx
CHAPTER 1: INTRODUCTION	1
1.1 Background	1
1.2 Thesis objectives	3
1.3 Thesis outline	4
CHAPTER 2: LITERATURE REVIEW	6
2.1 Introduction	6
2.2 Starches	6
2.2.1 Rice starches	10
2.3 Solid polymer electrolytes (SPE)	11
2.4 Iodide salts	16
2.5 Imidazolium based ionic liquids	17
2.6 The dye-sensitized solar cells (DSSC)	19
2.6.1 Basic principles and structure	20
2.6.2 Dye sensitizer	22
2.7 Summary	24

CHAPTER 3: EXPERIMENTAL METHODS	25
3.1 Introduction	25
3.2 Materials	25
3.2.1 Solid polymer electrolytes (materials)	25
3.2.2 Dye-sensitized solar cell fabrication (materials)	26
3.3 Preparation of solid polymer electrolytes	26
3.3.1 The rice starch and iodide salt systems	26
3.3.2 The rice starch, iodide salt and ionic liquid systems	28
3.4 Dye-sensitized solar cell (DSSC) fabrication	31
3.4.1 Conducting glass substrate	31
3.4.2 Double-layer photo-active electrode	31
3.4.2.1 First layer of photo-active electrode	32
3.4.2.2 Second layer of photo-active electrode	33
3.4.2.3 Dye solution	33
3.4.3 Counter electrode	34
3.4.4 DSSC fabrication	35
3.5 Measurement and characterization	36
3.5.1 Electrochemical impedance spectroscopy (EIS)	37
3.5.1.1 Ionic conductivity measurement	45
3.5.1.2 Temperature-dependent study	46
3.5.2 Fourier transform infrared spectroscopy (FTIR)	47
3.5.3 X-ray diffraction (XRD)	48
3.5.4 Thermogravimetric analysis (TGA)	50
3.5.5 Differential scanning calorimetry (DSC)	51
3.5.6 Current-voltage (J-V) characterization	53
3.6 Summary	54

CHAPTER 4: RESULTS AND DISCUSSION ON SYSTEMS BASED ON THREE DIFFERENT IODIDE SALTS	55
4.1 Introduction	55
4.2 EIS characterization	55
4.2.1 Ionic conductivity	55
4.2.2 Temperature-dependent ionic conductivity	68
4.3 FTIR characterization	71
4.4 XRD characterization	77
4.5 Thermal study – TGA	82
4.6 Thermal study – DSC	90
4.7 J-V characteristics	95
4.8 Summary	96
CHAPTER 5: RESULTS AND DISCUSSION ON SYSTEMS BASED ON TWO DIFFERENT IONIC LIQUIDS	97
5.1 Introduction	97
5.2 EIS characterization	97
5.2.1 Ionic conductivity	97
5.2.2 Temperature-dependent ionic conductivity	104
5.3 FTIR characterizarion	107
5.4 XRD characterization	109
5.5 Thermal study – TGA	112
5.6 Thermal study – DSC	118
5.7 J-V characteristics	121
5.8 Summary	129
CHAPTER 6: DISCUSSIONS ON DIFFERENCES OF FIVE SYSTEMS	130
6.1 Introduction	130

6.2	EIS characterization	130
6.2.1	Ionic conductivity	130
6.2.2	Temperature-dependent ionic conductivity	133
6.3	FTIR and XRD structural characterizations	133
6.4	TGA and DSC thermal studies	134
6.5	J-V characteristics	134
6.6	Summary	138
CHAPTER 7: CONCLUSION AND SUGGESTIONS FOR FUTURE RESEARCH		139
REFERENCES		142

LIST OF FIGURES

Figure 2.1: Amylose structure	8
Figure 2.2: Amylopectin structure	9
Figure 2.3: Structure of MPII ionic liquid (Aldrich)	18
Figure 2.4: Structure of HMII ionic liquid (Aldrich)	19
Figure 2.5: Schematic view of dye-sensitized solar cell	21
Figure 2.6: Structure of N719 dye (Aldrich)	23
Figure 3.1: The typical SPE film with rice starch and iodide salt	28
Figure 3.2: A typical view of SPE using rice starch, sodium iodide ionic liquid	30
Figure 3.3: A SPE film after addition of iodine	30
Figure 3.4: The FTO glass after first layer coating (with P90)	32
Figure 3.5: The electrode after second layer preparation (with P25)	33
Figure 3.6: Photo-anode electrode after soaking in N719 dye	34
Figure 3.7: The fabricated DSSC	35
Figure 3.8: The setup for DSSC characterization with Sun simulator	36
Figure 3.9: Schematic view of an impedance experiment	37
Figure 3.10: Explanation of polarization in sample cell	39
Figure 3.11: Schematic view of equivalent circuit for sample cell	39
Figure 3.12: Schematic view of Cole-Cole plot	46
Figure 3.13: Schematic view for working principle of X-ray diffractometer	50
Figure 3.14: Typical graph for current density vs voltage	53
Figure 4.1: Cole-Cole plot of pure rice starch (RS-0)	56
Figure 4.2: Cole-Cole plot of system 1 (RS:LiI) for (a) RS-1, (b) RS-2, (c) RS-3, (d) RS-4, (e) RS-5 and (f) RS-6	57
Figure 4.3: Cole-Cole plot for RS-7 with 35 wt.% of LiI	58
Figure 4.4: Conductivity of RS:LiI at different LiI content room temperature	60

Figure 4.5: Cole-Cole plot of system 2 (RS:NH ₄ I) for (a) RN-1, (b) RN-2, (c) RN-3, (d) RN-4, (e) RN-5, (f) RN-6, (g) RN-7 and (h) RN-8	61
Figure 4.6: Cole-Cole plot of RN-9	62
Figure 4.7: Variation of ionic conductivity with NH ₄ I salt in RS:NH ₄ I system	64
Figure 4.8: Cole-Cole plot for (a) RNa-1,(b) RNa-2,(c) RNa-3,(d) RNa-4, (e) RNa-5, (f) RNa-6, (g) RNa-7 and (h) RNa-8	65
Figure 4.9: Cole-Cole plot of RNa-9	66
Figure 4.10: Variation of ionic conductivity with different NaI salt content	68
Figure 4.11: Temperature-dependent ionic conductivity of rice starch and lithium iodide system.	69
Figure 4.12: Temperature-dependent ionic conductivity of RS:NH ₄ I system	70
Figure 4.13: Temperature-dependent ionic conductivity of RS:NaI system	71
Figure 4.14: FTIR spectra of RS-0, pure LiI, RS-5, RS-6 and RS-7	72
Figure 4.15: FTIR spectra of RS-0, NH ₄ I, RN-7,RN-8, RN-9 polymer electrolytes	75
Figure 4.16: FTIR spectra of RS-0,NaI,RNa-7,RNa-8, RNa-9 polymer electrolytes	76
Figure 4.17: XRD patterns of RS:LiI polymer electrolyte system for (a) RS-5, (b) RS-6, (c) RS-7, (d) pure rice starch (RS-0), and (e) pure lithium iodide salt	78
Figure 4.18: XRD patterns of polymer electrolytes in RS:NH ₄ I system for (a) RN-7, (b) RN-8, (c) RN-9, (d) pure rice starch (RS-0) and (e) NH ₄ I	79
Figure 4.19: XRD patterns of polymer electrolytes in RS:NaI system for (a) RNa-7, (b) RNa-8, (c) RNa-9, (d) pure rice starch (RS-0) and (e) NaI salt	81
Figure 4.20: TGA thermograms of pure rice starch (RS-0)	82
Figure 4.21: TGA results for RS-5	83
Figure 4.22: TGA results for RS-6	83
Figure 4.23: TGA results for RS-7	84
Figure 4.24: Comparison of TGA curves in RS:LiI system	85
Figure 4.25: TGA results for RN-7	86
Figure 4.26: TGA results for RN-8	86
Figure 4.27: TGA results for RN-9	87

Figure 4.28: TGA thermograms of RS-0, RN-7, RN-8, RN-9 in RS:NH ₄ I system	87
Figure 4.29: TGA thermograms of RNa-7	88
Figure 4.30: TGA thermograms of RNa-8	89
Figure 4.31: TGA thermograms of RNa-9	89
Figure 4.32: TGA thermograms for RS-0, RNa-7, RNa-8 and RNa-9 in RS:NaI system	90
Figure 4.33: DSC thermograms of pure rice starch, RS-5, RS-6, and RS-7	91
Figure 4.34: DSC thermograms of RN-7, RN-8, and RN-9 polymer electrolytes	92
Figure 4.35: DSC thermograms of RNa-7, RNa-8, RNa-9 polymer electrolytes	94
Figure 4.36: Photocurrent density versus potential (J-V) DSSC fabricated RNa-9	95
Figure 5.1: Cole-Cole plot of (a) RNaP-1, (b) RNaP-2 and (c) RNaP-3	98
Figure 5.2: Cole-Cole plot for RNaP-4	99
Figure 5.3: Variation of Ionic conductivity with MPII ionic liquid content	101
Figure 5.4: Cole-Cole plot of (a) RNaH-1 (b) RNaH-2 and (c) RNaH-3	102
Figure 5.5: Cole-Cole plot for RNaH-4	103
Figure 5.6: Variation of Ionic conductivity with HMII ionic liquid content.	105
Figure 5.7: Temperature-dependent ionic conductivity results of RNaP-1, RNaP-2, RNaP-3 and RNaP-4.	105
Figure 5.8: Temperature-dependent ionic conductivity of RS:NaI:HMII system	106
Figure 5.9: FTIR spectra of RNa-9, MPII, RNaP-2, RNaP-3 and RNaP-4 solid polymer electrolytes	107
Figure 5.10: FTIR spectra of RNa-9, HMII, RNaH-2, RNaH-3 and RNaH-4	108
Figure 5.11: XRD patterns of (a) RNaP-2, (b) RNaP-3, (c) RNaP-4, (d) MPII and (e) RNa-9	110
Figure 5.12: XRD patterns of polymer electrolytes for (a) RNaH-2, (b) RNaH-3 (c) RNaH-4, (d) HMII and (e) RNa-9	111
Figure 5.13: TGA thermograms for RNaP-1	112
Figure 5.14: TGA thermograms for RNaP-2	113

Figure 5.15: TGA thermograms for RNaP-3	113
Figure 5.16: TGA thermograms for RNaP-4	114
Figure 5.17: TGA thermograms for RNaP-1, RNaP-2, RNaP-3 and RNaP-4	115
Figure 5.18: TGA thermograms for RNaH-1	116
Figure 5.19: TGA thermograms for RNaH-2	116
Figure 5.20: TGA thermograms for RNaH-3	117
Figure 5.21: TGA thermograms for RNaH-4	117
Figure 5.22: TGA thermograms of RNaH-1, RNaH-2, RNaH-3 and RNaH-4	118
Figure 5.23: DSC thermograms for RNaP-1, RNaP-2, RNaP-3 and RNaP-4	119
Figure 5.24: DSC thermograms for RNaH-2, RNaH-3 and RNaH-4	120
Figure 5.25: J-V graphs for (a) RNaP-1, (b) RNaP-2 and (C) RNaP-3	122
Figure 5.26: J-V graph of RNaP-4	123
Figure 5.27: Variation of energy conversion efficiency with MPII ionic liquid	125
Figure 5.28: J-V graphs of (a) RNaH-1, (b) RNaH-2 and (c) RNaH-3	126
Figure 5.29: J-V graph for RNaH-4	127
Figure 5.30: Variation of energy conversion efficiency with HMII ionic liquid	129
Figure 6.1: Ionic conductivity of RS: LiI, RS:NH ₄ I, RS:NaI systems at different salt contents	131
Figure 6.2: Ionic conductivity of RNaP and RNaH systems at different ionic liquid contents	132
Figure 6.3: Photocurrent density versus cell potential (J-V) for DSSC fabricated using RNa-9, RNaP-1, RNaP-2, RNaP-3 and RNaP-4	135
Figure 6.4: Photocurrent density versus cell potential (J-V) for DSSC fabricated using RNa-9, RNaH-1, RNaH-2, RNaH-3 and RNaH-4	136
Figure 6.5: Variation of efficiency with MPII and HMII ionic liquid contents	137

LIST OF TABLES

Table 3.1: Designation of RS:LiI, RS:NH ₄ I and RS:NaI systems	27
Table 3.2: Designation of RNaP and RNaH systems	29
Table 4.1: Bulk resistances in RS:LiI system	56
Table 4.2: Designation and ionic conductivity in RS:LiI system	59
Table 4.3: Bulk resistance values in RS:NH ₄ I system	62
Table 4.4: Designation and ionic conductivity of RS:NH ₄ I system	63
Table 4.5: Bulk resistance for polymer electrolytes in RS:NaI system	64
Table 4.6: Ionic conductivity and designation of RS:NaI system	67
Table 4.7: Band assignments and infrared wavenumbers for pure rice starch	72
Table 4.8: Band assignments and wavenumbers for RS:NH ₄ I system	74
Table 4.9: Band assignments and wavenumbers for polymer electrolytes	76
Table 4.10: TGA and DSC data for RS:LiI polymer electrolyte system	91
Table 4.11: TGA and DSC data for RS:NH ₄ I polymer electrolyte system	93
Table 4.12: TGA and DSC data for RS:NaI polymer electrolyte system	95
Table 5.1: Bulk resistance values in RNaP system	97
Table 5.2: Designation and ionic conductivity of RS:NaI:MPII solid polymer	100
Table 5.3: Bulk resistance values as EIS data for RNaH system	101
Table 5.4: Designation and ionic conductivity of RNaH polymer electrolytes	104
Table 5.5: TGA and DSC thermograms for RS:NaI:MPII solid polymer electrolyte	119
Table 5.6: TGA and DSC thermograms for RS:NaI:HMII solid polymer electrolyte	121
Table 5.7: Dye-sensitized solar cell parameters for RS:NaI:MPII system	124
Table 5.8: Dye-sensitized solar cell parameters for RS:NaI:HMII system	128
Table 6.1: Comparison of this work with other works on efficiency enhancement	138

LIST OF SYMBOLS AND ABBREVIATIONS

$\tan \delta$:	Loss tangent
ε_0	:	Permittivity of the free space.
ε^*	:	Complex permittivity
ε'	:	Real part of complex permittivity
ε''	:	Imaginary part of complex permittivity
η	:	Energy conversion efficiency
θ	:	Incident angle
μ	:	Mobility
ρ	:	Density
ρ_0	:	Density of the gas
σ	:	Ionic conductivity
$\sigma(\omega)$:	Total frequency dependent conductivity
σ_{ac}	:	AC-conductivity
σ_0	:	Pre-exponential factor
τ_0	:	Free ion life-time
B	:	Susceptance
C	:	Geometrical capacitance
C_0	:	Vacuum capacitance
C_e	:	Capacitance without double-layer
D	:	Diffusion coefficient
E_a	:	Activation energy
G	:	Conductance
m	:	Mass of ionic carrier
k	:	Boltzmann constant
n	:	Number density of mobile ions
M_n	:	Molar mass
M^*	:	Complex modulus
M_r	:	Real part of complex modulus
M_i	:	Imaginary part of complex modulus
T_{dc}	:	Decomposition temperature
T_g	:	Glass transition temperature

$T_{g,\infty}$:	Maximum glass transition temperature by theory
P_{in}	:	Incident light power
$P(E)$:	Number of transitions per unit time
R_b	:	Bulk resistance
v	:	Velocity of the free ions
Y^*	:	Complex admittance
Y_r	:	Real part of complex admittance
Y_i	:	Imaginary part of complex admittance
Z^*	:	Complex impedance
Z'	:	Real part of complex impedance
Z''	:	Imaginary part of complex impedance
Z	:	Valency of ion
Z_A	:	Magnitude of impedance
DSC	:	Differential scanning calorimetry
DSSC	:	Dye-sensitized solar cell
EIS	:	Electrochemical impedance spectroscopy
FTIR	:	Fourier transform infrared
FTO	:	Fluorine doped tin oxide
HMII	:	1-hexyl-3-methylimidazolium iodide
HOMO	:	Highest occupied molecular orbital
IL	:	Ionic liquid
ITO	:	Indium tin oxide
LUMO	:	Lowest unoccupied molecular orbital
MPII	:	1-methyl-3-propylimidazolium iodide
PE	:	Polymer electrolyte
PTFE	:	Polytetrafluoroethylene
SPE	:	Solid polymer electrolyte
TGA	:	Thermogravimetric analysis
XRD	:	X-ray diffraction

LIST OF PUBLICATIONS AND PAPERS PRESENTED

Published Articles

M. H. Khanmirzaei, S. Ramesh (2015) Polymer electrolyte based dye-sensitized solar cell with rice starch and 1-methyl-3-propylimidazolium iodide ionic liquid, **Materials & Design**, DOI: 10.1016/j.matdes.2015.06.113 (IF=3.501; Q1)

M. H. Khanmirzaei, S. Ramesh, K. Ramesh (2015) Effect of different iodide salts on ionic conductivity and structural and thermal behavior of rice-starch-based polymer electrolytes for dye-sensitized solar cell application, **Ionics**, 21 (8) 2383-2391. (IF=1.836; Q2)

M. H. Khanmirzaei, S. Ramesh (2014) Nanocomposite Polymer Electrolyte based on Rice Starch/Ionic Liquid/TiO₂ Nanoparticles for Solar Cell Application, **Measurement**, 58 (0) 68-72. (IF=1.526 ; Q1)

M. H. Khanmirzaei, S. Ramesh (2014) Studies on biodegradable polymer electrolyte rice starch (RS) complexed with lithium iodide, **Ionics** 20 (5) 691-695. (IF=1.836; Q2)

S. Akbarzadeh, A. K. Arof, S. Ramesh, **M. H. Khanmirzaei**, R. M. Nor (2014) Prediction of conductivity by adaptive neuro-fuzzy model, **PloS ONE**, 9 (3) Article Number-e92241. (IF=3.534; Q1)

M. H. Khanmirzaei, S. Ramesh (2013) Ionic transport and FTIR properties of lithium iodide doped biodegradable rice starch based polymer electrolytes, **International Journal of Electrochemical Science** 8 (7) 9977-9991. (IF=1.956; Q3)

Submitted Articles

M. H. Khanmirzaei, S. Ramesh (2015) Dye-Sensitized Solar Cells Based on Solid Polymer Electrolytes Using Rice Starch and 1-Hexyl-3-Methylimidazolium Iodide Ionic Liquid, **Organic Electronics**, Under Revision (IF= ; Q1)

M. H. Khanmirzaei, S. Ramesh (2015) Hydroxypropyl Cellulose Based Non-Volatile Gel Polymer Electrolytes for Dye-Sensitized Solar Cell Applications using ionic liquid, **Scientific Reports**, Under Review (IF= ; Q1)

Patents

M. H. Khanmirzaei, S. Ramesh, Fabrication of dye sensitized solar cells using environmental friendly low cost biopolymer rice starch based polymer electrolytes as green energy generator, (2014).

M. H. Khanmirzaei, S. Ramesh, Novel solvent free hydroxyl propyl cellulose based gel biopolymer electrolyte as environmental friendly and non-volatile electrolyte layer for biopolymer based dye sensitized solar cells, (2014), PI 2014701877.

Conferences

M. H. Khanmirzaei, S. Ramesh, K. Ramesh, Calcium Iodide and Hydroxypropyl Cellulose Based Gel Polymer Electrolytes for Dye-Sensitized Solar Cell, International Conference - Advances in Functional Materials (AFM 2015), NY, USA, 29 June – 3 July 2015. (Poster)

M. H. Khanmirzaei, S. Ramesh, Gel Polymer Electrolyte Using Biopolymer Hydroxypropyl Cellulose and Sodium Iodide for Dye-Sensitized Solar Cell Application, ASIA - PACIFIC SOLAR RESEARCH CONFERENCE, Stream: The 9th Aseanian Conference on Dye-Sensitized and Organic Solar Cells (DSC-OPV9), University of NSW, Sydney, **Australia**, 8 Dec. – 10 Dec. 2014. (**Abstract**)

M. H. Khanmirzaei, S. Ramesh, Biopolymer Hydroxypropyl Cellulose based Non-volatile Gel Polymer Electrolytes for Dye Sensitized Solar Cell Applications, 65th Annual Meeting of the International Society of Electrochemistry (ISE-2014), Symposium 7, Dye Sensitized Solar Cells, Lausanne, **Switzerland**, 31 Aug. – 5 Sept. 2014. (**Poster**)

M. H. Khanmirzaei, S. Ramesh, Effect of Imidazolium Iodide Based Ionic Liquids on Ionic Conductivity and Efficiency of Dye Sensitized Solar Cells Using Biodegradable Rice Starch Based Polymer Electrolytes, 65th Annual Meeting of the International Society of Electrochemistry (ISE-2014), Symposium 7, Dye Sensitized Solar Cells, Lausanne, **Switzerland**, 31 Aug. – 5 Sept. 2014. (**Poster**)

M. H. Khanmirzaei, S. Ramesh, Ionic conductivity enhancement of biodegradable based polymer electrolytes using 1-Hexyl-3-methylimidazolium iodide ionic liquid for electrochemical applications, International Conference on Ionic Liquids (ICIL - 2013), Langkawi, **Malaysia**, 11 – 13 December 2013. (**Poster**)

M. H. Khanmirzaei, S. Ramesh, Environmental friendly low cost biodegradable polymer based dye sensitized solar cells as future green energy generator, 2nd International Conference on Solar Energy Materials, Solar Cells & Solar Energy Application (Solar Asia - 2013), Kuala Lumpur, **Malaysia**, 22 – 24 August 2013. (**Poster**)

M. H. Khanmirzaei, Ionic conductivity enhancement of biodegradable polymer electrolyte using different iodide salts dopants, Physics Colloquium 2013, Physics Department, University of Malaya, Kuala Lumpur, **Malaysia**, 04-05 June 2013. Local- (**Oral**)

M. H. Khanmirzaei, S. Ramesh, Nanocomposite polymer electrolytes based on rice starch/ionic liquid/TiO₂ nanoparticles for solar cell application, 4th International Conference on Functional Materials & Devices (ICFMD - 2013), Penang, **Malaysia**, 08 – 11 April 2013. (**Oral**)

CHAPTER 1

INTRODUCTION

1.1 BACKGROUND

Biodegradable polymers have economic and environmental benefits due to being cheap in cost, environmental friendly, nontoxic, abundance in nature, climate protection through CO₂ reduction, water solubility, good thermal, mechanical, and adhesive properties, and good ability of film forming (Kumar et al., 2012; Lenz, 1993; Liew et al., 2012; Lörcks, 1998). Utilizing environmental friendly polymers in polymer electrolytes and electronics field can be good replacement for some harmful existing materials and admirable category for green energy applications such as solar cells, specifically, dye sensitized solar cells, super capacitors, batteries, etc. Nowadays, due to non-environmental friendly effects of many synthetic polymers, biodegradable-based polymers have much attraction and portion in investigations.

Biodegradable polymers have been greatly involved in many applications with no harm for environment (Aoyagi et al., 2008; Armentano et al., 2010; Boley et al., 2000; Gunatillake et al., 2006; Imasaka et al., 1992; M. Kim et al., 2012; Lakshmi et al., 2003; E. Leclerc et al., 2004; Eric Leclerc et al., 2004; Lu et al., 2004; Middleton et al., 2000; Nair et al., 2007; Nishat et al.; Schnabelrauch et al., 2002; Shaarawy et al., 2009; Sinha Ray et al., 2005; Tian et al., 2012; Winzenburg et al., 2004; Xu et al., 2012; Yamamoto et al., 2005). Currently, biodegradable polymer electrolytes are being used for electrochemical applications in rechargeable lithium batteries (Fonseca et al., 2006; Polo Fonseca et al., 2006; Zhu et al., 2013), solar cells (Strange et al., 2008), dye sensitized solar cells (R. Singh et al., 2013), supercapacitors (Sudhakar et al., 2012), and fuel cells (Tripathi et al., 2011).

Among biodegradable polymers, natural polymers like starches have wide range of applications in drug delivery (Brouillet et al., 2008; Calinescu et al., 2012; Lemieux et al., 2009; Pu et al., 2011; Saboktakin et al., 2011; Sen et al., 2009; X. Wang et al., 2011), food packaging (Arvanitoyannis et al., 1998) and medicine (Rodrigues, 2012). Starch based solid polymer electrolytes (Kumar et al., 2012; Lopes et al., 2003; Marcondes et al., 2010; Mattos et al., 2007; Ning, Xingxiang, Haihui, & Benqiao, 2009; Ning, Xingxiang, Haihui, & Jianping, 2009; Ramesh et al., 2012a, 2012b; Sudhakar et al., 2012), and even rice starch based polymer electrolytes (Khanmirzaei et al., 2013, 2014a, 2014b; C. T. Kim et al., 1999; Samutsri et al., 2012; Viturawong et al., 2008), have impressive investigations on conductivity, rheological, structural and thermal properties and applications. One of the biggest challenges in polymer and salt complex is obtaining highly conducting films. Some attempts to increase ionic conductivity (Kaplan et al., 1989; Kiran Kumar et al., 2011; Su'ait et al., 2011) show importance of salt on performance of conduction. Kobayashi et al. (Kobayashi et al., 1992) reported that several lithium salt and salt contents can deeply affect the ion conductivity characteristics. Consequently, attempts to get better ionic conductivity between different polymers and salts are still in progress. Furthermore, ionic conductivity can be increased with other additives such as ionic liquids and fillers (Cho et al., 2007; Choi et al., 2011; Kurc, 2014; Li et al., 2014; Zalewska et al., 2014).

In this work, rice starch from starch group was used as fairly studied in literatures, and iodide salts were used to examine new possible properties on ionic conductivity, and dielectric parameters, and to develop dye sensitized solar cells (Nei de Freitas et al., 2008) to evaluate performance and energy conversion efficiency. Furthermore, rice starch is a good candidate among the other starches, because the rice starch has high amylose and low viscosity (Zhang et al., 2013).

As 1,4- α linkages in amylose are more stable and less steric than 1,6- α linkages, the mobile ions after addition of salt attach more on the amylose units. Thus, rice starches with high amylose content are expected to have more mobile ions and higher ionic conductivity (Khanmirzaei et al., 2013). Polymer electrolytes based on rice starch incorporated with lithium iodide, ammonium iodide and sodium iodide were prepared. The effect of iodide salts on conductivity, structural and thermal properties were studied using electrochemical impedance spectroscopy (EIS), Fourier transform infrared (FTIR), thermogravimetric analysis (TGA) and differential scanning calorimetry (DSC). Consequently, ionic liquids (ILs) have been introduced due to some advantageous properties such as non-flammability, high thermal stability, high ionic conductivity and negligible volatility (Arbizzani et al., 2011; Ueki et al., 2008). Therefore, ionic liquids have become good candidates to enhance ionic conductivity in polymer electrolyte systems, and in this work the ionic conductivity was further enhanced using ionic liquids namely, 1-methyl-3-propylimidazolium iodide (MPII) and 1-hexyl-3-methylimidazolium iodide (HMII). The polymer electrolytes based dye-sensitized solar cells were fabricated and analyzed under the Sun simulator.

1.2 THESIS OBJECTIVES

In the present work, the ionic conductivity, dielectric parameters, structural, thermal, and solar cell application and characteristics of rice starch based polymer electrolytes are discussed widely. The main objectives of the present work can be categorized by the below statements:

- To prepare rice starch based solid polymer electrolyte films using iodide salts for dye-sensitized solar cell applications and optimize the composition of the systems.

- To enhance the ionic conductivity and increase the ionic carriers of the solid polymer electrolytes (SPEs) using suitable ionic liquids for efficient dye sensitized solar cell applications.
- To characterize the samples to study ionic conductivity, structural and thermal behaviors.
- To fabricate dye sensitized solar cells (DSSCs) and to obtain DSSC related parameters and measure the energy conversion efficiency of the fabricated cells.

According to the knowledge of the authors, rice starch based solid polymer electrolytes are introduced into dye sensitized solar cell application as an environmental friendly source for the first time.

1.3 THESIS OUTLINE

The current thesis is expressed in 7 chapters. Chapter 1 is an introduction of the present work. Literature review is included in Chapter 2 containing history, structure and properties of starches, iodide salts and ionic liquids. The basic principles of dye sensitized solar cells are presented in Chapter 2. Chapter 3 is about experimental methods in four subtitles introducing materials used in this work, preparation techniques, characterizations and dye-sensitized solar cell fabrication procedures.

The results and discussions of the present work including five systems are described in Chapters 4 and 5, where the discussions on differences between five systems are expressed in Chapter 6. The ionic conductivity study, structural characterizations including FTIR and XRD, thermal studies using TGA and DSC, and dye-sensitized solar cell (DSSC) characterization for the first three systems based on rice starch and LiI, NH₄I and NaI iodide salts discussed in Chapter 4.

In Chapter 5, two systems based on rice starch, and MPIO and HMIO ionic liquids discussed for ionic conductivity study, structural characterizations including FTIR and XRD, thermal studies using TGA and DSC, and dye-sensitized solar cell characterization. Chapter 6 deals with discussions on differences and comparisons between five systems based on the results obtained by EIS, FTIR, XRD, TGA, DSC and DSSC characterizations. Finally, Conclusion and suggestions for the future work are represented in Chapter 7.

CHAPTER 2

LITERATURE REVIEW

2.1 INTRODUCTION

In this chapter, the literature review will be discussed to introduce the background of some materials used in this work. This chapter focuses on subjects such as starches, solid polymer electrolytes, iodide salts, imidazolium iodide based ionic liquids and dye-sensitized solar cells.

2.2 STARCHES

The history of starch is mainly unrecorded. The production of flour from grinding stones using starch grains was a normal practice across the Europe leastwise ~ 30000 years ago (Revedin et al., 2010). The starch is a carbohydrate including a large number of glucose units linked by glycosidic bonds. This polysaccharide is derived from most green plants such as potatoes, maize (corn), wheat, rice and cassava. The starch is white, odorless and tasteless powder which is normally soluble in warm or hot water. Starch structures as a polysaccharide are less varied than those of proteins, hence the more limited role of polysaccharides in living systems. They can have well-defined structures that vary with functional role of the polysaccharide in the living organism, and can be structural components of the cell walls of plants, or they can be involved in antigen-antibody recognition and hormone receptor interactions, or they may simply act as energy reserves.

Starches from various plant origins exhibit characteristic functional properties, depending on a number of integrated factors that include polymer composition, molecular structure, interchain organization, and minor constitutions (such as lipids, proteins, and phosphate ester groups).

Moreover, chemical, enzyme, and physical modification of starch structure, with either preservation or destruction of the native granular form, offer alternative routes of imparting certain functionality for this biopolymer. Starch modification is a common feature of many processed foods, having both textural and nutritional implications. Recent advances in the physical chemistry and structure of starch also reveal many similarities with synthetic semicrystalline polymers (Tegge, 1987).

Furthermore, the size, distribution, shape, and morphology of starch granules are markedly dependent on the botanical source, such as cereal starches which they are generally small and polyhydric, whereas tuber starches are large and ellipsoid or spherical (Zobel, 1988).

The starch consists of two types of macromolecules namely amylose and amylopectin. In most polysaccharides like starch, amylose and amylopectin are heterogeneous, exhibiting a wide distribution of molecular sizes and structures.

Most starches contain between 20% and 35% amylose. Starch owes much of its functionality to the fine structure and relative proportion of these polysaccharides (amylose and amylopectin) as well as to the physical organization of starch polymers into larger structural domains in the solid state (Biliaderis, 1998).

Amylose is the linear and helical polymer made up of D-glucose units and constitutes about 20 % of starch which has α -1,4-glucosidic linkages. The amylose provides energy for plants, because they can easily digest compared to amylopectin. Figure 2.1 indicates structure of amylose.

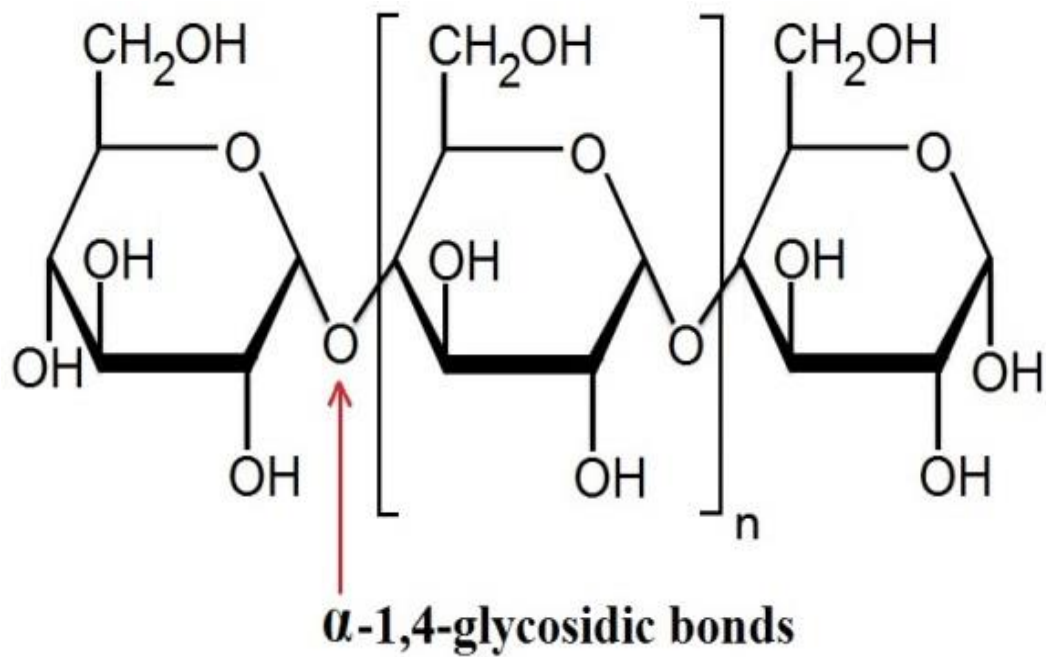


Figure 2.1: Amylose structure

Amylopectin is one of the largest known naturally occurring polymers and constitutes about 80 % of starch. Amylopectin is a highly branched polymer of glucose with α -1,6-glycosidic and α -1,4-glycosidic linkages. The α -1,6-glycosidic and α -1,4-glycosidic linkages are represented with amylopectin structure as shown in Figure 2.2.

The bulk of starch consists of amylopectin and molecules are larger than amylose molecules. The amylopectin molecules consist of several amylose molecules joined by oxygen bridges from the end of one amylose unit to a site along the chain of another amylose unit (Brady et al., 2004).

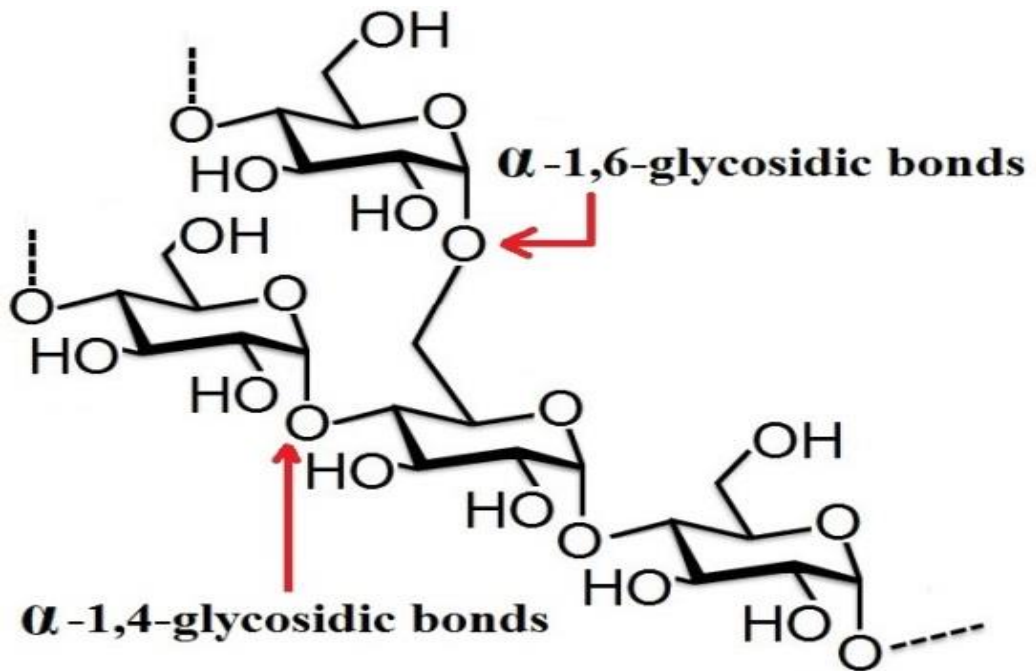


Figure 2.2: Amylopectin structure

There are some differences between amylose and amylopectin. Both amylose and amylopectin are soluble in hot water, but amylose does not form gel where amylopectin form gel. On the other hand, normally, all kinds of starch become soluble in hot water. Another difference is related to structure of amylose and amylopectin, as the structure of amylose is linear, it occupies less space compared to the amylopectin component.

Furthermore, starch gelation is important stage which requires some discussions. Starch gels are readily formed when gelatinized starch dispersions of sufficient concentration (usually > 6 wt.%) are cooled to room temperature. On cooling a starch paste, the exuded amylose from the swollen granules forms an interpenetrating network via interchain associations that surrounds the gelatinized granules. In this respect, starch gels can be regarded as hydrated polymer composites where swollen, amylopectin-enriched granules (filler particles) are embedded in and reinforce a continuous matrix of entangled amylose molecules (Ring, 1985).

The mechanical properties of such a material would depend on the rheological characteristics of the amylose matrix, the volume fraction and the deformability of the gelatinized granules, and the interactions between the dispersed and the continuous phases.

The long-term changes in rigidity and crystallinity of starch gels, related to amylopectin crystallization, correspond kinetically with staling events of aging items (Kulp et al., 1981). Thus, information concerning the rates of amylopectin crystallization has implications on the storage stability of starch based products. The presence of microcrystalline junctions in aged products has a direct bearing on the retrogradation kinetics from the respective of temperature-time-water content dependence of the crystallization process. The melting enthalpy increase for retrograded starch shows that crystallization occurs at a faster rate and to a greater extent when a lower single storage temperature is employed between -1 and 43 °C (Nakazawa et al., 1985; van Soest et al., 1994). Furthermore, in retrograded potato starch and cooked grains, storage at refrigeration temperatures resulted in the formation of less perfect crystallites than those formed on storage at room temperature. This is in accord with classical polymer crystallization theory (Jankowski et al., 1986), which predicts growth of more imperfect crystals with increasing degree of supercooling.

2.2.1 RICE STARCHES

Generally, rice starch is prepared from broken white rice. The broken grains are soaked for several hours in a caustic soda solution, and at the end, the alkali is washed away with water. The softened grains are ground with more caustic soda solution, and the resulting mass is submitted to centrifugation in a drum.

The starch layer is agitated with water (often with addition of 25 % formaldehyde solution), and the resulting starch liquor is dewatered, washed on a continuous rotary vacuum filter, re-suspended in water, and finally dewatered in a perforated basket centrifuge to about 35 % moisture. In modern processing it is usual to roll out a thick layer of moist starch, which is then slowly dried and falls to pieces as crystals (Kent-Jones, 2014).

Rice starches have low viscosity and high amylose content (Zhang et al., 2013). Amylose content in rice starches are about ~27 % of rice starch (Mutters et al., 2009; Panlasigui et al., 1991). As 1,4- α linkages in amylose are more stable and less steric than 1,6- α linkages, the mobile ions after addition of salt attach more on the amylose units. Thus, rice starches with more amylose will have more mobile ions and expect to have higher conductivity and more amorphism and shift in thermograms as will be discussed in this work. These reasons provide more interest to study on rice starch in this work.

2.3 SOLID POLYMER ELECTROLYTES (SPE)

The polymer electrolytes are electrolytic materials that offer many advantages in the area of large, high energy density batteries for electric propulsion and in fuel cells for electric vehicle or stationary applications. At the other end of the spectrum, polymer electrolytes are of interest for small, portable electronic devices where the battery represents a significant proportion of the device's size and weight. This chapter focuses on relevant structural, physical and electrical properties of these materials and on the related sectors where there has been considerable industrial input. Solid polymer electrolytes (SPEs) have been known for more than 30 years since their discovery by Peter V. Wright (Wright, 1975), which the major focus on technological potential is observed by Michel Armand et al (Armand, 1983; Armand et al., 1979).

The SPEs are solid solutions of monovalent (LiClO_4 , NaClO_4 , LiCF_3SO_3 , LiBF_4 , etc.) or divalent ($\text{Ca}(\text{ClO}_4)_2$, MgCl_2 , $\text{Mg}(\text{CF}_3\text{SO}_3)_2$) metal salts in the polymers, of which the pioneer, first and most studied was (and still is) the poly(ethylene oxide) (PEO). Consequently, the motion of the ions in the polymeric matrices in the absence of a solvent is a relatively new phenomenon whose existence and importance have been recognized only in the past decades (Armand, 1986; Bruce, 1997; Cameron, 1988; Dunsch, 1988; Gray, 1997; Schultze, 1996; Skotheim, 1988; Takahashi, 1989; Vincent, 1987; Wright, 1975). The macromolecules act as a solvent for a salt which become partially dissociated in the matrix, leading to electrolyte behavior. No small molecules are required for the conducting process, though the polymer–salt complex is regularly made from a solution of both constituents (Sequeira et al., 2010). The conductive complexes formed between solvating molecules and metal salts have been a challenging contest for the scientific community. The SPEs have been widely studied as they are a promising alternative to replace inorganic electrolytes and liquid crystals used in batteries, sensors and various electrochemical devices, among others. Up to now, unsettled questions remain concerning extend of dissociation and the transport numbers. These materials have kept their promises for applications in batteries, and the technological implications of their use are now generally accepted (Armand, 1994).

Between electronic and ionic conducting polymers, the latter (colorless) donate electron pairs from heteroatoms included in the macromolecular array from ‘s’ orbitals to Lewis acids (cations), where the former (highly absorbing) release single electrons from their conjugated ‘ π ’ system upon oxidative doping, with the formation of polarons (radical cations) possibly as dimers (bi-polarons). The ionic conductivity of the polymer electrolytes is typically 100 to 1000 times lower than liquid- or ceramic-based electrolytes.

Although higher conductivities are preferable, and indeed a great deal of effort has gone into improving the bulk ionic conductivity of polymer electrolytes over the years, 100 or 1000 times of increases are not essential, as a thin film electrochemical cell configuration can largely compensate for the lower values. Consequently, the term polymer electrolyte has come to denote any polymer based structure with remarkable ionic conductivity. These are found with a wide ambit of solid like characters. Low molecular weight polymers are regularly liquids so the range can be from liquids to very hard materials. Generally, the solid character of polymers is related to the molecular weight of the polymer. Some polymers can sort out at the molecular level in such a manner as to be crystalline. Since conductivity comes through molecular motion in the structure, crystalline polymers have low conductivity as the 'dry' polymer electrolyte is a single phase, non-crystalline material containing dissolved salt, and where the ions of the salt are mobile. The increasing need for novel electrolytes that have high conductivity, high lithium ion transport number, a wide electrochemical stability window, and are suitable for lithium batteries with safe operation is stimulating the third generation materials to be amorphous to temperatures as low as $-40\text{ }^{\circ}\text{C}$ and have conductivity at room temperature of the order of 10^{-3} S/cm , approaching that of liquid electrolytes (Sequeira et al., 2010).

Moreover, in polymer electrolytes, the mechanism of the interaction between polymer and salt can be explained with ion solvation by the polymer. Due to the presence of polar groups in polymers, it can be expected that they will behave as high-molecular-weight solvents and dissolve salts to make a stable ion-polymer complexes. A salt can only be dissolved in a solvent if the associated energy and entropy changes produce a general decrease in the free energy of the system. This emerges when the interaction between the ionic species and the coordinating groups on the polymer chain compensates for the loss of salt lattice energy (Vincent, 1987).

When a salt is dissolved in a polymer matrix, the conductivity of that polymer increases due to the concentration of charge carriers. The increase in entropy is realized by destruction of the crystal lattice and also by gross deformations in the polymer structure. Some net decrease in entropy may arise from localized ordering of the polymer host by the ions. The enthalpy of solvation is essentially the result of electrostatic interactions between the cation positive charge and the negative charge on the dipolar groups of the polymer or of partial sharing of a lone pair of electrons on a coordinating atom in the polymer, leading to a coordinate bond. The lattice energy effects may be compensated for by such factors as a low value of cohesive energy density and vacancy formation, favored by a low glass transition temperature, Lewis acid-base interactions between the coordinating sites on the polymer and the ions, and long-range electrostatic forces such as cation-anion interplay energies. Furthermore, for a specific cation-polymer coordination group, the distance apart of the coordinating groups and the polymer's ability to accept conformations that permit multiple inter- and intramolecular coordination are momentous (Gray, 1991).

Furthermore, in polar solvents such as water or methanol, hydrogen bonding is important for specific anion solvation, whereas aprotic liquids and solvating polymers have negligible anion stabilization energies. Differences in the general solvation energies of anions occur as the dielectric constant of the solvent varies. On passing from a polar, protic medium through to a less polar one, most anions are destabilized, the destabilization being greatest when the charge density and basicity of the ion are low ($F^- \gg Cl^- > Br^- > I^- \sim SCN^- > ClO_4^- \sim CF_3SO_3^- > BF_4^- \sim AsF_6^-$) (Marcus, 1987). The most suitable options of anion for aprotic, low-dielectric-constant dipolar polymer based polymer electrolytes are those to the right of the preceding series. These are large anions, with delocalized charge, are too weak bases with low ion-dipole stabilization energies.

In addition, their lattice energies are moderately low with little tendency to form tight ion pairs. These particular anions may be either soft (Γ^-) or hard (ClO_4^-) bases. In general, the formation of polymer electrolytes is controlled by the cation solvation energy in contrary to the salt lattice energy.

In solid polymer electrolyte preparation, the most common method of producing polymer electrolyte thin films is by solvent casting. This involves preparing a solution of the polymer and salt. This solution is cast into formers on a polytetrafluoroethylene (PTFE) surface, the solvent is removed by slow evaporation, and the final film is heated under vacuum to remove residual solvent. Many polymer electrolytes are semicrystalline and crystal formation may be significantly affected by the nature of the solvent, by the rate of the solvent removal, and by traces of residual solvent which is capable of acting either as nucleation sites or as a plasticizer.

In addition, the temperature at which films undergo final drying is important. Higher temperature usually induce the formation of high-melting spherulites as the sample cools (Cole et al., 1989). Consistency in casting techniques is important, but in practice, no common criteria are universally observed (Gray, 1991).

Among some electrochemical applications of polymer electrolyte, such as batteries, supercapacitors and electrochromic devices; dye-sensitized solar cells are another significant application of polymer electrolytes. The interest in this application is growing, reflected in the increased number of papers published each year concerning this application (De Freitas et al., 2010).

2.4 IODIDE SALTS

The salts normally refer to the ionic compounds which is result of reaction between an acid and a base. The salts also can be formed by other reactions such as reactions between a metal and an acid, a metal and a non-metal, a base and an acid anhydride, an acid and a basic anhydride. Most of the salts can dissolve in water. Each salt contains anions and cations, which cause to compound becomes electrically neutral. The ions in the salts can be inorganic such as chloride (Cl^-), or organic such as acetate ($\text{C}_2\text{H}_3\text{O}_2^-$); and also can be monatomic such as fluoride (F), or polyatomic such as sulfate (SO_4^{2-}) (Kurlansky, 2002).

The iodide salts are a compound which consists of iodine (I). Mainly there are two types of iodide salts one contain small cations such as lithium iodide (LiI), ammonium iodide (NH_4I), sodium iodide (NaI) and potassium iodide (KI), and the other contain large cations such as tetra-n-butylammonium (TBA^+) cation which combine with iodine and form tetra-n-butylammonium iodide (TBAI). The iodide salts are necessary in polymer electrolyte based dye-sensitized solar cell fabrications as iodide anions in iodide salts are required to provide redox mediator as will be discussed in this chapter section 2.6.

Lithium iodide (LiI) is compound of lithium and iodine. LiI has molar mass of 133.85 g/mol with melting point of 469 °C, which is soluble in water and ethanol. LiI has application in battery and dye-sensitized solar cell as an electrolyte. Ammonium iodide (NH_4I), compound of ammonium and iodine, has 144.94 g/mole and melting point of 551 °C. NH_4I is easily soluble in water. Sodium iodide (NaI) as a crystalline solid, compound of sodium and iodine, which has 149.89 g/mole and melting point of 661 °C. NaI is soluble in water, methanol and acetone.

2.5 IMIDAZOLIUM BASED IONIC LIQUIDS

The ionic liquids (ILs) are salts in the liquid state. One of the first truly room temperature ionic liquids was ethyl ammonium nitrate ($\text{C}_2\text{H}_5\text{NH}_3^+.\text{NO}_3^-$) (m.p. 12 °C), synthesized in 1914 by Paul Walden (Walden, 1914).

Some ionic liquids are considered as non-ionizing (e.g. non-polar), highly viscous and frequently exhibit low vapor pressure. Their other properties are varied that many have low combustibility, excellent thermal stability, wide liquid regions, and favorable solvating properties for a range of polar and non-polar compounds. Normally, ionic liquids have high mobility and ion conducting. Many categories of chemical reactions, such as Diels-Alder reactions and Friedel-Crafts reactions, can be carried out utilizing ionic liquids as solvents. Recent work has demonstrated that ionic liquids can serve as solvents for biocatalysis (Walker et al., 2004). The miscibility of ionic liquids with water or organic solvents differs with side chain lengths on the cation and with choice of anion. They can be functionalized to act as acids, bases or ligands, and have been utilized as precursor salts in the preparation of stable carbenes. Due to their specific properties, ionic liquids are attracting expanding attention in many fields, such as organic chemistry, electrochemistry, physical chemistry, catalysis and engineering.

Furthermore, between ionic liquids, imidazole based salts where the imidazole ring is in the cation are known as imidazolium salts. These salts are formed from the protonation or substitution at nitrogen of imidazole. These salts have been utilized as ionic liquids and precursors to stable carbenes. Salts where a deprotonated imidazole is an anion are likewise possible; these salts are known as imidazolate or imidazolidate salts.

Moreover, electrolytes containing imidazolium based ionic liquids such as 1-propyl-3-methylimidazolium iodide (MPII) (Fei et al., 2006) and 1-hexyl-3-methylimidazolium iodide (HMII) (M. Wang et al., 2006) ionic liquids provide excellent efficiencies and great stability in dye-sensitized solar cells when subjected to an accelerated light soaking test.

The 1-propyl-3-methylimidazolium iodide (MPII) ionic liquid ($C_7H_{13}IN_2$) has molar mass of 252.10 g/mol. Figure 2.3 shows the structure of MPII ionic liquid. Consequently, 1-hexyl-3-methylimidazolium iodide (HMII) ionic liquid ($C_{10}H_{19}IN_2$) has a molar mass of 294.18 g/mol. Figure 2.4 illustrates the structure of HMII, denoting extra 6 CH_2 bonds compared with MPII ionic liquid.

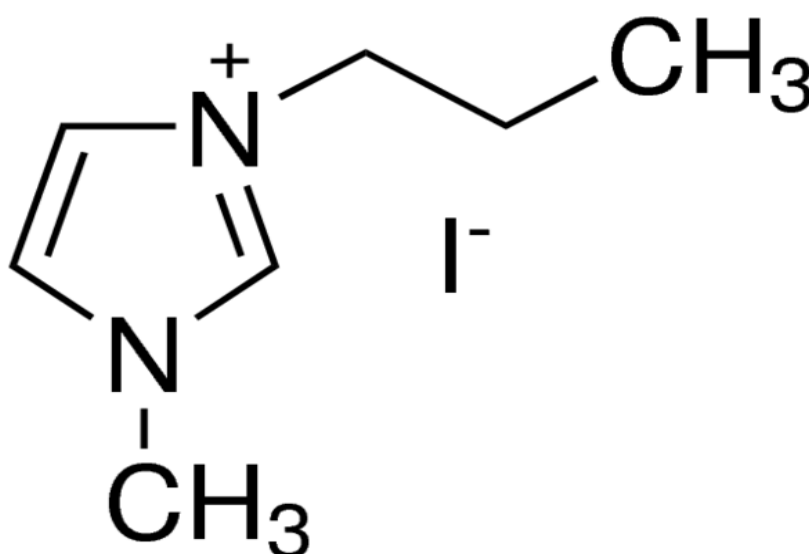


Figure 2.3: Structure of MPII ionic liquid (Aldrich)

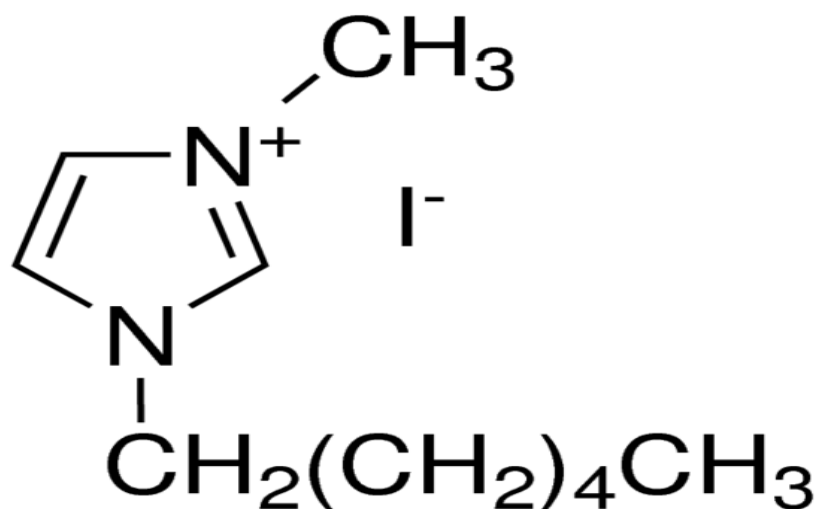


Figure 2.4: Structure of HMII ionic liquid (Aldrich)

2.6 THE DYE-SENSITIZED SOLAR CELLS (DSSC)

The dye-sensitized solar cell is a low-cost solar cell belonging to thin film solar cell groups. The DSSC is also known as Gratzel cell which invented by Brian Oregan and Michael Gratzel in 1991 (Oregan et al., 1991). This solar cell is based on colloidal TiO₂ films. Each DSSC contains three major parts namely photo-anode electrode, counter electrode and electrolyte. Photo-anode electrode is a glass substrate with a conductive layer such as indium tin oxide (ITO) or fluorine doped tin oxide (FTO) which coated with TiO₂ paste and soaked in ruthenium based dye. Counter electrode is normally coated with platinum. The electrolyte is normally three types, solid, gel and liquid type. The electrolyte is containing iodide, which in this work solid polymer electrolyte with iodide was used. Since the DSSC consist of combinations of several materials, the properties of each component directly influence the kinetics and reactions.

Thus, device performance depends on the morphology, optical and electrical properties of the porous semiconductor film; the chemical, electrochemical, photophysical and photochemical properties of the dye; the electrochemical and optical properties of the redox couple and solvent in the electrolyte; and the electrochemical properties of the counter-electrode.

The efficiency of a DSSC in the process for energy conversion depends on the relative energy levels and the kinetics of electron transfer processes at the sensitized semiconductor/electrolyte interface (DE FREITAS et al., 2010).

2.6.1 BASIC PRINCIPLES AND STRUCTURE

The dye-sensitized solar cells are working with some procedures which will be mentioned here. At the first, light will be absorbed by dye as a sensitizer (light absorption) and results in the injection of the electron in the conduction band (charge carrier transport) in the TiO₂ layer as mesoporous oxide based semiconductor and provide the electricity. In the redox mediator provided by iodide, the dye molecule will be regenerated at the counter electrode and the process will continuously repeat. The structure and principles of DSSC is demonstrated in Figure 2.5.

The mechanisms can also be explained and formulated, where after absorption of light by dye (S) there is formation of electronically excited state (S^{*}):



In the next step, the excited dye can involve in decay which is emission or injecting electrons in conduction band of TiO₂ by oxidization of dye (S⁺):



Through the mesoporous network of particles, the injected electrons travel to reach the counter electrode and go through the external circuit.

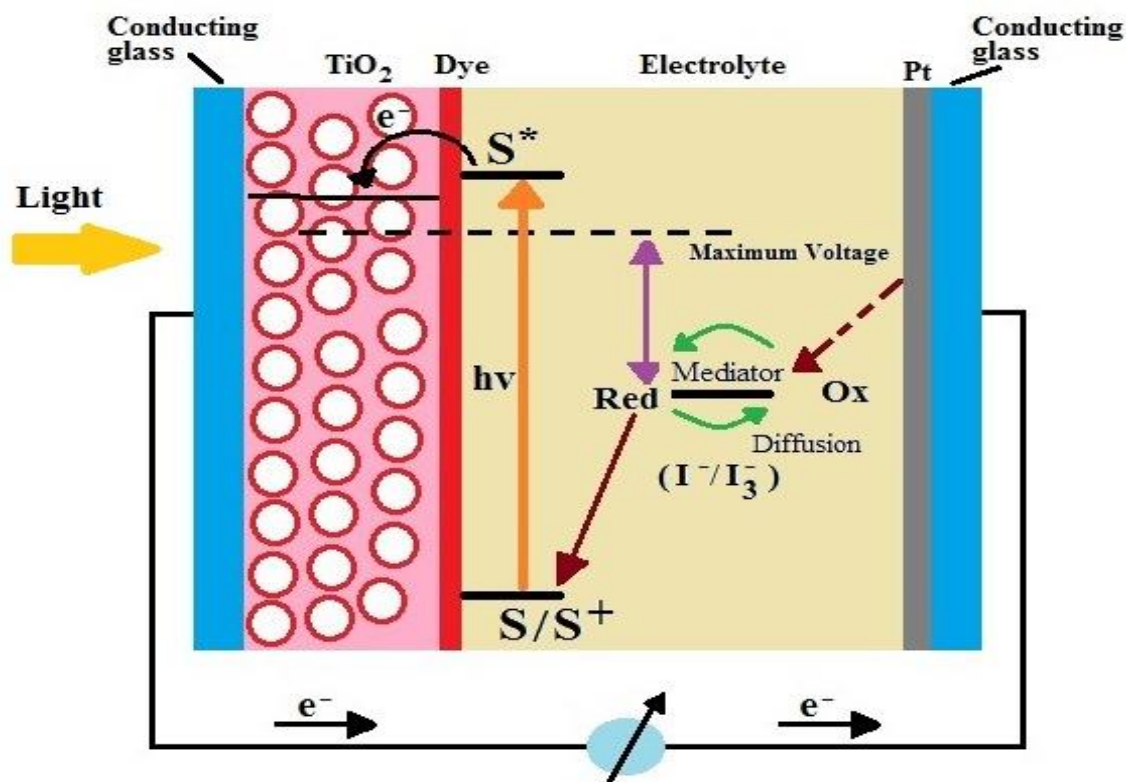


Figure 2.5: Schematic view of dye-sensitized solar cell

The oxidized dye returns back, by the donor (iodide) in the electrolyte, to the ground state (regeneration):



There is another phenomenon that happens in the cell without measurable photocurrent in the absence of a redox mediator which is called recombination. The recombination of the oxidized dye takes place with the electrons in TiO₂ layer:



In the counter electrode the electrons that reach through the external circuit reduce the oxidized iodide (I₃⁻) which is regeneration of I⁻ in this cycle repeats:



This process is conversion of sunlight to the electricity. According to Hara et al., the energy conversion efficiency of the dye-sensitized solar cell is affected by four energy levels of the ground state (HOMO), the excited state (LUMO), Fermi level in TiO₂ layer and the redox power of mediator (I⁻/I³⁻) (Hara et al., 2005). HOMO level refers to the highest occupied molecular orbital, where LUMO level is lowest unoccupied molecular orbital. The HOMO level is to organic semiconductors what the valence band maximum is to inorganic semiconductors and quantum dots. The Fermi level refers to the total electrochemical potential for electrons. Moreover, for the devices based on ruthenium complexes dyes, liquid electrolytes and nanocrystalline TiO₂, the charge injection is a very fast process, usually in the femtosecond time domain. On the other hand, the recombination is much slower, and occurs over a much longer timescale (several microseconds or longer). This difference of several orders of magnitude for the forward and reverse electron transfer rates allows the efficient processing of the charge separated products, i.e. the reduction of the dye cation by iodide and the percolation of the injected electrons in the TiO₂ film to arrive at the back contact (Kelly et al., 2001).

2.6.2 DYE SENSITIZER

In dye-sensitized solar cells, the dye is one of the key components for high power conversion efficiencies. The ideal sensitizer should be able to absorb the light spectra below the wavelength of 920 nm. As another requirement for dye sensitizer, it must carry attachment groups such as phosphonate or carboxylate to graft to the semiconductor oxide surface (Grätzel, 2003). There are many investigations on synthesis of the dyes to satisfy the mentioned requirements with high stability.

The ruthenium based dyes are one of the successful sensitizers for mesoporous solar cells. One of the highly used pioneering ruthenium based dyes is cis-Bis(isothiocyanato) bis(2,2'-bipyridyl-4,4'-dicarboxylato) with commercial name of N3.

Among the other ruthenium based dyes, Di-tetrabutylammonium cis-bis(isothiocyanato) bis(2,2'-bipyridyl-4,4'-dicarboxylato) ruthenium (II) known as N719 is one of the highly studied ruthenium-based dyes with high performance, and it is modified dye to increase device voltage and finally efficiency of the cell, which used in this work. Figure 2.6 shows the structure of N719.

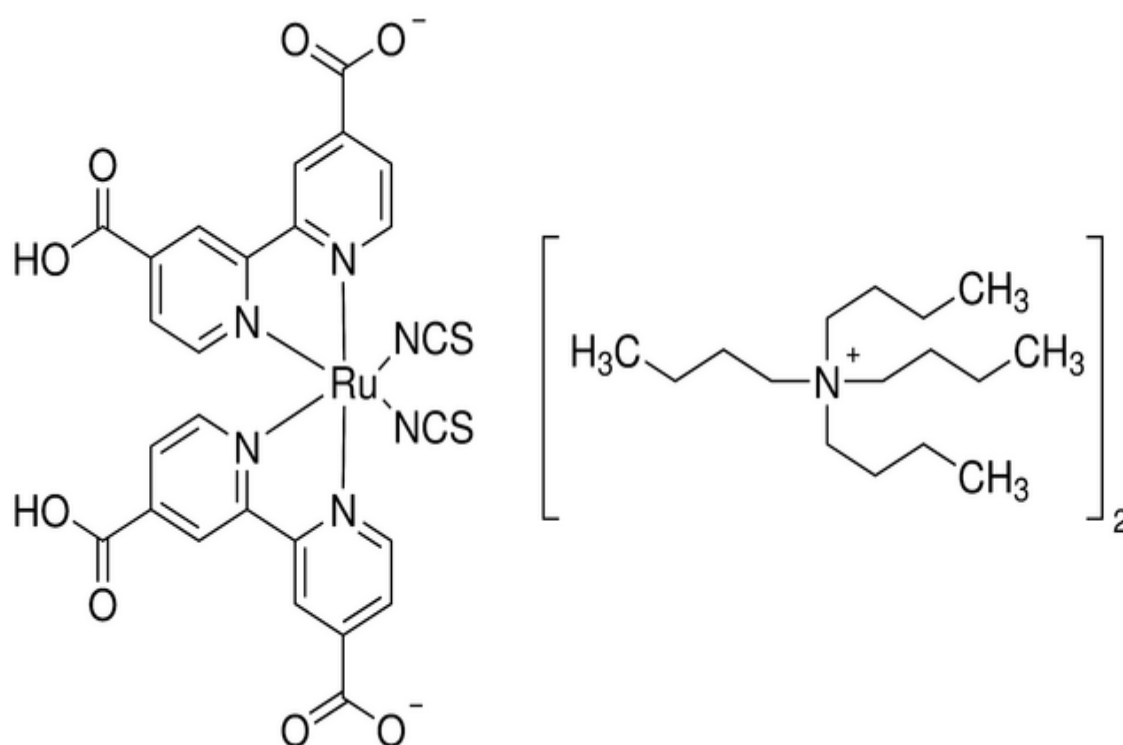


Figure 2.6: Structure of N719 dye (Aldrich)

Compared to N3 dye, N719 has some advantages such as (a) a higher ground state of the binding moiety thus increasing electrostatic binding onto the TiO₂ surface at lower pH values, (b) the decreased charge on the dye attenuating the electrostatic repulsion in between adsorbed dye units and thereby increasing the dye loading, (c) increasing the stability of solar cells towards water-induced dye desorption, and (d) the oxidation potential of these complexes is cathodically shifted compared to that of the N3 sensitizer, which increases the reversibility of the ruthenium III/II couple, leading to enhanced stability (Klein et al., 2004).

2.7 SUMMARY

This chapter discussed the current literature related to the starches, solid polymer electrolytes and dye-sensitized solar cells, and the characteristics of each subject. The following chapter will elaborate on the methodology and procedures for solid polymer electrolyte preparation, dye-sensitized solar cell (DSSC) fabrication and characterizations including EIS, FTIR, XRD, TGA, DSC and DSSC characterization.

CHAPTER 3

EXPERIMENTAL METHODS

3.1 INTRODUCTION

The methodology and procedures for polymer electrolyte preparation, dye-sensitized solar cell fabrication and characterizations such as impedance spectroscopy, structural, thermal and solar cell characterization are discussed in this chapter. In the first part of chapter the materials and chemicals used are discussed as well.

3.2 MATERIALS

The materials used are divided into two major parts. First category is in solid polymer electrolyte preparation and the other in dye-sensitized solar cell preparation.

3.2.1 SOLID POLYMER ELECTROLYTES (MATERIALS)

In solid polymer electrolyte (SPE) preparation, polymer, some iodide salts and some imidazolium iodide based ionic liquids were used. Rice starch (RS) was used as biopolymer. Lithium iodide (LiI), Ammonium iodide (NH₄I) and Sodium iodide (NaI) were used as iodide salts. In addition, 1-methyl-3-propylimidazolium iodide (MPII) and 1-hexyl-3-methylimidazolium iodide (HMII) were used as ionic liquids. Rice starch (RS) purchased from Sigma-Aldrich and was used without further purification. Lithium iodide salt (LiI) was purchased from Aldrich (crystalline powder, 99.9 % trace metals basis). Ammonium iodide (NH₄I) and sodium iodide (NaI) were purchased from Sigma-Aldrich (assay \geq 99%). 1-methyl-3-propylimidazolium iodide (MPII) and 1-hexyl-3-methylimidazolium iodide (HMII) were purchased from Aldrich. The rice starch, lithium iodide, ammonium iodide, sodium iodide, MPII and HMII were kept dry before use.

3.2.2 DYE-SENSITIZED SOLAR CELL FABRICATION (MATERIALS)

Mainly, dye-sensitized solar cells consist of anode electrode, cathode electrode and electrolyte. The materials for electrolyte preparation are the items discussed in section 3.2.1 on SPE preparation. The other materials are related to electrodes treatments and preparations. The TiO₂ nanopowder of two grades namely TiO₂ P90 (with particle size 14 nm) and P25 (with particle size 21 nm) were purchased from AEROXIDE. The Triton X-100 was purchased from Sigma-Aldrich. The Carbowax was purchased from Supelco Analytical. The magic tape (3M) purchased was of the Scotch brand.

3.3 PREPARATION OF SOLID POLYMER ELECTROLYTES

In this work, the solid polymer electrolytes (SPEs), which consist of five systems, were prepared using solution cast technique. The first three systems are only rice starch (RS) and iodide salt based systems. The other two systems contained rice starch and sodium iodide incorporated with imidazolium iodide based ionic liquids.

3.3.1 THE RICE STARCH AND IODIDE SALT SYSTEMS

The first three systems were prepared using rice starch (RS). Rice starch and lithium iodide (LiI) as RS:LiI system, rice starch and ammonium iodide (NH₄I) as RS:NH₄I system and rice starch and sodium iodide (NaI) as RS:NaI system, and their designations and compositions are illustrated in Table 3.1. All the first three systems follow the equation: RS+ X wt.% Y (X=5, 10, 15, 20, 25, 30, 35, 40, 45; Y=LiI, NH₄I and NaI).

Only for RS:LiI system, the LiI amount continued until 35 wt.%, since when there is a higher concentration of LiI, the solid films became very sticky making them difficult to handle and to cast. Distilled water as solvent was used with amount of ~25 ml for each sample.

Appropriate amounts of RS, as tabulated in Table 3.1, were added into the distilled water and heated until 80 °C and kept at this temperature for about 15 min to gelatinize the rice starch. After gelatinization of the rice starch appropriate amounts of iodide salt (LiI, NH₄I and NaI) were added as listed in Table 3.1. The mixtures were stirred to obtain a homogenous solution that is later casted onto a Teflon petri dish.

Furthermore, the remaining amount of water was evaporated in a drying oven at 60 °C for 24 h. After drying, the solid polymer electrolytes were casted and analyzed with EIS directly at room temperature.

Table 3.1: Designation of RS:LiI, RS:NH₄I and RS:NaI systems

Designation			RS:X (wt.%) Composition, (X=LiI, NH ₄ I, NaI)
RS:LiI	RS:NH ₄ I	RS:NaI	
RS-0	-	-	100:0
RS-1	RN-1	RNa-1	95:5
RS-2	RN-2	RNa-2	90:10
RS-3	RN-3	RNa-3	85:15
RS-4	RN-4	RNa-4	80:20
RS-5	RN-5	RNa-5	75:25
RS-6	RN-6	RNa-6	70:30
RS-7	RN-7	RNa-7	65:35
-	RN-8	RNa-8	60:40
-	RN-9	RNa-9	55:45

Figure 3.1 exhibits an example of SPE film using rice starch and iodide salt. For dye-sensitized solar cell application, for system 3, iodine as redox mediator (to provide I⁻/I₃⁻ redox) was added to the mixtures where the molar ratio of sodium iodide and iodine (NaI:I₂) is (10:1).

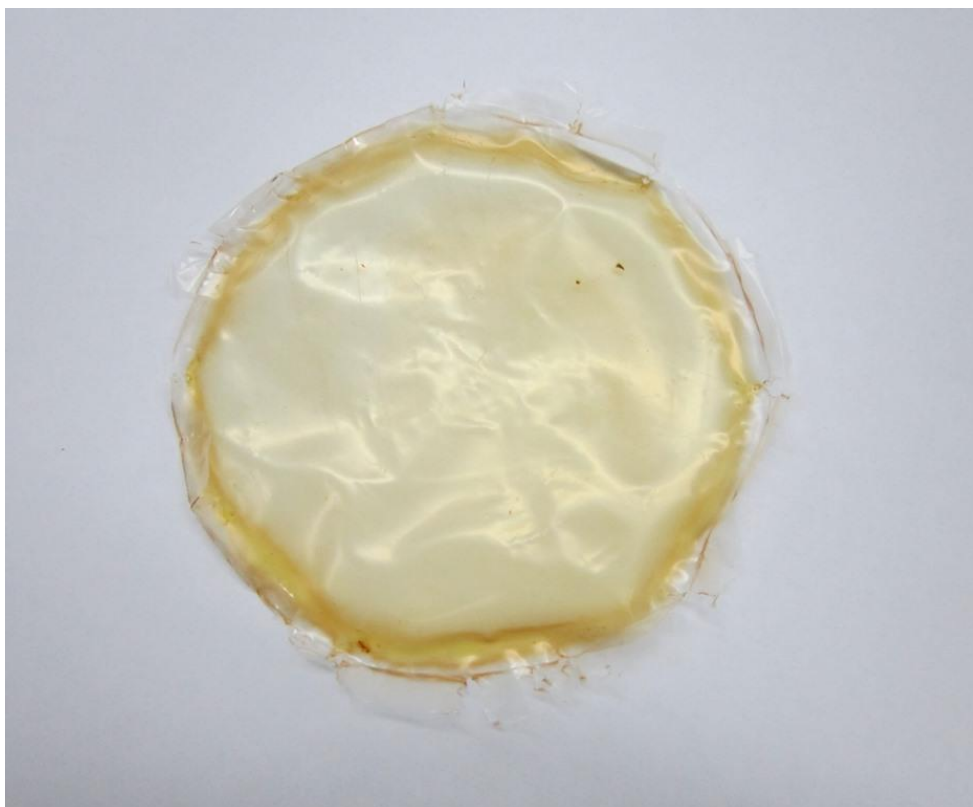


Figure 3.1: The typical SPE film with rice starch and iodide salt

3.3.2 THE RICE STARCH, IODIDE SALT AND IONIC LIQUID SYSTEMS

RS:NaI:MPII and RS:NaI:HMII systems were prepared with the incorporation of RS biopolymer, NaI salt, MPII (for RS:NaI:MPII system) and HMII (for RS:NaI:HMII system) ionic liquids. NaI salt was used in two last systems, as rice starch with NaI among the first three systems showed the highest ionic conductivity in 45 wt. % of NaI. The solid polymer electrolytes were prepared using the solvent cast method. The RS biopolymer and NaI weight ratios were optimized to get the highest ionic conductivity at 55 wt.% for rice starch and 45 wt.% for sodium iodide and designated as RNa-9. Systems 4 and 5 follow the equation: RS:NaI:X IL (X=5, 10, 15, 20 wt.%, IL=MPII and HMII) and the designations are introduced in Table 3.2. Distilled water with the amount of ~15 ml was used as solvent for each sample.

Appropriate amounts of rice starch were added into the distilled water and heated until 80 °C and kept at this temperature for about 15 min to gelatinize the rice starch.

After gelatinization, appropriate amounts of sodium iodide salt (NaI) were added as in Table 3.2. After further stirring, the temperature was fixed at about 60 °C before the addition of ILs to make a better complexation of polymer and ionic liquid. Appropriate amounts of MP11 and HM11 ionic liquids were added to the solution according to the systems and designations as shown in Table 3.2.

Table 3.2: Designation of RNaP and RNaH systems

Designation		Ionic liquid (g) (MP11, HM11)	RS:NaI:X (wt.%) Composition, (X=MP11, HM11)
RS:NaI:MP11	RS:NaI:HM11		
RNaP-1	RNaH-1	0.1	52.25:42.75:5
RNaP-2	RNaH-2	0.2	49.5:40.5:10
RNaP-3	RNaH-3	0.3	46.75:38.25:15
RNaP-4	RNaH-4	0.4	44:36:20

Figure 3.2 shows the SPE prepared using ionic liquid which illustrates more flexibility compared to the SPE without ionic liquid. Iodine as redox mediator (to provide I^-/I_3^- redox) was added to the mixtures where the molar ratio of sodium iodide and iodine (NaI:I₂) is (10:1).

Figure 3.3 shows the SPE after the addition of iodine. The mixtures were further stirred to obtain a homogenous solution and then casted onto a Teflon petri dish. The excess remaining waters were evaporated by drying in the oven at 55 °C for 24 h. After drying, the SPEs were casted and analyzed directly using EIS at room temperature.

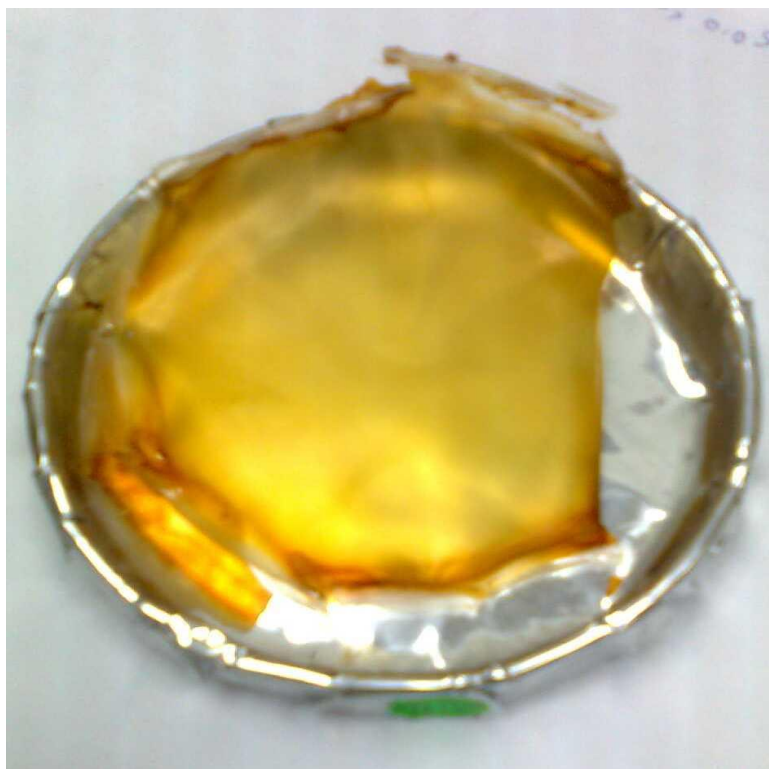


Figure 3.2: A typical view of SPE film using rice starch, sodium iodide and ionic liquid



Figure 3.3: A SPE film after addition of iodine

3.4 DYE-SENSITIZED SOLAR CELL (DSSC) FABRICATION

The DSSCs were fabricated in three major steps including photo-active electrode preparation, counter electrode preparation and SPE preparation. The fabrications of DSSCs were also involved in the substrate treatment as well.

3.4.1 CONDUCTING GLASS SUBSTRATE

In the electrode preparation, the conducting glass substrate is utilized. Two most commonly used conducting glasses are indium tin oxide (ITO) and fluorine doped tin oxide (FTO). In this work, the FTO substrate was used for photo anode and counter electrodes. Before coating on the FTO glass, the FTO substrate should be cleaned. The FTO glass was cleaned with the following procedures. First, the FTO glasses were washed with soap, and then were rinsed off and washed in running water. Then, the FTO glasses were placed in a beaker with a little distilled water and two drops of H_2SO_4 , and sonicated for about 10 minutes. After the sonication process, the FTO glasses were transferred to another beaker which is filled with 2-propanol. Then the beaker was heated on a hotplate until some small air bubbles were observed to come up and the FTO glasses were lifted with tweezers and placed on a tissue and wiped.

3.4.2 DOUBLE-LAYER PHOTO-ACTIVE ELECTRODE

The photo-anode or photo-active electrode was prepared by coating two layers of TiO_2 based paste. For the first layer, the TiO_2 paste with grade P90 was used and spin coated on the substrate. The particle size of P90 is small (~14 nm) to reduce any short circuit caused by dye leakage to the FTO surface directly. The second layer which is TiO_2 paste with grade P25 (25 nm) was doctor bladed onto the FTO glass. In the second layer preparation, the TiO_2 with a bigger particle size was used to make a very porous layer to trap more dyes for more sensitization. Finally, the photo-anode electrode was soaked in the N719 dye solution to trap the dyes on the electrode.

3.4.2.1 FIRST LAYER OF PHOTO-ACTIVE ELECTRODE

For the first layer which is spin coated, 0.5 g of TiO_2 (P90) was ground for 30 minutes with 2 ml HNO_3 (pH=1) in an agate mortar and spin coated on FTO at 1000 rpm for 2 seconds and after that with 2350 rpm for 60 seconds. Finally, the substrate sintered at 450 °C for 30 min and cooled down very slowly to room temperature. Figure 3.4 shows the FTO substrate after preparation of the first layer.

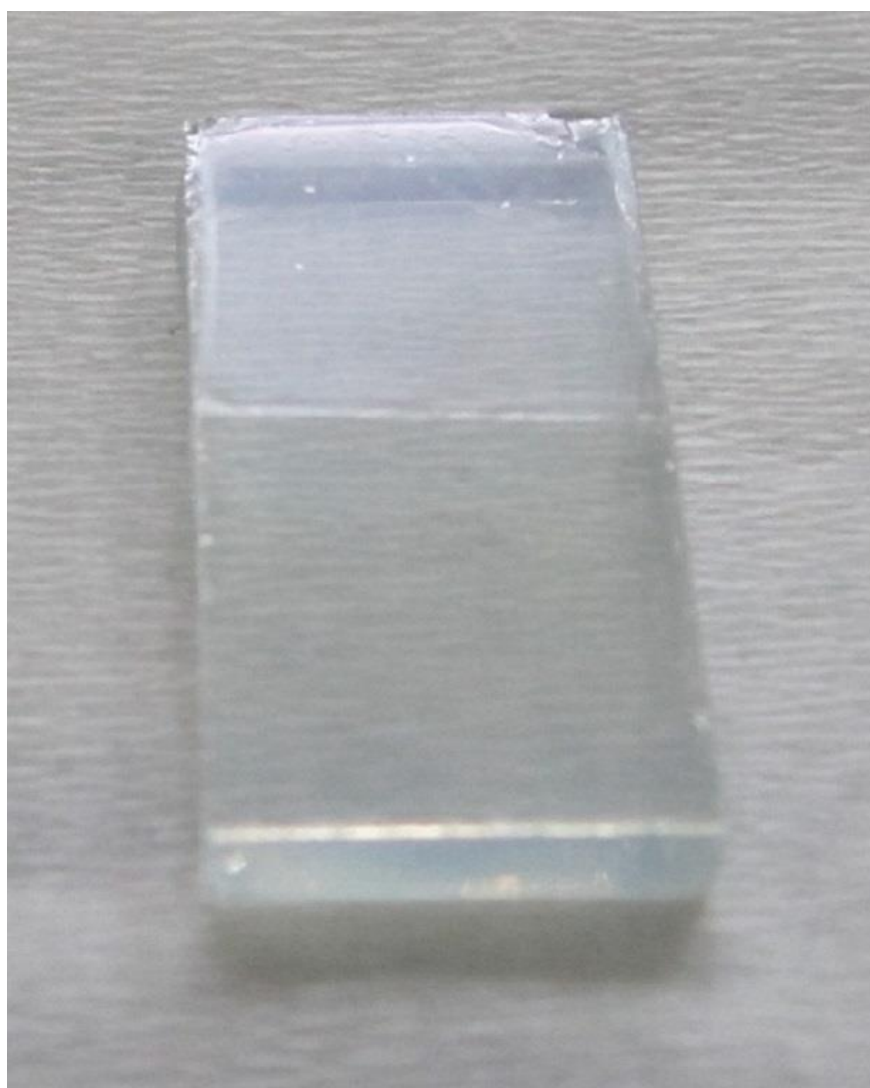


Figure 3.4: The FTO glass after first layer coating (with P90)

3.4.2.2 SECOND LAYER OF PHOTO-ACTIVE ELECTRODE

For the second layer, 0.5 g of TiO₂ (P25) was grounded for 30 minutes with 2 ml HNO₃ (pH=1) in an agate mortar with 1 drop of Triton X-100 and 0.1 g Carbowax and later the solution was doctor bladed on the first layer which the thickness was controlled using magic tape, and then sintered at 450 °C for 30 min. Figure 3.5 demonstrates the prepared photo-anode electrode.

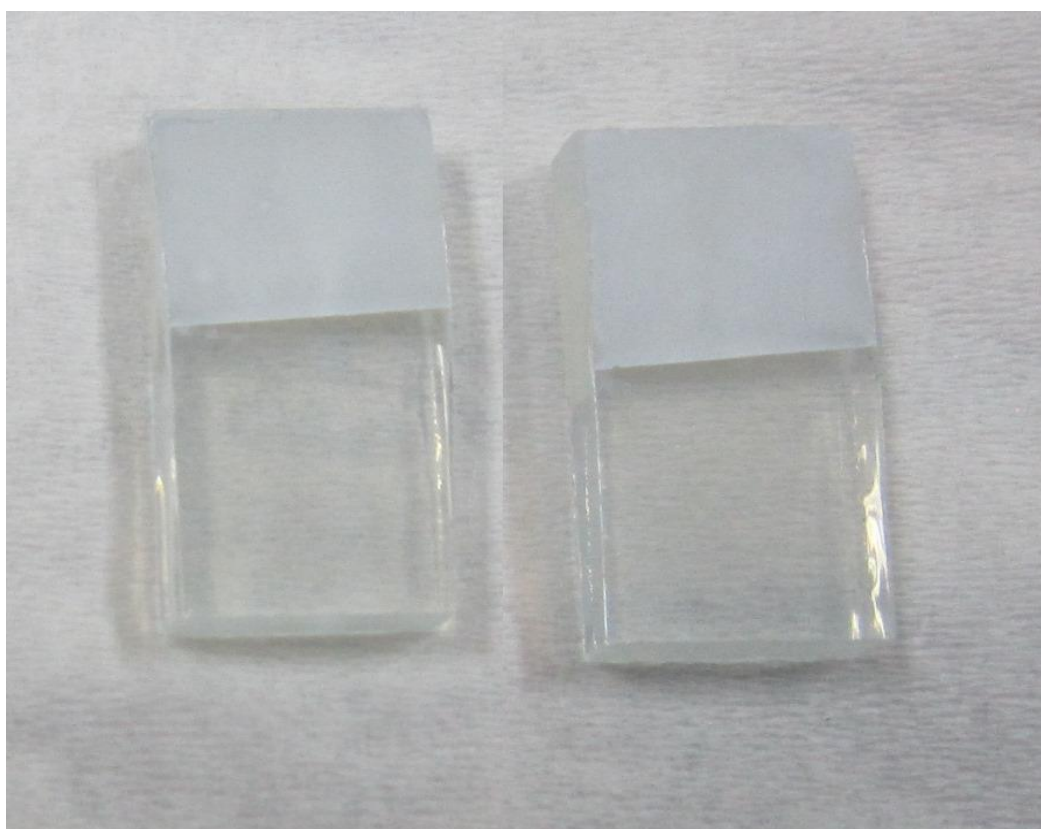


Figure 3.5: The electrode after second layer preparation (with P25)

3.4.2.3 DYE SOLUTION

The solution was prepared to soak the photo-active electrode and trap the dyes inside the very porous second TiO₂ layer. For the dye solution preparation, 5 mg N719 dye powder mixed with 10 ml ethanol and stirred for about 10 minutes without any heating. Finally the prepared photo-anode was soaked in N719 dye solution for 24 hr.

Then the electrodes were used for DSSC fabrication. Figure 3.6 shows the final product of photo-anode electrode after cleaning the conducting parts.

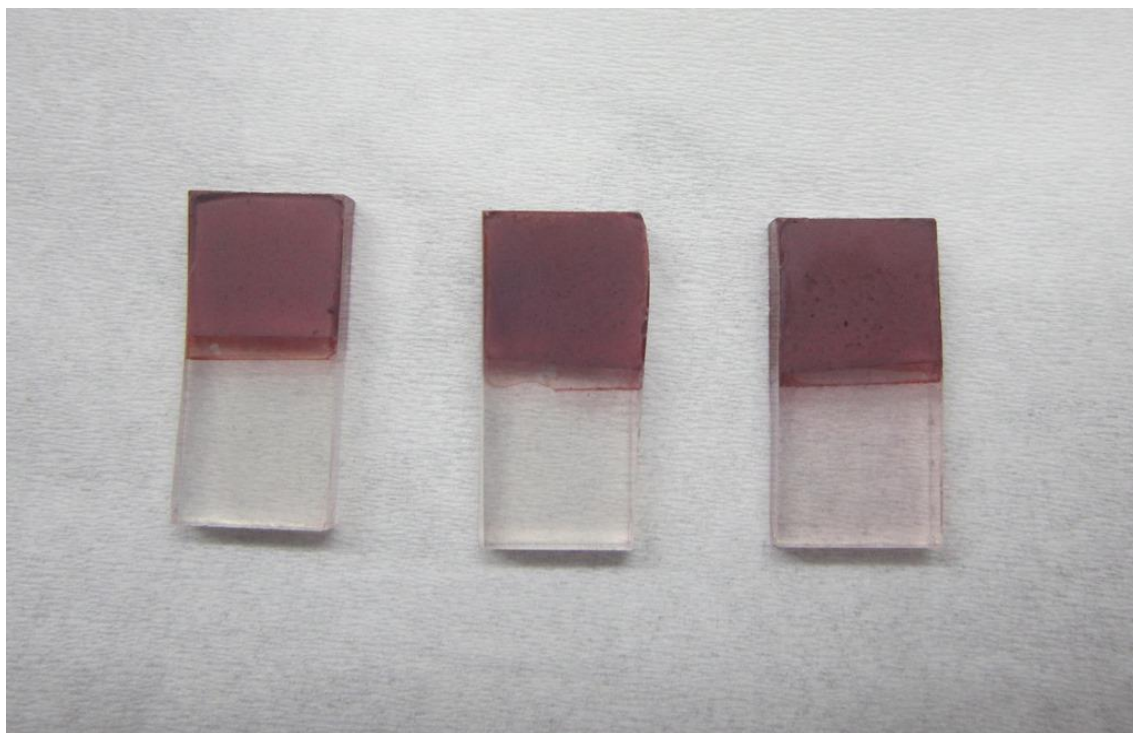


Figure 3.6: Photo-anode electrode after soaking in N719 dye

3.4.3 COUNTER ELECTRODE

The cathode or counter electrode was prepared using commercial platinum solution in three layers. In the first layer, some drops of Pt solution were applied on the FTO surface and spin coated with 1000 rpm for 4 seconds and quickly 2350 rpm for 45 seconds. The coated substrate was sintered at 450 °C for 5 to 10 minutes and cooled down to room temperature.

For second layer preparation, the same procedures as the first layer were repeated. Finally, the third layer was prepared same as first layer but sintered at 450 °C for 30 minutes.

3.4.4 DSSC FABRICATION

Each DSSC was fabricated by using photo-anode electrode, counter electrode and solid polymer electrolyte (SPE). The SPEs were sandwiched between photo-anode and counter electrodes and fixed with a clip. The fabricated DSSC follows the configuration of Glass/FTO/TiO₂(P90)/TiO₂(P25)/N719-Dye/SPE/Pt/FTO/Glass. The prepared DSSCs were analyzed under the Sun simulator. Figure 3.7 exhibits the fabricated DSSC and the setup for the DSSC characterization under the Sun simulator is illustrated in Figure 3.8.



Figure 3.7: The fabricated DSSC

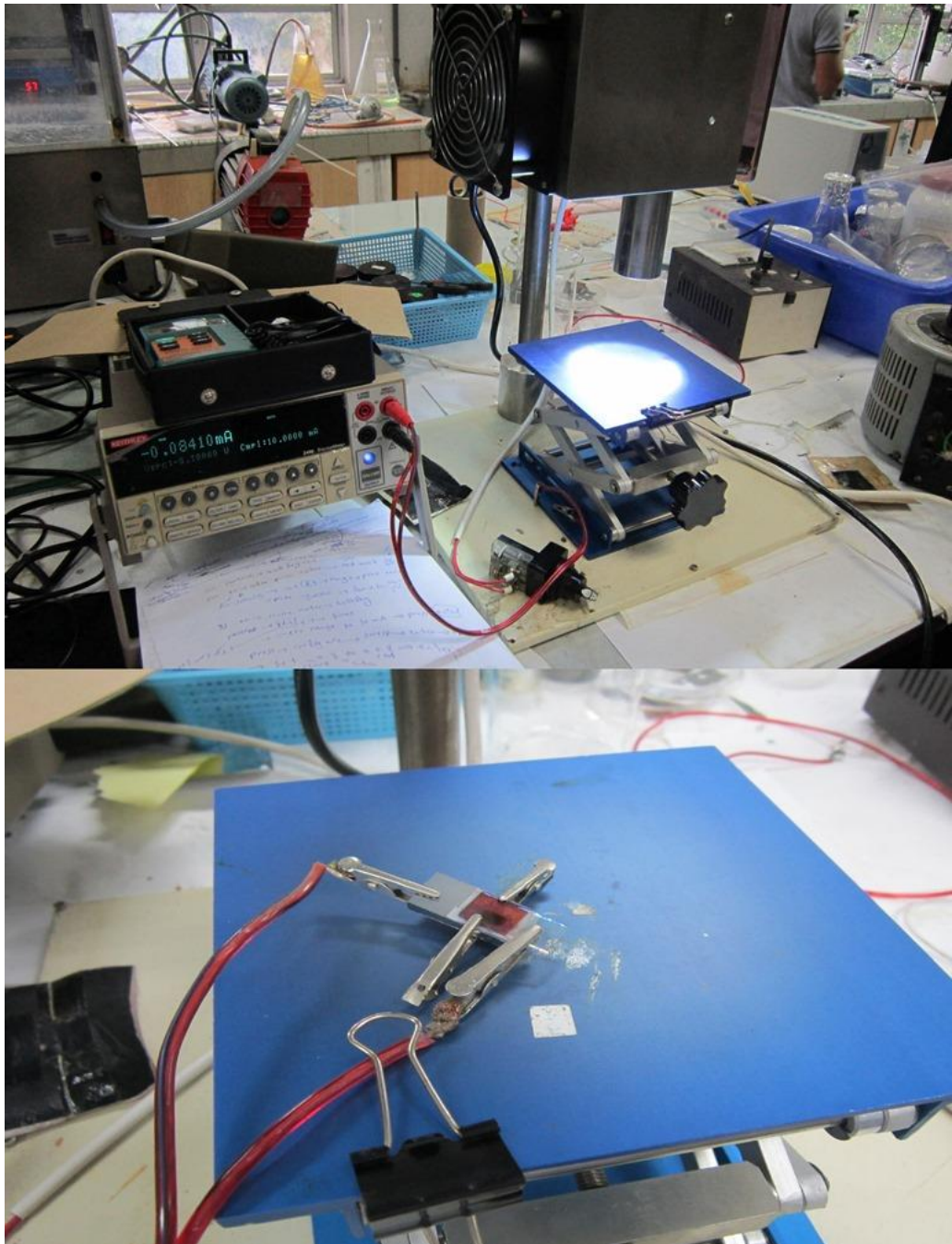


Figure 3.8: The setup for DSSC characterization with Sun simulator

3.5 MEASUREMENT AND CHARACTERIZATION

Several characterization methods were utilized to study the ionic conductivity, structural, thermal and photovoltaic properties and behaviors of SPEs and DSSs. For ionic conductivity studies, the electrochemical impedance spectroscopy (EIS) was used.

Structural properties of SPEs were studied with Fourier transform infrared spectroscopy (FTIR) and X-Ray diffraction (XRD). Thermal behaviors of SPEs were studied using thermogravimetric analysis (TGA) and differential scanning spectroscopy (DSC).

3.5.1 ELECTROCHEMICAL IMPEDANCE SPECTROSCOPY (EIS)

The electrochemical impedance spectroscopy (EIS), also known as dielectric spectroscopy is one of the most popular analytical tools in materials research (Lvovich, 2012) which measures the dielectric parameters of the sample as a function of frequency (Kremer et al., 2003; Volkov et al., 2003). The impedance is a simple concept which can be explained by Ohm's Law ($R=V/I$). The working principle of impedance experiment can be explained in Figure 3.9 (which the sample with electrodes behaves like a capacitor with surface (A) and distance (d). In this case, the polymer electrolyte sample can be sandwiched between two stainless steel electrodes).

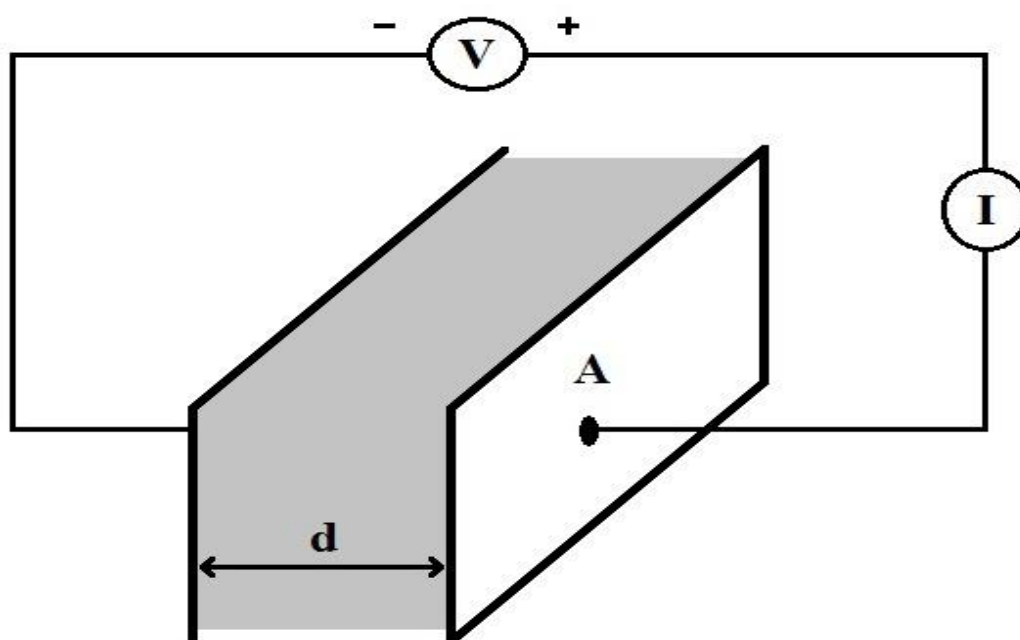


Figure 3.9: Schematic view of an impedance experiment

After applied working voltage (V), the current will pass through the sample and resistance known as bulk resistance (R_b) can be defined as

$$R_b = \rho \frac{d}{A} \quad (3.1)$$

where ρ (ohm.cm) is characteristic resistivity, and inverse of resistivity is conductivity σ ($\text{ohm}^{-1} \text{cm}^{-1}$ or S cm^{-1}). Then the conductivity can be defined as

$$\sigma = \frac{d}{R_b A} \quad (3.2)$$

In the experiments normally the applying voltage is AC voltage; the sinusoidal voltage will be applied. The resulting input voltage with applied frequency will be time dependent in the form of (Blythe, 1979; Volkov et al., 2003)

$$V(t) = V_A \sin(2\pi ft) = V_A \sin(\omega t) \quad (3.3)$$

and

$$I(t) = I_A \sin(\omega t + \phi) \quad (3.4)$$

According to Ohm's Law, the complex impedance will be

$$Z^*(\omega) = \frac{V(t)}{I(t)} = \frac{V_A \sin(\omega t)}{I_A \sin(\omega t + \phi)} = Z_A \frac{\sin(\omega t)}{\sin(\omega t + \phi)} \quad (3.5)$$

where Z_A is magnitude of impedance.

In the electrolyte based systems which electrolytes are sandwiched between two electrodes (sample cell), the electrical circuit (after applying sinusoidal voltage with certain signal) forms double-layer in interfaces between electrode and electrolyte. The double-layer results in polarization according to Figure 3.10. There are two double-layers which act as two capacitors with capacitance C_e . Without considering the double-layer, there is geometrical capacitance (C) formed by electrolyte and electrodes.

Moreover, the bulk resistance of the electrolyte is represented by R (Bandara; et al., 2011).

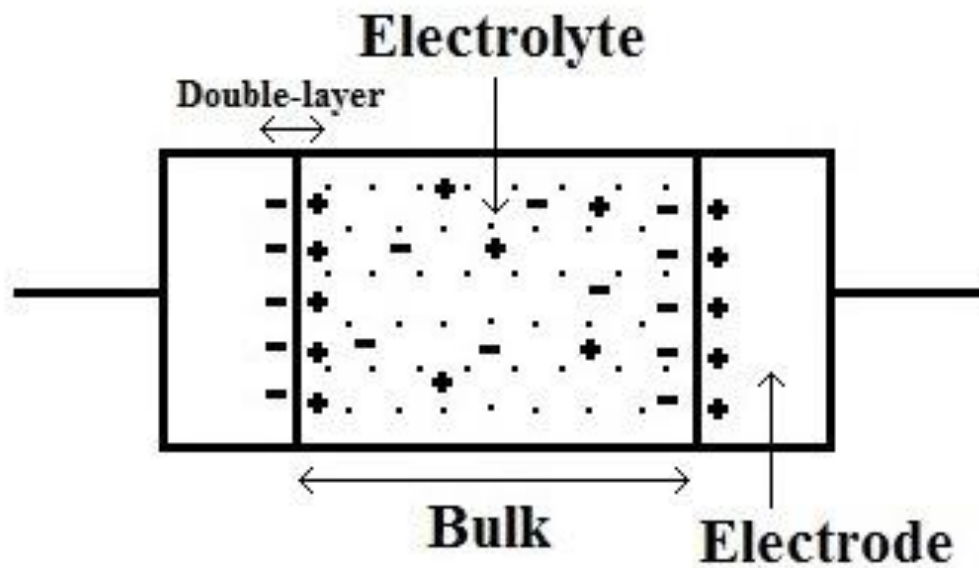


Figure 3.10: Explanation of polarization in sample cell

Consequently, the circuit can be expressed as simple equivalent circuit with schematic view according to Figure 3.11.

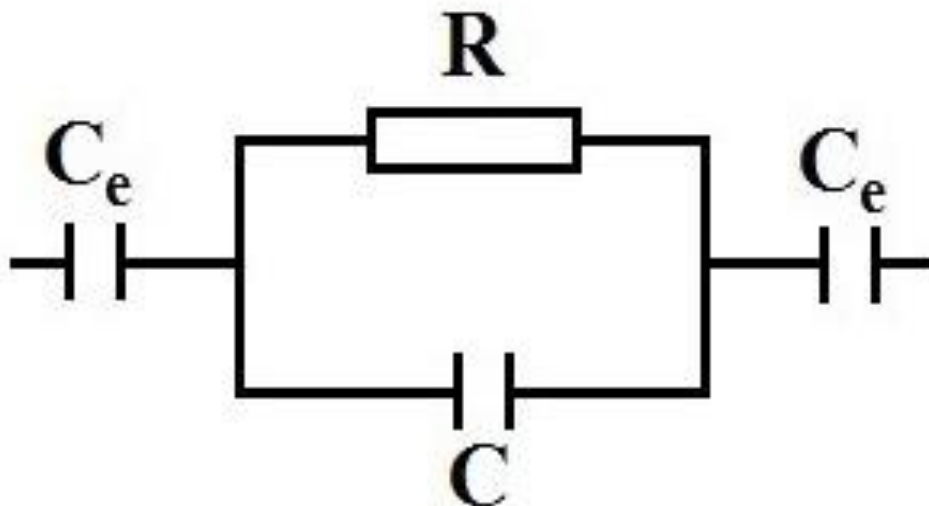


Figure 3.11: Schematic view of equivalent circuit for sample cell

Thus, the total complex impedance of the sample cell can be derived from previous equation as

$$Z^*(\omega) = \frac{R}{1 + j\omega RC} + \frac{2}{j\omega C_e} \quad (3.6)$$

The complex impedance can be expressed as

$$Z^* = Z' + iZ'' \quad (3.7)$$

Therefore, the real and imaginary part of complex impedance will be

$$Z' = \frac{R}{1 + \omega^2 R^2 C^2} \quad (3.8)$$

and

$$Z'' = -\left(\frac{\omega R^2 C}{1 + \omega^2 R^2 C^2} + \frac{2}{\omega C_e} \right) \quad (3.9)$$

One of the other important dielectric parameters is complex permittivity (ε^*). This parameter can be calculated by real and imaginary parts of complex impedance. On the other hand, the real (ε') and imaginary (ε'') parts of complex permittivity ($\varepsilon^* = \varepsilon' + i\varepsilon''$) can be calculated by below equations

$$\varepsilon' = \frac{Z''}{\omega C_0 (Z'^2 + Z''^2)} \quad (3.10)$$

$$\varepsilon'' = \frac{Z'}{\omega C_0 (Z'^2 + Z''^2)} \quad (3.11)$$

where Z' and Z'' are real and imaginary parts of complex impedance. Here $C_0 = \varepsilon_0 A/L$ represents vacuum capacitance related to electrodes and sample configuration, A is surface area of blocking electrodes, L is thickness of sample, and ε_0 is the permittivity of the free space. The real and imaginary parts of permittivity are also known as dielectric constant and dielectric loss, respectively.

Capacitance is another dielectric parameter can be calculated using real and imaginary parts of complex impedance:

$$C' = \frac{-Z''}{\omega(Z'^2 + Z''^2)} \quad (3.12)$$

$$C'' = \frac{Z'}{\omega(Z'^2 + Z''^2)} \quad (3.13)$$

That means

$$C' = -C_0 \varepsilon' \quad (3.14)$$

$$C'' = C_0 \varepsilon'' \quad (3.15)$$

Conductance (G) and susceptance (B) are other dielectric parameters that can be expressed as below

$$G = \frac{Z'}{(Z'^2 + Z''^2)} \quad (3.16)$$

$$B = \frac{-Z''}{(Z'^2 + Z''^2)} \quad (3.17)$$

Furthermore, other important dielectric parameters are modulus (M) and admittance (Y) which defined as

$$M^* = \frac{1}{\varepsilon^*} = j\omega C_0 Z^* \quad (3.18)$$

$$Y^* = \frac{1}{Z^*} = j\omega C_0 \varepsilon^* \quad (3.19)$$

where M^* ($=M_r + iM_i$) and Y^* ($=Y_r + iY_i$) are complex modulus and complex admittance, respectively.

Consequently, Equations 3.18 and 3.19 can be rearranged as

$$M^* = \frac{1}{\varepsilon^*} = \frac{\varepsilon'}{\varepsilon'^2 + \varepsilon''^2} - i \frac{\varepsilon''}{\varepsilon'^2 + \varepsilon''^2} \quad (3.20)$$

$$Y^* = \frac{1}{Z^*} = \frac{Z'}{Z'^2 + Z''^2} - i \frac{Z''}{Z'^2 + Z''^2} = G + iB \quad (3.21)$$

Thus real and imaginary parts of modulus and admittance can be derived from above equations as

$$M_r = \frac{\varepsilon'}{\varepsilon'^2 + \varepsilon''^2} \quad (3.22)$$

$$M_i = \frac{-\varepsilon''}{\varepsilon'^2 + \varepsilon''^2} \quad (3.23)$$

$$Y_r = \frac{Z'}{Z'^2 + Z''^2} \quad (3.24)$$

$$Y_i = \frac{-Z''}{Z'^2 + Z''^2} \quad (3.25)$$

One of the other useful dielectric parameters is loss tangent ($\tan \delta$), which can be obtained from following equation

$$\tan \delta = \frac{\varepsilon''}{\varepsilon'} \quad (3.26)$$

where ε' and ε'' are the real and imaginary parts of complex permittivity. The loss tangent is also known as dielectric constant and dielectric loss respectively.

After introduction of dielectric parameters, the total conductivity can be expressed. The total conductivity is combination of dc conductivity (which explained in Equation 3.2) and ac-conductivity which varies with frequency. Total conductivity can be expressed as (Elliott, 1987; Mott; et al., 1979):

$$\sigma(\omega) = \sigma_{dc} + \sigma_{ac} = \sigma_{dc} + A\omega^s \quad (3.27)$$

and

$$\sigma_{ac} = A\omega^s \quad (3.28)$$

where A is a parameter dependent on temperature and s is the frequency exponent (<1).

To calculate ac-conductivity, parameter s should be calculated. On the other hand, for ac- conductivity another equation is expressed as

$$\sigma_{ac} = \omega \varepsilon_0 \varepsilon' \tan \delta \quad (3.29)$$

Substituting Equation (3.26) for $\tan \delta$ in Equation (3.29) results in

$$\sigma_{ac} = \varepsilon_0 \varepsilon'' \omega \quad (3.30)$$

Finally, using Equations (3.28) and (3.30)

$$\varepsilon_0 \varepsilon'' \omega = A\omega^s \quad (3.31)$$

Hence

$$\varepsilon'' = \frac{A}{\varepsilon_0} \omega^{s-1} \quad (3.32)$$

This can be written as

$$\ln \varepsilon'' = \ln \frac{A}{\varepsilon_0} + (s-1) \ln \omega \quad (3.33)$$

The above equations can be rearranged as a simple formula for ac-conductivity:

$$\sigma_{ac} = \varepsilon_0 \varepsilon'' \omega = \omega \varepsilon_0 \left[\frac{Z'}{Z'^2 + Z''^2} \right] \times \left(\frac{t}{A\omega \varepsilon_0} \right) = \left[\frac{Z'}{Z'^2 + Z''^2} \right] \times \left(\frac{t}{A} \right) \quad (3.34)$$

In the EIS study, the ionic transport mechanism is very important to figure out. The mechanism for polymer electrolytes can be expressed by the Rice and Roth (Rice et al., 1972) model.

This model shows the ionic conductivity of mobile ions has relation with some other transport parameters as

$$\sigma = \frac{2}{3} \left[\frac{(Ze)^2}{kTm} \right] n E_a \tau_0 \exp\left(\frac{-E_a}{kT}\right) \quad (3.35)$$

where Ze denotes the charge carried by an ion belonging to the conducting species which Z is valency of ion, k is Boltzmann constant, m is mass of ionic carrier, n is the number density of mobile ions, τ_0 is the free ion life-time. τ_0 can be obtained from the mean free pass relation expressed by ($\ell = v\tau_0$), v is velocity of the free ions ($= \sqrt{2E/m}$).

The transport parameters such as mobility (μ) and diffusion coefficient (D) can be obtained from relationship between mobility and conductivity, and from Einstein relation with determinate value of n and σ as expressed below:

$$\mu = \frac{\sigma}{ne} \quad (3.36)$$

and

$$D = \frac{kT\sigma}{ne^2} \quad (3.37)$$

where e is electronic charge.

Another transport parameter which can be obtained by EIS results is the number of transitions per unit time, $P(E)$, which is denoted by equation below (Rice et al., 1972):

$$P(E) = \frac{1}{\tau_0} \exp\left(\frac{-E_a}{kT}\right) \quad (3.38)$$

where τ_0 is free ion life-time and E_a is activation energy.

3.5.1.1 IONIC CONDUCTIVITY MEASUREMENT

For the electrolyte and electrode cell, the previous equation for conductivity can be expressed as equation bellow

$$\sigma = \frac{L}{R_b A} \quad (3.39)$$

where σ is in $S\text{ cm}^{-1}$, L and A are the thickness of sample and area of blocking electrodes, respectively.

In the EIS experiment the results from frequency-dependent complex impedance can be used to draw Cole-Cole plots to represent real and imaginary parts of complex impedance to determine the bulk resistance.

The schematic view of Cole-Cole plot using EIS results is represented in Figure 3.12. According to Figure 3.12, the bulk resistance (R_b) can be measured, and with measuring the thickness of the sample with area of the electrode, the ionic conductivity using Equation (3.39) can be obtained.

In this work, the ionic conductivity studies were carried out using electrochemical impedance spectroscopy (EIS) analyser, Hioki, 3532-50 LCR HiTESTER. The measurements were collected in frequency range of 50 Hz to 5 MHz. The samples were sandwiched between two stainless steel blocking electrodes with area of 2.98 cm^2 . Imaginary parts of impedance were automatically computed with LCR HiTESTER. Cole-Cole plots were used to determine bulk resistance (R_b) to calculate ionic conductivity (σ) using Equation (3.39). Thickness of the samples was measured using Mitutoyo digital gauge.

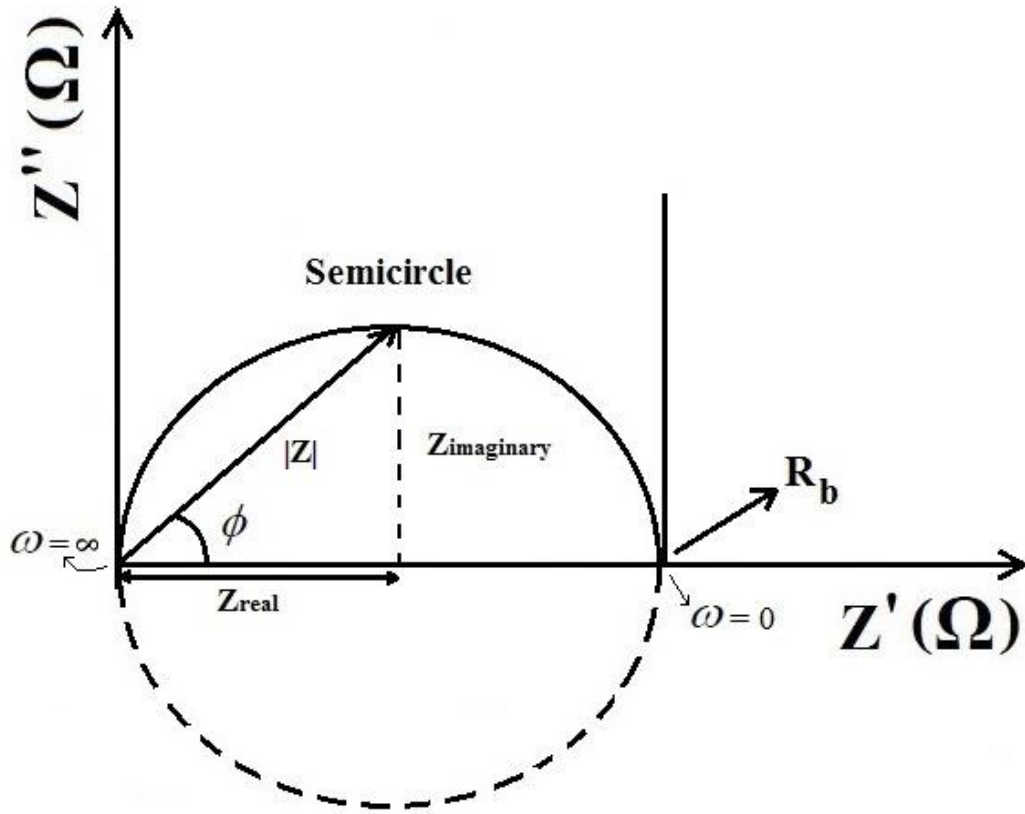


Figure 3.12: Schematic view of Cole-Cole plot

3.5.1.2 TEMPERATURE-DEPENDENT STUDY

The temperature-dependant ionic conductivity study helps the researchers to find out the investigated electrolyte system follows which model. Two major models for polymer electrolytes are Arrhenius and Vogel-Tammann-Fulcher (VTF) models (Bandara et al., 2012). Arrhenius thermal activated model which expresses the relation between conductivity and temperature as

$$\sigma = \sigma_0 \exp\left[\frac{-E_a}{kT}\right] \quad (3.40)$$

where T is temperature σ_0 is pre-exponential factor, E_a is activation energy and k is Boltzmann constant (eV/K).

Activation energy (eV) can be acquired from Equation (3.40). Normally activation energy can be calculated from logarithmic scale of ionic conductivity vs 1000/T plot where the σ unit is S cm^{-1} and temperature unit is in Kelvin.

In the VTF model, the behavior of the sample should be fitted in the VTF equation mentioned below

$$\sigma T^{1/2} = A \exp\left(\frac{-E_a}{K_B(T - T_0)}\right) \quad (3.41)$$

where T is the temperature, A is pre-exponential factor, T_0 is reference temperature related to glass transition temperature (T_g) (Y.-J. Wang et al., 2006).

In this work, the temperature-dependent behaviors of SPEs were studied using EIS analyzer (Hioki, 3532-50) with the forced convection oven (YIHDER-DK-500) between temperatures 30 to 100 °C. As all the SPEs follow Arrhenius thermal activated model, the activation energies were calculated using this model.

3.5.2 FOURIER TRANSFORM INFRARED SPECTROSCOPY (FTIR)

The infrared based spectroscopy has valuable information in determining the molecular structures. The information deduced from infrared spectrometers is complementary to that of other methods (Griffiths; et al., 2007). The infrared spectroscopy is based on vibration modes of molecules caused by infrared radiation. In infrared based spectroscopy, absorbed infrared spectrum of a material by passing infrared radiation through the sample is collected. The collected spectrum determines which fraction of infrared radiation is absorbed in each frequency. The frequency at each peak in absorption spectrum is equal to the frequency of the normal modes of vibration from the molecules of the sample. Normally, there are two types of infrared based spectroscopy to study polymers, dispersive and Fourier-transform instruments.

In dispersive instruments the infrared radiation is split into its constituent wavelengths by a monochromator. In the Fourier-transform instrument the infrared radiation for all wavelengths passes through the sample to the detector simultaneously. The detector measures the total transmitted intensity as a function of the displacement of one of the mirrors in a double-beam interferometer like Michelson interferometer. Finally, the separation of the wavelengths is done by performing mathematically Fourier transform on the intensity versus displacement data (Bower, 2002).

The FTIR analysis of polymer electrolytes is important factor to monitor polymer and salt complexation, ion-ion and ion-polymer interactions as a function of salt concentration (Selvasekarapandian et al., 2006). In this work, structural properties were analyzed using FTIR spectrometer (Thermo Scientific, Nicolet iS10). The wavenumbers region was between 4000 and 400 cm^{-1} with 2 cm^{-1} resolution. Nitrogen gas was used to blank FTIR in order to remove CO_2 and water from environment. Infrared spectra of samples were collected after background collection.

3.5.3 X-RAY DIFFRACTION (XRD)

X-rays are electromagnetic radiations with wavelength in the range of 10^{-9} to 10^{-11} m. The name X was given by Roentgen who accidentally discovered it in 1895 amid his uncertainty about its wave or corpuscular nature. As an electromagnetic radiation, X-rays travel in free space at the speed of light (3.00×10^8 m/s). Both X-rays and light affect photographic plates. But compare with the light, X-rays are more energetic than light, therefore it can penetrate solid object several centimeter thick while light cannot pass through opaque object as thin as ordinary paper. Light causes visual sensation to human eye while X-rays are invisible to human eye. Given the right conditions, both light and X-rays undergo reflection and diffraction.

Light undergoes refraction in transparent media while X-rays penetrate through the media without being refracted. The refractive index of X-rays in transparent media is equal to 1.

Normally, X-rays can be produced by any of the following ways:

- Bombarding a solid target usually made from high melting point metal such as tungsten and copper, with a beam of energetic electrons whereby the incident electrons knock off one of the inner shell electrons from the target atoms and resulting in the formation of a vacant electron site in the inner shell. An electron from an outer orbit fills the vacant site and releasing its excess energy in the form of X-ray photon.
- Decelerating a beam of electron by mean of an electromagnetic field; this cause the electron excess energy to be released in the form of X-rays photons.

The X-Ray diffractometer is an instrument to identify atomic and molecular structure of each sample. In the X-ray diffractometer, the energetic X-ray radiations is forwarded to the sample and reflected beams are collected and analyzed according to Figure 3.13 to determine the structure of the sample which follow the Bragg's law relation as stated below

$$2d \sin \theta = n\lambda \quad (3.42)$$

where d is spacing distance between atomic planes, θ is the incident angle, n is an integer and λ is the wavelength.

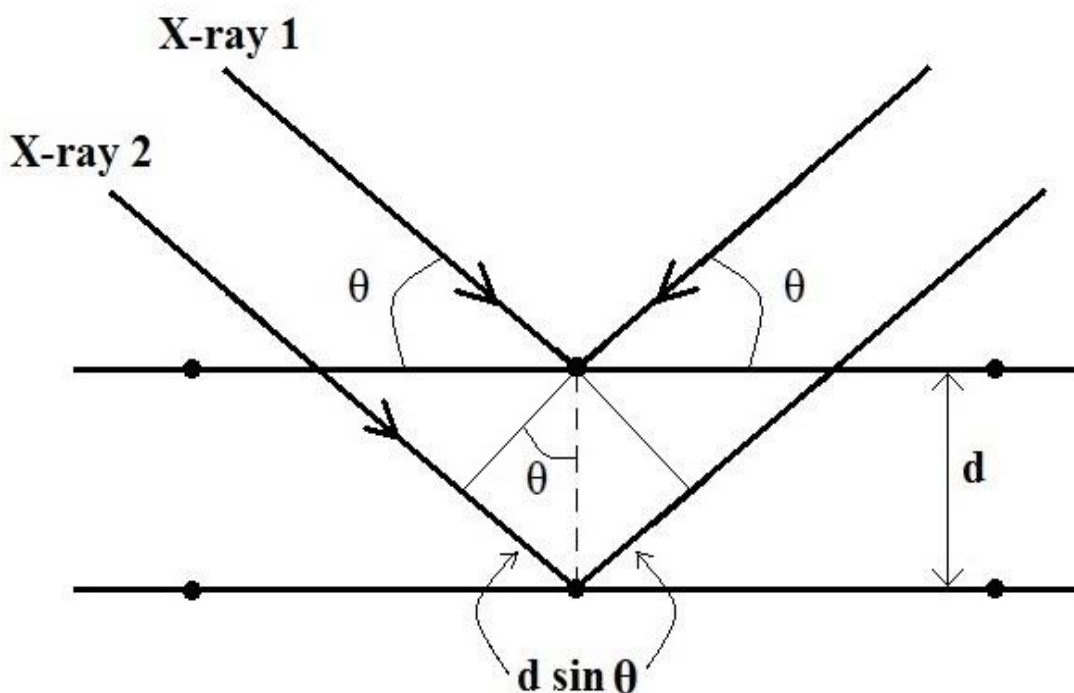


Figure 3.13: Schematic view for working principle of X-ray diffractometer

The XRD is used for structural studies to determine some properties of samples such as crystal structure, crystallinity, amorphous nature and molecular orientation. In this work XRD patterns of samples were recorded with XRD Siemens D 5000 diffractometer (40 kV, 40 mA) with Cu-K α radiation and wavelength of $\lambda=1.540600 \text{ \AA}$ for 2θ range of $5-80^\circ$ at ambient temperature.

3.5.4 THERMOGRAVIMETRIC ANALYSIS (TGA)

One of the thermal analysis methods is characterized by thermogravimetric analysis (TGA) which is based on weight changes of the sample versus temperature. On the other hand TGA is an experimental technique which weight of the sample is measured as a function of sample temperature or time. The sample is typically heated at a constant heating rate. To measure the weight change, the TGA instrument has a thermobalance.

To make the stable media and reduce the moisture, gas should flow during the experiment. Moreover, due to the density changes of gas, buoyancy corrections must be made in TGA measurements. Without buoyancy corrections sample will appear to show a mass increase during a heating experiment. TGA measurements are usually corrected for the effect of buoyancy by performing a blank (without a sample) measurement (Bottom, 2008). The temperature dependence of density at constant pressure can be expressed as

$$\rho = \rho_0 \frac{T_0}{T} \quad (3.43)$$

where ρ_0 is the density of the gas at the reference temperature T_0 which is normally room temperature (~ 25 °C) and T is the temperature in kelvin. For sample preparation the sample should be placed in a crucible. Normally, a sudden drop in weight change at a certain temperature shows the decomposition temperature of the sample.

In this work, the SPE samples were analyzed for thermogravimetric analysis (TGA) with TA Instrument Universal Analyzer TGA Q500. The Nitrogen flow rate for balance gas and sample gas were 40 and 60 ml/min, respectively. The samples were heated with ramping rate of 50 °C/min from 4 to 700 °C to obtain decomposition temperature (T_{dc}).

3.5.5 DIFFERENTIAL SCANNING CALORIMETRY (DSC)

A very important thermal technique to study on materials is differential scanning calorimetry (DSC). DSC has been used in many wide ranges of thermal studies of materials including polymers and plastics, foods and pharmaceuticals, glasses and ceramics, proteins and life science materials (Gabbott, 2008).

A DSC analyzer measures the energy changes when a sample is heated, cooled or held isothermally, together with the temperature at which these changes occur.

The DSC study allows measuring some important thermal parameters such as heat flow, specific heat (C_p), glass transition temperature (T_g) and enthalpy. There are two holders of crucible. The sample should be placed in one crucible same as TGA instruments. Consequently, a similar empty crucible (without sample) is placed as reference in the second holder. The temperature applies to two holders and is changed at the constant rate of $dT/dt (= \dot{T})$, while the two holders are ideally maintained at the same temperature by a feedback loop. Moreover, an extra energy Q must be supplied to the sample holder at a rate dQ/dt to maintain its temperature the same as that of the reference holder. The rate (dQ/dt) is registered by the instrument and plotted either against T or against time t (Bower, 2002). The plotted results in heat and cool processes will be used to measure some important parameters especially glass transition temperature (T_g), melting point and crystallization temperature. Normally, the temperature where a small gap in heat flow vs temperature results appears is known as glass transition temperature, which is the temperature assigned to a region above which amorphous (non-crystalline) materials are fluid or rubbery and below which they are immobile and rigid, simply frozen in a disordered, non-crystalline state. To avoid moisture and instability condition during the experiment, nitrogen gas should flow through the sample and reference holders (Gabbott, 2008).

Polymer electrolyte samples were analyzed for DSC using TA Instrument Universal Analyzer DSC Q2000 with refrigerated cooling system (RCS90). The experiment was performed under nitrogen flow rate of 50 ml/min. Samples followed the range of 3-5 mg weight and were sealed in the Tzero aluminum hermetic pan. The samples were analyzed in heat-cool-heat process within 4 cycles with heating and cooling rate of 10 °C/min. At first, the system was equilibrated at 105 °C for 2 min for isothermal purposes and equilibrated at -80 °C for cycle 1.

In cycle 2, the rate of 10 °C/min was applied from -80 °C to 200 °C. In cycle 3, this procedure applied to -80 °C from the previous cycle. Finally, in cycle 4 this process applied to 200 °C.

3.5.6 CURRENT-VOLTAGE (J-V) CHARACTERIZATION

Generally, the dye-sensitized solar cells (DSSCs) are examined after fabrication under Sun simulators. The light from Sun simulator received by DSSC will excited the cell (as explained in chapter 2) and the cell produces the electricity. The results of current and voltage collected from cell and current or current density vs voltage is used to study the characteristic parameters of cell and finally to measure the energy conversion efficiency of the cell. Figure 3.14 shows typical graph of current density versus voltage.

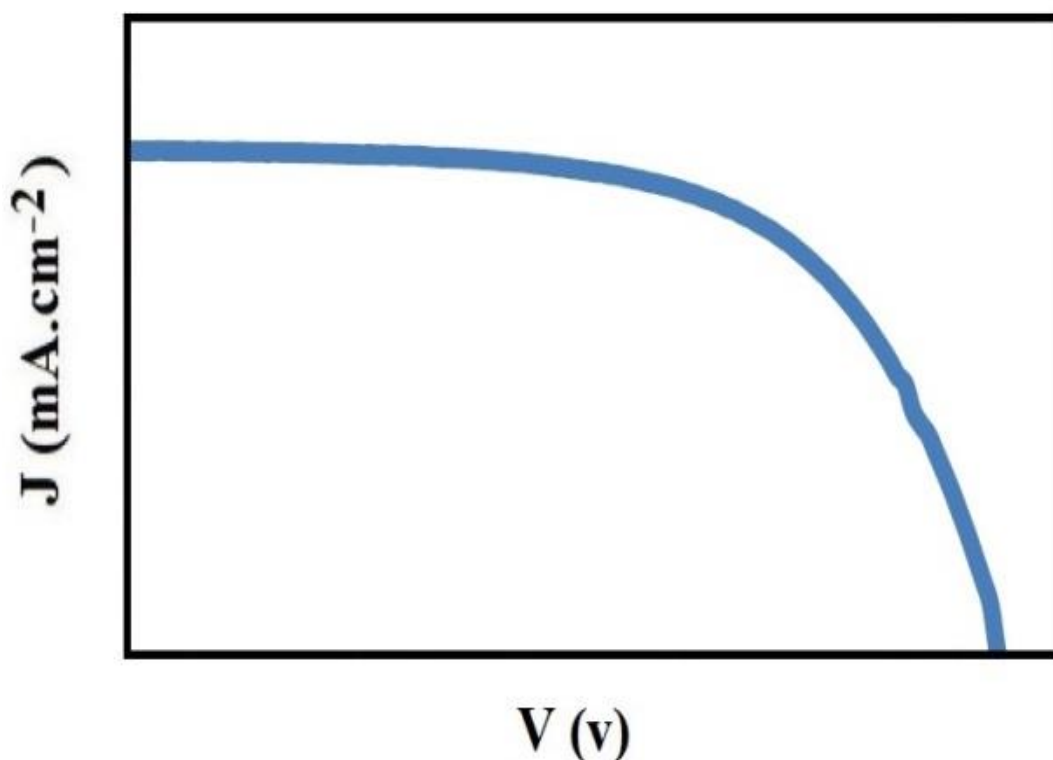


Figure 3.14: Typical graph for current density vs voltage

One important factor to measure the efficiency is fill factor (FF). The fill factor of a solar cell is the ratio of the maximum power output ($V_{\max} \times J_{\max}$) versus its 'dummy' power output ($V_{oc} \times J_{sc}$). The FF is a key parameter in evaluating the performance of solar cells. Normally, the fill factor is between 0 and 1, and defined by (Nelson, 2003):

$$FF = \frac{J_{\max} V_{\max}}{J_{sc} V_{oc}} \quad (3.44)$$

where J_{\max} (mA cm^{-2}) and V_{\max} (V) are the current density and voltage at maximum power output, and J_{sc} (mA cm^{-2}) and V_{oc} (V) are short-circuit current density and open-circuit voltage. Furthermore, the efficiency (η) can be calculated using below equation (Hagfeldt et al., 2010):

$$\eta = \frac{J_{sc} \cdot V_{oc} \cdot FF}{P_{in}} \quad (3.45)$$

where P_{in} is incident light power in mW/cm^2 unit. The 100 mW/cm^2 is applied for analyzed DSSCs under Sun simulator.

In this work, the DSSCs were analyzed to measure J-V curve under Sun simulator (white light illumination of 1000 W m^{-2} defined as incident light power, P_{in}) with Keithley 2400 electrometer. Active area was fixed at 0.25 cm^2 .

3.6 SUMMARY

The experimental methods including SPE preparations, DSSC fabrication and related characterizations are discussed in this chapter. The results and discussions will be expressed in the following chapter for systems based on iodide salts.

CHAPTER 4

RESULTS AND DISCUSSION ON SYSTEMS BASED ON THREE DIFFERENT IODIDE SALTS

4.1 INTRODUCTION

The SPEs in the RS:LiI, RS:NH₄I and RS:NaI systems based on LiI, NH₄I and NaI iodide salts were analyzed using different characterizations of EIS, FTIR, XRD, TGA and DSC, and DSSC characterization for RNa-9 in RS:NaI system were discussed in this chapter. The pure rice starch, designated as RS-0. The solid polymer electrolytes (SPEs) in RS:LiI system are RS-1, RS-2, RS-3, RS-4, RS-5, RS-6 and RS-7. The SPEs in RS:NH₄I system are RN-1, RN-2, RN-3, RN-4, RN-5, RN-6, RN-7, RN-8 and RN-9. The SPEs in RS:NaI system are RNa-1, RNa-2, RNa-3, RNa-4, RNa-5, RNa-6, RNa-7, RNa-8 and RNa-9.

4.2 EIS CHARACTERIZATION

The SPEs were examined using EIS to study the ionic conductivity of SPEs based on LiI, NH₄I and NaI iodide salts, and discussed in two sections: ionic conductivity and temperature-dependent ionic conductivity study in sections 4.2.1 and 4.2.2, respectively.

4.2.1 IONIC CONDUCTIVITY

The ionic conductivity was measured for pure rice starch (RS-0), and for SPEs in RS:LiI system namely RS-1, RS-2, RS-3, RS-4, RS-5, RS-6 and RS-7 with the composition expressed in Table 4.1. Sample preparation in this system above the 35 wt. % LiI was not applicable as the SPE was difficult to cast, very sticky and not easy to handle. The Figure 4.1 demonstrates the Cole-Cole plot for pure rice starch (RS-0) which exhibits a big bulk resistance (R_b) and low ionic conductivity which behave like an insulator.

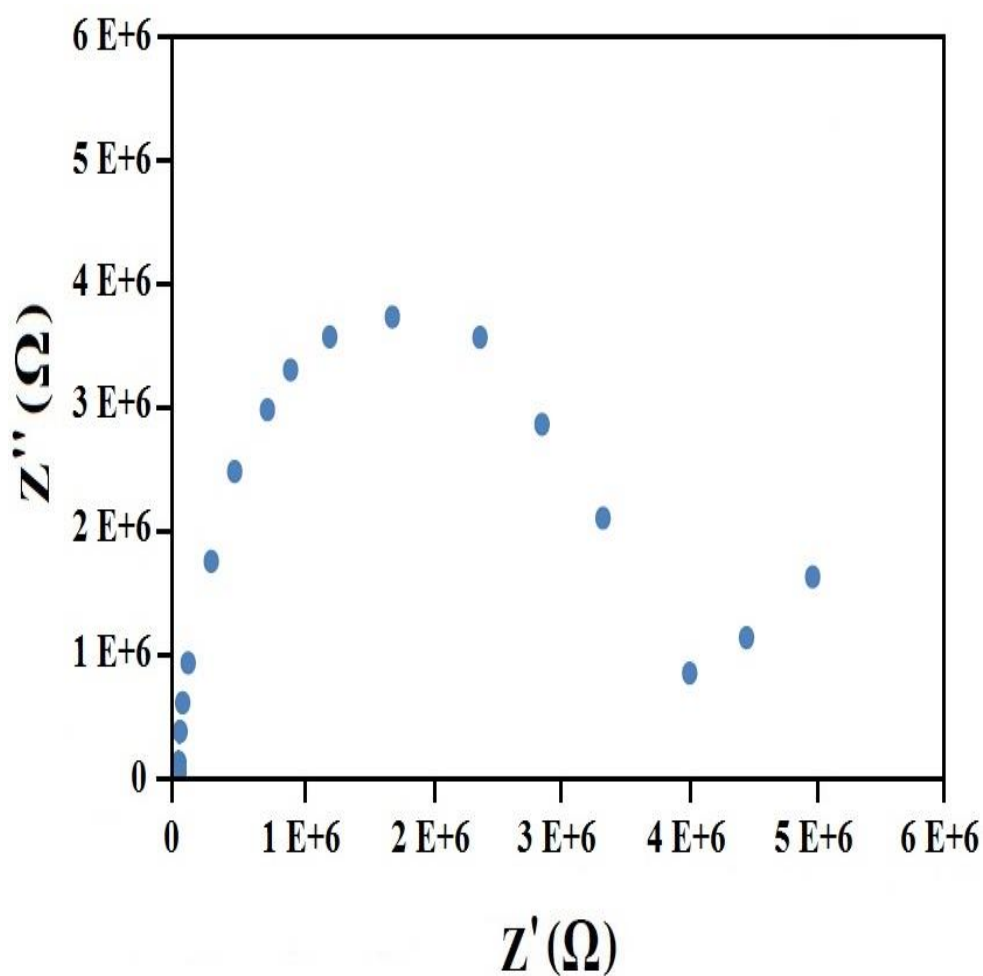


Figure 4.1: Cole-Cole plot of pure rice starch (RS-0)

Figure 4.2 shows the Cole-Cole plots of RS:LiI system for (a) RS-1, (b) RS-2, (c) RS-3, (d) RS-4, (e) RS-5 and (f) RS-6. R_b values have been obtained for samples with different LiI salt ratios. Average thickness of samples is 0.0107 cm for RS:LiI system.

Table 4.1: Bulk resistances in RS:LiI system

Designation	RS:LiI (wt.%)	Bulk resistance, $R_b (\Omega)$
RS-0	100:0	4.00×10^6
RS-1	95:5	3.14×10^5
RS-2	90:10	9.57×10^4
RS-3	85:15	2.26×10^5
RS-4	80:20	1.43×10^4
RS-5	75:25	1.03×10^3
RS-6	70:30	9.81×10^2
RS-7	65:35	9.60×10^1

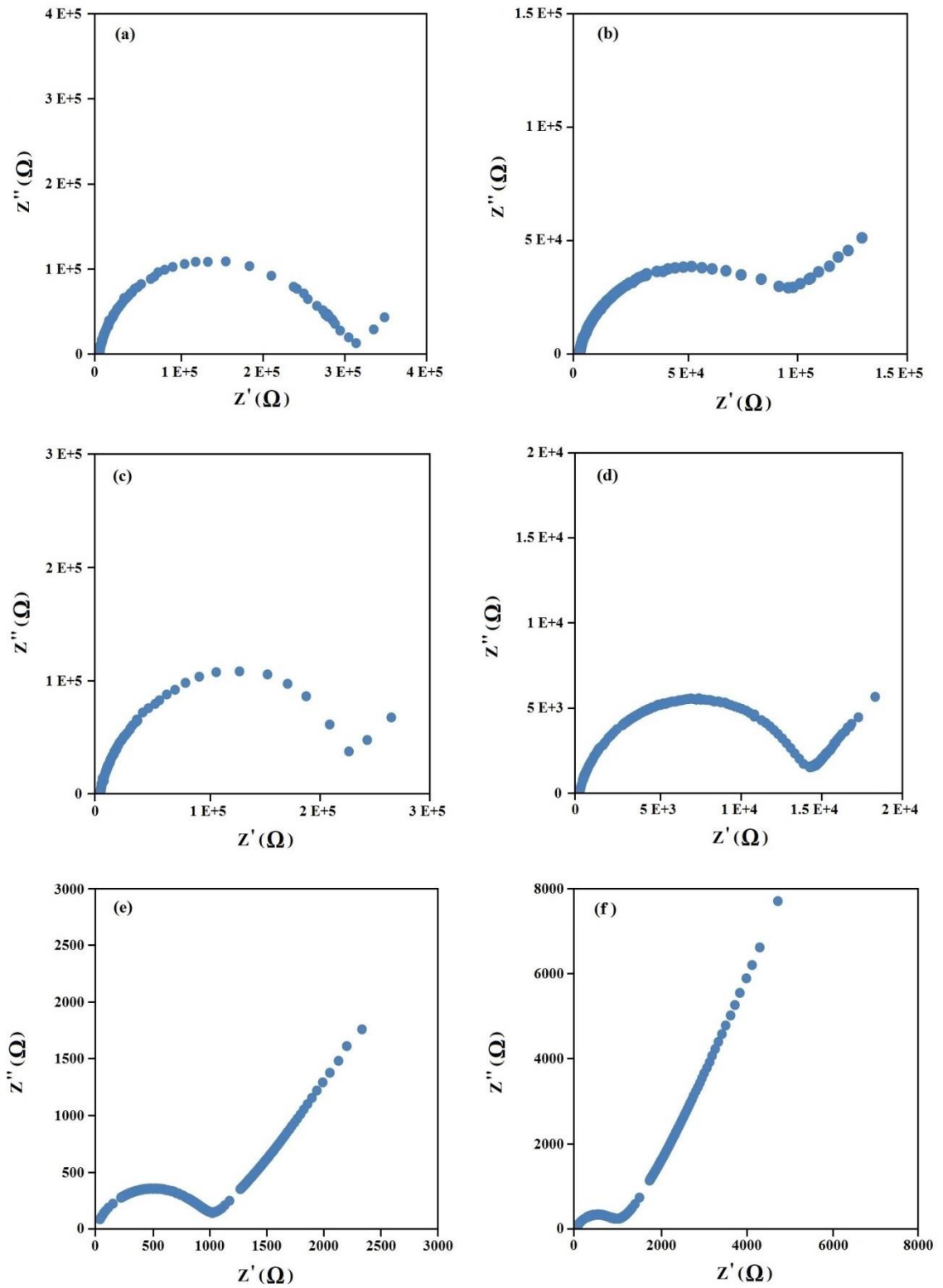


Figure 4.2: Cole-Cole plot of system 1 (RS:LiI) for (a) RS-1, (b) RS-2, (c) RS-3, (d) RS-4, (e) RS-5 and (f) RS-6

The RS-7 sample has achieved the highest ionic conductivity in RS:LiI system according to Cole-Cole plot demonstrated in Figure 4.3.

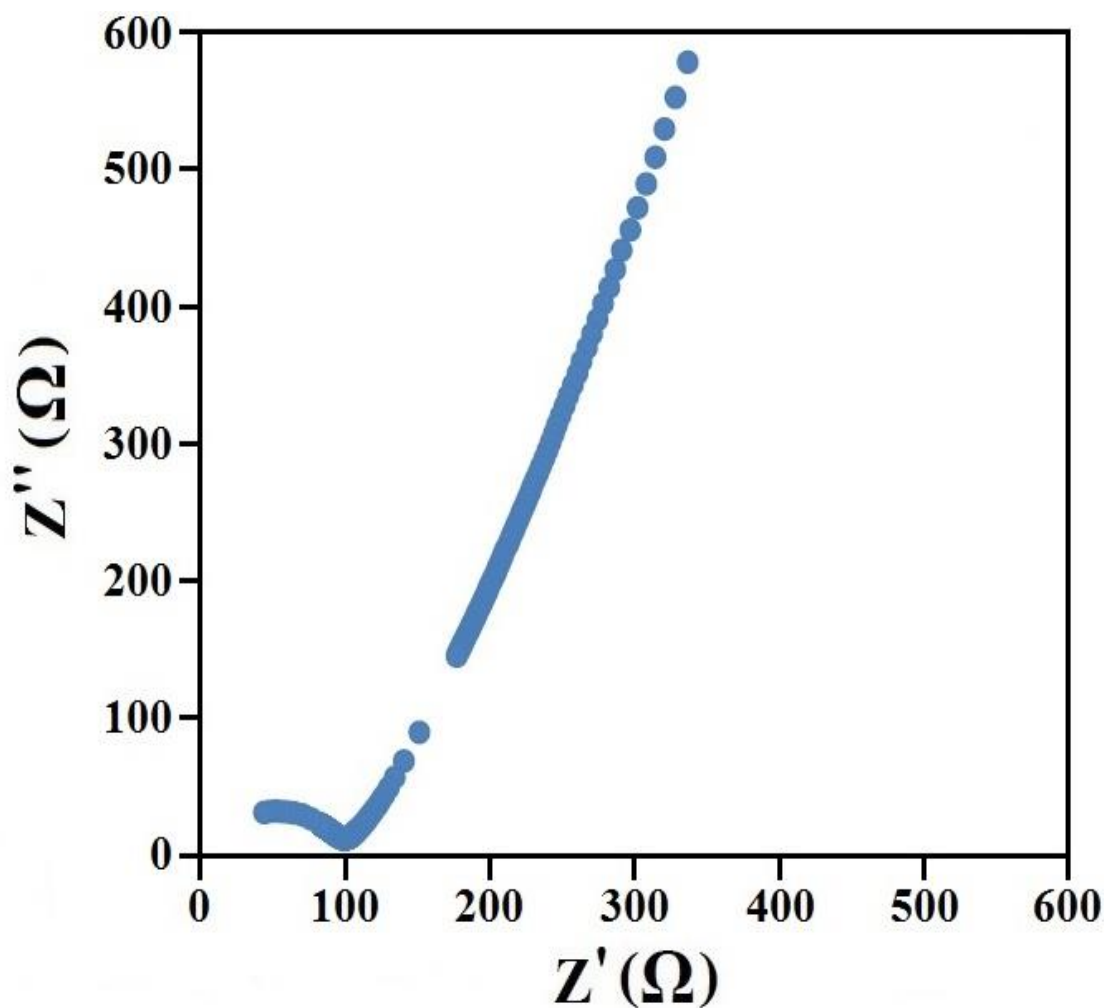


Figure 4.3: Cole-Cole plot for RS-7 with 35 wt.% of LiI

The bulk resistance for all SPEs in RS:LiI system is shown in Table 4.1. It is found that the lowest R_b is achieved in RS-7 with 35 wt.% LiI.

The ionic conductivity for each SPE determined using Equation (3.39) and EIS data. Table 4.2 exhibits the ionic conductivities measured for all SPEs in RS:LiI system.

Table 4.2: Designation and ionic conductivity in RS:LiI system.

Designation	RS:LiI (wt.%) Composition	Conductivity, σ (S cm ⁻¹)
RS-0	100:0	6.87×10^{-10}
RS-1	95:5	1.87×10^{-8}
RS-2	90:10	3.33×10^{-8}
RS-3	85:15	1.66×10^{-8}
RS-4	80:20	1.59×10^{-7}
RS-5	75:25	2.47×10^{-6}
RS-6	70:30	3.83×10^{-6}
RS-7	65:35	4.68×10^{-5}

Figure 4.4 illustrates the variation of ionic conductivity with different LiI content. Figure 4.4 shows increase in the ionic conductivity with the addition of LiI salt. Ionic conductivity after addition of more than 15 wt.% of LiI increases dramatically until 35 wt.% LiI.

According to Table 4.2 the highest achieved ionic conductivity is 4.68×10^{-5} S cm⁻¹ for RS-7 SPE with 35 wt.% of LiI at room temperature. In this work, dependence of ionic conductivity on lithium iodide concentration reveals effect of lithium iodide salt on conductivity after interaction with polymer.

According to Figure 4.4, it is confirmed that LiI content has direct effect on conductivity, which sharp increase the ionic conductivity in higher salt content. The reason is the number of Li⁺ mobile ions in LiI salt as charge carriers. Increase in salt concentration, increases the number of Li⁺ mobile ions. Figure 4.4 shows a drop in ionic conductivity from 10 wt.% to 15 wt.% LiI. This is due to aggregation and accumulation of free ions in the polymer electrolyte preparation (Ren et al., 2014).

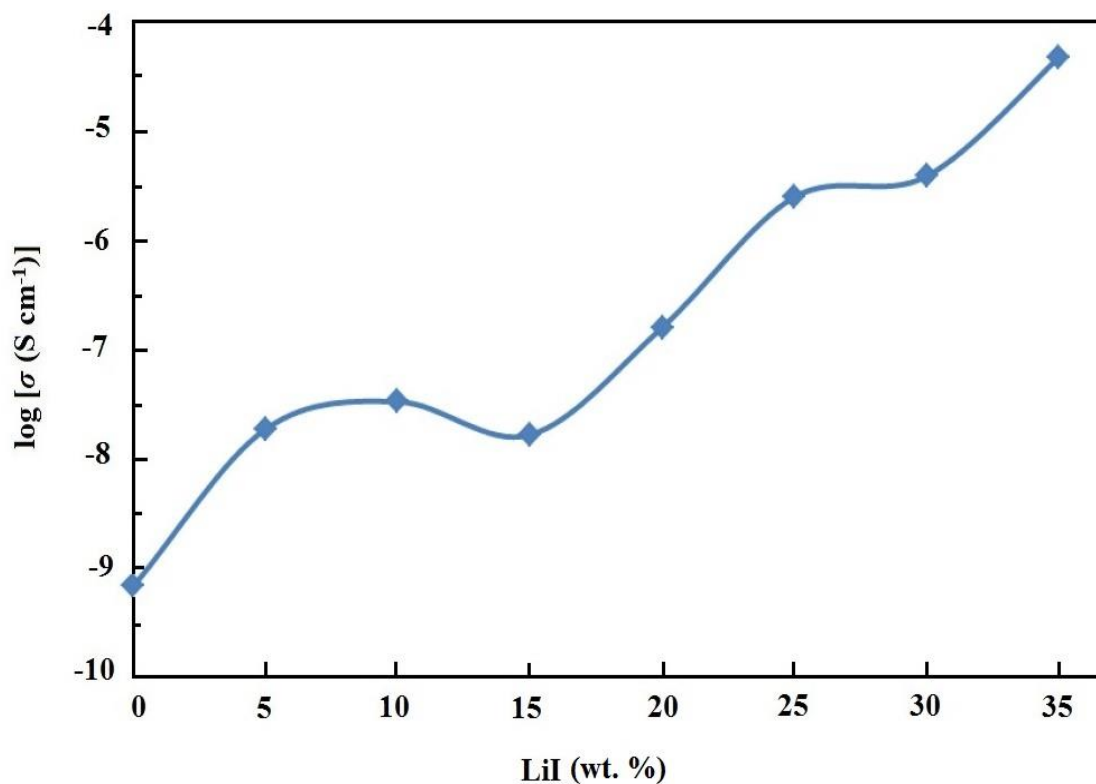


Figure 4.4: Conductivity of RS:LiI system at different LiI content at room temperature

In RS:NH₄I system, SPEs were analyzed using EIS. The ionic conductivity was measured for all samples. Figure 4.5 shows Cole-Cole plots of (a) RN-1, (b) RN-2, (c) RN-3, (d) RN-4, (e) RN-5, (f) RN-6, (g) RN-7 and (h) RN-8. Figure 4.5 indicates that the R_b decreases with increasing NH₄I salt content. This is due to increase in the number of mobile ions of NH₄I salt.

Figure 4.5 demonstrates Cole-Cole plot for RN-9 which represents the lowest R_b and resulting in highest achieved ionic conductivity in RS:NH₄I system.

The bulk resistance (R_b) values of RS:NH₄I system are depicted in Table 4.3. The lowest R_b has been found to be 17.3 Ω for RN-9 SPE with 45 wt.% of NH₄I salt.

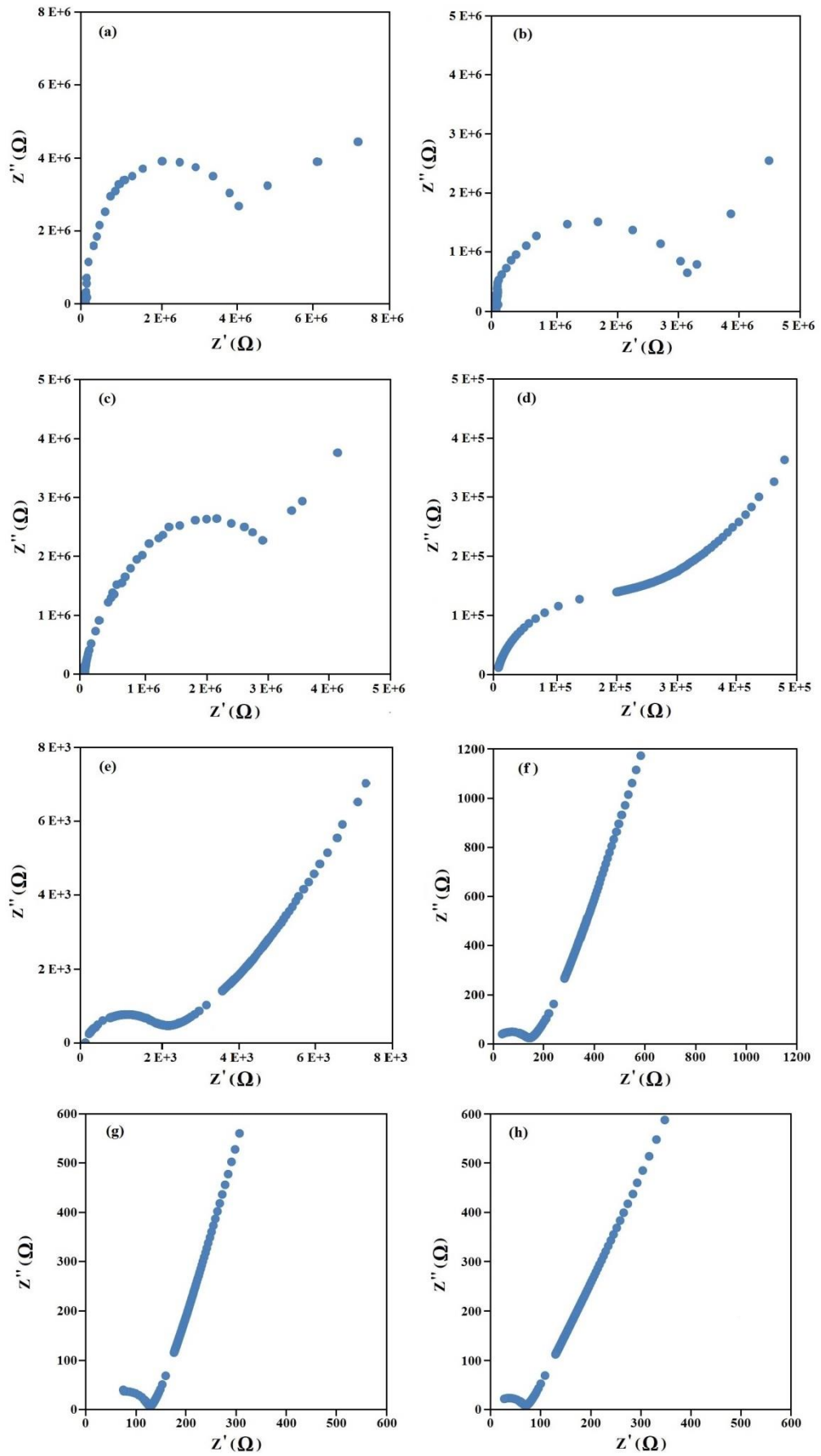


Figure 4.5: Cole-Cole plot of system 2 (RS:NH4I) for (a) RN-1, (b) RN-2, (c) RN-3, (d) RN-4, (e) RN-5, (f) RN-6, (g) RN-7 and (h) RN-8

Table 4.3: Bulk resistance values in RS:NH₄I system

Designation	RS:LiI (wt.%)	Bulk resistance, R_b (Ω)
RN-1	95:5	3.87×10^6
RN-2	90:10	3.15×10^6
RN-3	85:15	2.89×10^6
RN-4	80:20	2.36×10^5
RN-5	75:25	2.16×10^3
RN-6	70:30	1.48×10^2
RN-7	65:35	1.30×10^2
RN-8	60:40	7.03×10^1
RN-9	55:45	1.73×10^1

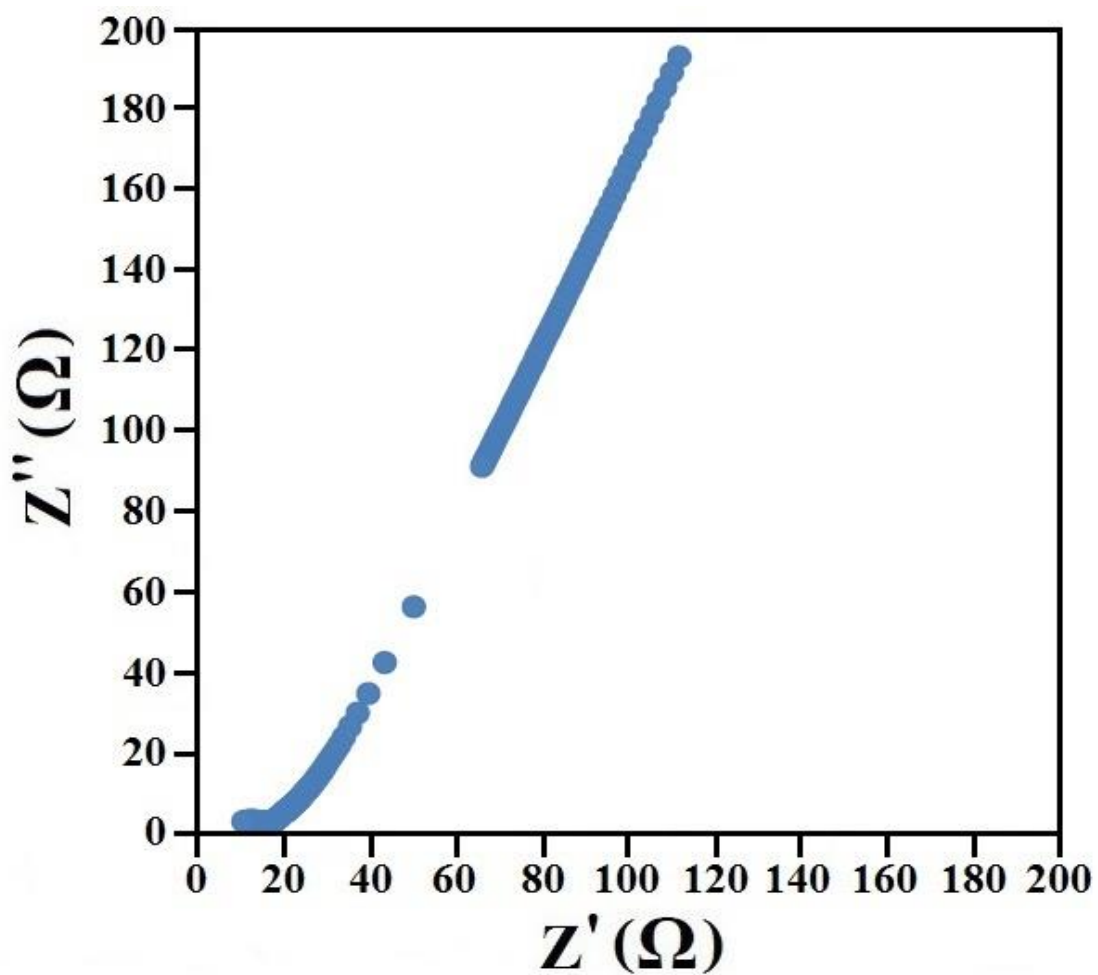


Figure 4.6: Cole-Cole plot of RN-9

The measured ionic conductivities are represented in Table 4.4. The highest ionic conductivity achieved for RS:NH₄I system is $1.39 \times 10^{-4} \text{ S cm}^{-1}$.

The results show that the ionic conductivity increases after the addition of NH₄I salt. This is due to increase of mobile ions of NH₄I salt incorporated in this system. On the other hand, the mobile ions can enhance the electrical performance in the system (R. Singh, Baghel, et al., 2014).

Table 4.4: Designation and ionic conductivity of RS:NH₄I system

Designation	RS:LiI (wt.%) Composition	Conductivity, σ (S cm ⁻¹)
RN-1	95:5	1.02×10^{-9}
RN-2	90:10	1.13×10^{-9}
RN-3	85:15	1.22×10^{-9}
RN-4	80:20	1.32×10^{-8}
RN-5	75:25	1.58×10^{-6}
RN-6	70:30	2.18×10^{-5}
RN-7	65:35	2.22×10^{-5}
RN-8	60:40	3.68×10^{-5}
RN-9	55:45	1.39×10^{-4}

Figure 4.7 shows the variation of the ionic conductivity with NH₄I iodide salt content. The graph indicates that after addition of 20 wt.% of NH₄I the ionic conductivity increases dramatically until reach to 45 wt.% of NH₄I.

In RS:NaI system, SPEs were analyzed using EIS to measure the ionic conductivity. Figure 4.8 shows Cole-Cole plot for RNa-1, RNa-2, RNa-3, RNa-4, RNa-5, RNa-6, RNa-7 and RNa-8. The graphs show the variation of R_b with different NaI salt content. The R_b decreases with the addition of NaI salt which results in higher ionic conductivity due to increasing mobile ions from NaI salt.

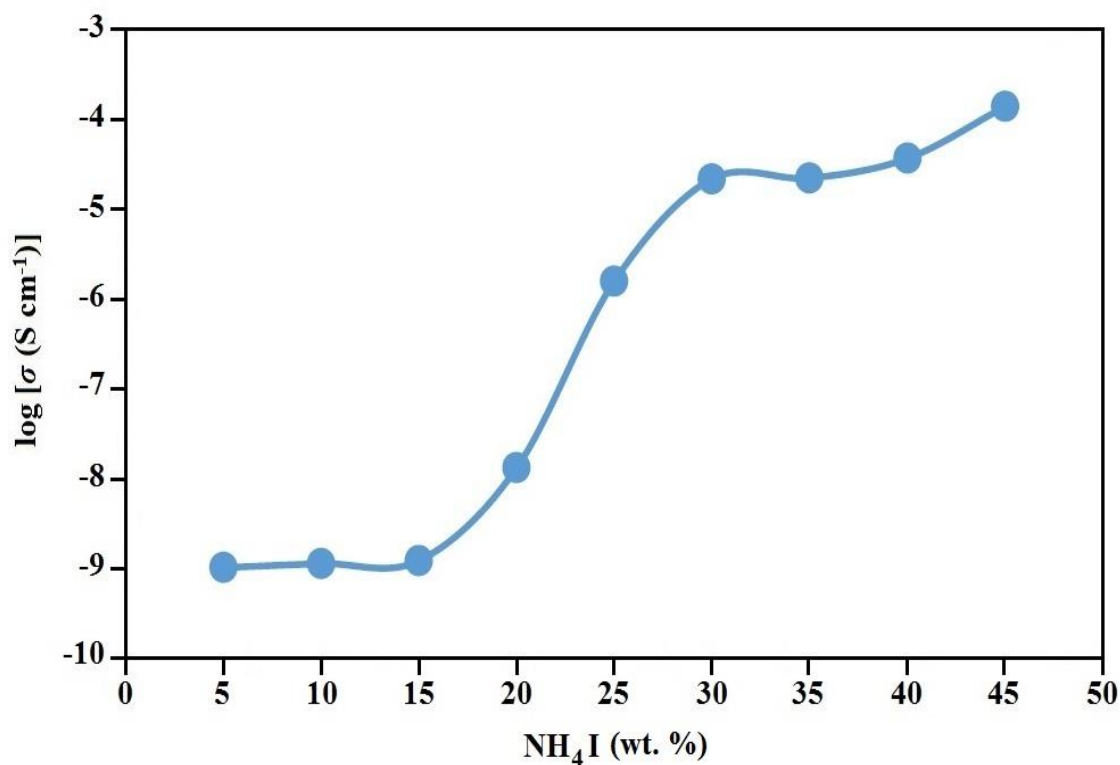


Figure 4.7: Variation of ionic conductivity with NH₄I salt content in RS:NH₄I system

Consequently, Figure 4.9 exhibits Cole-Cole plot for RNa-9 which has the lowest R_b .

The R_b values of all SPEs are inserted in Table 4.5.

Table 4.5: Bulk resistance for polymer electrolytes in RS:NaI system

Designation	RS:NaI (wt.%)	Bulk resistance, R_b (Ω)
RNa-1	95:5	8.79×10^5
RNa-2	90:10	2.49×10^5
RNa-3	85:15	6.70×10^4
RNa-4	80:20	1.80×10^4
RNa-5	75:25	1.04×10^5
RNa-6	70:30	9.02×10^3
RNa-7	65:35	2.25×10^2
RNa-8	60:40	5.21×10^1
RNa-9	55:45	1.14×10^1

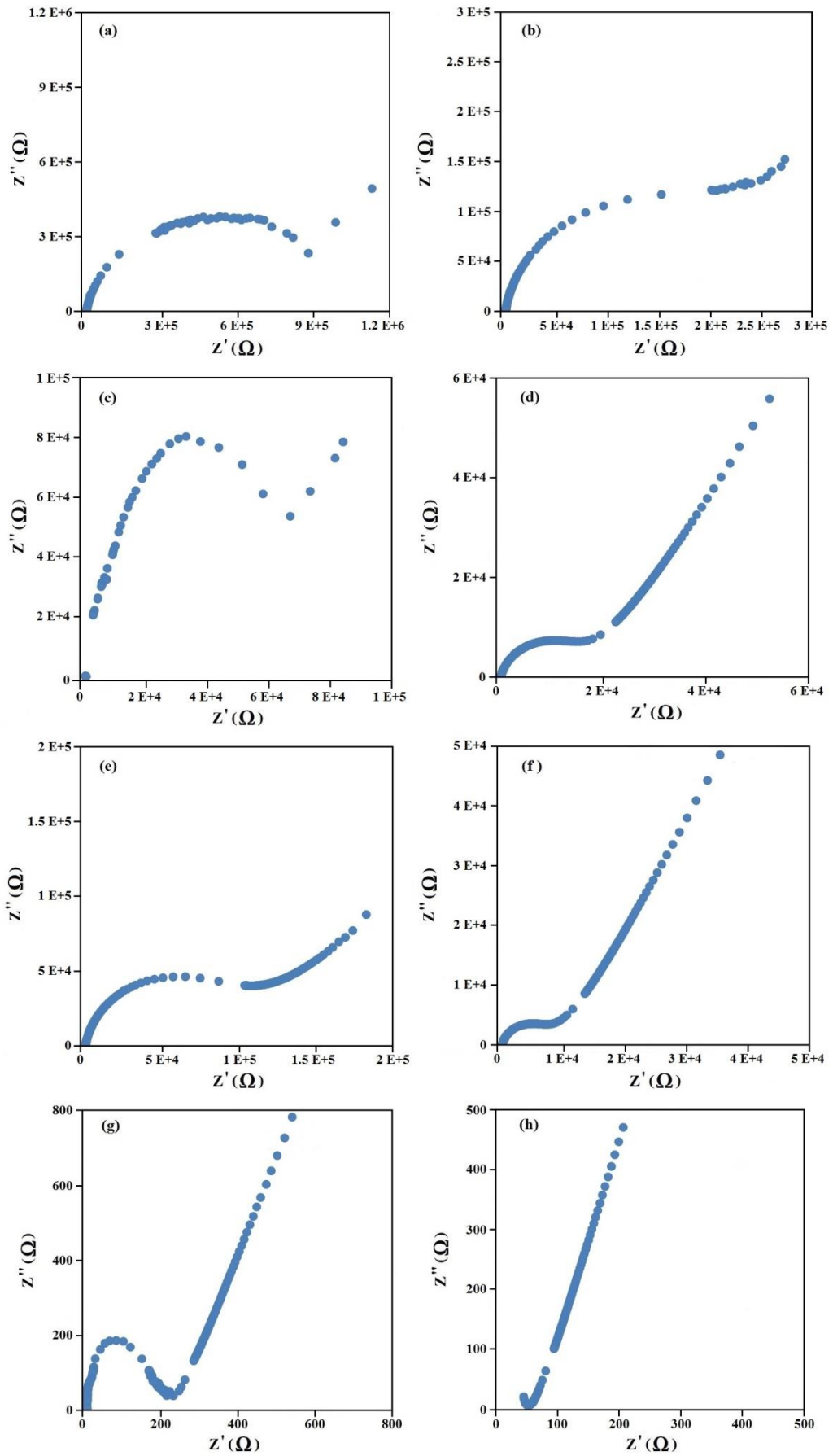


Figure 4.8: Cole-Cole plot for (a) RNA-1, (b) RNA-2, (c) RNA-3, (d) RNA-4, (e) RNA-5, (f) RNA-6, (g) RNA-7 and (h) RNA-8

Disappearance of semicircles after the addition of 40 wt.% of NaI in RNa-8 results in the conclusion that the charge carriers are ions and the total ionic conductivity is due to ion conduction (Klassen et al., 1998). In Figure 4.9, the equivalent circuit for the RNa-9 SPE is represented with the C_e as double layer capacitance, C for geometric capacitance and R as resistance with equivalent values of 1 μ F, 0.1 μ F and 100 ohm, respectively.

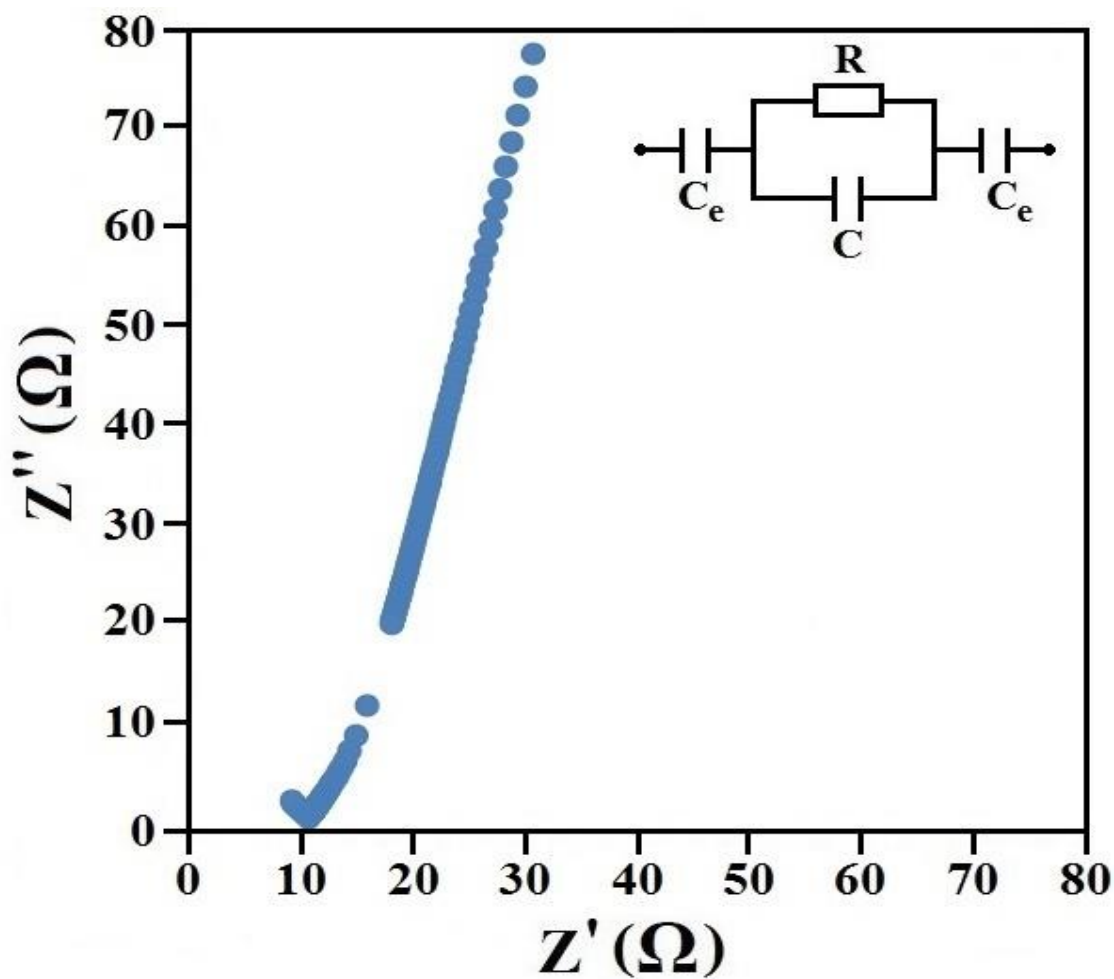


Figure 4.9: Cole-Cole plot of RNa-9

The ionic conductivity values at room temperature obtained from EIS data for each SPE in RS:NaI system is depicted in Table 4.6. According to Table 4.6, the highest ionic conductivity of 4.79×10^{-4} ($S\ cm^{-1}$) was achieved in RNa-9 with the addition of 45 wt.% of NaI salt content.

Furthermore, by comparing the EIS results in RS:LiI, RS:NH₄I and RS:NaI systems, the RNa-9 has the highest achieved ionic conductivity between these three systems which is in RS:NaI system with the incorporation of 45 wt.% NaI.

Table 4.6: Ionic conductivity and designation of RS:NaI system

Designation	RS:NaI (wt.%) Composition	Conductivity, σ (S cm ⁻¹)
RNa-1	95:5	3.32×10^{-9}
RNa-2	90:10	9.03×10^{-9}
RNa-3	85:15	4.56×10^{-8}
RNa-4	80:20	1.55×10^{-7}
RNa-5	75:25	3.03×10^{-8}
RNa-6	70:30	3.05×10^{-7}
RNa-7	65:35	1.40×10^{-5}
RNa-8	60:40	5.22×10^{-5}
RNa-9	55:45	4.79×10^{-4}

Figure 4.10 demonstrates the variation of the ionic conductivity with different NaI salt content. The graph shows the ionic conductivity increases with the addition of NaI salt. This is due to increase of mobile ions of iodide salts incorporated in systems. On the other hand, the mobile ions can enhance the electrical performance in the system (R. Singh, Baghel, et al., 2014).

Figure 4.10 further reveals that the ionic conductivity drop from 20 wt.% to 25 wt.% of NaI salt. This is due to aggregation and accumulation of free ions in the polymer electrolyte preparation (Ren et al., 2014). The addition of NaI salt above 25 wt.% makes more clusters in NaI to be closer. This could help to increase the ionic conductivity above the amount of 25 wt.% NaI salt.

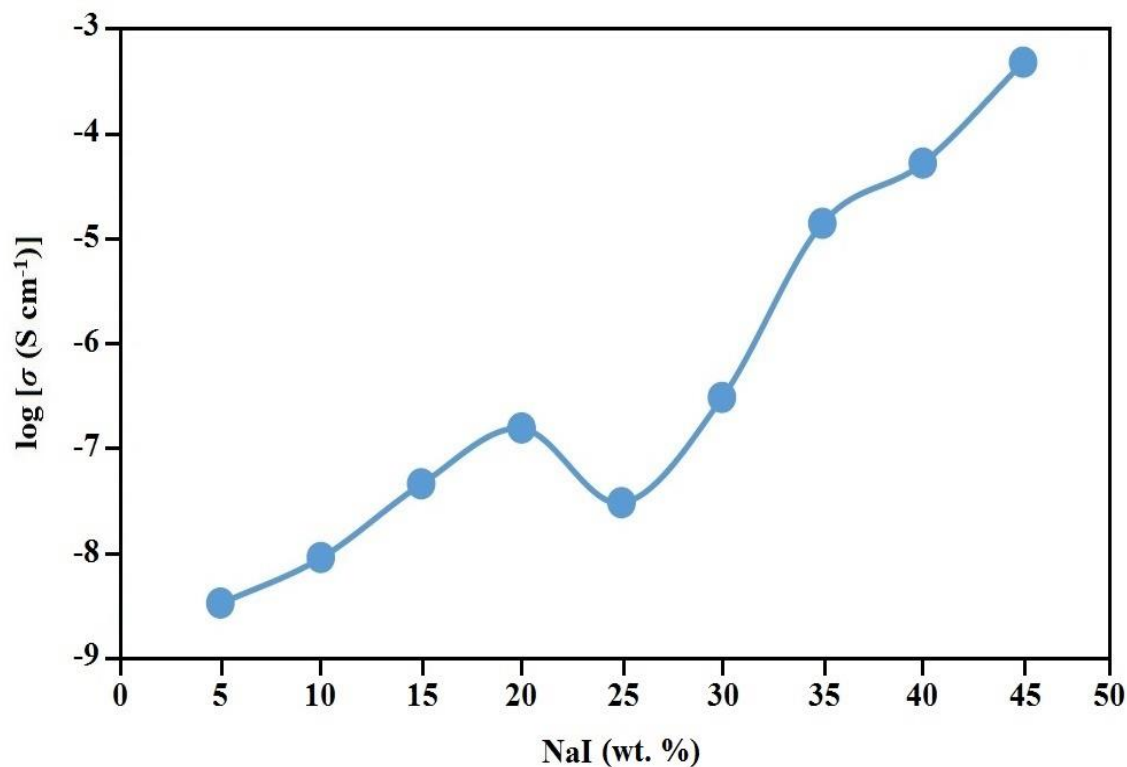


Figure 4.10: Variation of ionic conductivity with different NaI salt content

4.2.2 TEMPERATURE-DEPENDENT IONIC CONDUCTIVITY

The temperature-dependent study on ionic conductivity was carried out to analyze the mechanism of ionic conduction and related model. Figure 4.11 demonstrates the $\log \sigma$ versus $1000/T$ for various samples of RS-0, RS-5, RS-6 and RS-7 in temperature range from 30 °C to 100 °C. Results show that ionic conductivity increases with increase in temperature. This is due to bond rotations which result in faster ion movements as temperature increases (Baskaran et al., 2004; Subba Reddy et al., 2003). Regressions ($R^2 \sim 1$) show best confirmation of results lying on straight lines.

Figure 4.11 indicates that the temperature-dependence behavior of RS:LiI system follows Arrhenius thermal activated model. Activation energies (E_a) acquired from Equation (3.40). Activation energies of 0.46, 0.45 and 0.41 eV calculated for RS-5, RS-6 and RS-7, respectively. Activation energy decreases with increase of conductivity which is related to increase of LiI content.

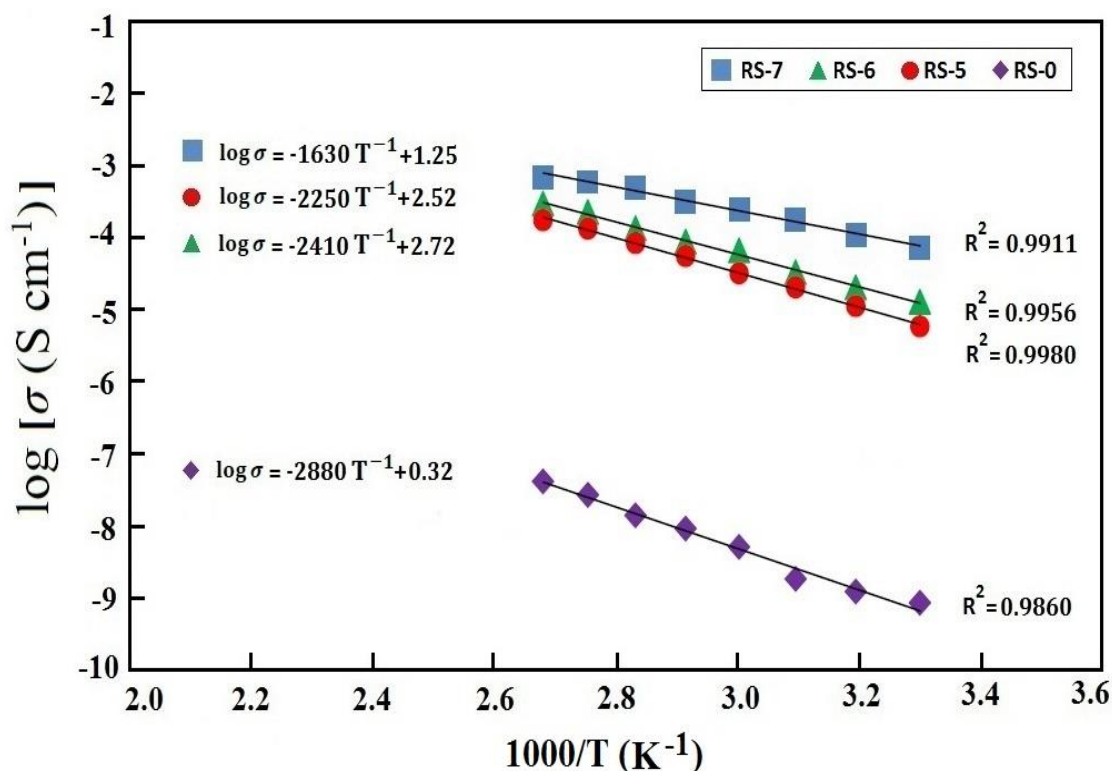


Figure 4.11: Temperature-dependent ionic conductivity of rice starch and lithium iodide system

Addition of salt produces more sites for ionic transport between conducting band and valence band which deduce to lower the band gap as activation energy. This fact means ions at higher salt concentration needed less energy for transformation between transit sites to increase the ionic conductivity. The mechanism is hopping Li^+ ions on vacant places and increases in mobile ion numbers, results in increase of ionic conductivity (Uma et al., 2003).

In RS: NH_4I system, temperature-dependent ionic conductivity study was performed for RN-7, RN-8 and RN-9. Figure 4.12 illustrates temperature-dependent results for the solid polymer electrolytes for RN-7, RN-8 and RN-9. The regression values ($R^2 \sim 0.99$) show that each SPE follows Arrhenius thermal activated model.

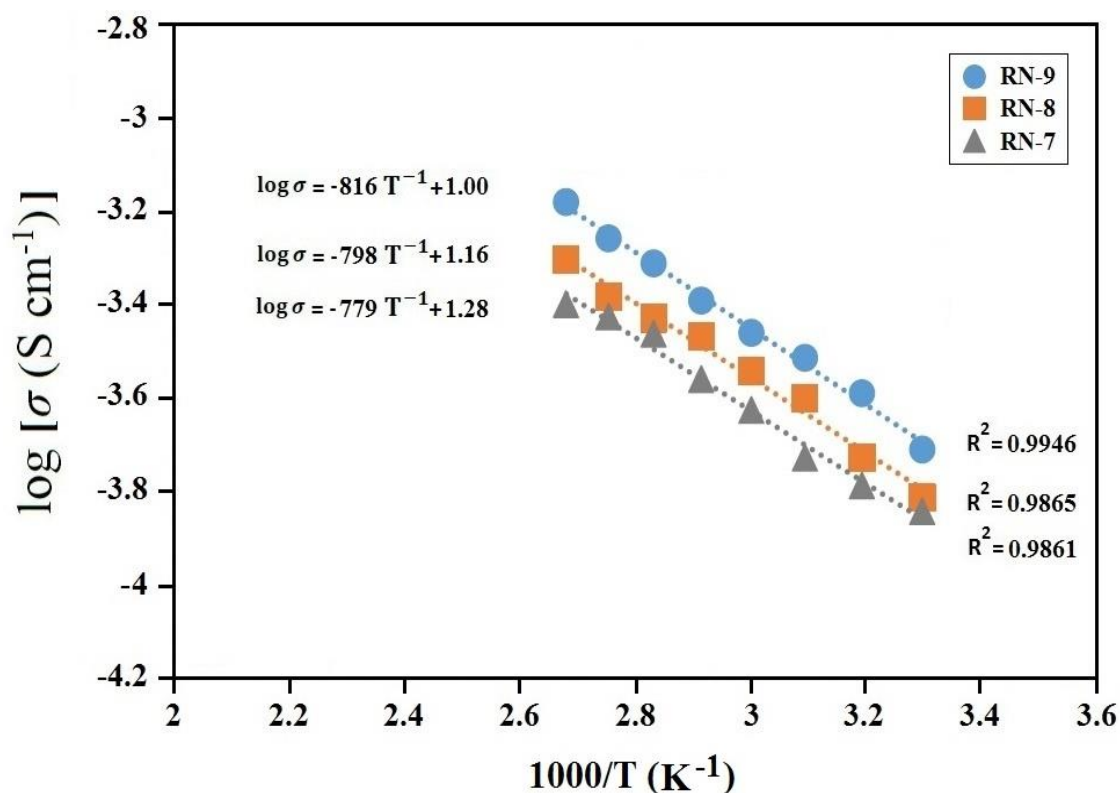


Figure 4.12: Temperature-dependent ionic conductivity of RS:NH₄I system

The activation energies calculated for RN-7, RN-8 and RN-9 are 0.16, 0.158 and 0.154 eV, respectively. The results show that activation energy decreases with an increase of ionic conductivity and the lowest activation energy is for sample RN-9 as the highest achieved ionic conductivity.

Figure 4.13 illustrates temperature-dependent ionic conductivity results for the solid polymer electrolytes of RNa-7, RNa-8 and RNa-9. The regression values ($R^2 \sim 0.99$) show each system follows Arrhenius thermal activated model according to Equation (3.40). The activation energies calculated for RNa-7, RNa-8 and RNa-9 are 0.156, 0.131 and 0.110 eV, respectively. The results show that increasing in the ionic conductivity has been achieved with decrease in activation energy. The lowest activation energy is for sample RNa-9 as highest achieved ionic conductivity.

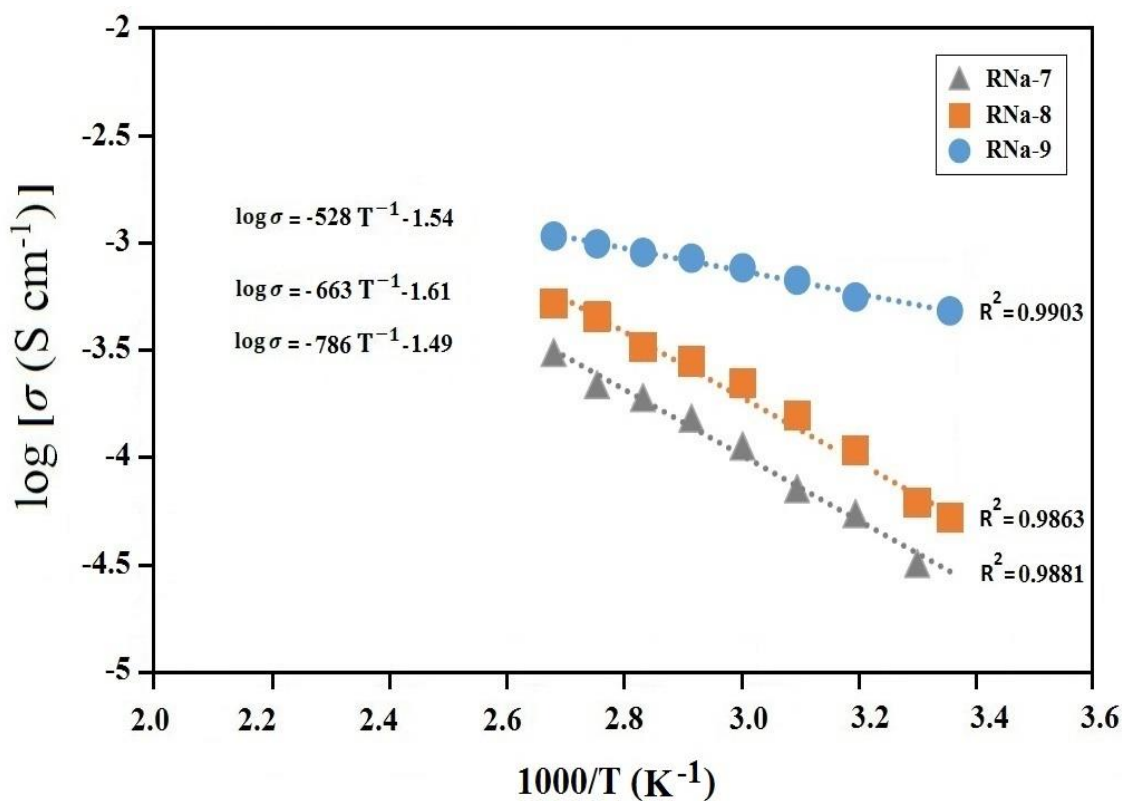


Figure 4.13: Temperature-dependent ionic conductivity of RS:NaI system

4.3 FTIR CHARACTERIZATION

The FTIR analysis of polymer electrolytes is important factor to monitor polymer and salt complexation, ion-ion and ion-polymer interactions as a function of salt concentration (Selvasekarapandian et al., 2006). In RS:LiI system, the complexation between RS and LiI salt was investigated using FTIR spectroscopy. Figure 4.14 shows FTIR spectra of pure rice starch (RS-0), pure LiI, RS-5, RS-6 and RS-7 at different wavenumbers between 4000 and 400 cm^{-1} .

The important band assignments for pure rice starch (RS-0) are represented in Table 4.3 (Kizil et al., 2002; Pretsch; et al., 2009).

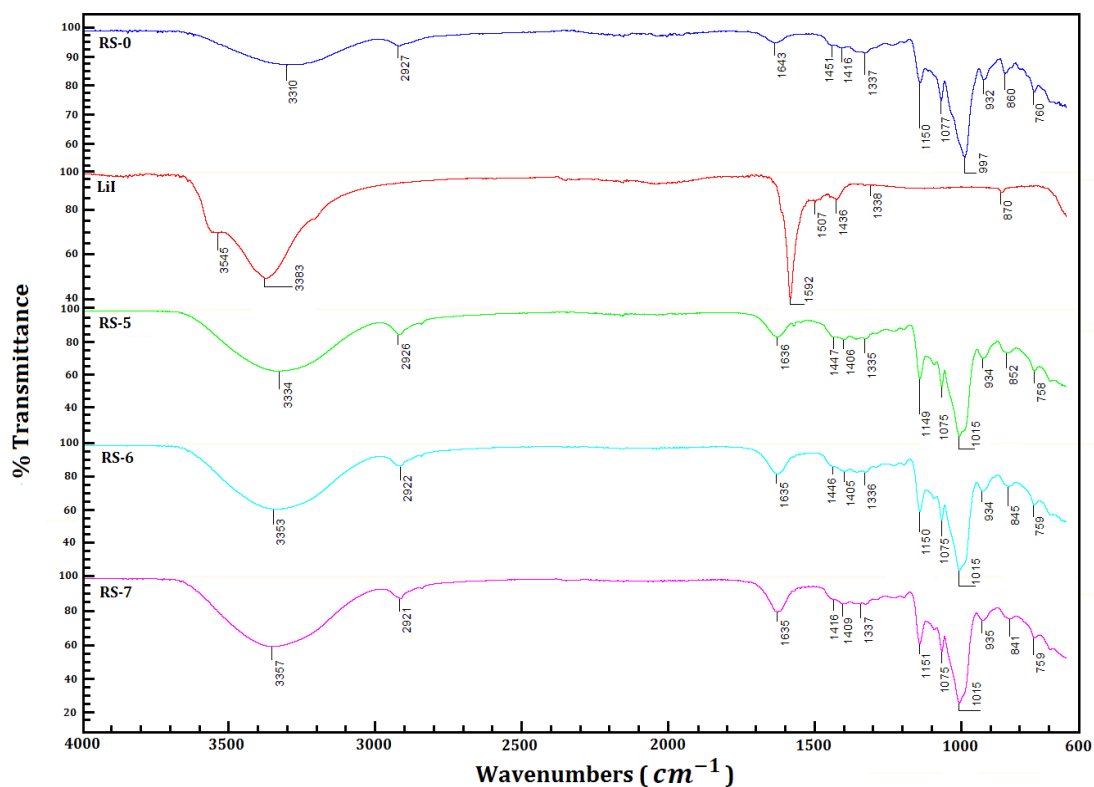


Figure 4.14: FTIR spectra of RS-0, pure LiI, RS-5, RS-6 and RS-7

Table 4.7: Band assignments and infrared wavenumbers for pure rice starch

Sample	Band assignment	Wavenumber (cm ⁻¹)
RS	O-H stretching (broad)	3310
	C-H ₂ deformation (<i>m</i>) -(CH ₂)	2927
	H ₂ O in amorphous regions of starch	1643
	C-H bending (<i>v</i>) - (CH ₂)	1451
	C-O-H bending , C-H twisting (CH ₂)	1337
	C-O stretching (<i>s</i>)	1150
	C-O-H bending (<i>s</i>)	1077
	C-H bending (<i>v</i>)	997
	Skeletal mode vibrations of α -1,4-glycosidic linkages, (C-O-C)	932
	C-H deformation	860
	C-C stretching (<i>v</i>)	760

note: RS= Rice Starch, (*s*)= strong, (*m*)= medium, (*v*)= variable

Shifts of peaks at 1643, 1451 and 860 cm^{-1} for pure rice starch (RS-0), after addition of LiI salt, confirms complexation between rice starch (RS) and LiI. In Figure 4.14, the peak at 1643 cm^{-1} for pure RS (RS-0) is shifted to lower frequencies of 1636 and 1635 cm^{-1} for RS-5 and RS-7, respectively, due to influence of the peak in LiI salt bonding and interaction, which is the evidence of complexation between rice starch polymer and LiI salt.

Moreover, the peak at 1451 cm^{-1} in pure rice starch, characteristic of C–H bending (CH_2) is shifted to lower frequencies at 1447, 1446 and 1416 cm^{-1} in RS-5, RS-6 and RS-7, respectively, expressing complexation with LiI salt. In lower frequency range there is also evidence of complexation at peak of C–H bond at 860 cm^{-1} which is shifted to lower frequencies of 852, 845 and 841 cm^{-1} in RS-5, RS-6 and RS-7 respectively.

The FTIR spectra for RS: NH_4I system are represented in Figure 4.15 at different wavenumbers between 4000 and 400 cm^{-1} . The band assignments for polymer electrolyte contents according to literatures (Kizil et al., 2002; Pretsch; et al., 2009; V. K. Singh et al., 2013) are depicted in Table 4.8.

The results show the peaks in pure rice starch (RS-0) shifts to another frequency after the addition of ammonium iodide salt.

The peak in 3310 cm^{-1} for RS-0, which refers to O-H stretching, shifts to lower frequencies of 3222, 3197 and 3197 cm^{-1} in RN-7, RN-8 and RN-9, respectively after incorporation of NH_4I .

Table 4.8: Band assignments and wavenumbers for RS:NH₄I system

Wavenumbers, cm ⁻¹			Band Assignments
RS	NH ₄ I	RS+NH ₄ I	
3310		3357, 3191	O-H stretching (broad)
	3091, 3082		N-H stretch, alkynes
2927		2926	C-H ₂ deformation (<i>m</i>) -(CH ₂)
	2798		H-C=O : C-H stretch, aldehydes
1643		1623	H ₂ O in amorphous regions of starch
	1616		C-C stretch(in ring), aromatic
1451			C-H bending (<i>v</i>) - (CH ₂)
	1375		NH ₄ asymmetric H-N-H deformation
1337			C-O-H bending , C-H twisting (CH ₂)
1150		1149	C-O stretching (<i>s</i>)
1077		1074	C-O-H bending (<i>s</i>)
997		1015	C-H bending (<i>v</i>)
932		930	Skeletal mode vibrations of α -1,4-glycosidic linkages, (C-O-C)
860		851	C-H deformation
760		762	C-C stretching (<i>v</i>)

note: RS= Rice Starch, (*s*)= strong, (*m*)= medium, (*v*)= variable

In other peaks like 997 cm⁻¹, referring to C-H bending, in RS-0 the frequency shifts to higher frequencies of 1012, 1013 and 1015 cm⁻¹ due to complexation and interaction of NH₄I salt. The shifts express that the complexation between polymer (RS-0) and salt (NH₄I) has occurred (Khanmirzaei et al., 2015).

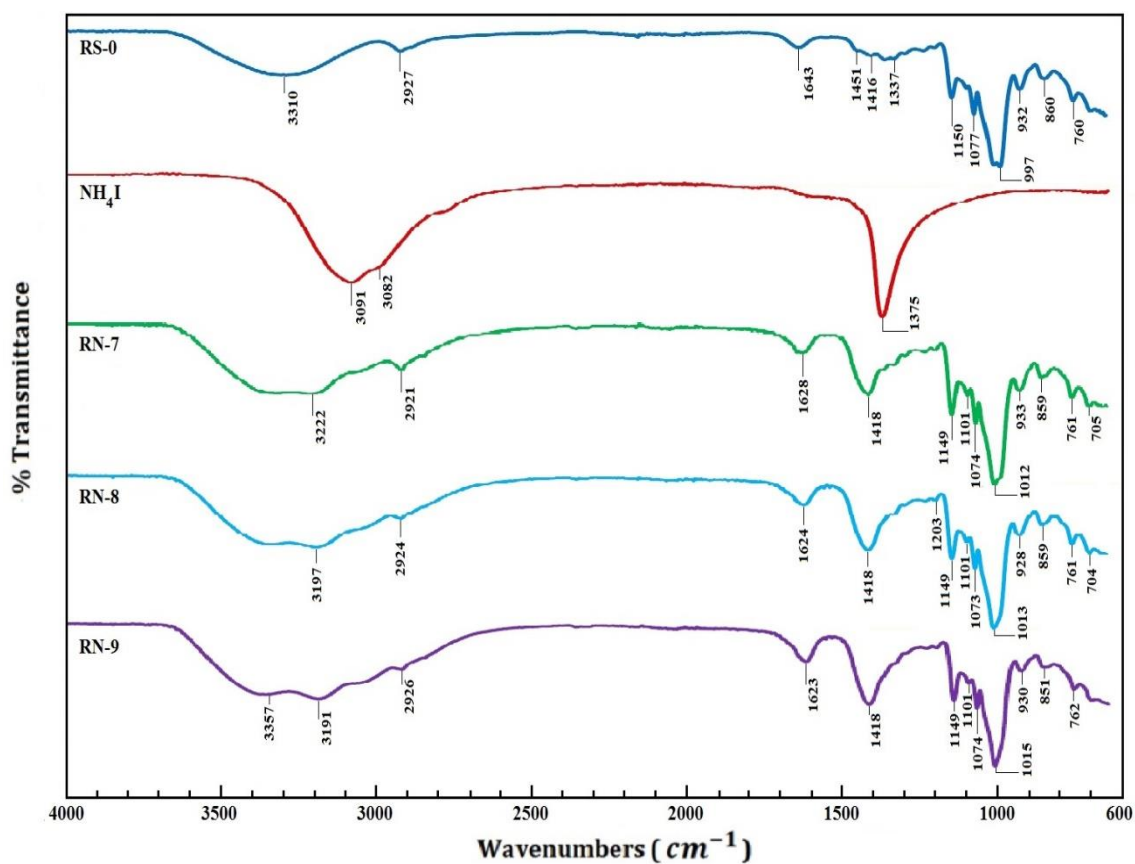


Figure 4.15: FTIR spectra of RS-0, NH₄I, RN-7, RN-8 and RN-9 polymer electrolytes

The FTIR spectra for RS:NaI system are illustrated in Figure 4.16. The band assignments for polymer electrolyte contents according to literatures (Kizil et al., 2002; Pretsch; et al., 2009; V. K. Singh et al., 2013) are depicted in Table 4.9. The broad peak at 3310 cm^{-1} for RS-0, representing the O-H stretching, shifts to higher frequencies of 3356 , 3354 and 3373 cm^{-1} in RN-7, RN-8 and RN-9, respectively, after addition of NaI salt.

The peak at 1643 cm^{-1} for RS-0 shifts to lower frequencies of 1635 , 1635 and 1624 cm^{-1} in RN-7, RN-8 and RN-9, respectively. The shifts in FTIR spectra due to addition of NaI salt reveals that the complexation between rice starch and NaI salt has occurred.

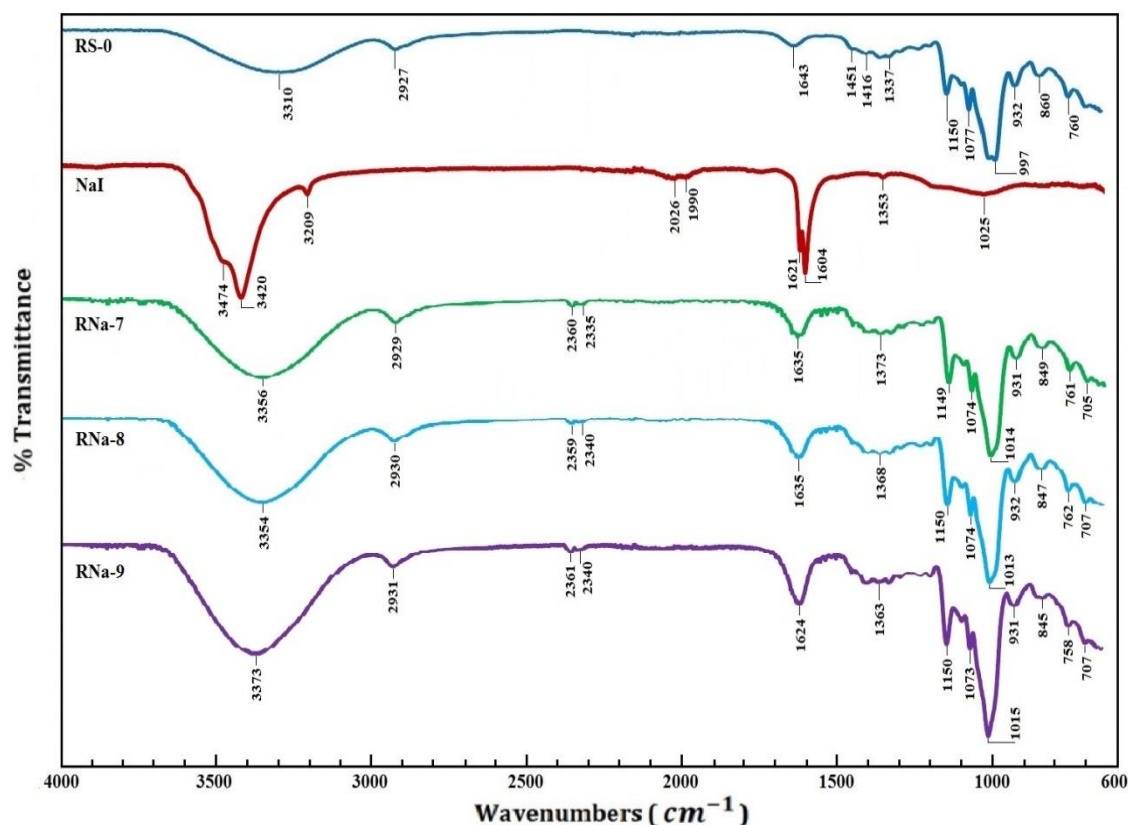


Figure 4.16: FTIR spectra of RS-0, NaI, RNa-7, RNa-8 and RNa-9 polymer electrolytes

Table 4.9: Band assignments and wavenumbers for polymer electrolytes

Wavenumbers, cm^{-1}		Band Assignments
RS	RS+NaI	
3310	3373	O-H stretching (broad)
2927	2931	C-H ₂ deformation (<i>m</i>) -(CH ₂)
1643	1624	H ₂ O in amorphous regions of starch
1451	-	C-H bending (<i>v</i>) - (CH ₂)
1337	1363	C-O-H bending , C-H twisting (CH ₂)
1150	1150	C-O stretching (<i>s</i>)
1077	1073	C-O-H bending (<i>s</i>)
997	1015	C-H bending (<i>v</i>)
932	931	Skeletal mode vibrations of α -1,4-glycosidic linkages, (C-O-C)
860	845	C-H deformation
760	758	C-C stretching (<i>v</i>)

note: RS= Rice Starch, (*s*)= strong, (*m*)= medium, (*v*)= variable

4.4 XRD CHARACTERIZATION

The XRD patterns further confirmed complexation between RS and LiI salt in RS:LiI system. The XRD recorded patterns of SPEs are illustrated in Figure 4.17. The figure shows XRD patterns of (a) RS-5 (25 wt.% LiI), (b) RS-6 (30 wt.% LiI), (c) RS-7 (35 wt.% LiI), (d) RS-0 (pure rice starch), and (e) LiI salt. Figure 4.17 (e) shows very sharp crystalline peak at $2\theta = 21^\circ$ and other crystalline peaks at $2\theta = 12$ and 30° for lithium iodide salt denoting crystalline characteristic of LiI salt.

Pure rice starch pattern in (d) exhibits amorphous characteristics with small peak at $2\theta = 19^\circ$ and broad hunch at $2\theta = 17-22^\circ$. After addition of LiI salt, the peaks in pure rice starch shifted and 2θ increased slightly to the range of $20-25^\circ$ for RS-5, $19-21^\circ$ for RS-6, and $19-22^\circ$ for RS-7 as highest LiI salt concentration and ionic conductivity in this system.

The results confirm that the intensity of the broad range of sample decreasing with doping of LiI salt which is evidence of dissolution of salt because of elimination of the peaks in salt patterns.

The XRD patterns further confirm complexation of polymer with salt which disorders the crystallinity and oriented arrangement of system. The XRD patterns further emphasize that addition of salt increases the amorphous behavior of the RS:LiI system which enhances the ionic conductivity (R. Singh et al., 2013) and increase the ion mobility and flexibility of polymer structure.

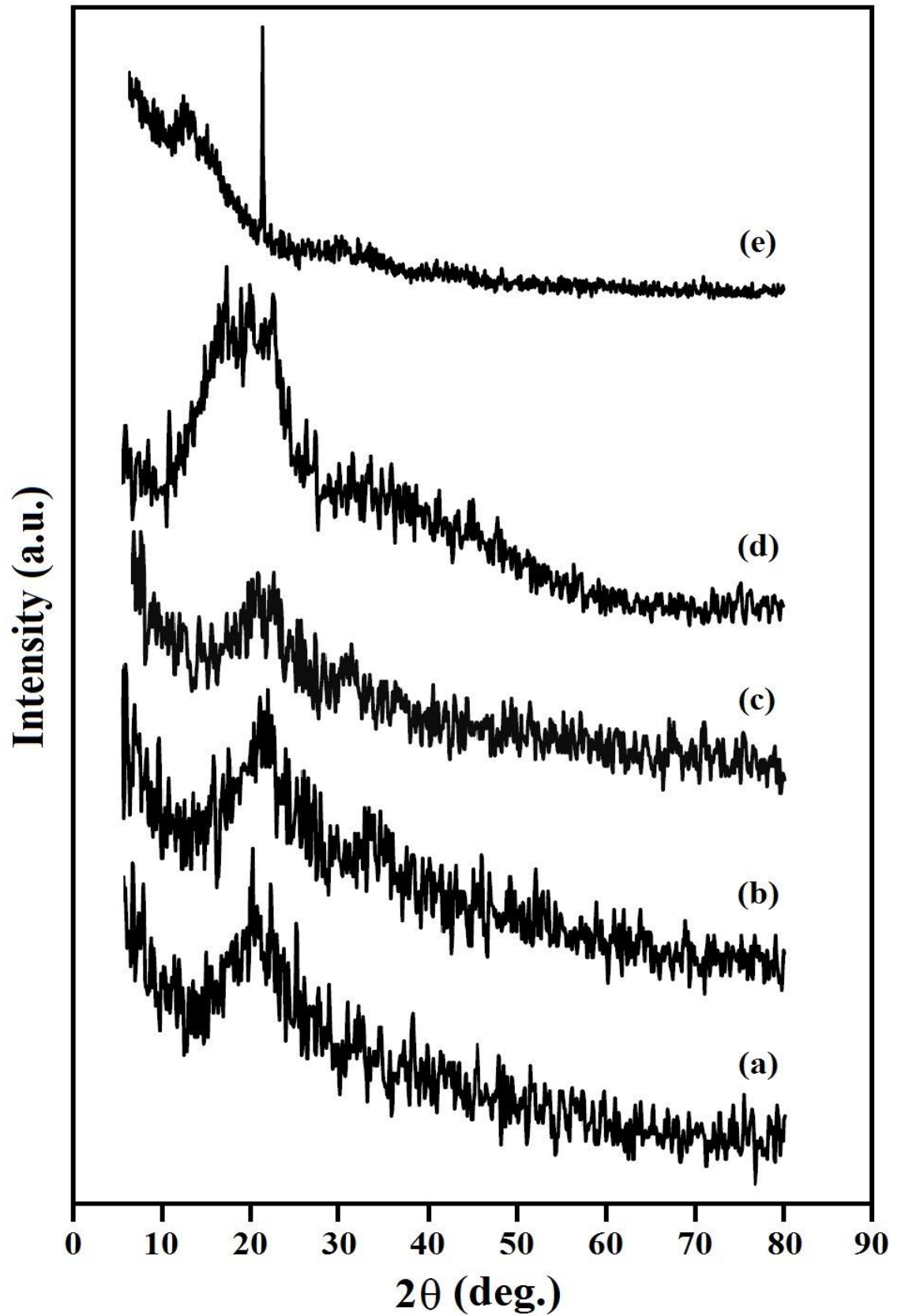


Figure 4.17: XRD patterns of RS:LiI polymer electrolyte system for (a) RS-5, (b) RS-6, (c) RS-7, (d) pure rice starch, and (e) pure lithium iodide salt

In RS:NH₄I system, the XRD patterns of RS:NH₄I system with ammonium iodide are represented in Figure 4.18. The graph shows XRD patterns of (a) RN-7, (b) RN-8, (c) RN-9, (d) RS-0 (pure rice starch) and (e) NH₄I.

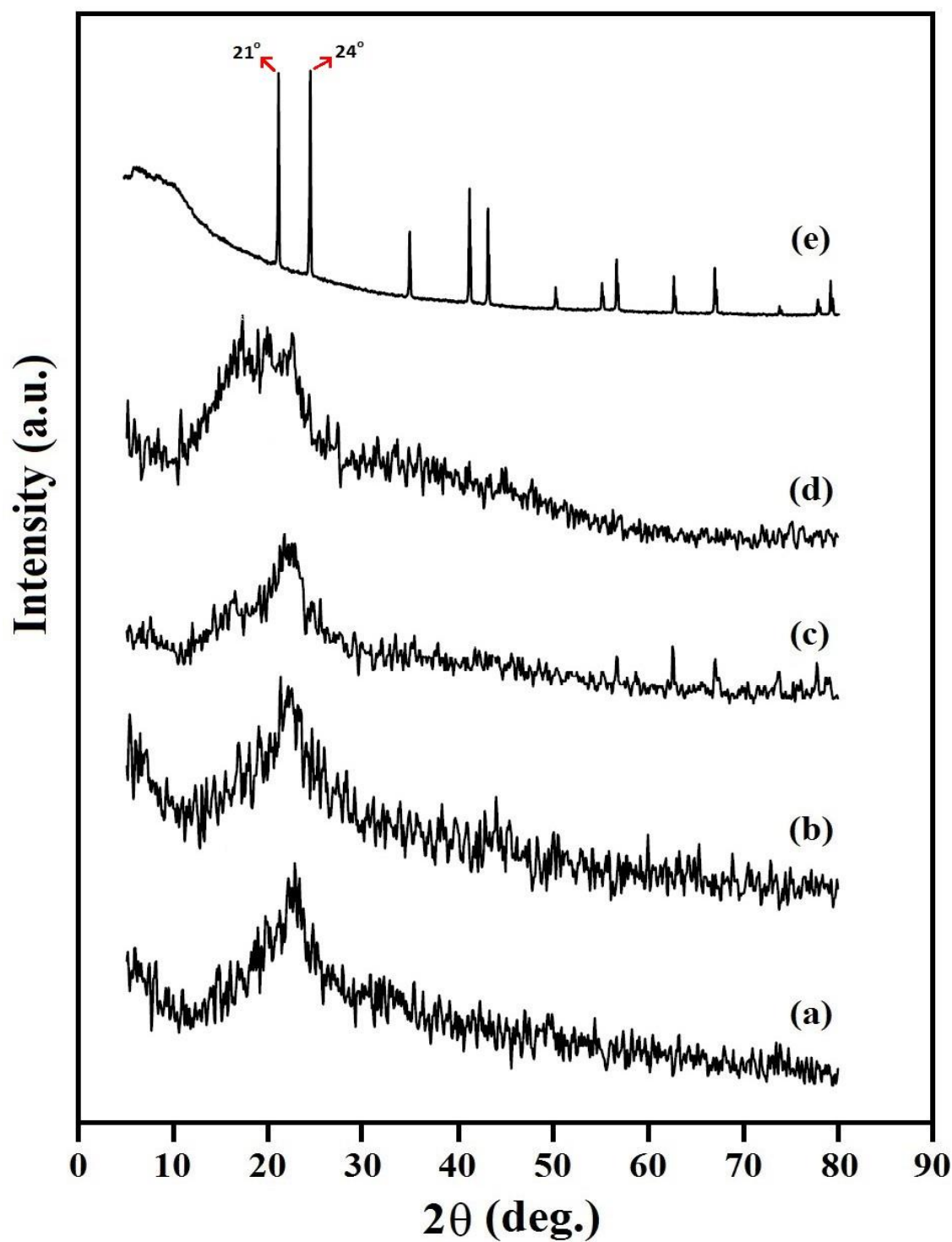


Figure 4.18: XRD patterns of polymer electrolytes in RS:NH₄I system for (a) RN-7, (b) RN-8, (c) RN-9, (d) pure rice starch (RS-0) and (e) NH₄I

The ammonium iodide patterns show crystalline characteristics with sharp peaks at $2\theta = 21$ and 24° , and some other peaks are at $2\theta = 35, 41$ and 43° . Pure rice starch pattern in Figure 5.6(d) exhibits amorphous characteristics with small peak at $2\theta = 19^\circ$ and broad hunch at $2\theta = 17-22^\circ$.

After incorporation of NH_4I salt the peaks in RS-0, shifts to higher range of $19-25^\circ$ for RN-7, $18-25^\circ$ for RN-8 and $19-25^\circ$ for RN-9. The shifts confirm complexation of ammonium iodide salt with pure rice starch.

The graph shows elimination of peaks in ammonium iodide. The results indicate that the SPEs become more amorphous after addition of NH_4I salt which is another evidence of complexation between pure rice starch and NH_4I salt.

In RS:NaI system, the XRD patterns of RS:NaI system are demonstrated in Fig. 4.19 for (a) RNa-7, (b) RNa-8, (c) RNa-9, (d) pure rice starch and (e) NaI. Figure 4.19 (e) shows very sharp crystalline peak at $2\theta = 22.1$ and 46.7° , and some other crystalline peaks are at $2\theta = 15.5, 18.3$ and 42.5° for sodium iodide salt denoting crystalline characteristic of NaI salt.

The peaks in pure rice starch shifts to higher value after addition of NaI to range of $19-24^\circ$ in RNa-7, $19-25^\circ$ in RNa-8 and $18-25^\circ$ in RNa-9. The results show broadening of pure rice starch change and become more broaden and more amorphous after addition of sodium iodide salt. These results further confirm complexation of pure rice starch and NaI salt.

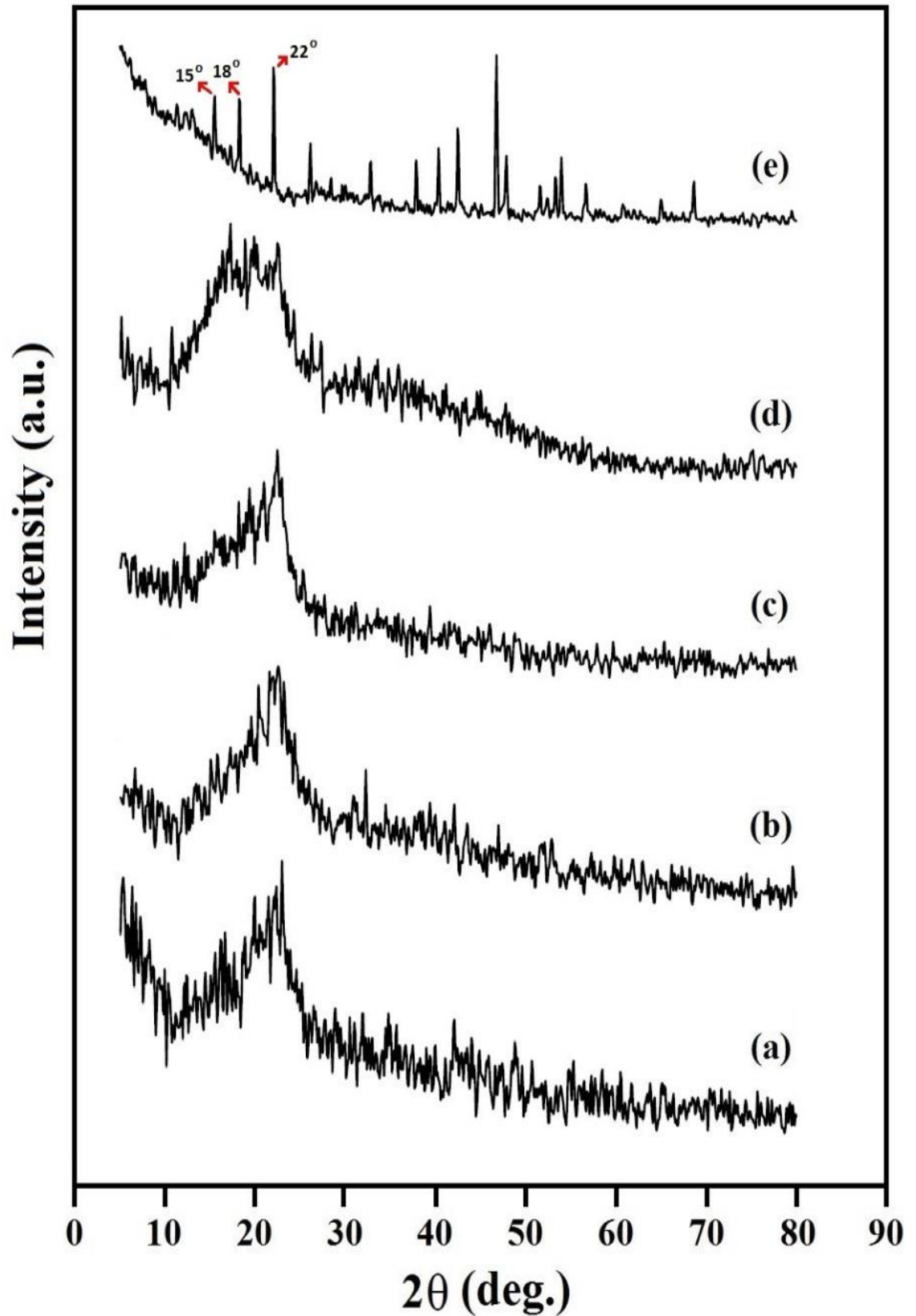


Figure 4.19: XRD patterns of polymer electrolytes in RS:NaI system for (a) RNa-7, (b) RNa-8, (c) RNa-9, (d) pure rice starch (RS-0) and (e) NaI salt

4.5 THERMAL STUDY - TGA

The thermal stability of samples was examined by TGA analysis. Figure 4.20 shows the results for selected SPEs for pure rice starch. TGA thermograms of RS-5 (25 wt.% LiI) is represented in Figure 4.21, RS-6 (30 wt.% LiI) in Figure 4.22, and RS-7 (35 wt.% LiI) in Figure 4.23 in RS:LiI system. All selected samples show one-step decomposition with different decomposition temperatures (T_{dc}). The decomposition temperature is the temperature where the weight change starts to decrease dramatically. Initial weight loss in range 70 to 100 °C in SPEs is due to the evaporation of trapped residual solvent or moisture (Mohamad et al., 2007). T_{dc} is ~292 °C for pure rice starch. T_{dc} for RS-5, RS-6, and RS-7 are ~245, 230, and 224 °C, respectively.

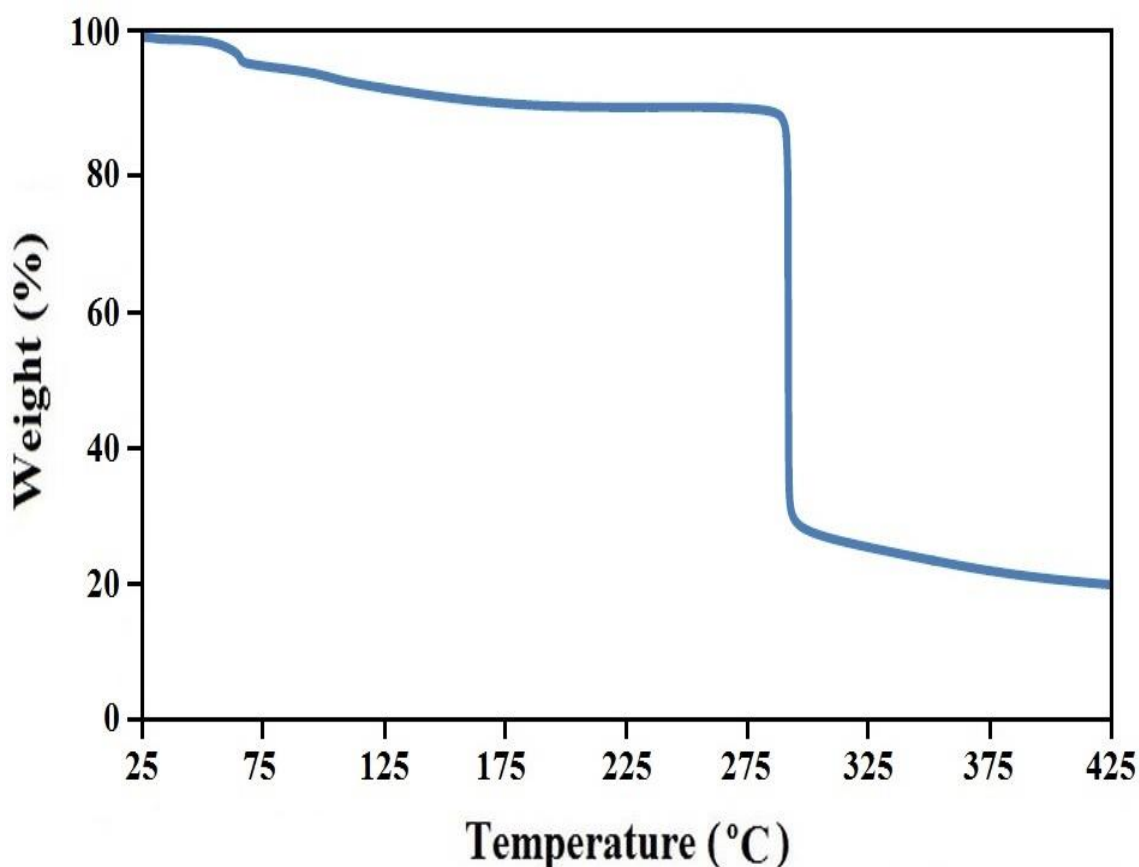


Figure 4.20: TGA thermograms of pure rice starch (RS-0)

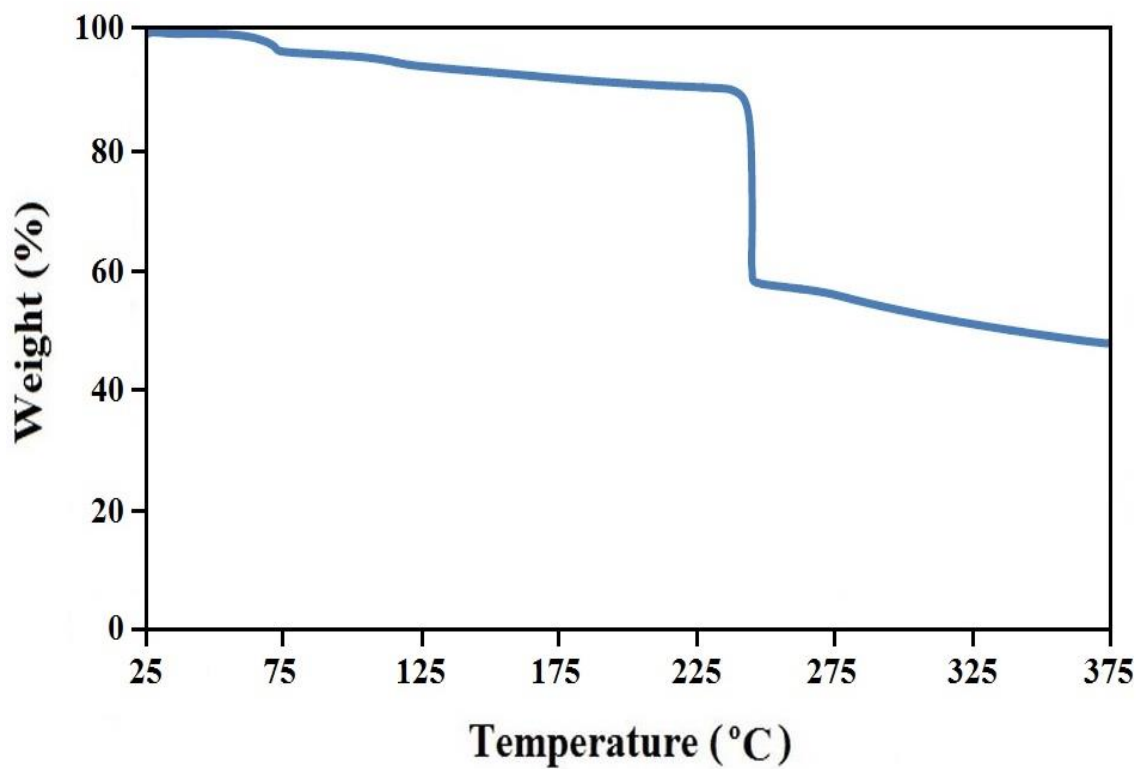


Figure 4.21: TGA results for RS-5

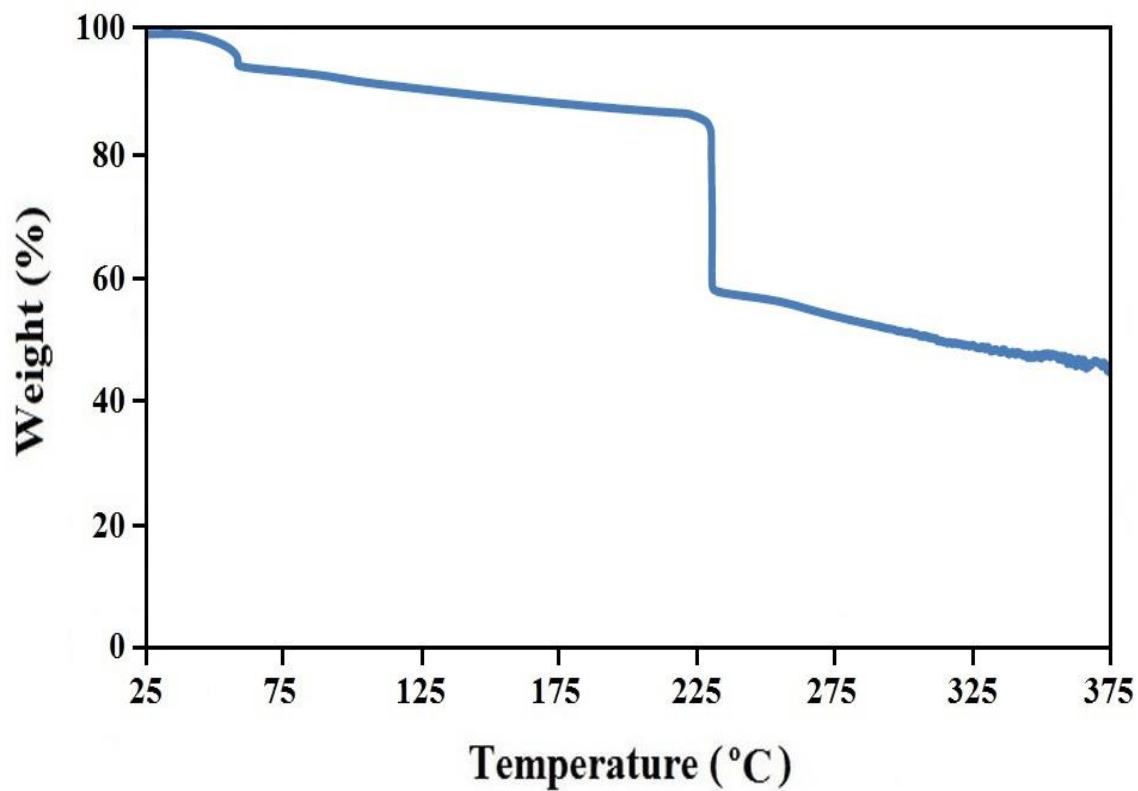


Figure 4.22: TGA results for RS-6

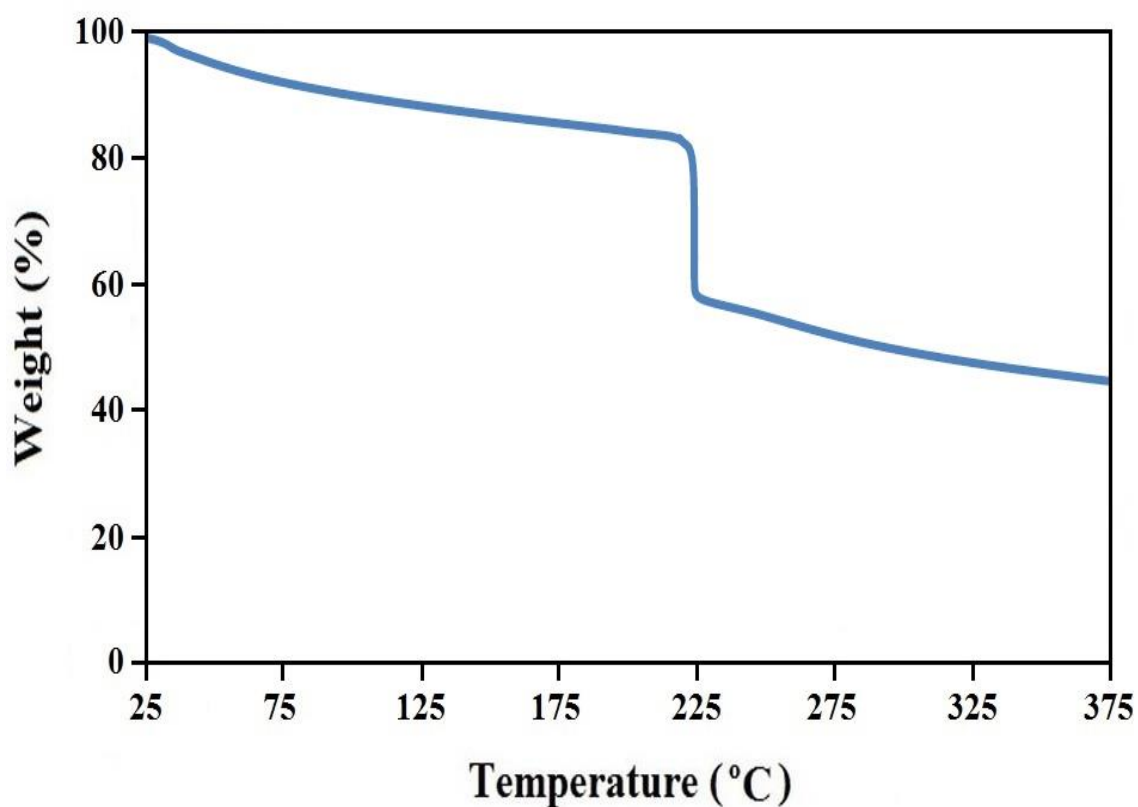


Figure 4.23: TGA results for RS-7

Figure 4.24 further shows the comparison between samples with different LiI salt content. The TGA results indicates that RS-7 with 35 wt.% of LiI shows more thermal stability compared with the other LiI concentrations. The results confirm that T_{dc} decreases with the addition of lithium iodide salt content.

In section 4.2, FTIR results confirmed that the complexation between RS and LiI at different band assignments has occurred (Khanmirzaei et al., 2013). This complexation can increase the thermal stability of RS:LiI system compared to RS without LiI (uncomplexed). This is the reason of decreasing T_{dc} with the addition of lithium iodide salt content, and reduction of rice starch content. From Figure 4.24, it is understood that pure rice starch (RS-0) has higher T_{dc} .

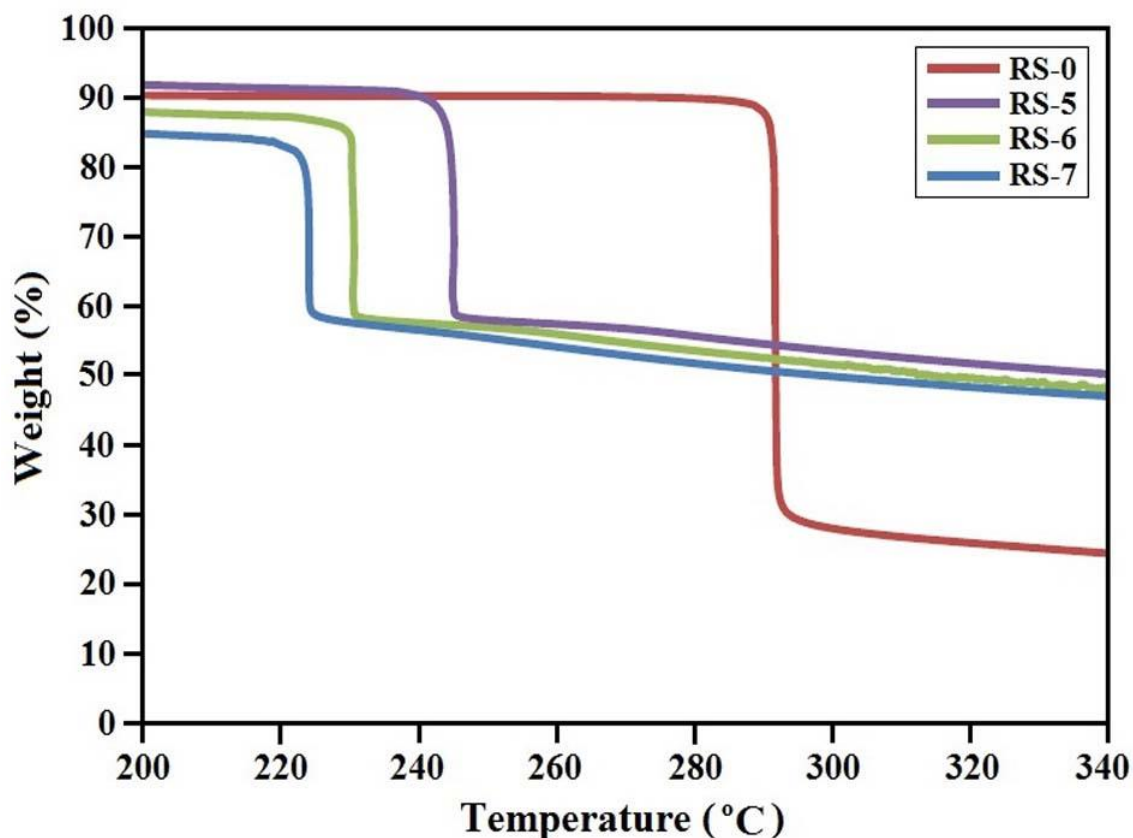


Figure 4.24: Comparison of TGA curves in RS:LiI system

In RS:NH₄I system, the SPEs in RS:NH₄I system containing RN-7, RN-8 and RN-9 were analyzed for TGA thermal analyzer. Figures 4.25, 4.26 and 4.27 show TGA results in RS:NH₄I system for RN-7, RN-8 and RN-9 SPEs, respectively.

Figure 4.28 shows the comparison between RS-0, RN-7, RN-8 and RN-9, respectively. The graph reveals that the decomposition temperature (T_{dc}) decreases dramatically from 292 °C (pure rice starch) to 187, 185 and 184 °C for RN-7, RN-8 and RN-9, respectively, after addition of NH₄I salt with one step decomposition. The lowest T_{dc} is 184 °C in RN-9 with the highest ionic conductivity in RS:NH₄I system. The shifts in T_{dc} indicate that the shift is as a result of NH₄I salt addition which further confirms complexation between RS and NH₄I salt. The T_{dc} values for RS:NH₄I system are represented in Table 4.11.

From Figure 4.28, it is observed that even though the T_{dc} values have shifted to lower temperature values, the thermal stability of SPEs incorporated with NH_4I salt is higher compared to pure rice starch (RS-0).

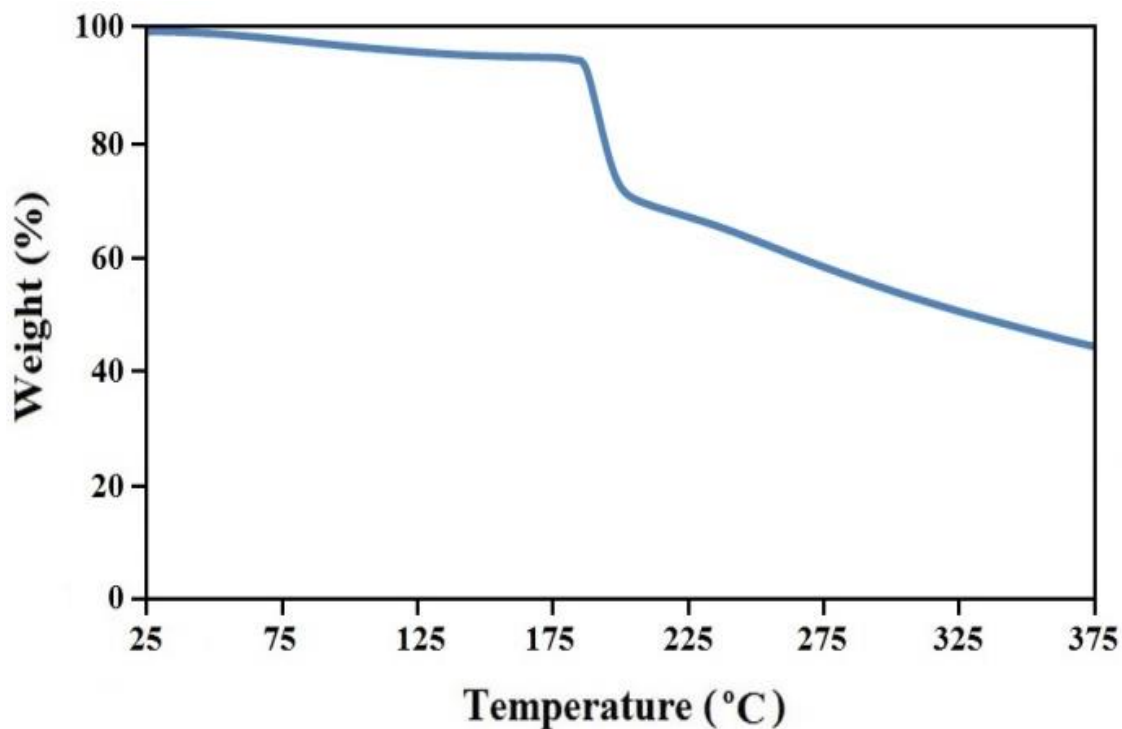


Figure 4.25: TGA results for RN-7

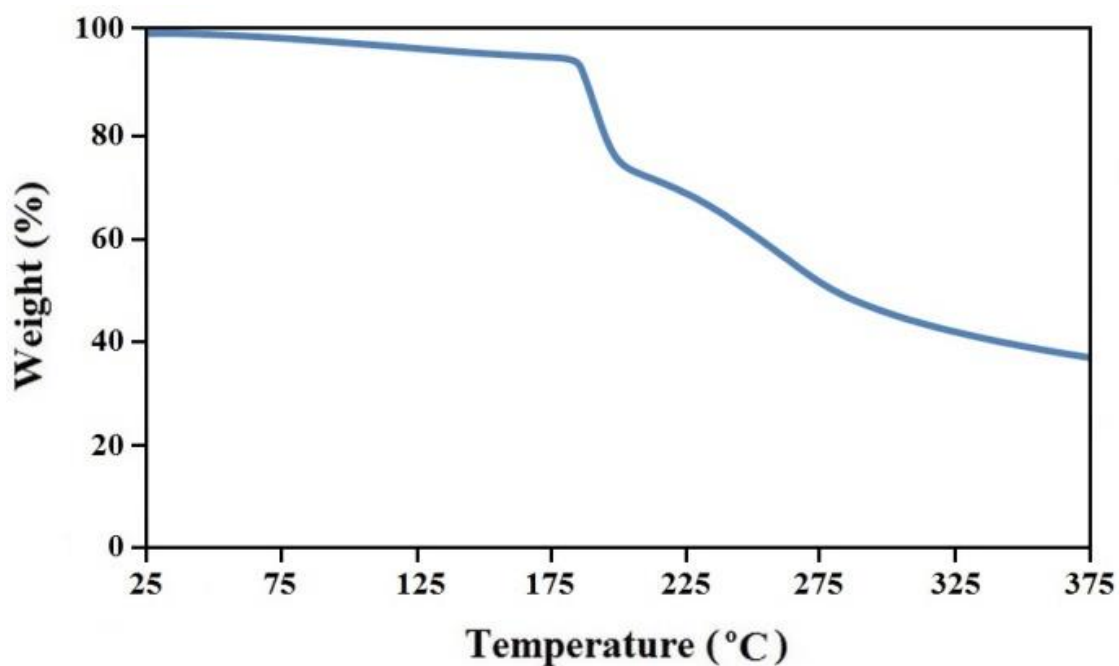


Figure 4.26: TGA results for RN-8

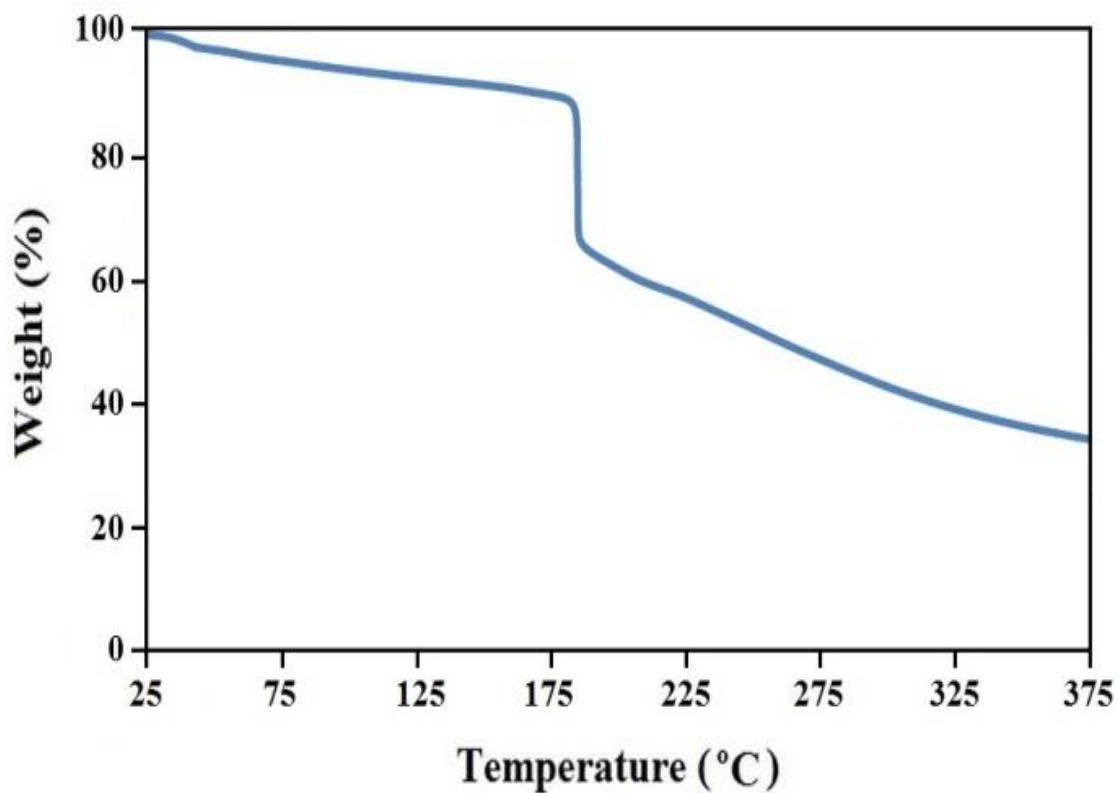


Figure 4.27: TGA results for RN-9

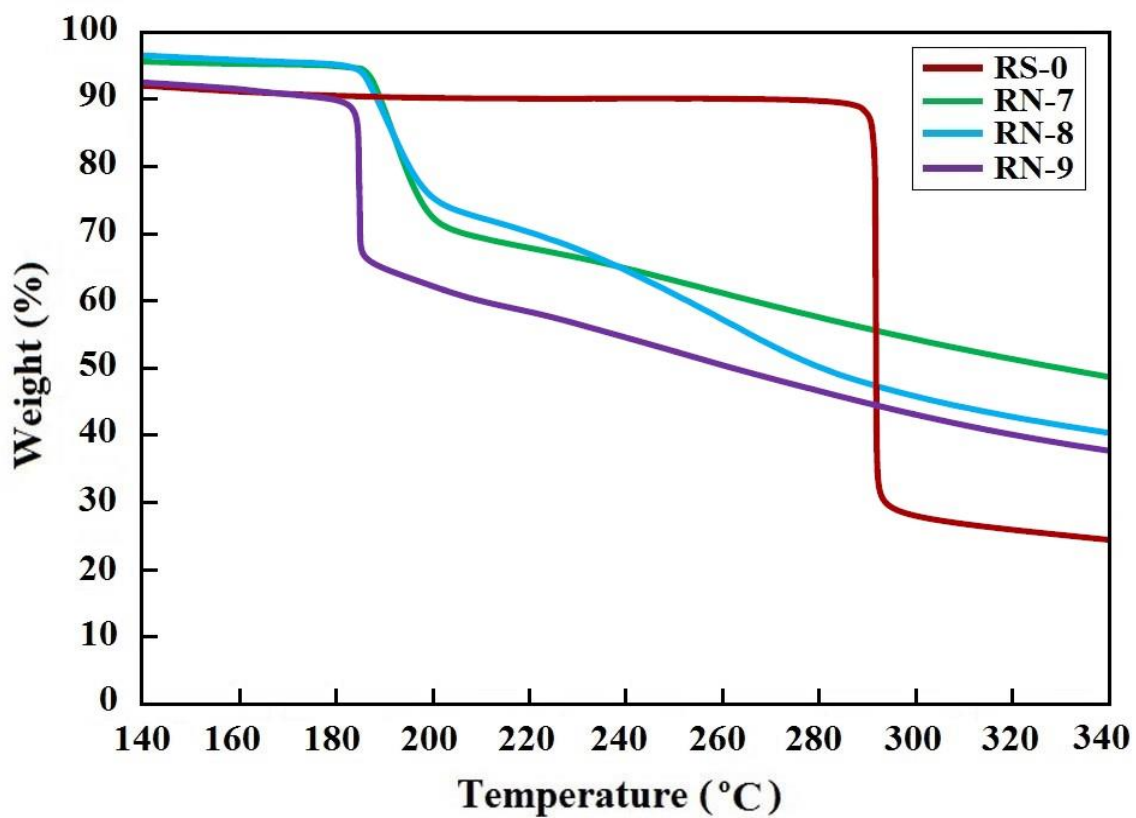


Figure 4.28: TGA thermograms of RS-0, RN-7, RN-8 and RN-9 in RS:NH₄I system

Thermal behavior of RS:NaI samples analyzed using TGA. Figures 4.29, 4.30 and 4.31 show TGA thermograms of RS:NaI system for RNa-7, RNa-8 and RNa-9. The graphs show T_{dc} decreases from 292 °C in pure rice starch to 245, 243 and 242 °C for RNa-7, RNa-8 and RNa-9, respectively, after addition of NaI salt.

The RNa-9 SPE shows the lowest T_{dc} of 242 °C with lowest weight change which indicates that RNa-9 has slightly more thermal stability compared with the RS-0, RNa-7, RNa-8 and RNa-9.

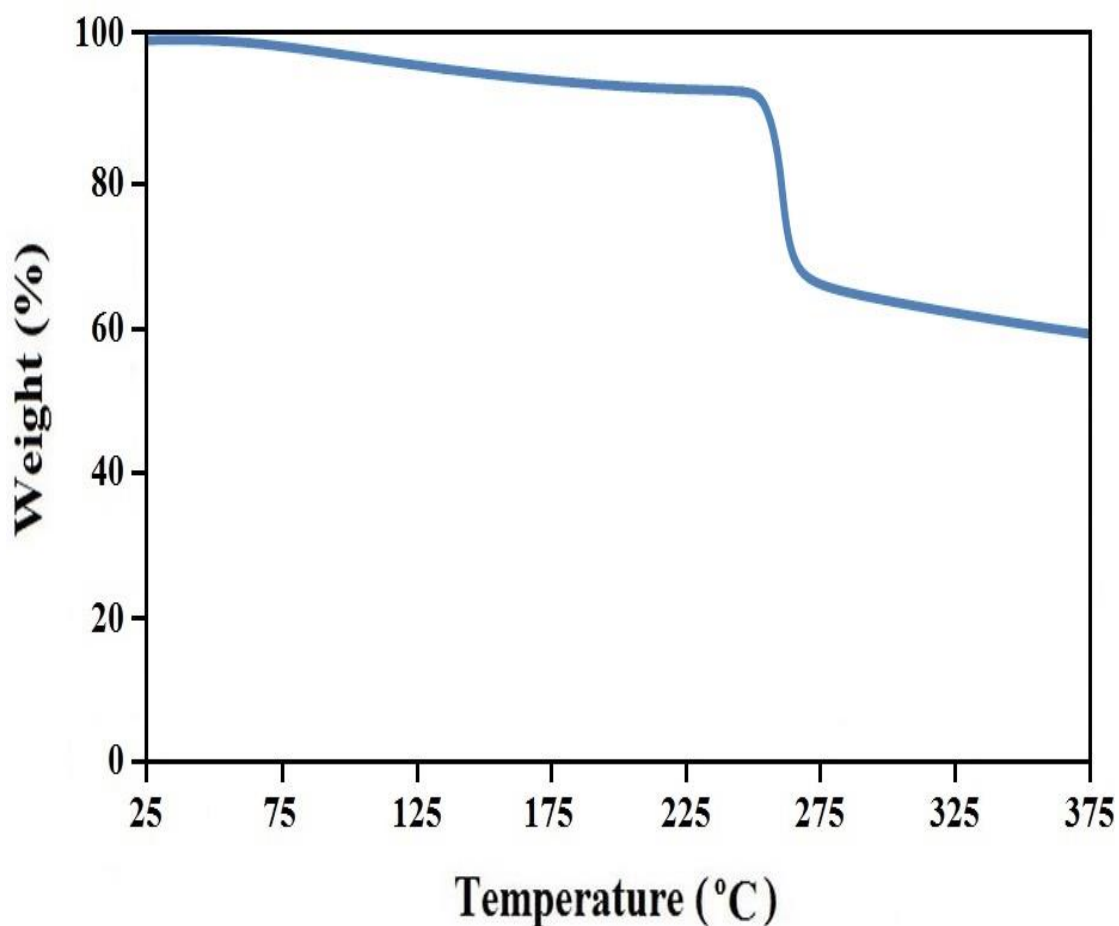


Figure 4.29: TGA thermograms of RNa-7

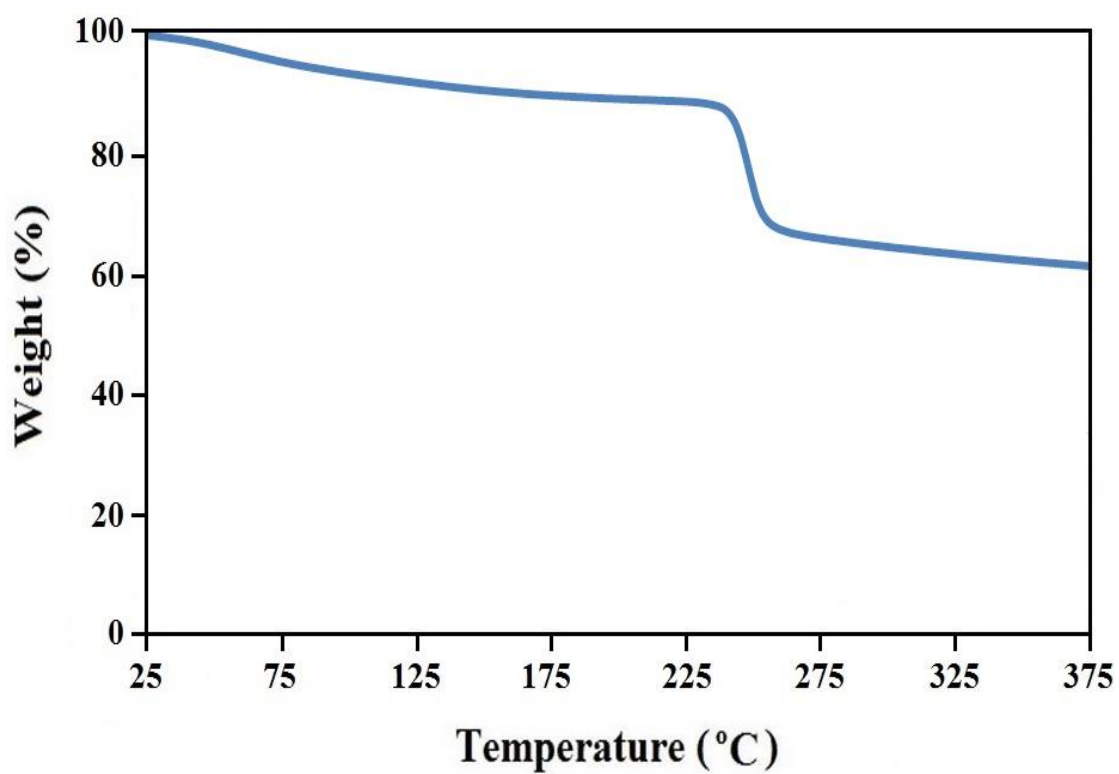


Figure 4.30: TGA thermograms of RNa-8

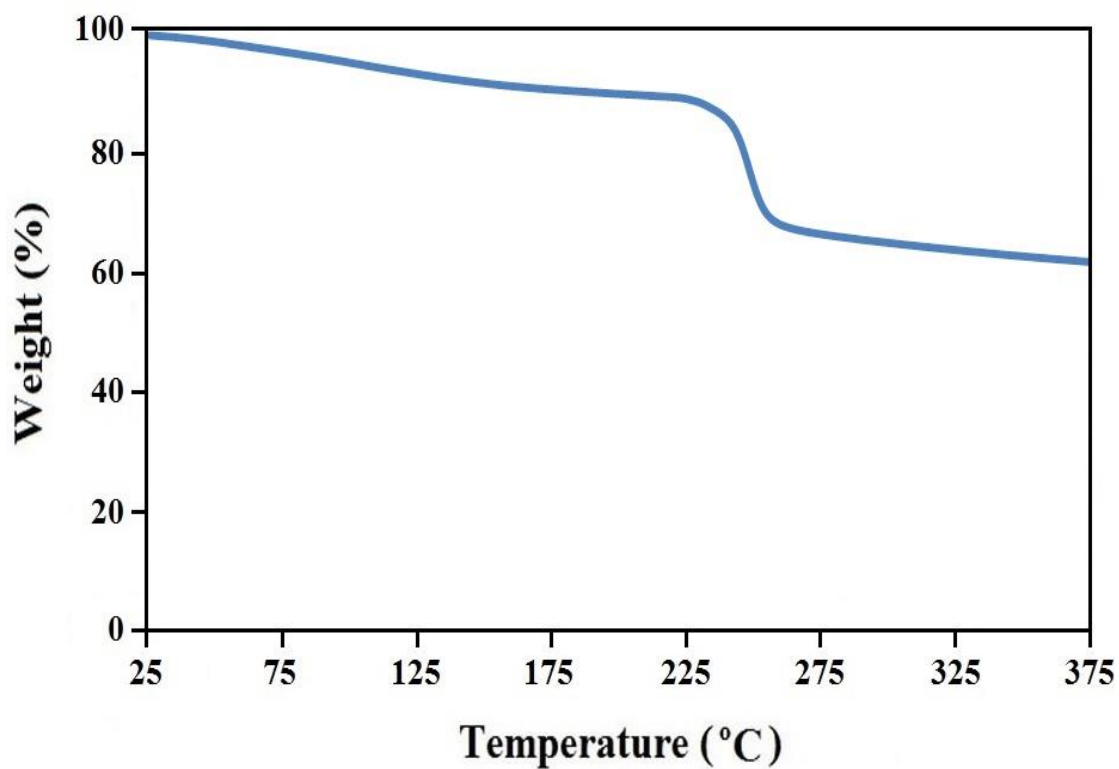


Figure 4.31: TGA thermograms of RNa-9

Figure 4.32 represents the comparison between RS-0, RNa-7, RNa-8 and RNa-9, and indicates that after addition of NaI salt the T_{dc} decrease sharply. The reason to decrease T_{dc} after addition of iodide salt can be due to complexation of rice starch and iodide salt and result in more segmental flexibility of polymeric network which can reduce the decomposition temperature of polymer electrolyte.

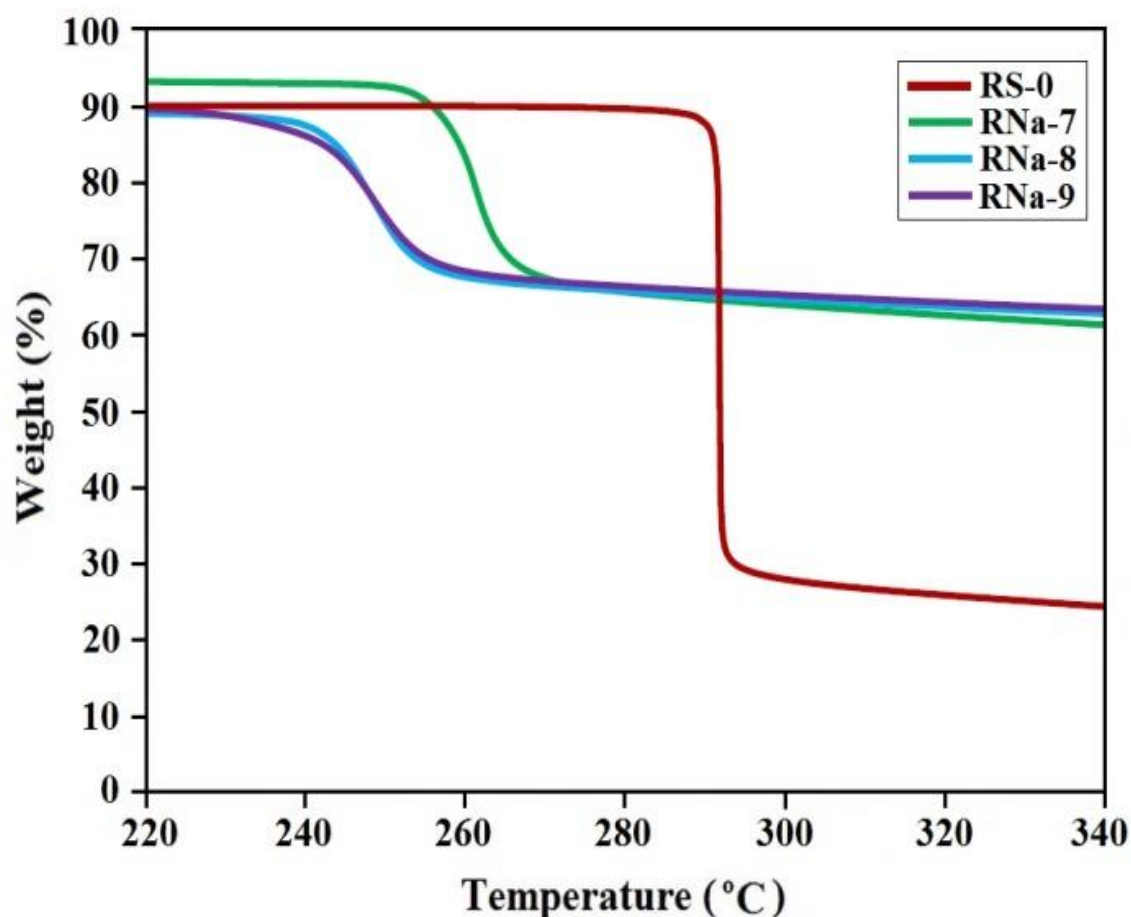


Figure 4.32: TGA thermograms for RS-0, RNa-7, RNa-8 and RNa-9 in RS:NaI system

4.6 THERMAL STUDY - DSC

The thermal properties of samples were further studied through DSC analysis. Figure 4.33 shows thermograms of samples for RS with and without the addition of salt in RS:LiI system. The results show small changes in heat flow from exothermic to endothermic which is known as glass transition temperature (T_g).

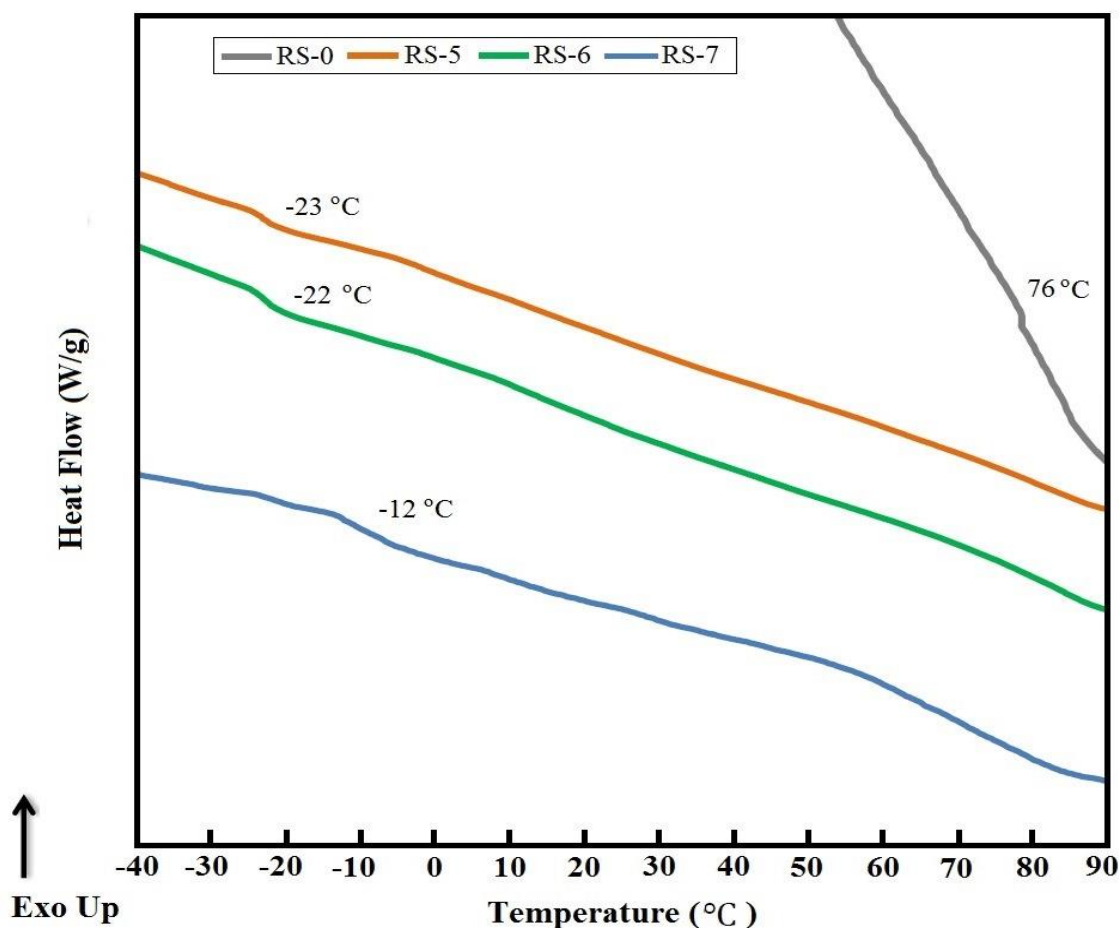


Figure 4.33: DSC thermograms of pure rice starch, RS-5, RS-6, and RS-7 polymer electrolytes

The T_g for pure rice starch is ~ 76 °C. The glass transition temperature decreases after the incorporation of LiI salt. T_g values are depicted in Table 4.10, for samples of RS-5, RS-6, and RS-7 are -23 , -22 , and -12 °C, respectively. Thermal parameters are listed in Table 4.10.

Table 4.10: TGA and DSC data for RS:LiI polymer electrolyte system

Samples	Decomposition temperature (T_{dc}) (°C)	Decomposition Steps	Glass transition temperature (T_g) (°C)
RS-0	292	Single step	76
RS-5	245	Single step	-23
RS-6	230	Single step	-22
RS-7	224	Single step	-12

The glass transition temperature decreases sharply from pure rice starch to RS-5 after addition of LiI salt. The reason can be expressed as transition of the sample from glassy state to rubbery state due to incorporation of LiI salt which results in more flexibility of the sample. The DSC results show T_g shifts to higher temperatures with increasing salt content. This is due to existing complexation with addition of salt with flexibility of polymer chains (Tominaga et al., 2005). Moreover, increase in the salt content and complexation with polymer results in the increasing number of ionic charge carriers, higher ionic conductivity, and more segmental flexibility of polymeric network due to complexation.

In RS: NH_4I system, the systems further analyzed for thermal study using DSC. The glass transition temperature (T_g) for pure rice starch is $\sim 76^\circ\text{C}$. Figure 4.34 exhibits the DSC results for RN-7, RN-8 and RN-9. The graph reveals that T_g values for samples of RN-7, RN-8 and RN-9 are -40 , -39 and -38°C , respectively.

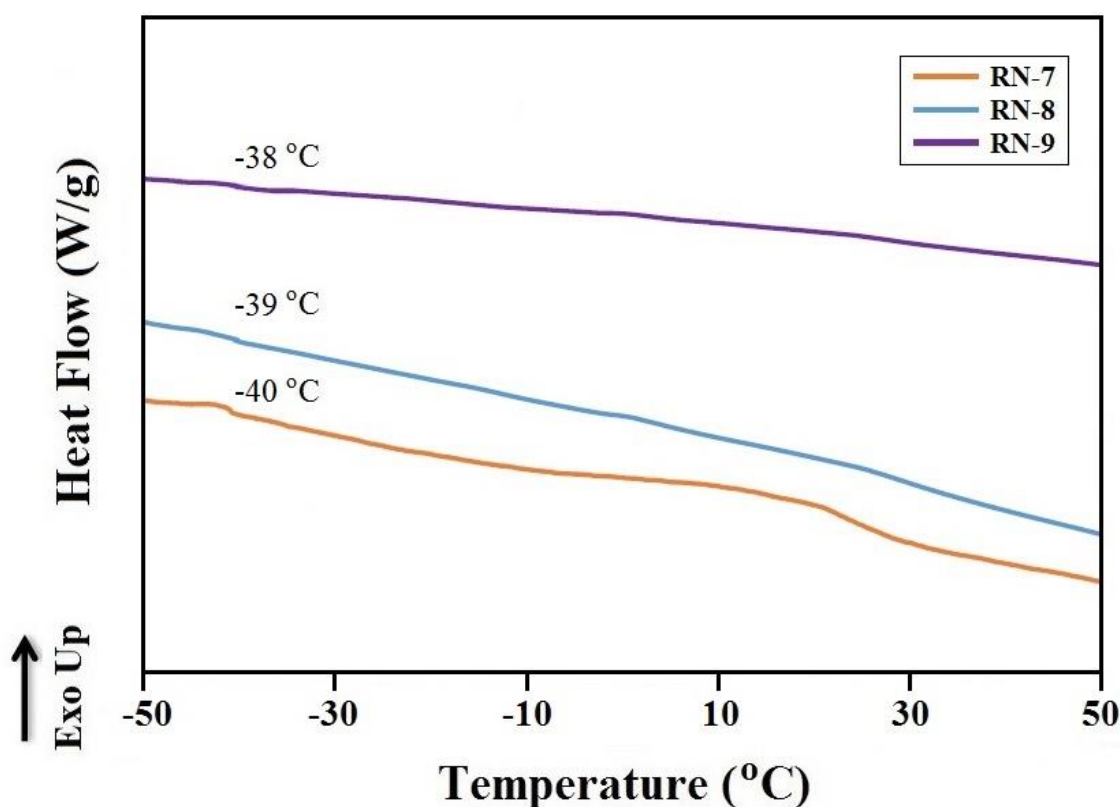


Figure 4.34: DSC thermograms of RN-7, RN-8, and RN-9 polymer electrolytes

The DSC results show that T_g shifts to higher temperatures with increasing iodide salt. This is due to existing complexation with addition of salt with flexibility of polymer chains (Tominaga et al., 2005). Another reason can be dissociation of ions which may act as transient cross-linking points in the polymer electrolyte (Nishimoto et al., 1999). The DSC thermal parameters are depicted in Table 4.11.

Table 4.11: TGA and DSC data for RS:NH₄I polymer electrolyte system

Samples	Decomposition temperature (T_{dc}) (°C)	Decomposition Steps	Glass transition temperature (T_g) (°C)
RS-0	292	Single step	76
RN-7	187	Single step	-40
RN-8	185	Single step	-39
RN-9	184	Single step	-38

The T_g value decreases sharply from pure rice starch to RN-7 after addition of NH₄I salt which is due transition of the sample from glassy state to rubbery state resulting in more flexibility of the sample.

Furthermore, thermal study on polymer electrolytes further confirm complexation of pure rice starch with iodide salt and results in changing thermal properties after addition of iodide salts.

In RS:NaI system, the RS:NaI system further analyzed for thermal study using DSC. The glass transition temperature (T_g) for pure rice starch is ~76 °C. After addition of salt, glass transition temperature decreases. Figure 4.35 exhibits DSC thermograms for RNa-7, RNa-8 and RNa-9, respectively. Consequently, in RS:NaI system, T_g for RNa-7, RNa-8 and RNa-9 are -43, -43 and -42 °C, respectively.

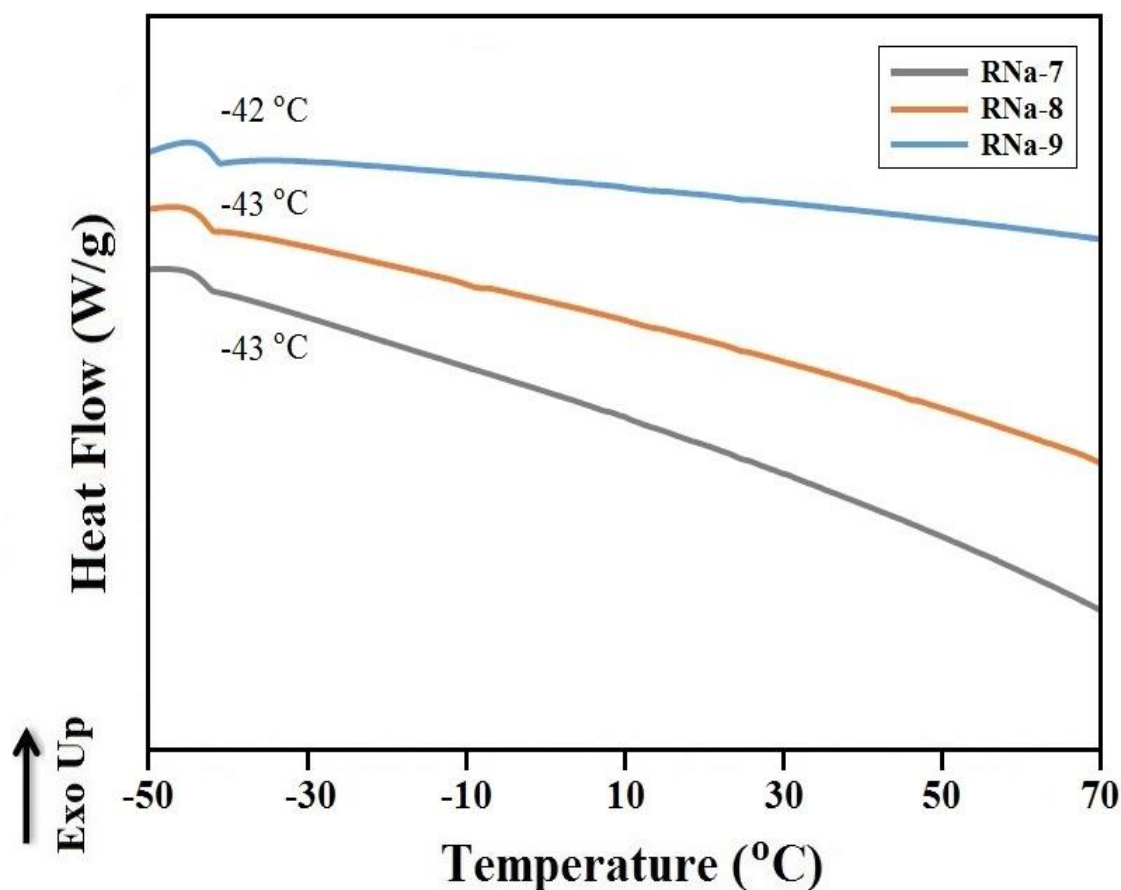


Figure 4.35: DSC thermograms of RNA-7, RNA-8, and RNA-9 polymer electrolytes

The results show that T_g shifts to higher temperatures with the addition of NaI salt. This is due to existing complexation with addition of salt with increasing the flexibility of polymer chains (Tominaga et al., 2005). Moreover, T_g increases with increasing iodide salt concentration, and resulting in increase of mobile ions and ionic conductivity. Therefore, the increase in the T_g can be attributed to dissociated ions, which may act as transient cross-linking points in the polymer electrolytes, and also decreases segmental motion of the matrix polymer, which directly reduces the ionic mobility (Nishimoto et al., 1999). In conclusion, thermal study on polymer electrolytes further confirm complexation of pure rice starch with iodide salt and results in changing thermal properties after addition of iodide salts. The thermal parameters are depicted in Table 4.12.

Table 4.12: TGA and DSC data for RS:NaI polymer electrolyte system

Samples	Decomposition temperature (T_{dc}) ($^{\circ}\text{C}$)	Decomposition Steps	Glass transition temperature (T_g) ($^{\circ}\text{C}$)
RS-0	292	Single step	76.00
RNa-7	245	Single step	-43 (-43.41)
RNa-8	243	Single step	-43 (-43.31)
RNa-9	242	Single step	-42

4.7 J-V CHARACTERISTICS

DSSC study was not conducted for the first two systems, due to low ionic conductivity, which results in low conversion energy and no significant performance of DSSC. Among the all first three systems, RNa-9 exhibited the highest ionic conductivity, and was used to fabricate DSSC. The J-V characteristic curve of fabricated Dye sensitized solar cell using RNa-9 with N719 dye is illustrated in Figure 4.36.

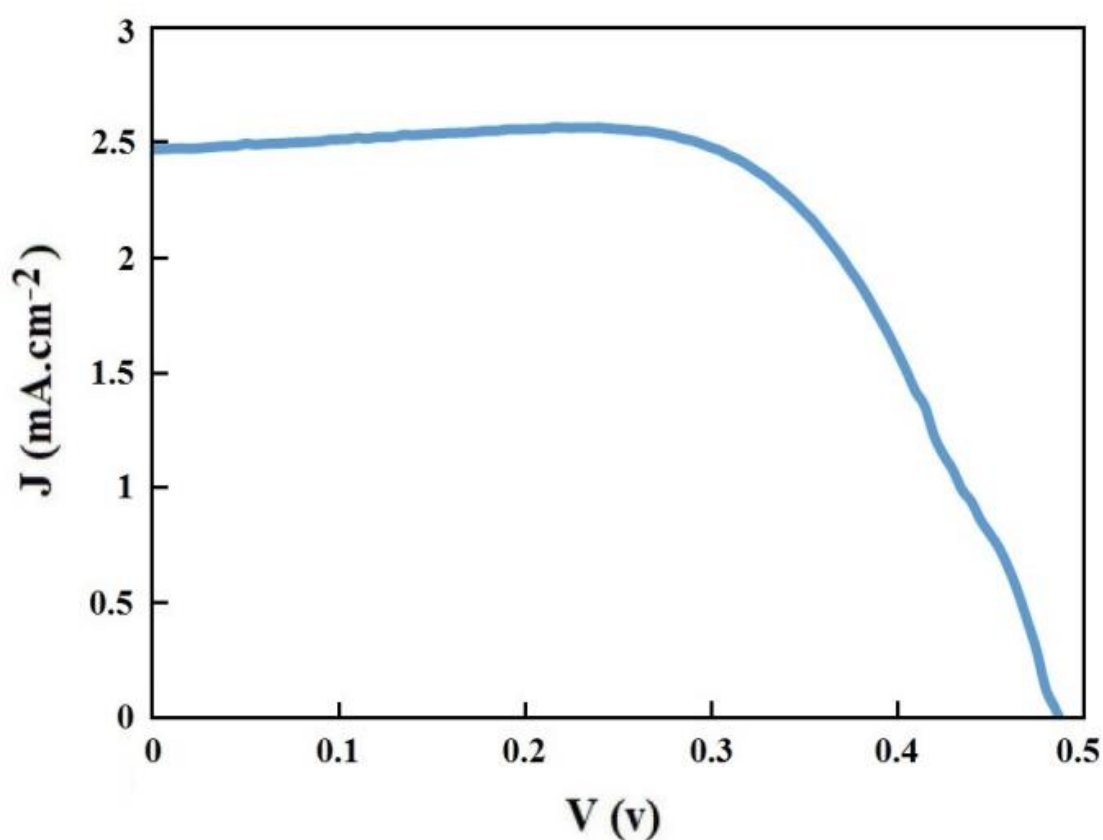


Figure 4.36: Photocurrent density versus cell potential (J-V) for DSSC fabricated using RNa-9

The DSSC cell was analyzed under Sun simulator with light power of 100 mW/cm^2 . DSSC parameters of J_{sc} , V_{oc} , ff and η in the RNa-9 based DSSC are $2.40 \text{ (mA cm}^{-2}\text{)}$, 0.485 (V) , 0.67 and 0.78 (\%) , respectively. Among the polymer electrolyte based DSSCs using biodegradable polymers, (R. Singh et al., 2013), achieved 0.54 \% with composition of Agarose:KI polymer electrolyte based DSSC. Subsequently, (R. Singh, et al., 2014) achieved efficiency of 0.63 \% with composition of Arrowroot Starch:KI polymer electrolyte based DSSC. This study shows enhanced energy conversion efficiency of 0.78 \% compared with some other studies performed recently using the biodegradable polymers.

4.8 SUMMARY

The results and discussion for first three systems, RS:LiI, RS:NH₄I and RS:NaI, expressed in this chapter. The results related to characterizations are demonstrated and discussed. The RNa-9 SPE in RS:NaI system represented the highest ionic conductivity among all the first three systems. The structural and thermal studies confirmed complexation between rice starch and LiI, NH₄I and NaI salts. The fabricated DSSC using RNa-9 showed the energy conversion efficiency of 0.78 \% . The following chapter will focus on last two systems incorporated with MP11 and HM11 ionic liquids. The results and discussion on two ionic liquid based systems will be elaborated and fabricated DSSCs using all ionic liquid based samples will be demonstrated.

CHAPTER 5

RESULTS AND DISCUSSION ON SYSTEMS BASED ON TWO DIFFERENT IONIC LIQUIDS

5.1 INTRODUCTION

The RS:NaI:MPII and RS:NaI:HMII systems incorporated with NaI, and MPII and HMII ionic liquids are discussed in this chapter. Results and discussion would be on ionic conductivity, structural, thermal and DSSC studies using EIS, FTIR, XRD, TGA, DSC and J-V analysis. The RNa-9 SPE from RS:NaI system which achieved the highest ionic conductivity was incorporated with MPII and HMII ionic liquids to enhance the ionic conductivity to further enhance the DSSC performance.

5.2 EIS CHARACTERIZATION

The SPEs in two ionic liquid based systems were examined using EIS for ionic conductivity and temperature-dependent ionic conductivity study. The results have been discussed in two sections namely 5.2.1 and 5.2.2.

5.2.1 IONIC CONDUCTIVITY

The solid polymer electrolytes in RS:NaI:MPII system were analyzed using EIS. Figure 5.1 shows Cole-Cole plot of RNaP-1, RNaP-2, RNaP-3. The graph shows small bulk resistances compared with the first three systems without ionic liquid. R_b values for SPEs in RS:NaI:MPII system are expressed in Table 5.1.

Table 5.1: Bulk resistance values in RNaP system

Designation	RS:NaI:MPII (wt.%)	Bulk resistance, R_b (Ω)
RNaP-1	52.25:42.75:5	8.67
RNaP-2	49.50:40.50:10	5.94
RNaP-3	46.75:38.25:15	5.33
RNaP-4	44.00:36.00:20	5.37

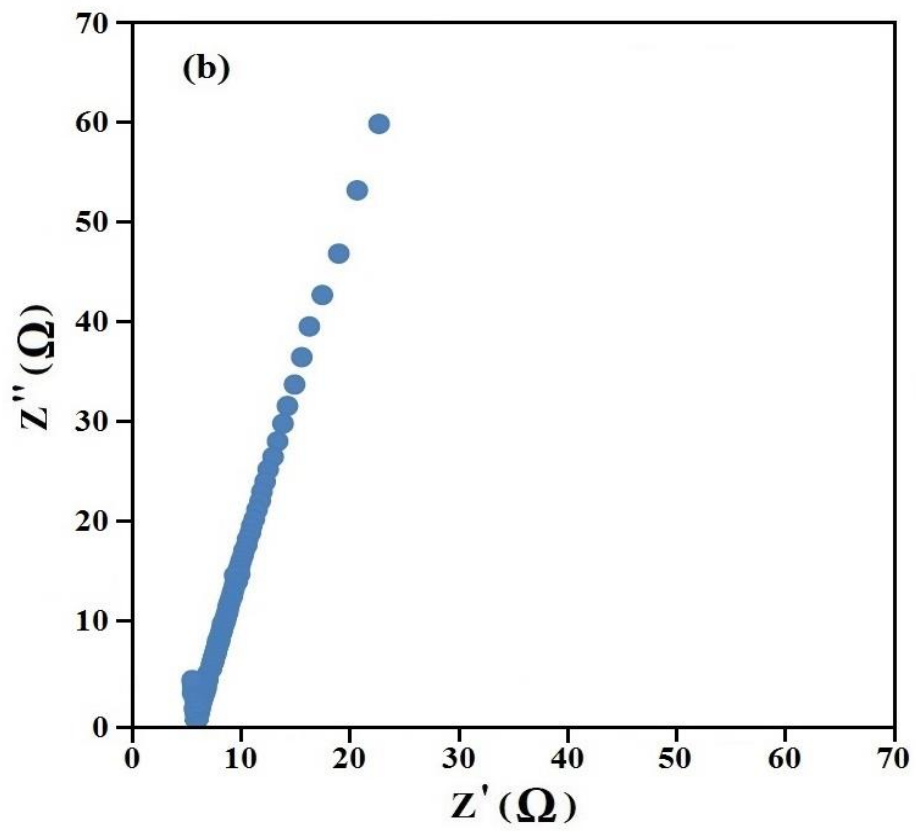
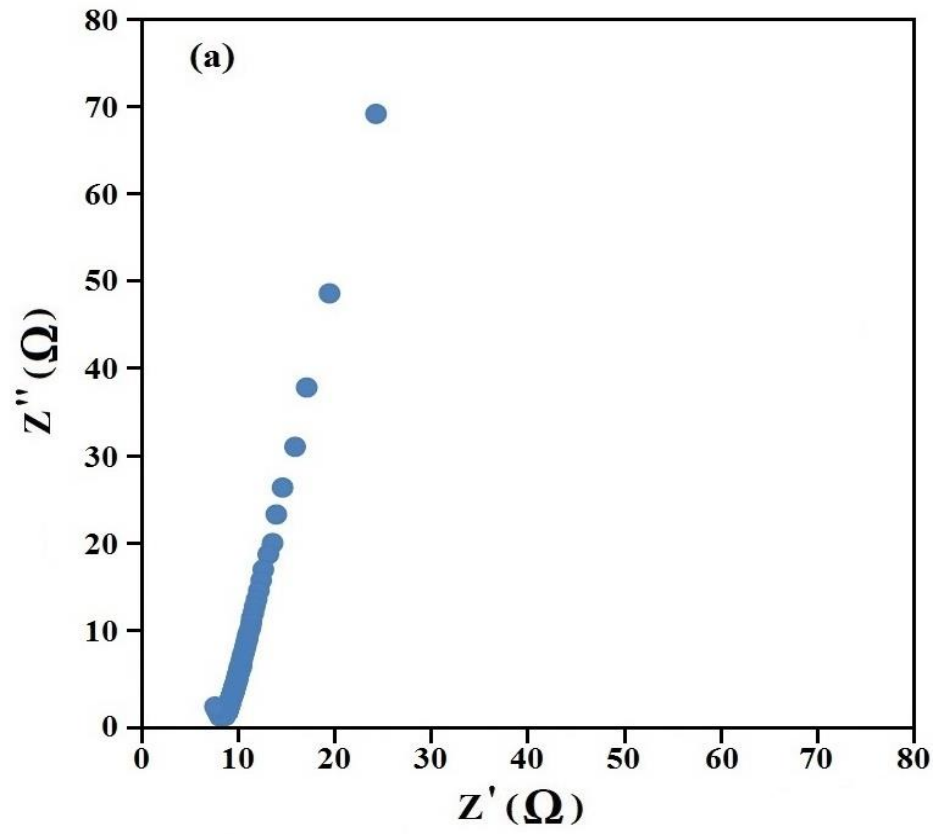
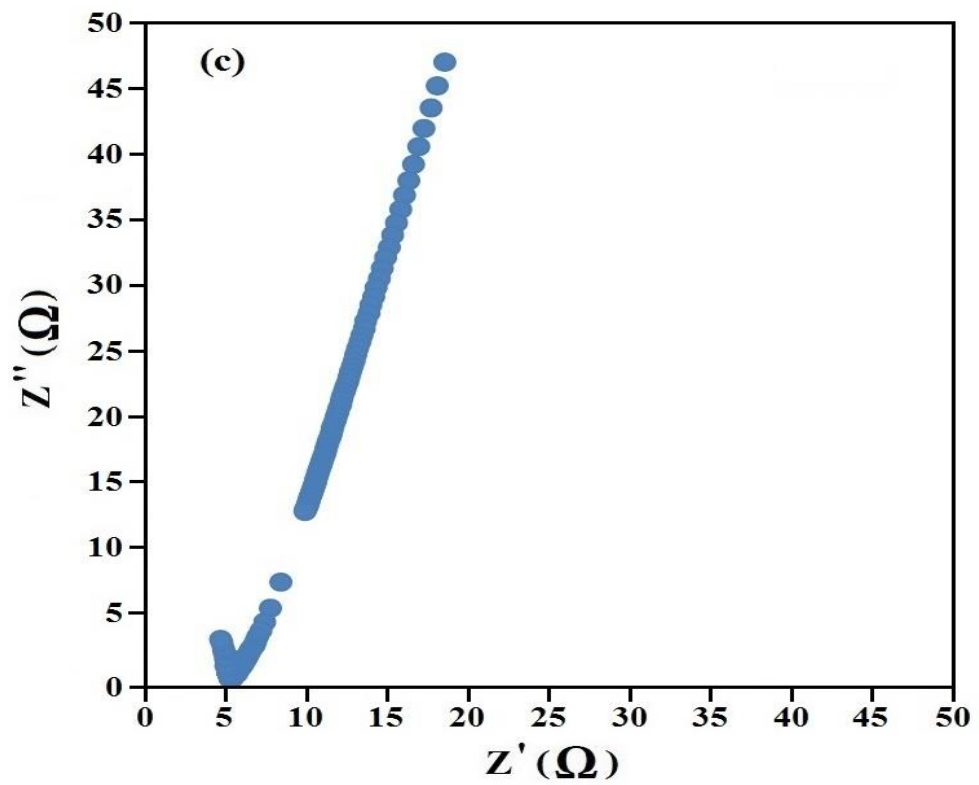


Figure 5.1: Cole-Cole plot of (a) RNaP-1, (b) RNaP-2 and (c) RNaP-3



‘Figure 5.1, continued’

The R_b increases with the addition of MPII ionic liquid content. Figure 5.2 exhibits RNaP-4 with 20 wt.% of MPII with the lowest bulk resistance in RS:NaI:MPII system.

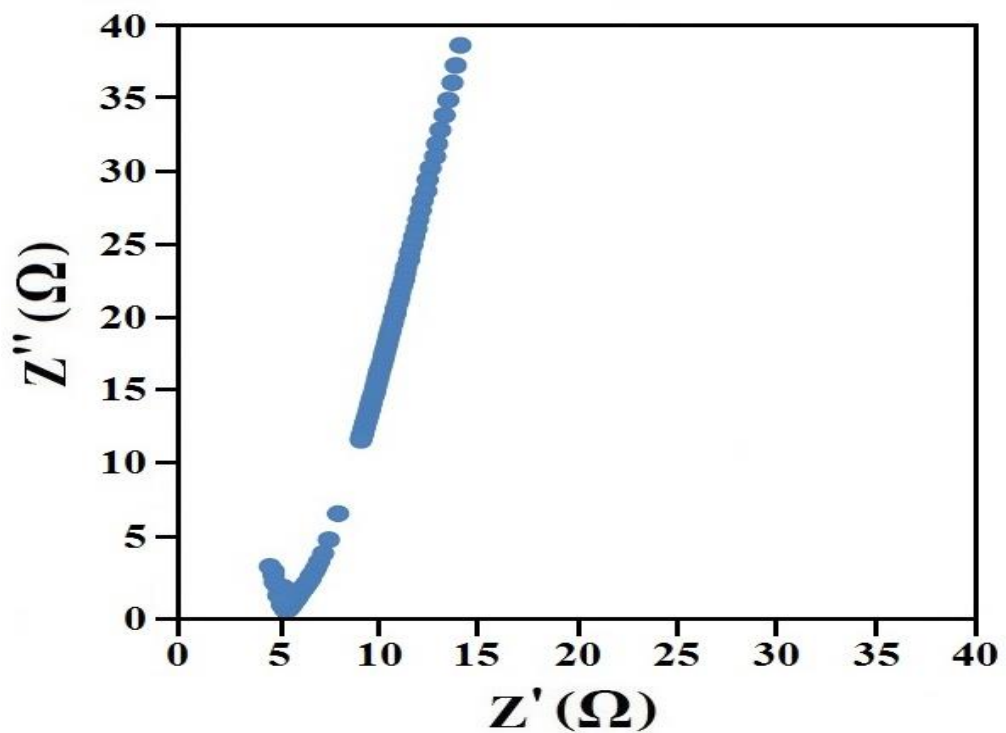


Figure 5.2: Cole-Cole plot for RNaP-4

The ionic conductivities were determined using EIS data. The highest ionic conductivity of 1.20×10^{-3} (S cm⁻¹) in RNaP-4 was achieved after addition of 20 wt.% of MPII ionic liquid. The ionic conductivities of all samples are inserted in Table 5.2.

Table 5.2: Designation and ionic conductivity of RS:NaI:MPII solid polymer electrolyte system

Designation	RS:NaI:MPII composition (wt.%)	MPII ionic liquid (g)	Conductivity, σ (S cm⁻¹)
RNa-9	55.00:45.00:0	0	4.79×10^{-4}
RNaP-1	52.25:42.75:5	0.1	5.81×10^{-4}
RNaP-2	49.50:40.50:10	0.2	7.12×10^{-4}
RNaP-3	46.75:38.25:15	0.3	9.88×10^{-4}
RNaP-4	44.00:36.00:20	0.4	1.20×10^{-3}

Figure 5.3 demonstrates the variation of ionic conductivity with the addition of MPII ionic liquid. Figure 5.3 indicates that the ionic conductivity increases with the addition of MPII. This is due to the increase of mobile ions after incorporation and addition of MPII ionic liquid. On the other hand, this is due to the high self-dissociating and ion-transporting abilities of the constituent ionic liquid, its conductivity increases with the carrier numbers in the polymer electrolytes. Besides that, the increase of the amount of the ionic liquid weakens the interaction among the polymer chains, accelerates the decoupling of the ion transport from polymer segmental motion (Jiang et al., 2006). There is a sharp increase in ionic conductivity after addition of MPII ionic liquid. The reason may be explained as the mobile ions movement is through the ionic liquid which has higher mobility compared with RS as a host.

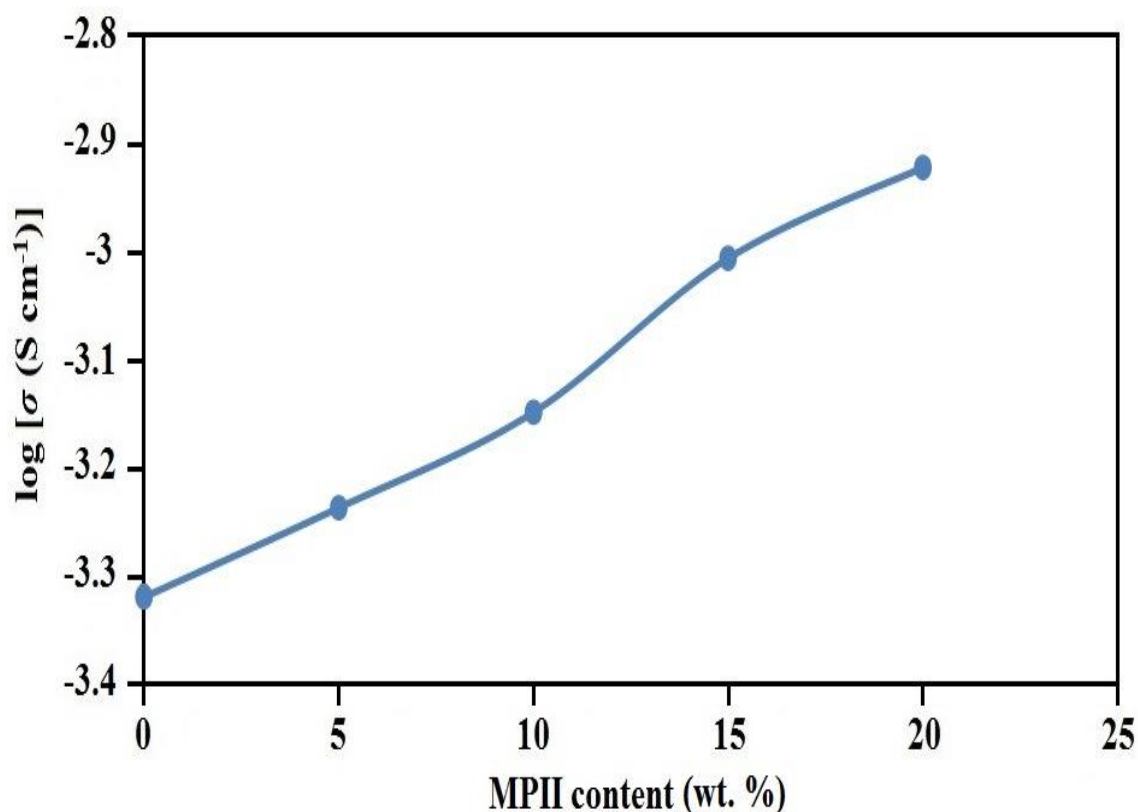


Figure 5.3: Variation of Ionic conductivity with MPII ionic liquid content

In RS:NaI:HMII system, the ionic conductivity is studied using EIS data. Figure 5.4 illustrates Cole-Cole plot of (a) RNaH-1, (b) RNaH-2 and (c) RNaH-3. The Figure shows significance decrease of bulk resistance (R_b) after incorporation of HMII ionic liquid compared with the three systems without ionic liquid. Furthermore, Figure 5.5 exhibits Cole-Cole plot for RNaH-4 with the lowest R_b in RS:NaI:HMII system with incorporation of 20 wt.% HMII ionic liquid. Table 5.3 shows R_b values for SPEs in RS:NaI:HMII system.

Table 5.3: Bulk resistance values as EIS data for RNaH system

Designation	RS:NaI:HMII (wt.%)	Bulk resistance, R_b (Ω)
RNaH-1	52.25:42.75:5	11.6
RNaH-2	49.5:40.5:10	5.89
RNaH-3	46.75:38.25:15	6.71
RNaH-4	44.00:36.00:20	2.66

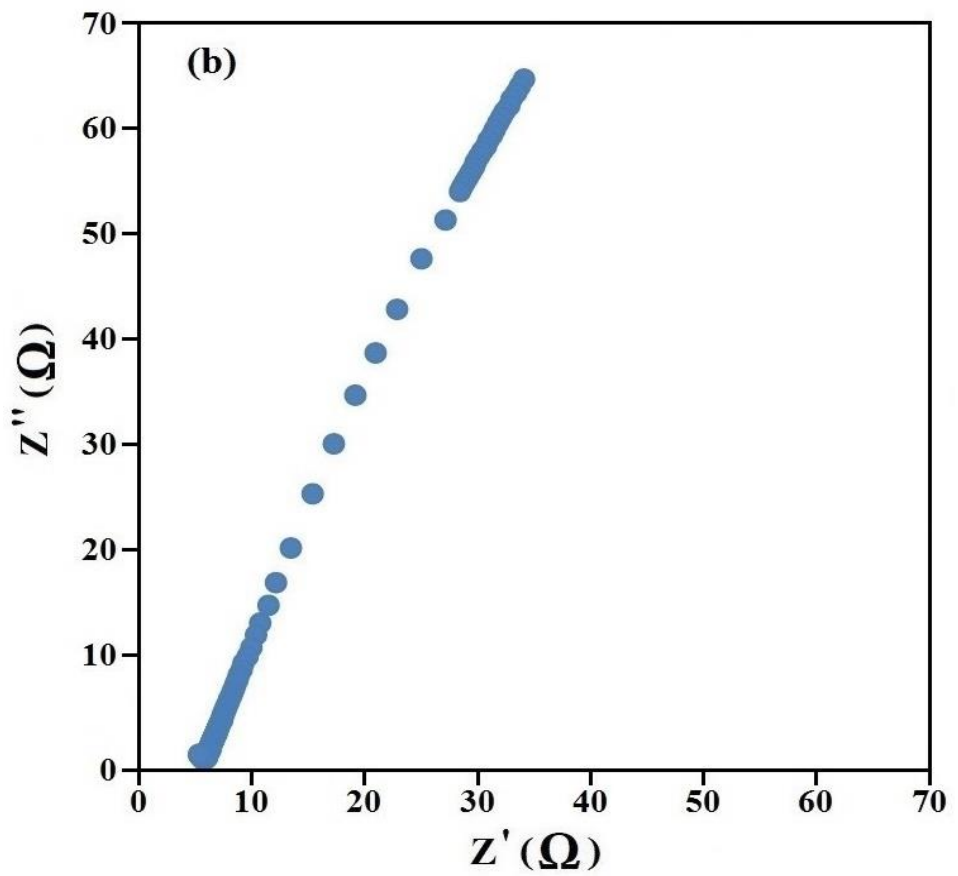
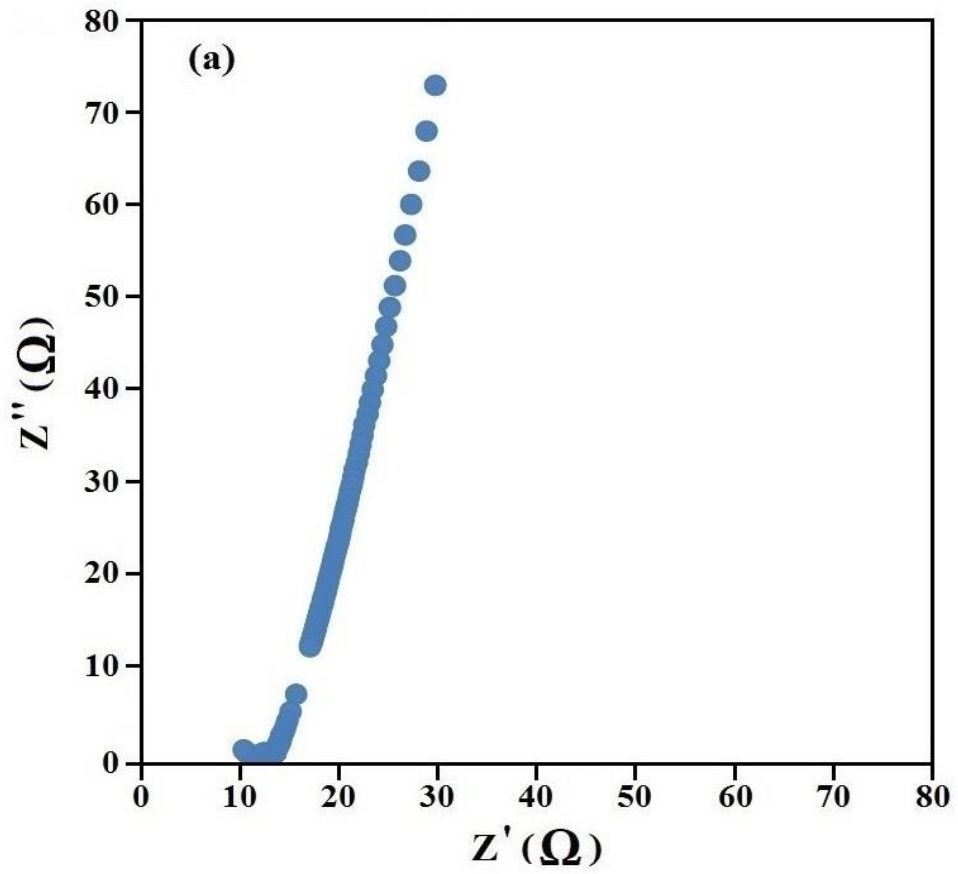
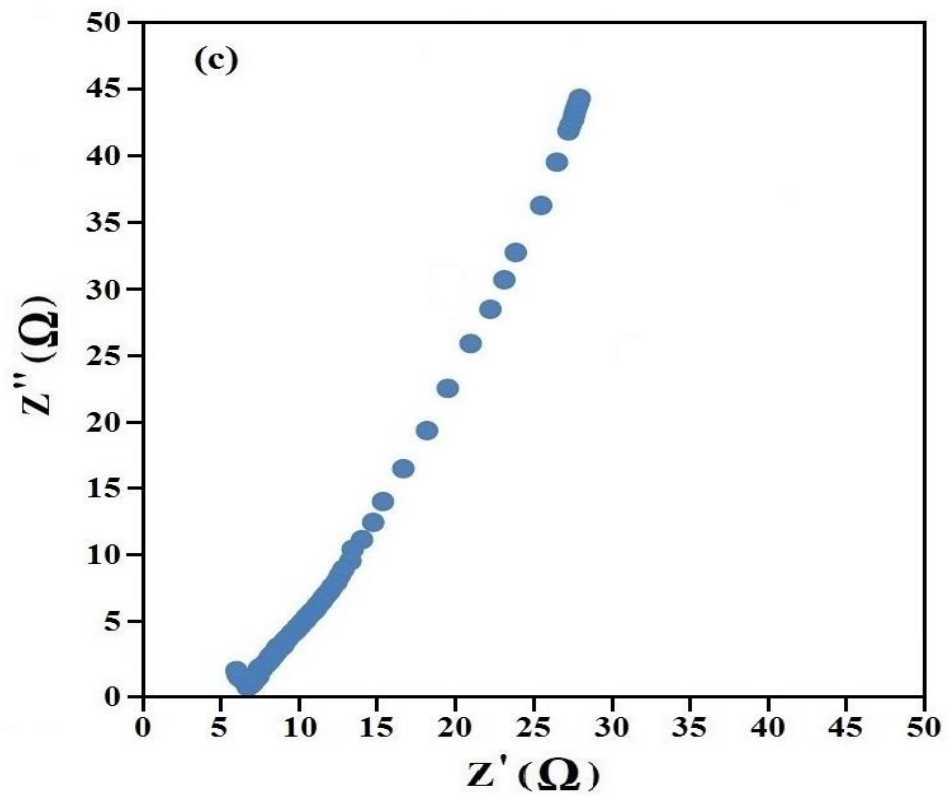


Figure 5.4: Cole-Cole plot of (a) RNaH-1 (b) RNaH-2 and (c) RNaH-3



'Figure 5.4, continued'

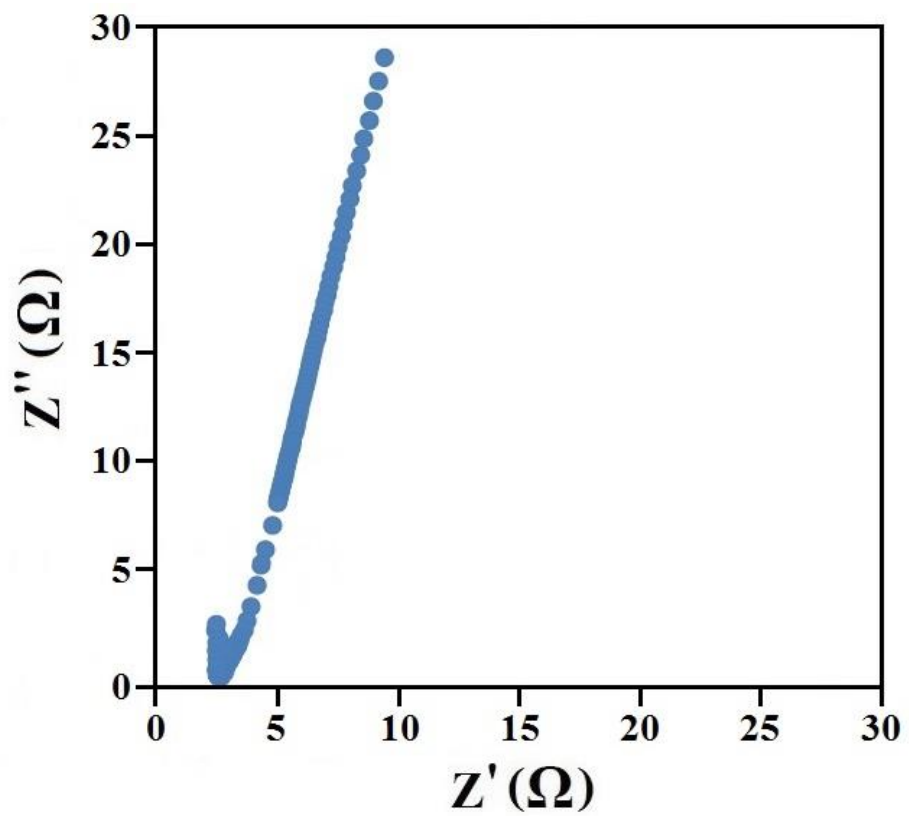


Figure 5.5: Cole-Cole plot for RNaH-4

The ionic conductivity measured using EIS data. Table 5.4 shows the ionic conductivity value for all the samples in the RS:NaI:HMII solid polymer electrolyte system.

RNaH-4 SPE showed the highest room temperature ionic conductivity among all the five different SPE systems in this study. The ionic conductivity value was found to be 1.83×10^{-3} (S cm⁻¹).

Table 5.4: Designation and ionic conductivity of RNaH polymer electrolyte systems

Designation	RS:NaI:HMII composition (wt.%)	HMII ionic liquid (g)	Conductivity, σ (S cm⁻¹)
RNa-9	55.00:45.00	0	4.79×10^{-4}
RNaH-1	52.25:42.75:5	0.1	5.18×10^{-4}
RNaH-2	49.50:40.50:10	0.2	8.03×10^{-4}
RNaH-3	46.75:38.25:15	0.3	1.03×10^{-3}
RNaH-4	44.00:36.00:20	0.4	1.83×10^{-3}

Figure 5.6 illustrates that the ionic conductivity increases upon addition of HMII due to the increase of mobile ions after incorporation of HMII due to higher self-dissociation of HMII ionic liquid as mentioned earlier for MPII based SPEs. The results show that there is a dramatic increase in ionic conductivity with the addition of 20 wt.% of HMII.

5.2.2 TEMPERATURE-DEPENDENT IONIC CONDUCTIVITY

The temperature-dependent ionic conductivity study was carried out for RS:NaI:MPII system. Figure 5.7 shows the temperature-dependent results for RNaP-1, RNaP-2, RNaP-3 and RNaP-4.

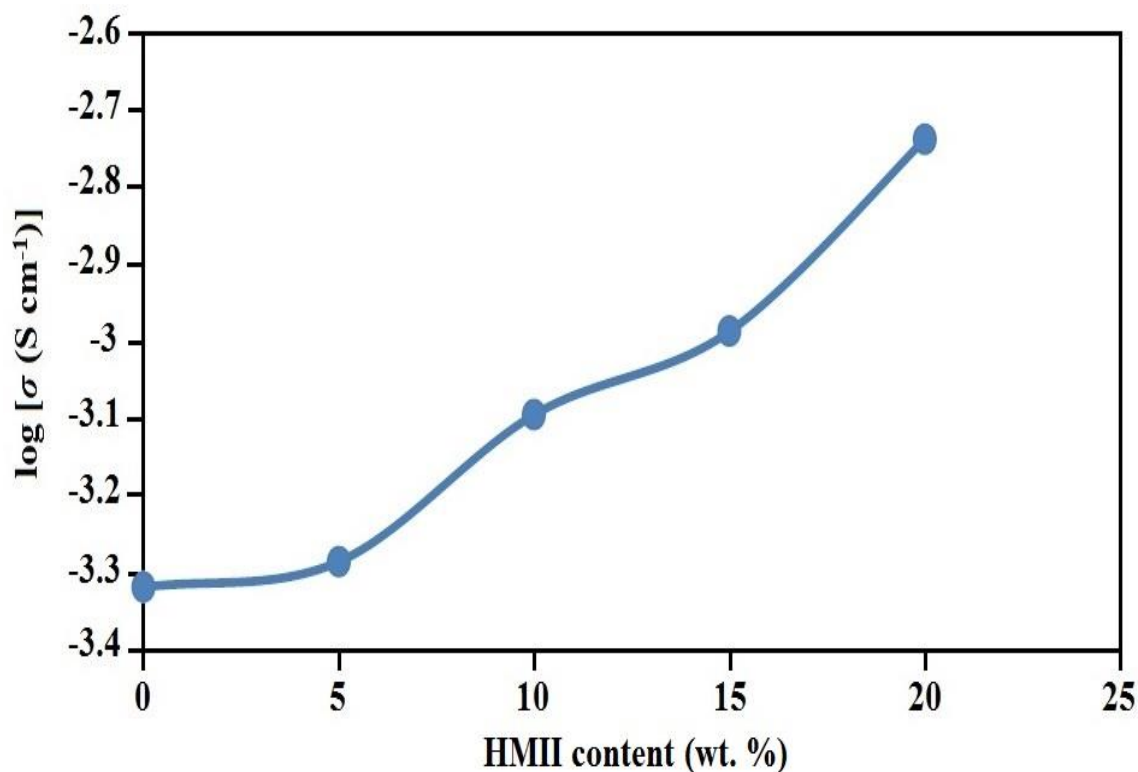


Figure 5.6: Variation of Ionic conductivity with HMII ionic liquid content

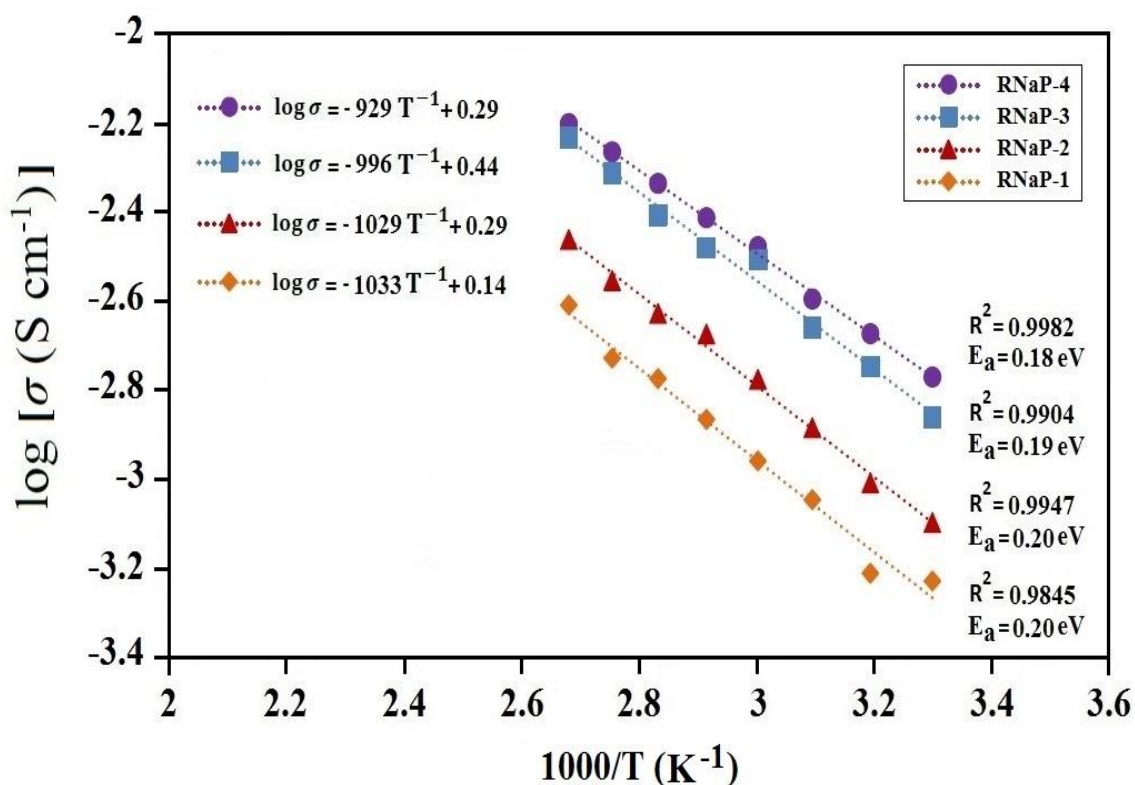


Figure 5.7: Temperature-dependent ionic conductivity results for RNaP-1, RNaP-2, RNaP-3 and RNaP-4

The regression values in graph shows all SPEs follow almost straight line, and then according to Equation (3.40), the RS:NaI:MPII system follows thermal activated model. The activation energies for RNaP-1, RNaP-2, RNaP-3 and RNaP-4 are 0.200, 0.207, 0.199 and 0.181 eV, respectively.

In RS:NaI:HMII system, temperature-dependent ionic conductivity of SPEs was studied. Figure 5.8 exhibits temperature-dependent ionic conductivity results for RNaH-1, RNaH-2 and RNaH-4.

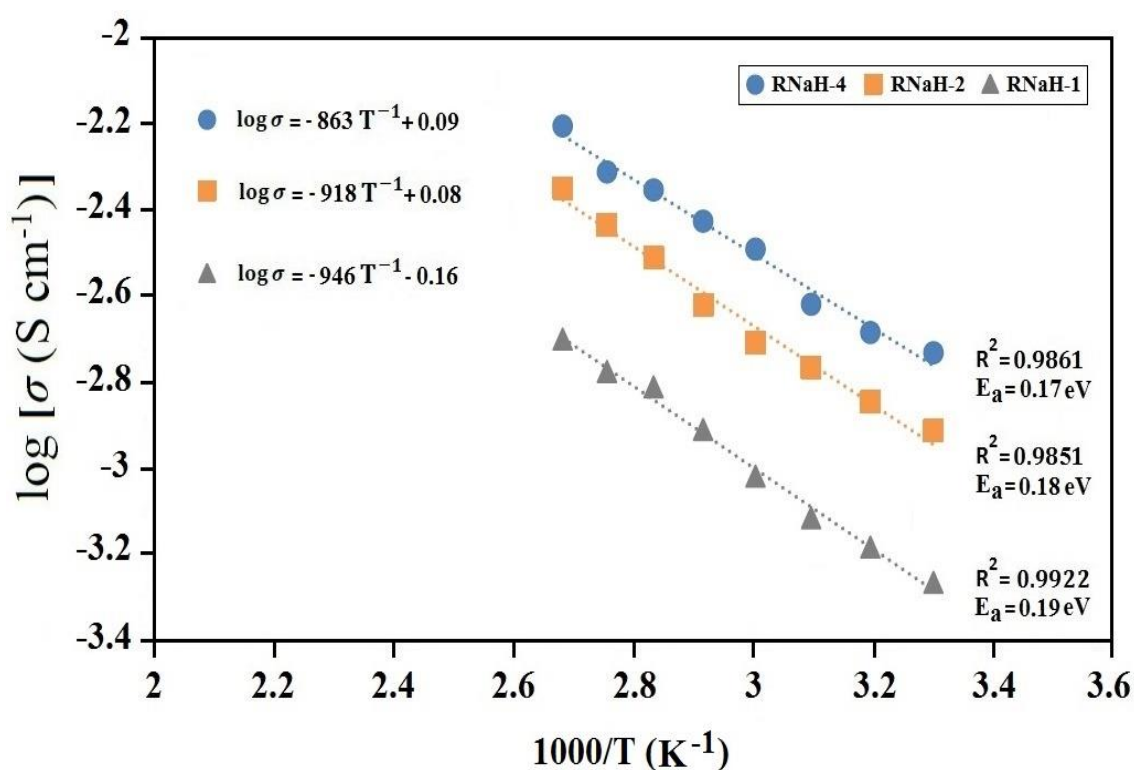


Figure 5.8: Temperature-dependent ionic conductivity of RS:NaI:HMII system

The regression values ($R^2 \sim 0.99$) show that the system follows Arrhenius thermal activated model. The activation energies calculated for RNaH-1, RNaH-2 and RNaH-4 are 0.19, 0.18 and 0.17, respectively. The results show that the activation energy decreases with increase of ionic conductivity which can be explained and expected according to Arrhenius relation in Equation (3.40).

5.3 FTIR CHARACTERIZATION

The FTIR spectra of RS:NaI:MPII solid polymer electrolyte system are represented in Figure 5.9 with wavenumbers between 4000 and 600 cm^{-1} .

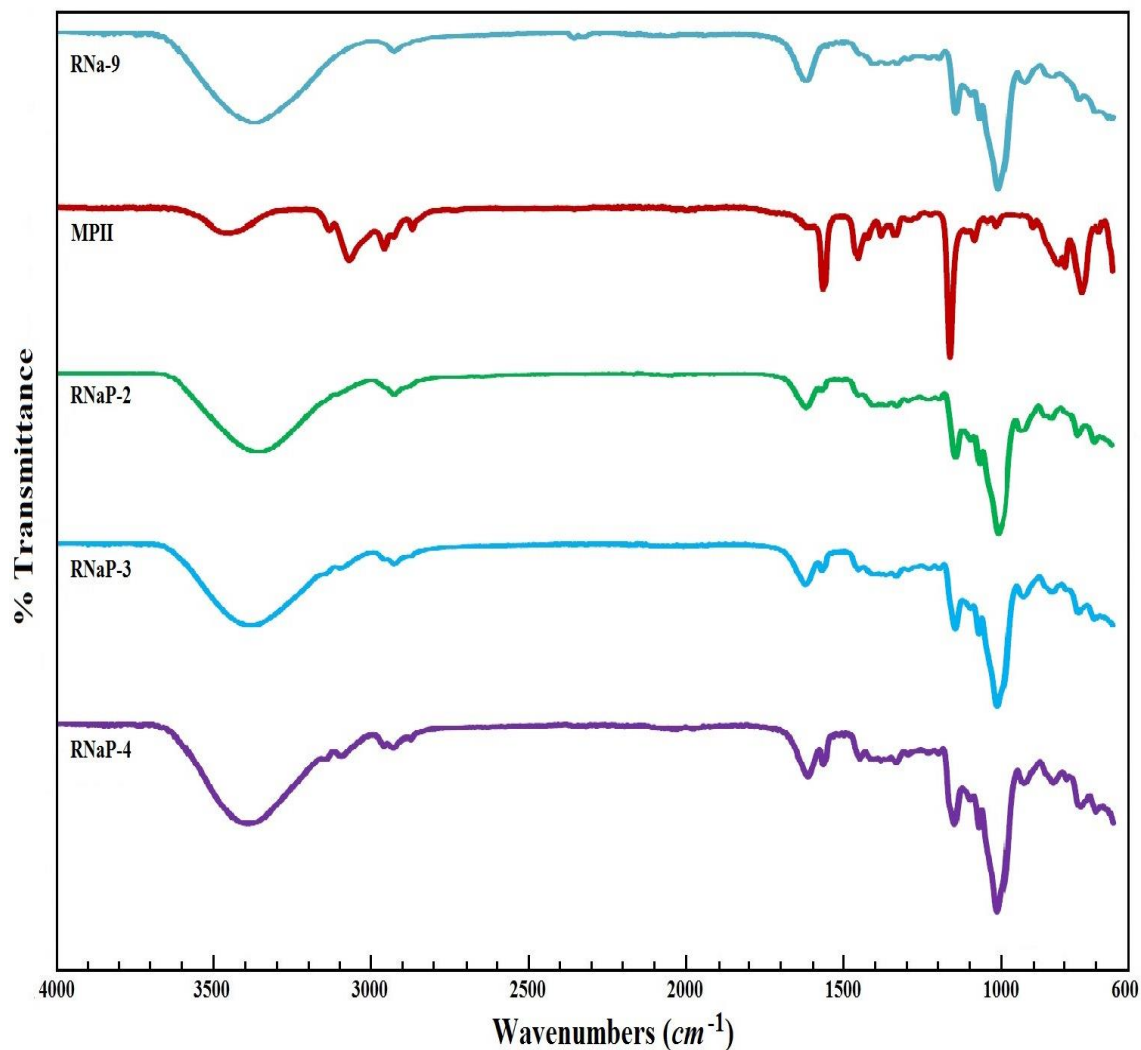


Figure 5.9: FTIR spectra of RNa-9, MPII, RNaP-2, RNaP-3 and RNaP-4 solid polymer electrolytes

The results show the peaks in RNa-9 shift after addition of MPII ionic liquid for RNaP-2, RNaP-3 and RNaP-4 samples. The important spectra range of 3453-3359, 3076-2931, 1624-1569, 1386-1336, 1167-1149, 845-820 and 761-749 cm^{-1} are referred to the O-H stretching (broad), C-H₂ deformation, C=C stretch, C-H bending, C-O stretching, C-H deformation and C-C stretching, respectively.

After addition of MPII ionic liquid, the peak at 3373 cm^{-1} shifts to 3359 , 3385 and 3397 cm^{-1} for RNaP-2, RNaP-3 and RNaP-4, respectively. Consequently, the results show the peak at 759 cm^{-1} in RNa-9 shifts to 759 , 757 and 754 cm^{-1} wavenumbers in RNaP-2, RNaP-3 and RNaP-4, respectively, after addition of MPII ionic liquid. The shifts of wavenumbers prove that the complexation between RS polymer and MPII ionic liquid occurred.

FTIR spectra of RS:NaI:HMII solid polymer electrolyte system are represented in Figure 5.10 at different wavenumbers between 4000 and 600 cm^{-1} . Figure 5.10 shows the FTIR results for RNa-9, HMII, RNaH-2, RNaH-3 and RNaH-4.

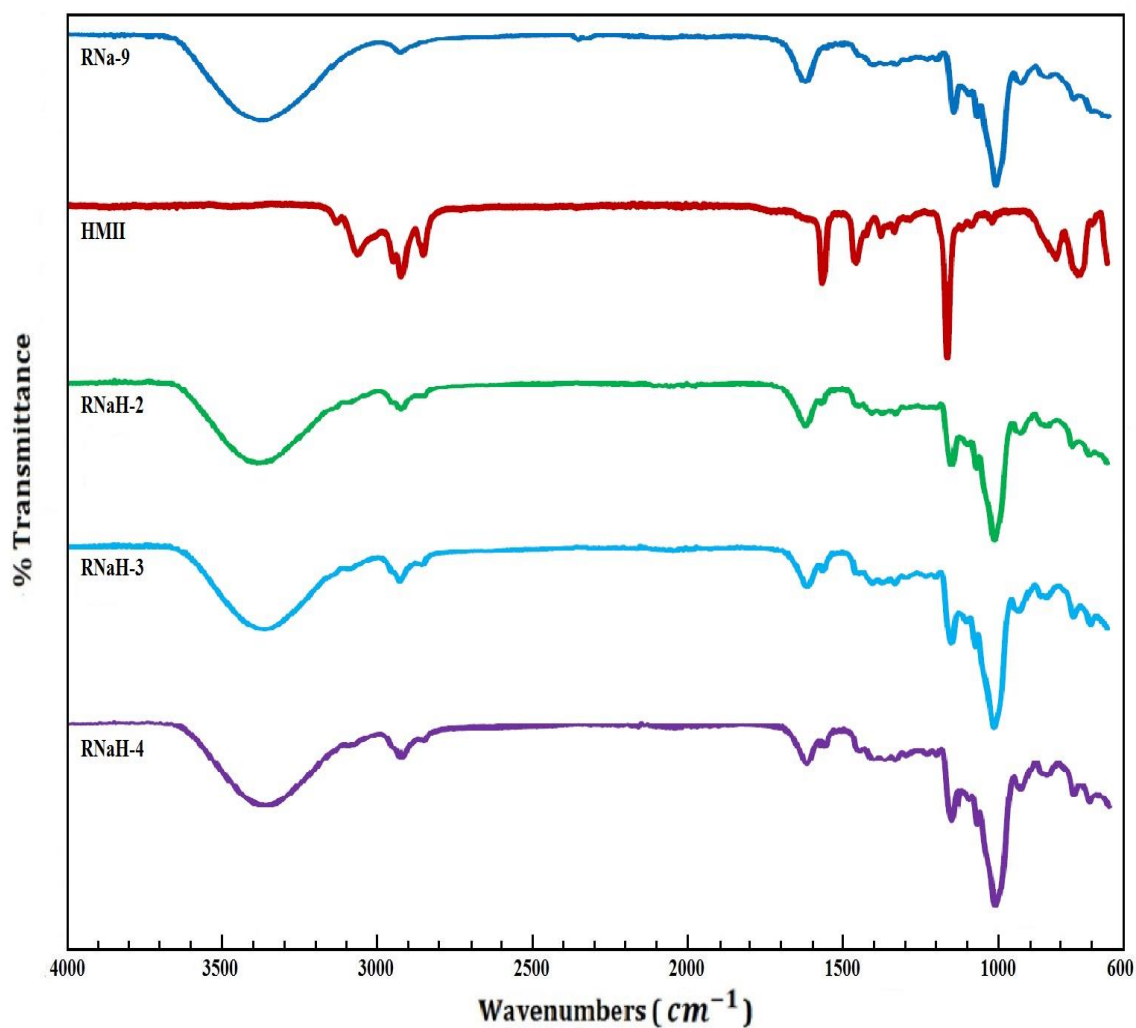


Figure 5.10: FTIR spectra of RNa-9, HMII, RNaH-2, RNaH-3 and RNaH-4

Spectra with the wavenumber range of 3392-2953, 3070-2856, 1624-1569, 1379-1335, 1156-1149, 846-817 and 761-747 cm^{-1} represents O-H stretching (broad), C-H₂ deformation, C=C stretch, C-H bending, C-O stretching, C-H deformation and C-C stretching, respectively.

The peak at 3373 cm^{-1} for RNa-9, due to peaks in HMII between 3070-2856 cm^{-1} , shifts to the higher frequencies of 3385, 3377 and 3375 cm^{-1} in RNaH-2, RNaH-3 and RNaH-4, respectively. Moreover, the peak at 759 cm^{-1} in RNa-9 also shifted to 760, 758, 757 cm^{-1} in RNaH-2, RNaH-3 and RNaH-4, respectively, after addition of HMII ionic liquid.

The results show that the peaks in RNa-9 (RS:NaI, 55:45 wt.%) which is without HMII ionic liquid shifts to lower frequency after addition of HMII ionic liquid. The variations of wavenumber with the addition of HMII confirm that complexation between polymer and ionic liquid has occurred.

5.4 XRD CHARACTERIZATION

Figure 5.11 exhibits the XRD patterns of (a) RNaP-2, (b) RNaP-3, (c) RNaP-4, (d) MPII and (e) RNa-9 in RS:NaI:MPII system. The RNa-9 XRD patterns represents amorphous characteristics with a small peak at $2\theta = 22^\circ$ and a broad hunch at $2\theta = 18-25^\circ$. The XRD patterns in MPII show a broad hunch at $2\theta = 15-24^\circ$. The results indicates that after addition of MPII ionic liquid the polymer electrolytes show more amorphous behavior with broader hunches of $2\theta = 18-26^\circ$, $16-24^\circ$ and $15-25^\circ$ for RNaP-2, RNaP-3 and RNaP-4, respectively. Moreover, the changes in broadening and amorphous nature of polymer electrolytes after addition of MPII ionic liquid further confirm complexation between polymer and ionic liquid.

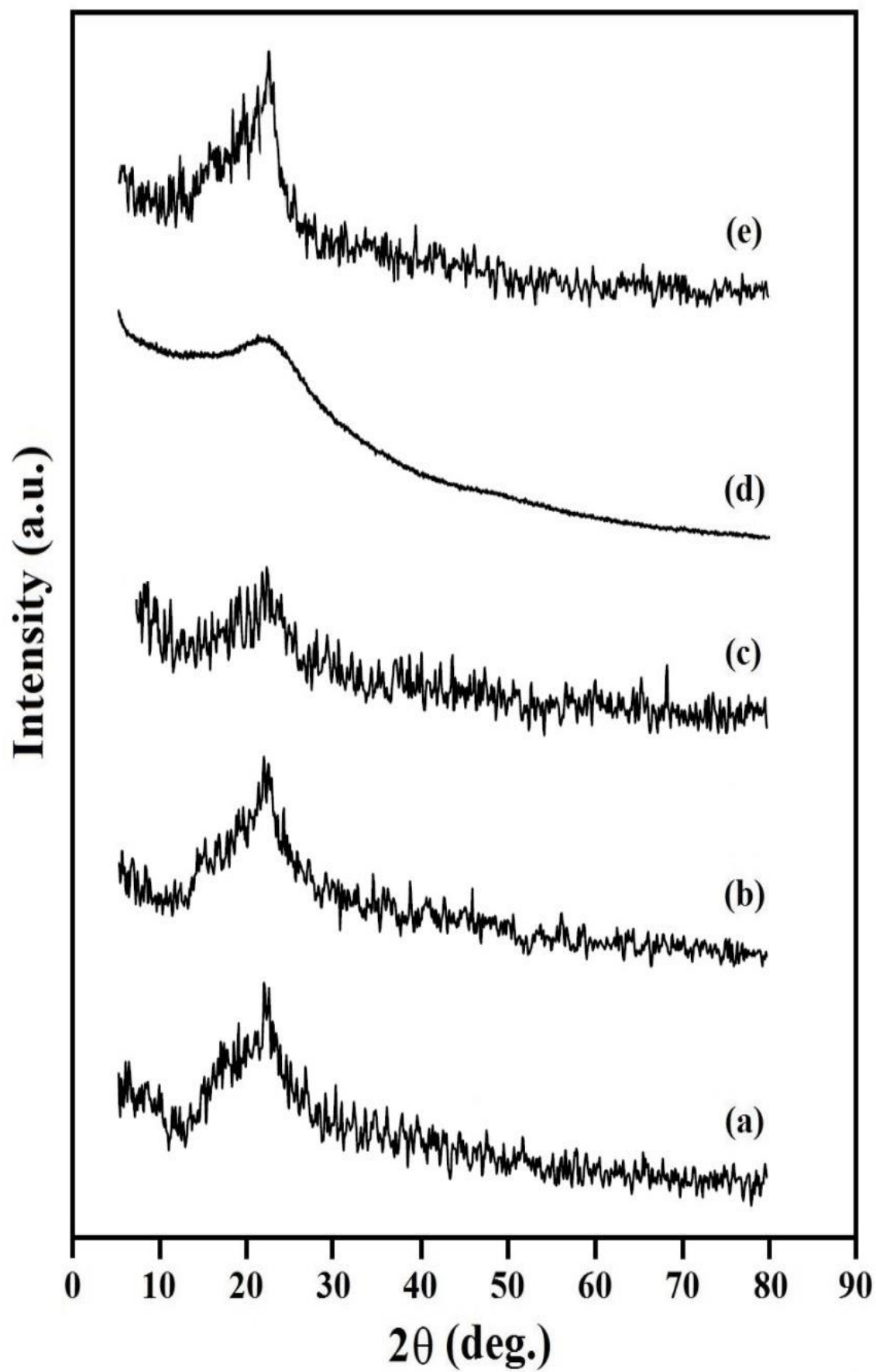


Figure 5.11: XRD patterns of (a) RNaP-2, (b) RNaP-3, (c) RNaP-4, (d) MPII and (e) RNa-9

XRD patterns of RS:NaI:HMII system is represented in Figure 5.12. The graph shows XRD patterns of (a) RNaH-2, (b) RNaH-3, (c) RNaH-4, (d) HMII (pure ionic liquid) and (e) RNa-9.

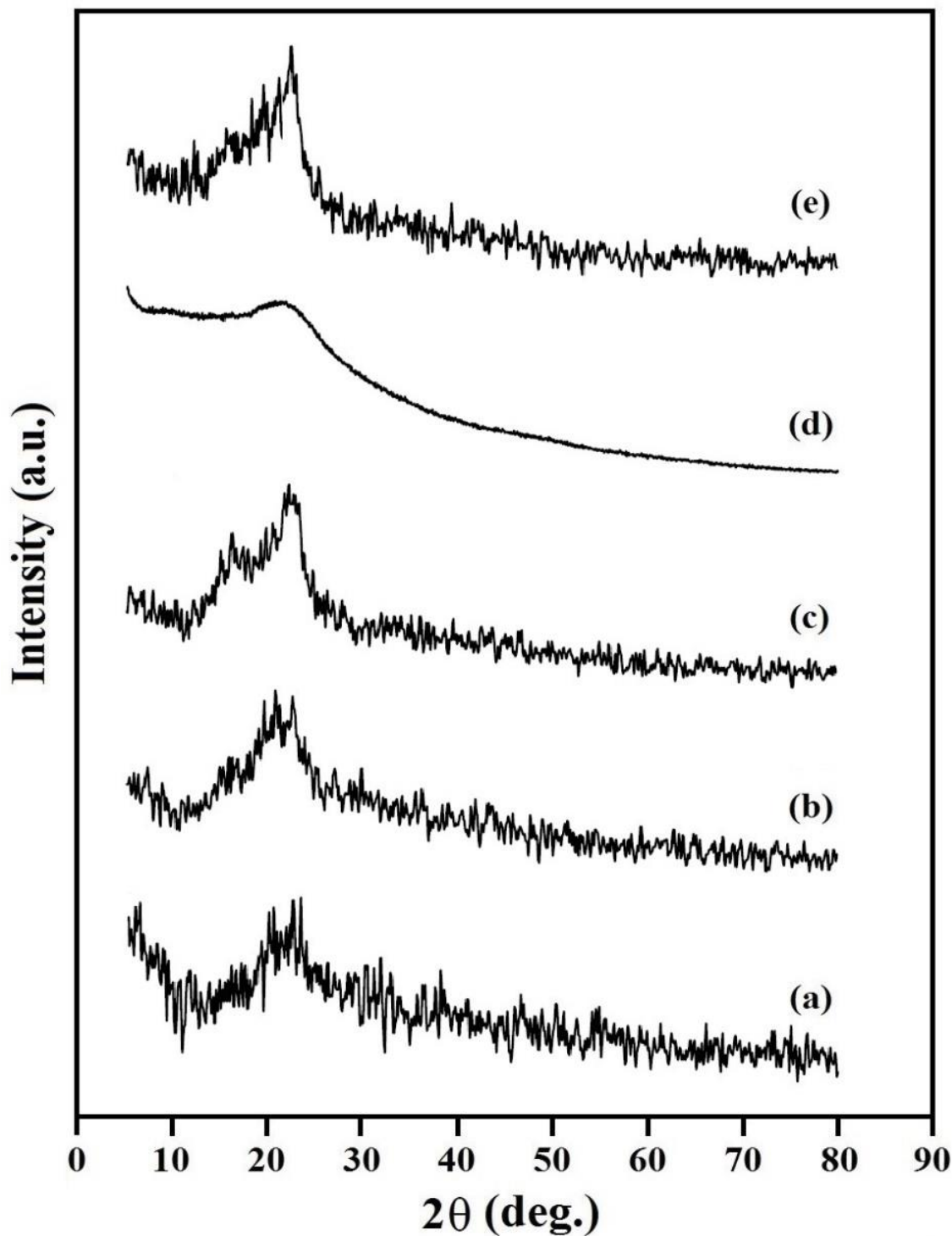


Figure 5.12: XRD patterns of polymer electrolytes for (a) RNaH-2, (b) RNaH-3, (c) RNaH-4, (d) HMII and (e) RNa-9

The RNa-9 with amorphous characteristics has a small peak at $2\theta = 22^\circ$ and a broad hunch at $2\theta = 18-25^\circ$. The XRD patterns of HMII ionic liquid show a broad hunch at $2\theta = 16-22^\circ$. After addition of HMII, the polymer electrolyte goes through more amorphous behavior with broader hunches of $2\theta = 18-22^\circ$, $16-22^\circ$ and $15-23^\circ$ in RNaH-2, RNaH-3 and RNaH-4, respectively. Consequently, the change in broadening and amorphous nature of the polymer electrolytes after addition of HMII confirms complexation between polymer electrolyte and HMII ionic liquid.

5.5 THERMAL STUDY – TGA

The ionic liquid based polymer electrolytes were further studied for thermal behavior using thermogravimetric analysis (TGA). Figures 5.13, 5.14, 5.15 and 5.16 illustrate TGA thermograms of RNaP-1, RNaP-2, RNaP-3 and RNaP-4, respectively.

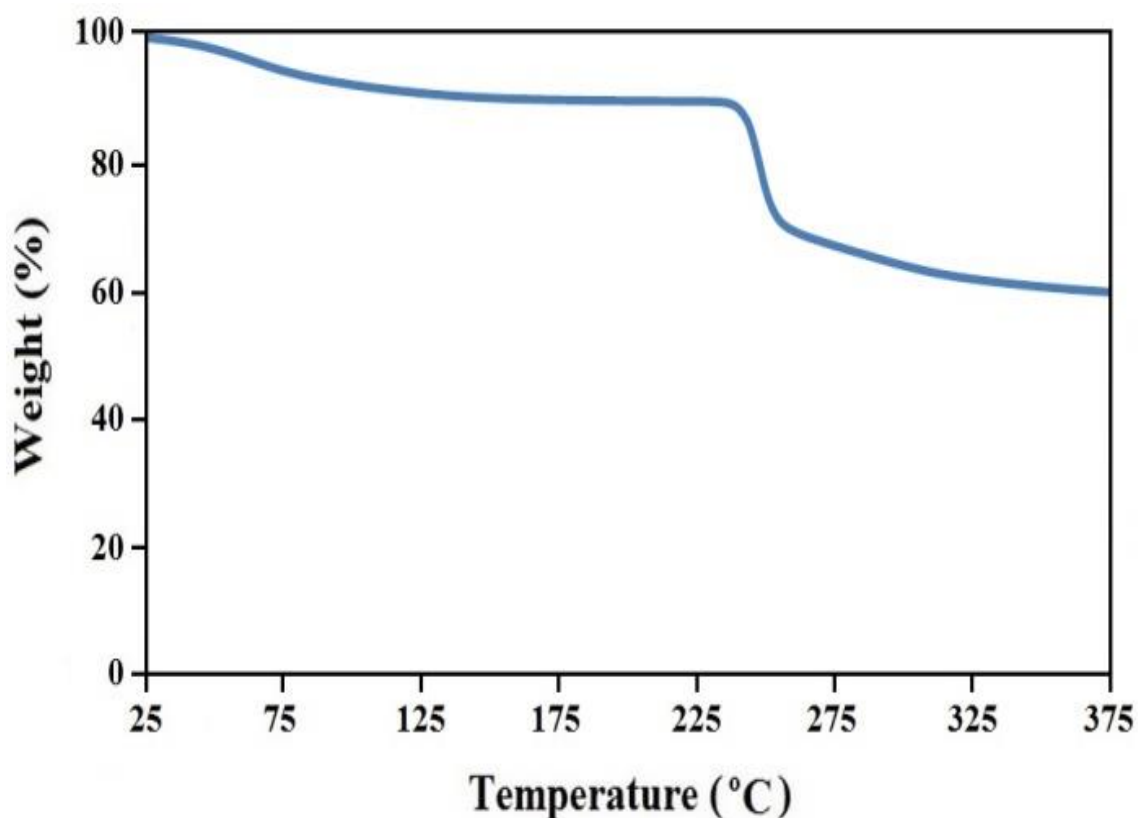


Figure 5.13: TGA thermograms for RNaP-1

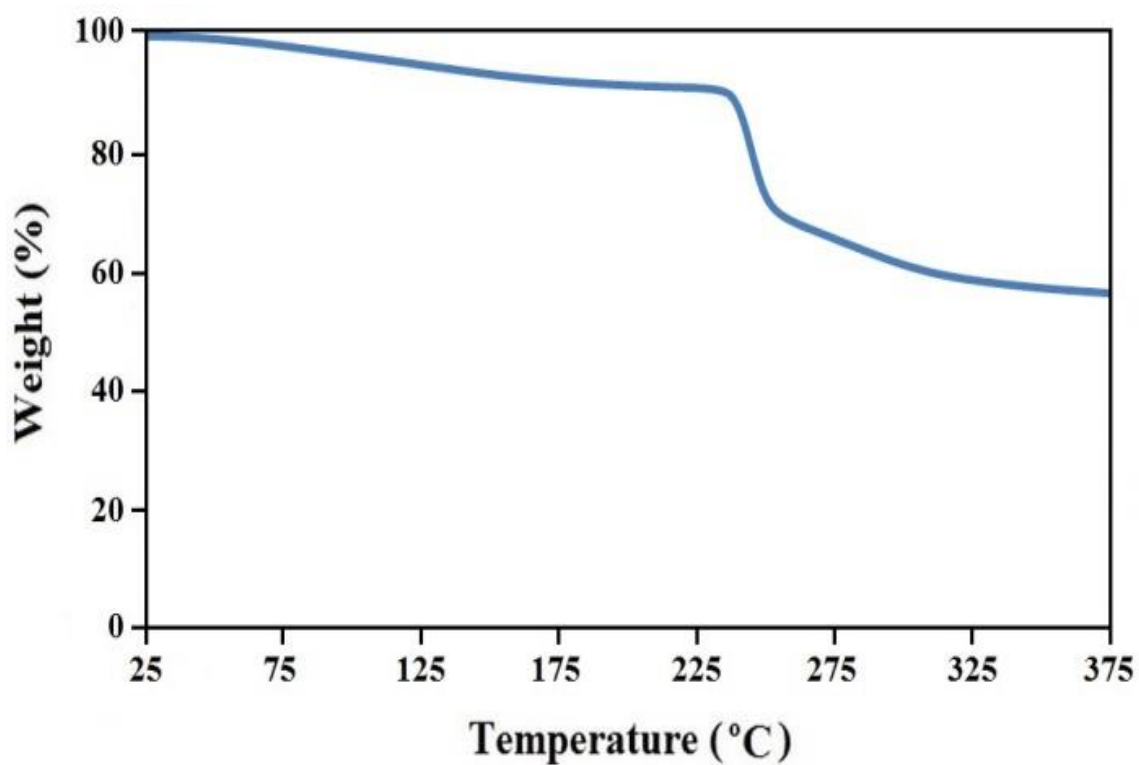


Figure 5.14: TGA thermograms for RNaP-2

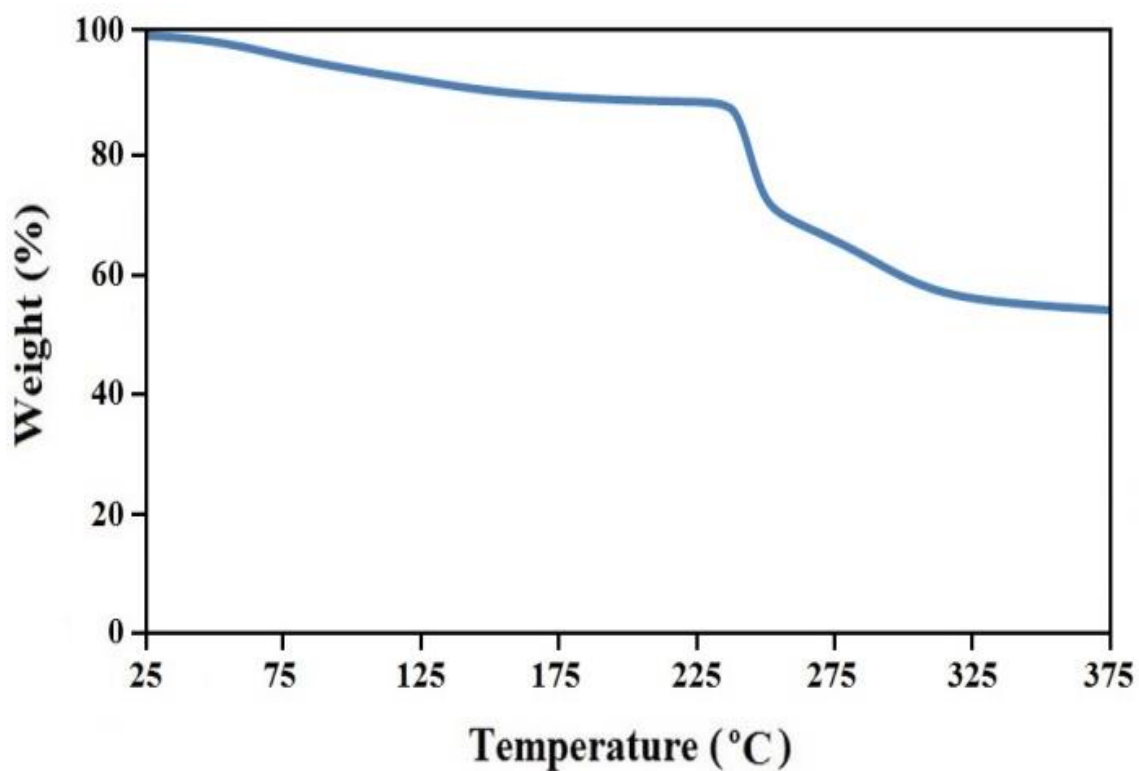


Figure 5.15: TGA thermograms for RNaP-3

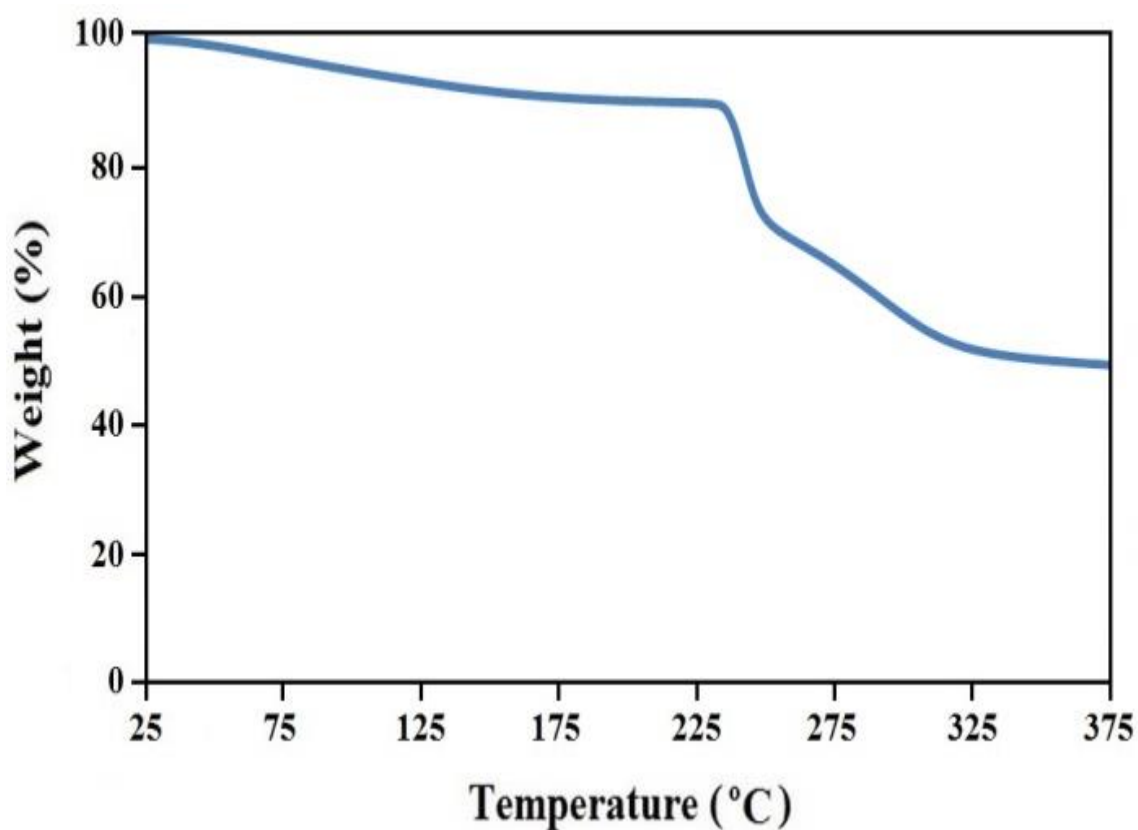


Figure 5.16: TGA thermograms for RNaP-4

The thermograms of TGA show the decomposition temperature (T_{dc}) of 242, 242, 239, 238 and 236 °C for RNa-9, RNaP-1, RNaP-2, RNaP-3 and RNaP-4, respectively. Figure 5.17 shows the comparison between the thermograms of SPEs in RS:NaI:MPII system. The figure indicates that T_{dc} decreases after addition of MPII ionic liquid. This is due to the complexation between polymer, salt and MPII ionic liquid and result in more segmental flexibility of polymeric network which can reduce the decomposition temperature of polymer electrolyte. The results further specifies that the RNaP-4 has the lowest weight loss compared with RNaP-1, RNaP-2 and RNaP-3 denoting more stability of SPE incorporated with 20 wt.% of MPII.

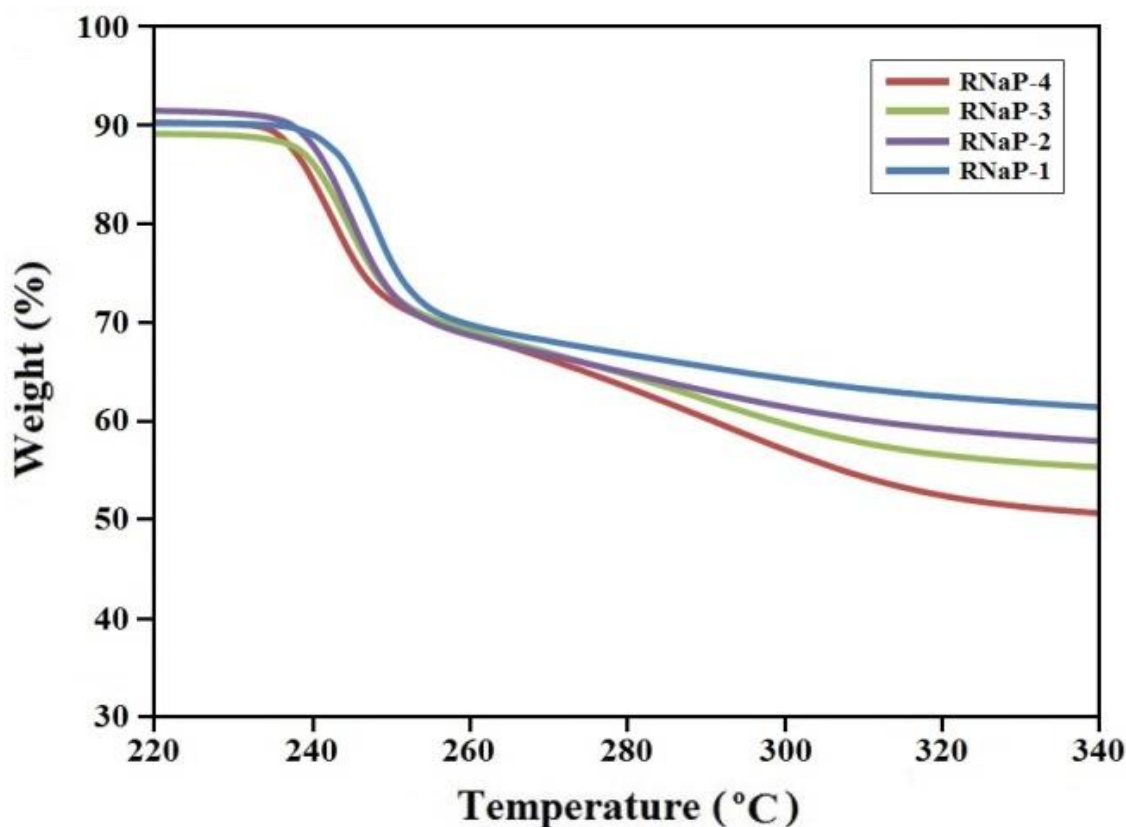


Figure 5.17: TGA thermograms for RNaP-1, RNaP-2, RNaP-3 and RNaP-4

The solid polymer electrolytes in RS:NaI:HMII system were studied for thermal behaviors using TGA as well. Figures 5.18, 5.19, 5.20 and 5.21, exhibit TGA thermograms of RNaH-1, RNaH-2, RNaH-3 and RNaH-4, respectively.

Figure 5.22 shows comparison between SPEs in RS:NaI:HMII system. The TGA results show decomposition temperatures (T_{dc}) for the samples. The decomposition temperature for RNaH-1, RNaH-2, RNaH-3 and RNaH-4 are 238, 239, 239 and 240 °C, respectively. The T_{dc} of the polymer electrolytes are included in Table 5.6. The variation of T_{dc} is due to existence of HMII ionic liquid in the structure and polymeric network of polymer electrolytes. The TGA results further demonstrates the lowest weight loss in RNaH-4. But T_{dc} increase with the addition of HMII ionic liquid, which can be related to hexyl (6 carbons) structure of HMII ionic liquid.

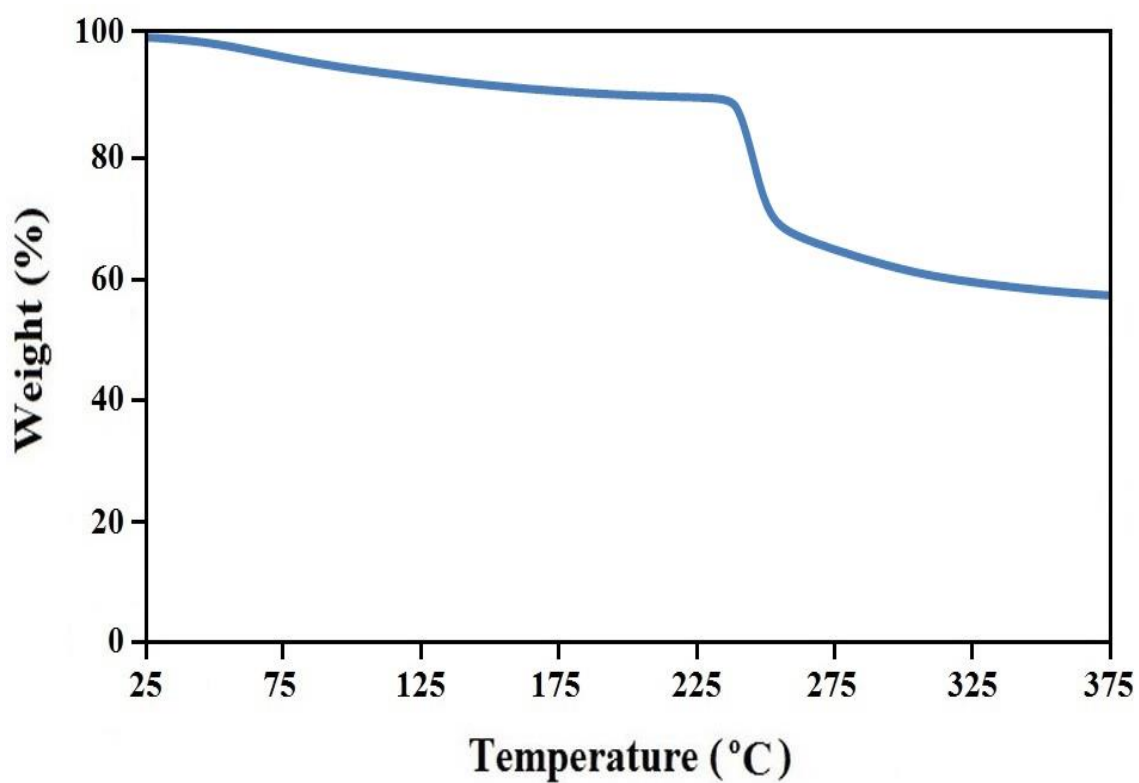


Figure 5.18: TGA thermograms for RNaH-1

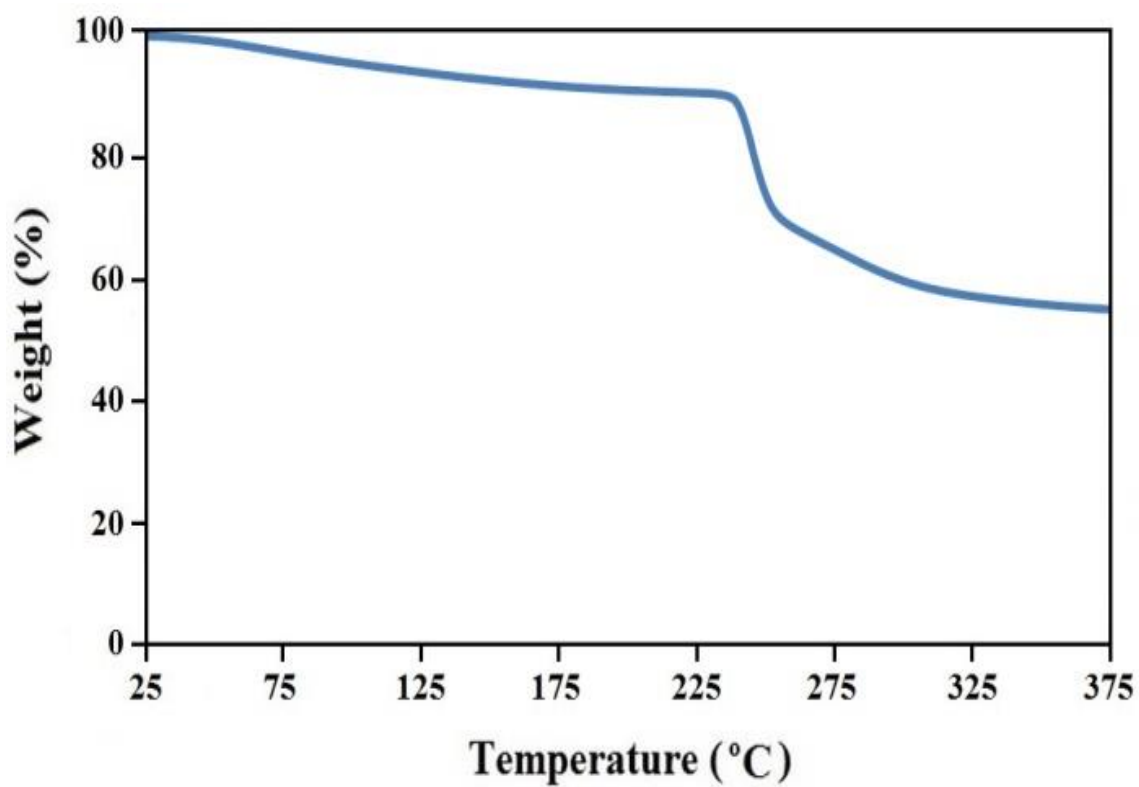


Figure 5.19: TGA thermograms for RNaH-2

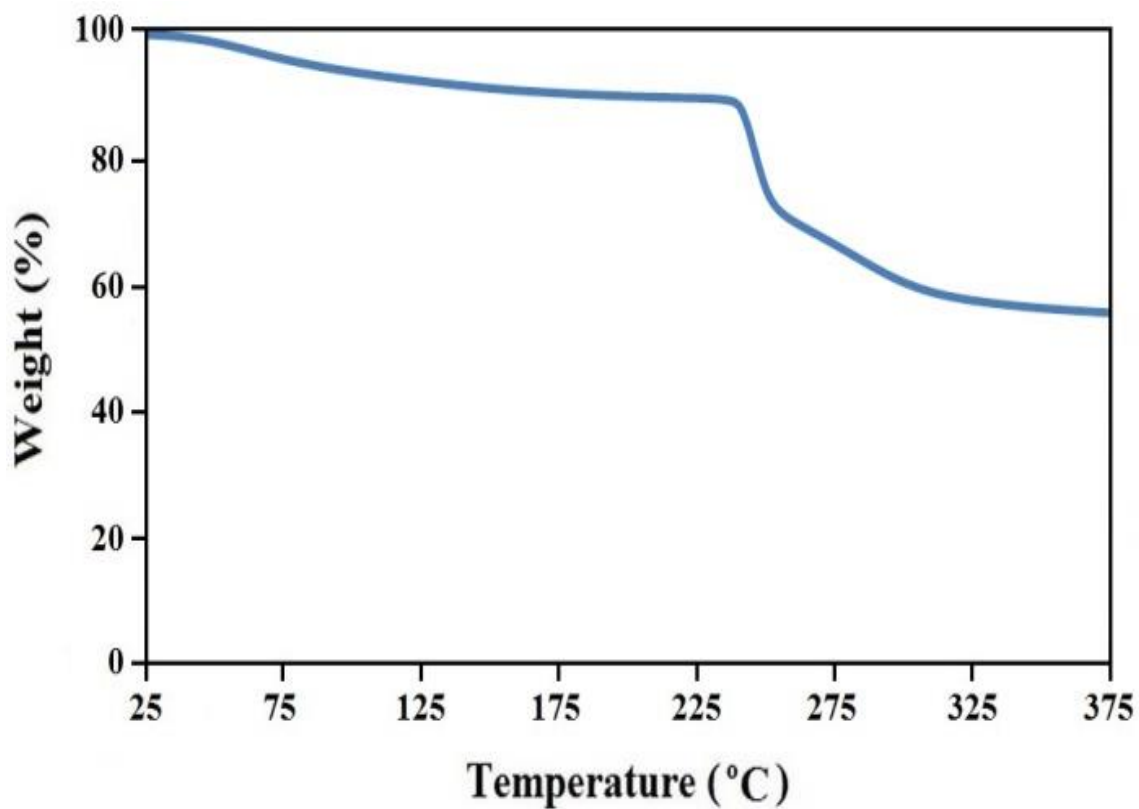


Figure 5.20: TGA thermograms for RNaH-3

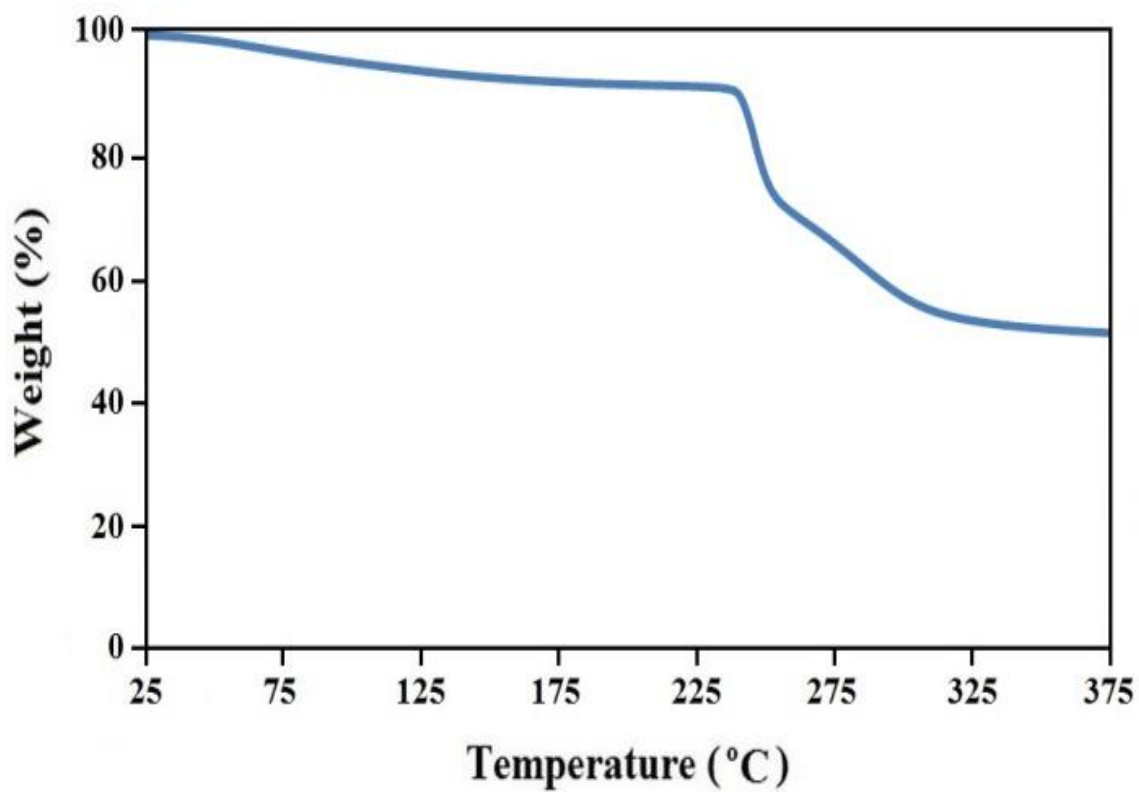


Figure 5.21: TGA thermograms for RNaH-4

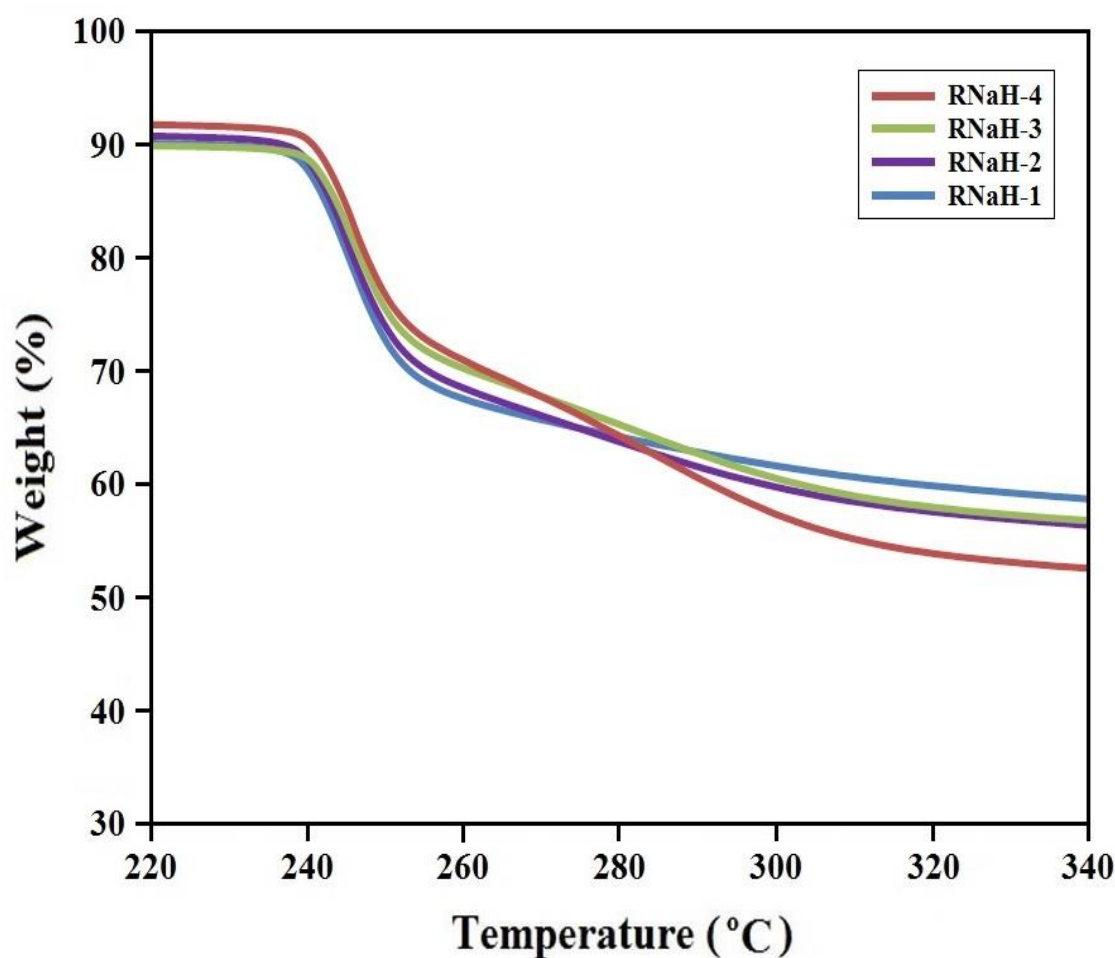


Figure 5.22: TGA thermograms of RNaH-1, RNaH-2, RNaH-3 and RNaH-4

5.6 THERMAL STUDY – DSC

The Figure 5.23 demonstrates the DSC thermograms of RNaP-1, RNaP-2, RNaP-3 and RNaP-4 SPEs in RS:NaI:MPII system. The DSC results exhibit glass transition temperature (T_g) for polymer electrolytes.

In RNa-9 polymer electrolyte, which is without MPII ionic liquid, T_g is $-42\text{ }^\circ\text{C}$. After addition of MPII ionic liquid, T_g decreases compared with RNa-9 without MPII ionic liquid. The thermal parameters are expressed in Table 5.5.

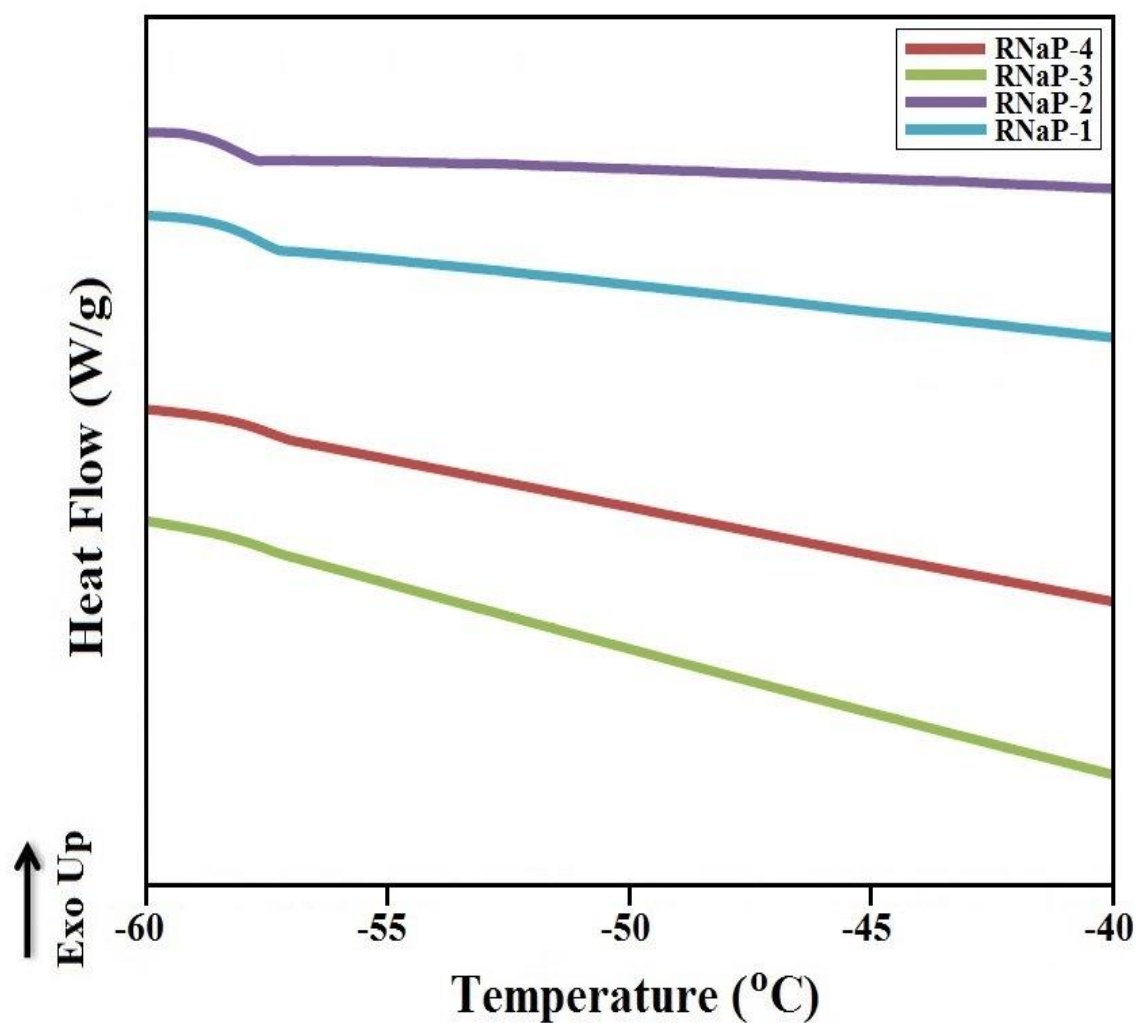


Figure 5.23: DSC thermograms for RNAP-1, RNAP-2, RNAP-3 and RNAP-4

Table 5.5: TGA and DSC thermograms for RS:NaI:MPII solid polymer electrolyte system.

Samples	Decomposition temperature (T _{dc}) (°C)	Glass transition temperature (T _g) (°C)
RNa-9	242	-42.00
RNaP-1	242	-58.31
RNaP-2	239	-58.22
RNaP-3	238	-57.79
RNaP-4	236	-57.08

The DSC thermograms in Figure 5.23 show T_g of -58.31, -58.22, -57.79 and -57.08 °C for RNAP-1, RNAP-2, RNAP-3 and RNAP-4, respectively.

The T_g changes after addition of ionic liquid can be related to complexation of polymer with salt and ionic liquid, and changes of flexibility of polymeric chains (Tominaga et al., 2005; Y.-J. Wang et al., 2005). The T_g in RNa-9 decreases after addition of ionic liquid which can be due to increase of polymer flexibility, higher amorphous phase, and possibility of reduction in the internal viscosity due to addition of MPII ionic liquid (Nithya et al., 2015; Ren et al., 2014).

In RS:NaI:HMII system, DSC analysis was carried out which is the DSC results are illustrated in Figure 5.24 for RNaH-2, RNaH-3 and RNaH-4. The glass transition temperature (T_g) for the samples from DSC results are represented in Table 5.6.

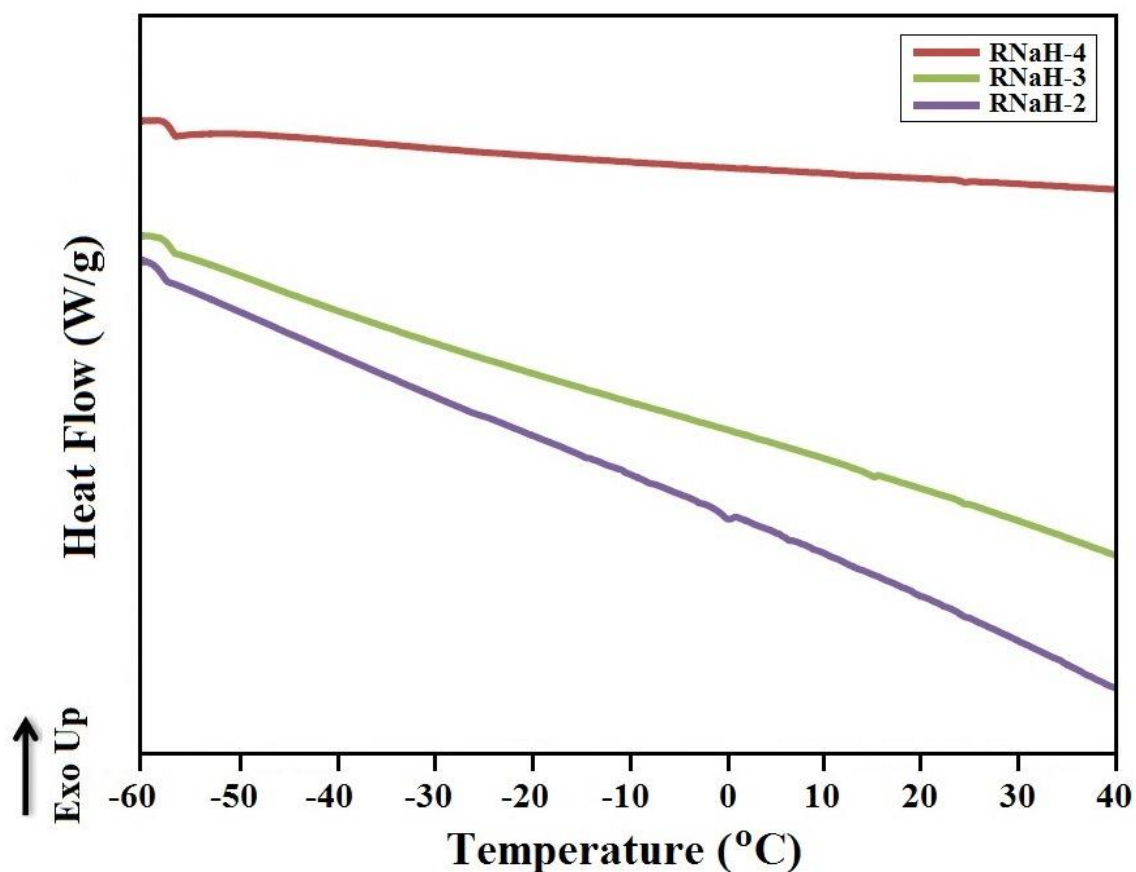


Figure 5.24: DSC thermograms for RNaH-2, RNaH-3 and RNaH-4

The DSC results demonstrate that T_g in RNa-9 solid polymer electrolyte (without ionic liquid) decrease after the addition of HMII ionic liquid.

This can be due to increase of polymer flexibility, higher amorphous phase, and possibility of reduction in the internal viscosity due to addition of MPII ionic liquid (Nithya et al., 2015; Ren et al., 2014).

Table 5.6: TGA and DSC thermograms for RS:NaI:HMII solid polymer electrolyte system

Samples	Decomposition temperature (T_{dc}) (°C)	Glass transition temperature (T_g) (°C)
RNa-9	242	-42.00
RNaH-1	238	-58.10
RNaH-2	239	-58.02
RNaH-3	239	-57.82
RNaH-4	240	-57.27

The DSC thermographs show the T_g is almost unchanged after addition of HMII which is around -58 °C. Moreover, since the increase in ionic conductivity with the addition of HMII (according to Figure 5.24) is due to increasing the number of charge carriers, therefore the T_g become almost unchanged in different HMII weight ratios (Bandara et al., 2012). The DSC thermal results further showed the effect of HMII ionic liquid on polymer electrolyte system.

5.7 J-V CHARACTERISTICS

The solid polymer electrolytes of RNaP-1, RNaP-2, RNaP-3 and RNaP-4 in RS:NaI:MPII system with N719 dye were used to fabricate DSSCs and analyzed under Sun simulator. The J-V characteristic curves of fabricated Dye-sensitized solar cells using RNaP-1, RNaP-2, RNaP-3 are illustrated in Figure 5.25.

Consequently, Figure 5.26 exhibits J-V result for RNaP-4 with the highest ionic conductivity in RS:NaI:MPII system.

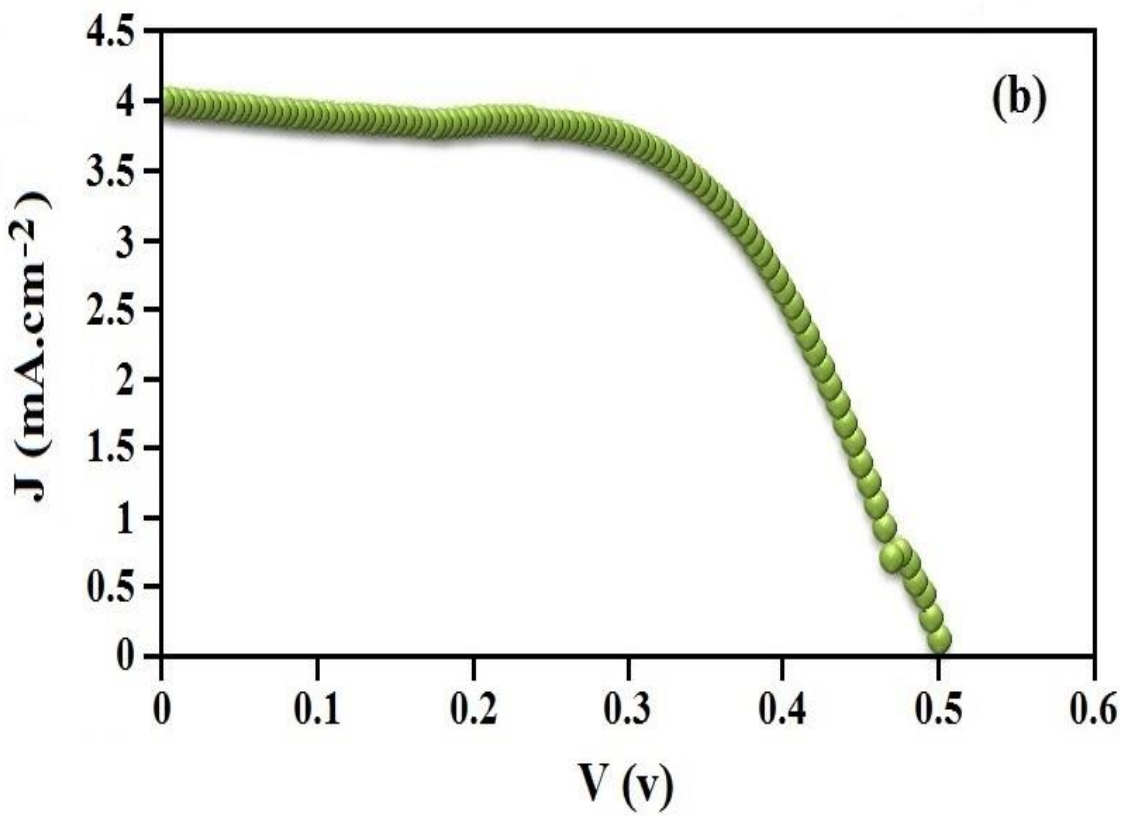
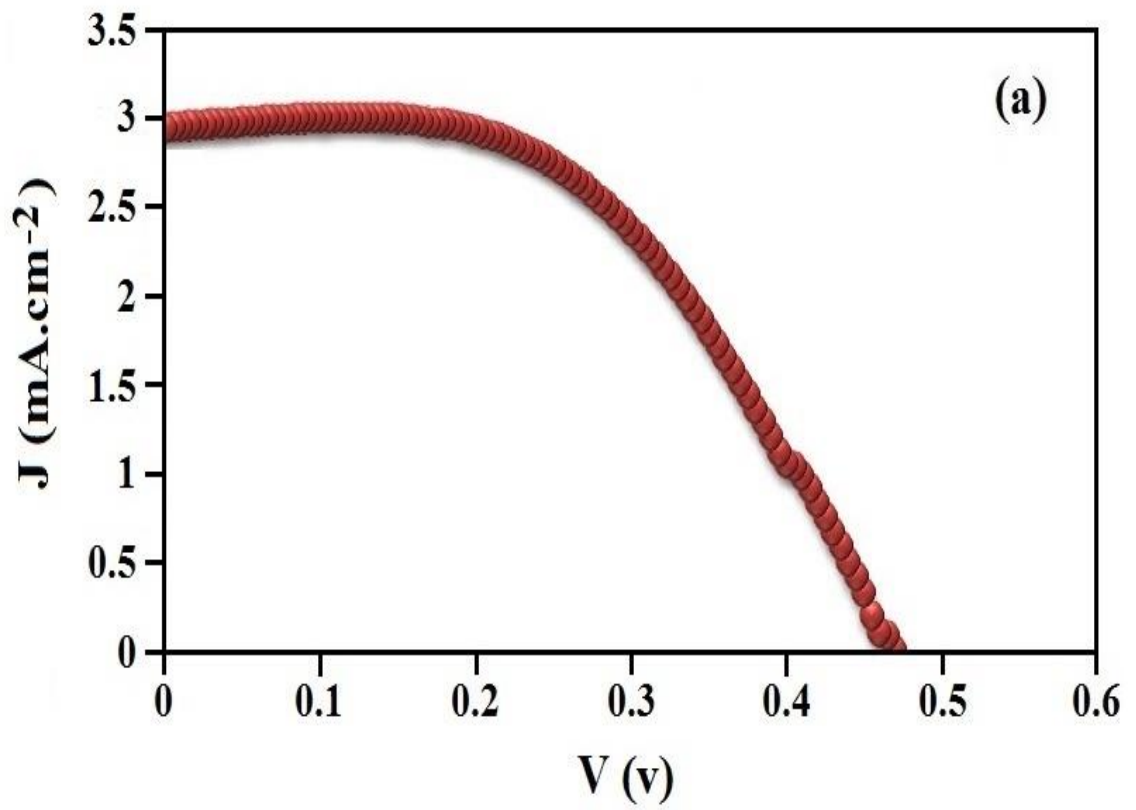
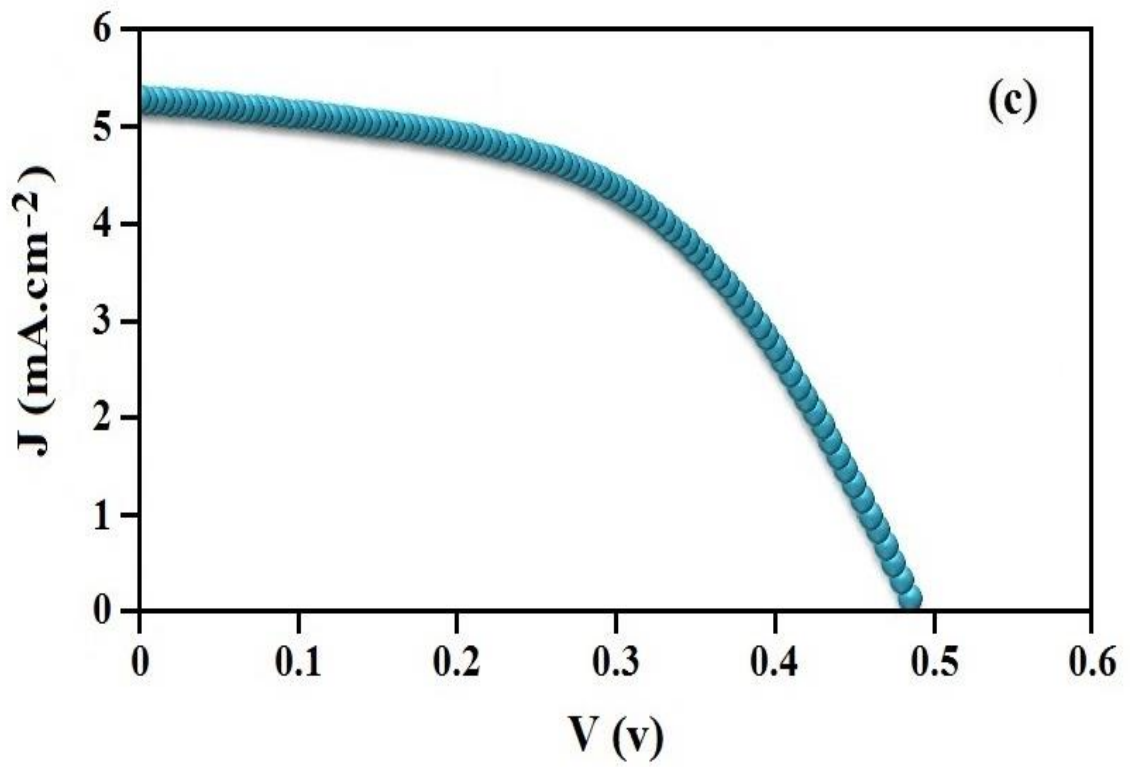


Figure 5.25: J-V graphs for (a) RNaP-1, (b) RNaP-2 and (c) RNaP-3



‘Figure 5.25, continued’

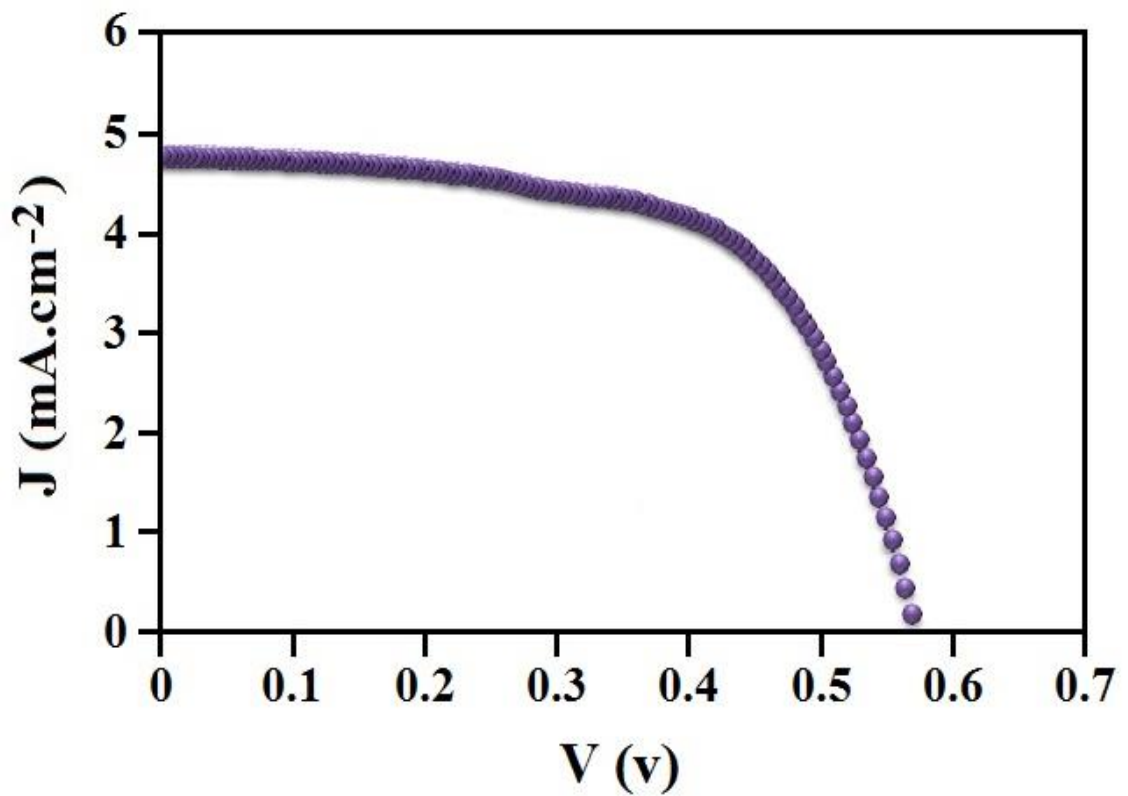


Figure 5.26: J-V graph of RNaP-4

The J-V graphs in Figures 5.25 and 5.26, in RS:NaI:MPII system, indicate that the energy conversion efficiency is increasing with the addition of MPII ionic liquid and reach to the maximum value achieved in RS:NaI:MPII system in RNaP-4 with 20 wt.% of MPII ionic liquid content.

The J-V parameters for all SPEs are expressed in Table 5.7. The results show the energy conversion efficiency of polymer electrolytes increases with the addition of MPII ionic liquid.

The highest energy conversion efficiency of 2.09 % was achieved after addition of 20 wt.% of MPII ionic liquid (RNaP-4). The other parameters of J_{sc} , V_{oc} and ff for RNaP-4 are $4.78 \text{ (mA cm}^{-2}\text{)}$, 0.57 (V) and 0.767 , respectively.

Table 5.7: Dye-sensitized solar cell parameters for RS:NaI:MPII system

Electrolyte	J_{sc} (mA cm⁻²)	V_{oc} (V)	FF (%)	Efficiency, η (%)
RNa-9	2.40	0.485	67.0	0.78
RNaP-1	2.94	0.47	51.6	0.71
RNaP-2	4.00	0.50	58.9	1.18
RNaP-3	5.27	0.485	51.9	1.33
RNaP-4	4.78	0.57	76.7	2.09

Moreover, Figure 5.27 exhibits the variation of energy conversion efficiency of SPEs in RS:NaI:MPII system with MPII ionic liquid content. The graph shows the efficiency increases exponentially when 20 wt.% of MPII is used, as increase of ionic conductivity. The increase is due to increasing the plasticization effect of MPII ionic liquid which cause to higher ionic movement over the rice starch network and mobility.

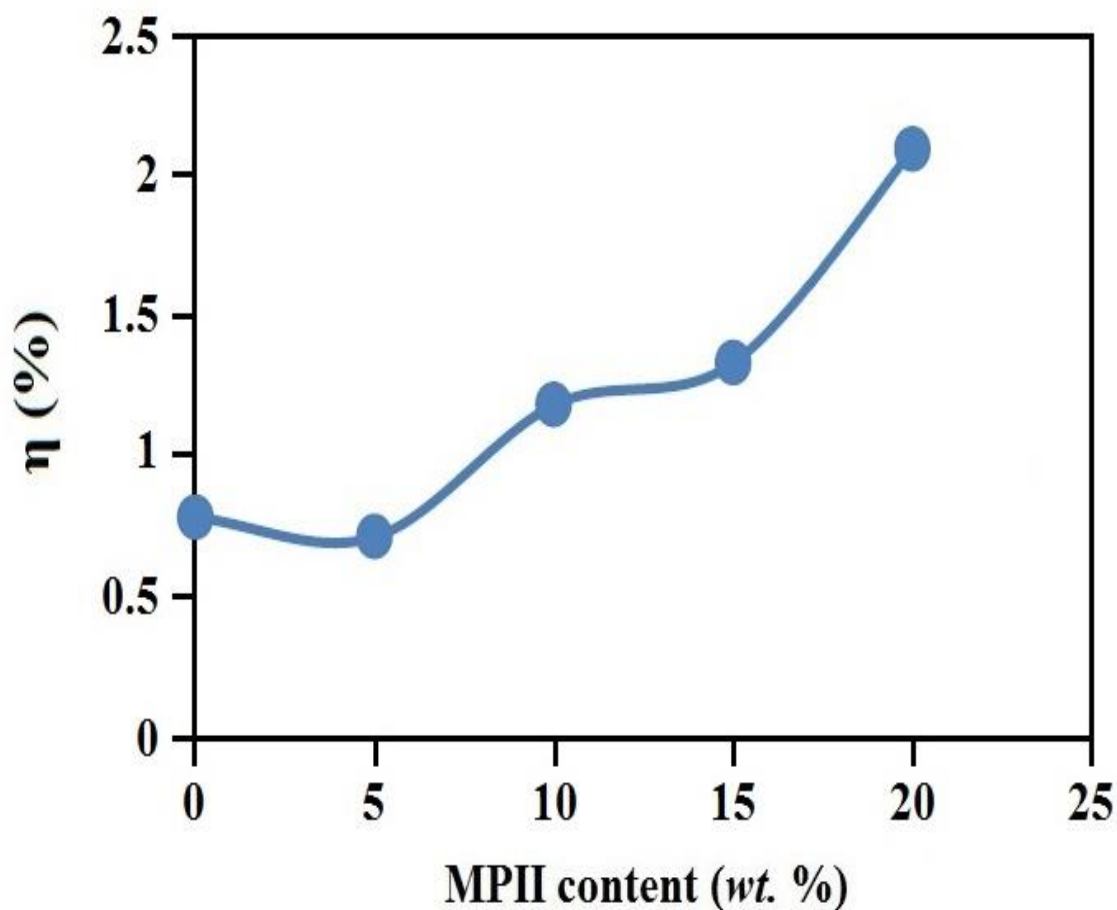


Figure 5.27: Variation of energy conversion efficiency with MPII ionic liquid content

In RS:NaI:HMII system, the solid polymer electrolytes of RNaH-1, RNaH-2, RNaH-3 and RNaH-4 are used to fabricate DSSC. The J-V characteristic curves of fabricated dye-sensitized solar cells are represented in Figure 5.28 for (a) RNaH-1, (b) RNaH-2 and (c) RNaH-3. The figure shows the current density increases upon increase of HMII ionic liquid content.

Figure 5.29 exhibits J-V curve of RNaH-4, with the highest ionic conductivity, which has highest short-circuit current density and highest open-circuit voltage in RS:NaI:HMII system.

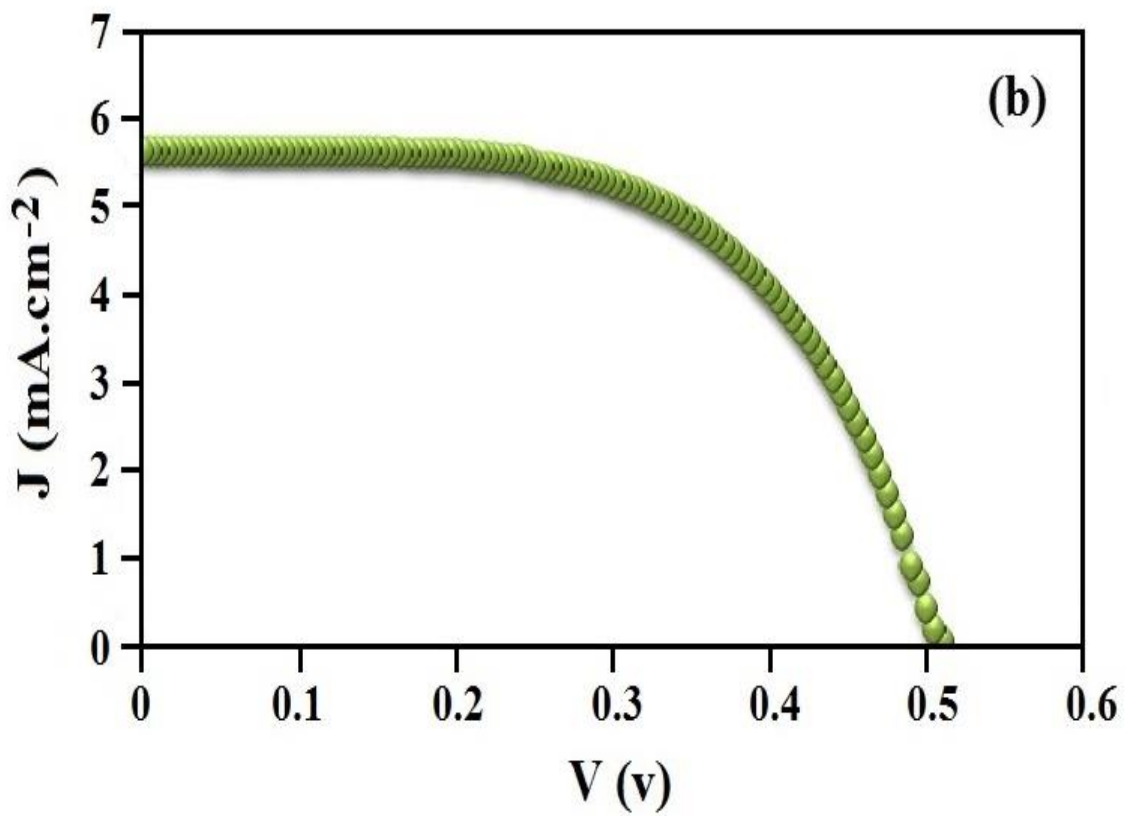
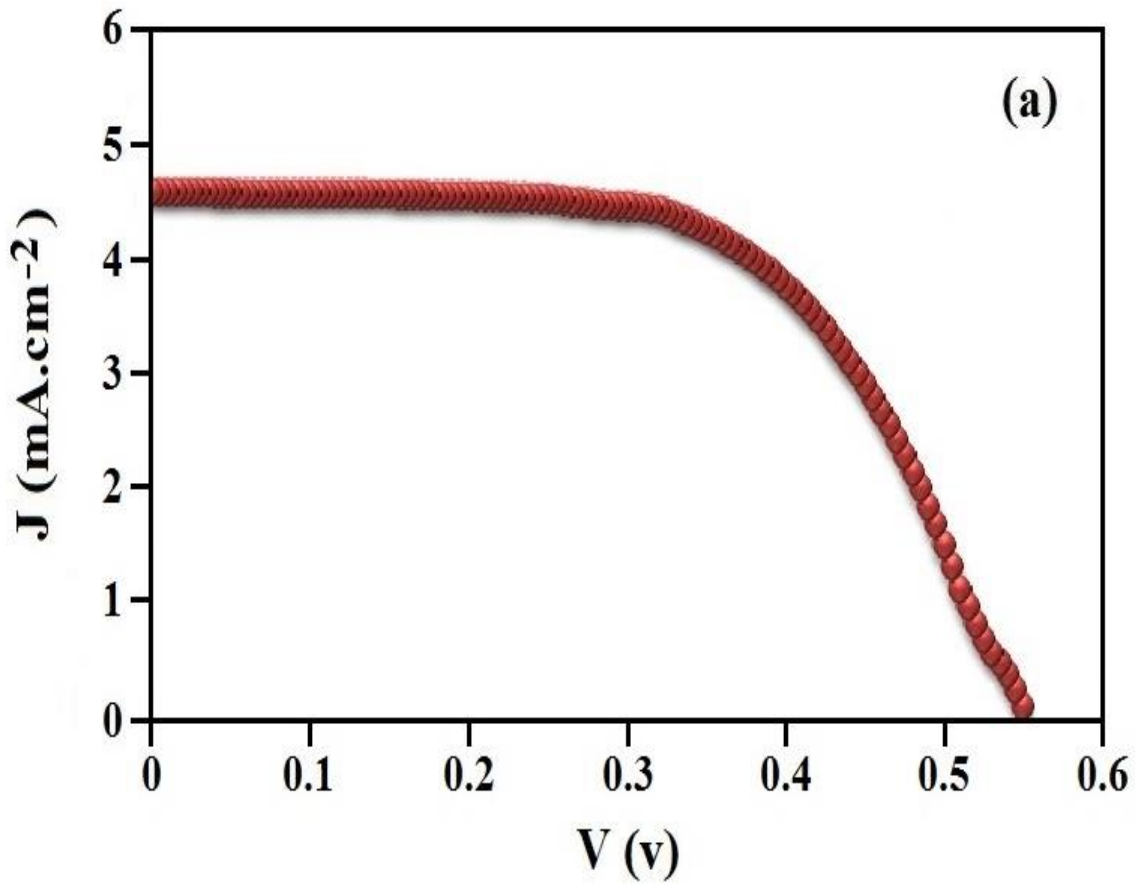
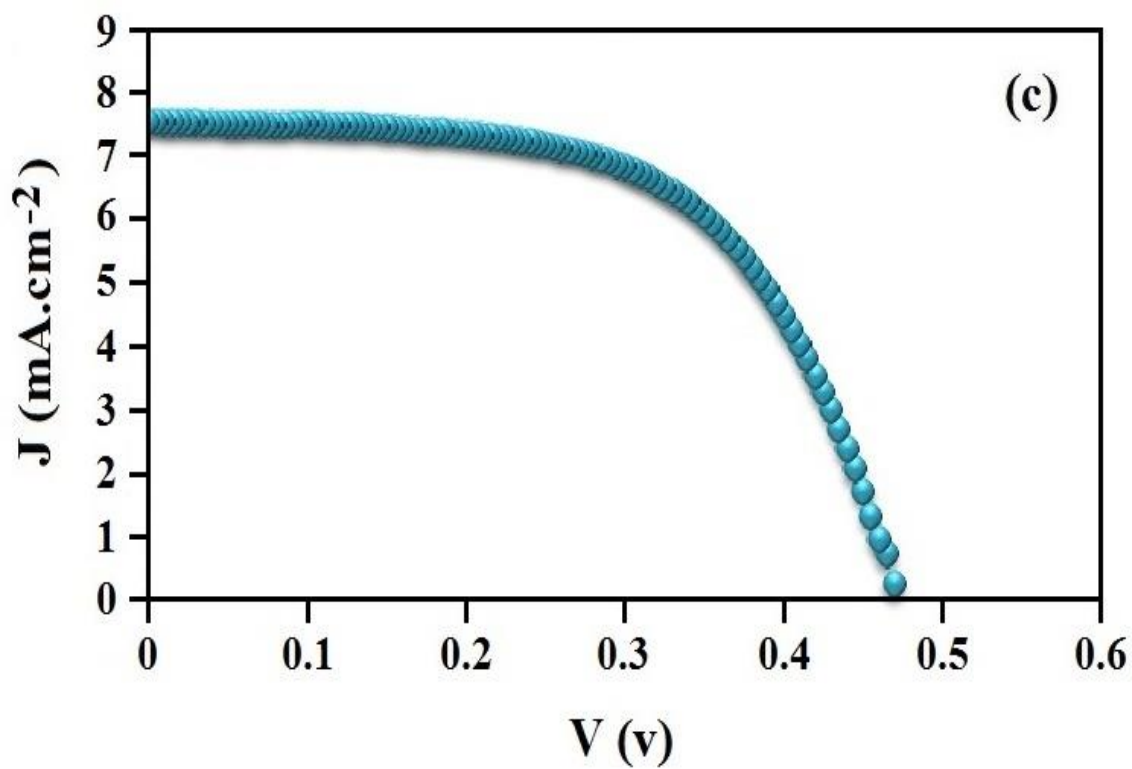


Figure 5.28: J-V graphs of (a) RNaH-1, (b) RNaH-2 and (c) RNaH-3



'Figure 5.28, continued'

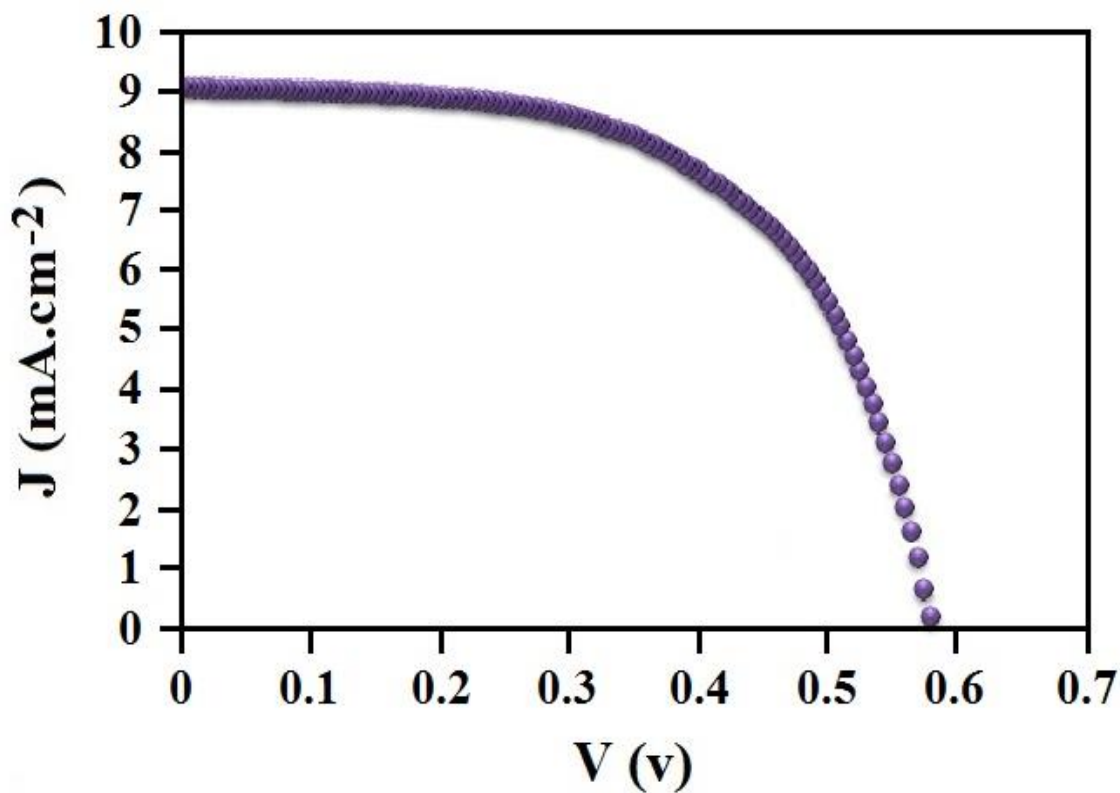


Figure 5.29: J-V graph for RNaH-4

Table 5.8 shows the DSSC related parameters for all SPEs in RS:NaI:HMII system. After addition of 20 wt.% HMII, the efficiency increases dramatically. The RNaH-4 with 20 wt.% of HMII shows the highest solar cell performance with DSSC parameters of J_{sc} , V_{oc} and ff with values of $9.07 \text{ (mA cm}^{-2}\text{)}$, 0.58 (V) and 0.65 , respectively, which exhibits the highest energy conversion efficiency (η) of 3.42% in the RS:NaI:HMII based DSSCs. Furthermore, this is the highest achieved energy conversion efficiency among all systems in this study.

Table 5.8: Dye-sensitized solar cell parameters for RS:NaI:HMII system

Electrolyte	$J_{sc} \text{ (mA cm}^{-2}\text{)}$	$V_{oc} \text{ (V)}$	FF (%)	Efficiency, η (%)
RNa-9	2.40	0.485	67.0	0.78
RNaH-1	4.58	0.55	60.2	1.52
RNaH-2	5.63	0.51	59.0	1.69
RNaH-3	7.54	0.47	64.1	2.27
RNaH-4	9.07	0.58	65.0	3.42

Figure 5.30 demonstrates the variation of the energy conversion efficiency with the addition of HMII ionic liquid. Figure 5.30 indicates that the energy conversion efficiency increases significantly after addition of HMII ionic liquid starting from 5 wt.% to 20 wt.% of HMII ionic liquid.

Consequently, efficiency increases dramatically after the addition of 15 and 20 wt.% of HMII ionic liquid. This can be due to more plasticization effect after the addition of HMII ionic liquid which results in the highest electron movement and mobility in RNaH-4 followed by increase in the current density of the solar cell.

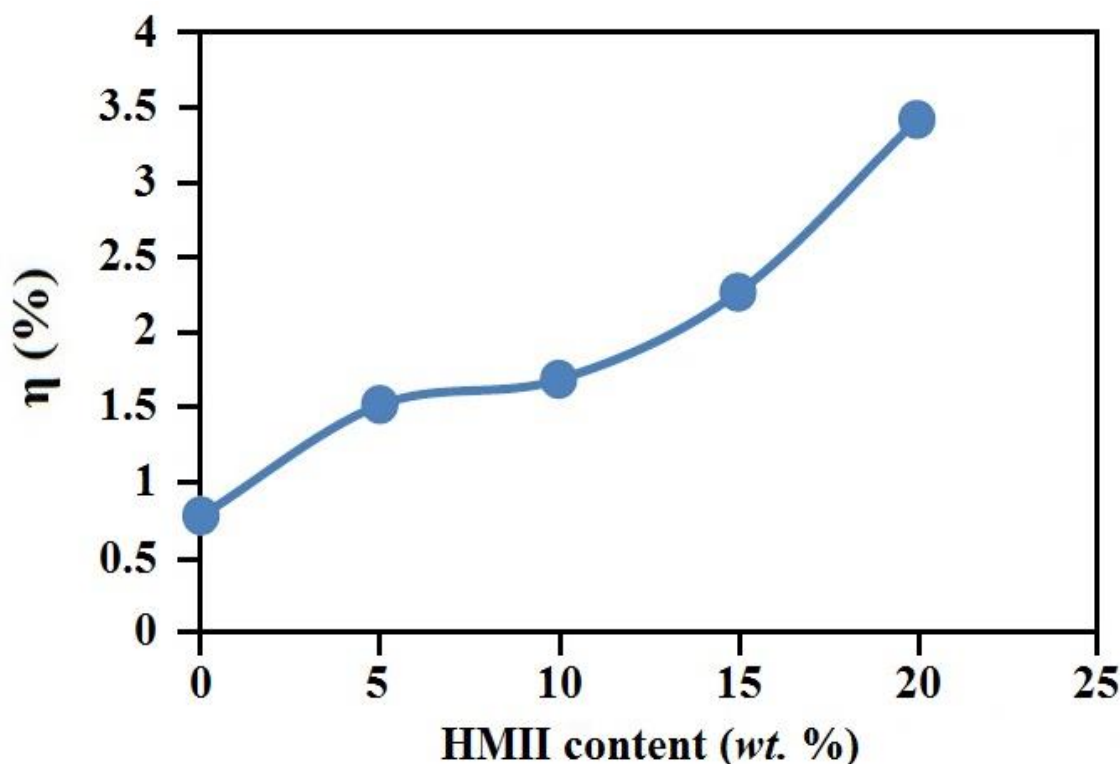


Figure 5.30: Variation of energy conversion efficiency with HMII ionic liquid content

5.8 SUMMARY

The results and discussion on two ionic liquid based systems using MPII and HMII were elaborated in this chapter. The ionic conductivity study, structural and thermal behaviors of RS:NaI:MPII and RS:NaI:HMII systems were discussed throughout the chapter. The DSSC characterizations of two ionic liquid based systems were discussed. The RNaH-4 incorporated with 20 wt.% of HMII showed the best energy conversion efficiency and performance among all systems. The following chapter will be allocated for the discussion on differences between five systems mentioned in previous chapters, Chapter 4 and Chapter 5, based on the results from ionic conductivity, structural, thermal and DSSC characterizations.

CHAPTER 6

DISCUSSIONS ON DIFFERENCES OF FIVE SYSTEMS

6.1 INTRODUCTION

This chapter covers the overall discussions on the SPE systems such as RS:LiI, RS:NH₄I, RS:NaI, RS:NaI:MPII and RS:NaI:HMII by comparing the results containing ionic conductivity, structural, thermal and DSSC studies performed in this study using EIS, FTIR, XRD, TGA, DSC and DSSC characterizations.

6.2 EIS CHARACTERIZATION

The EIS results from all the five systems have been discussed to compare of both ionic conductivity and temperature-dependent ionic conductivity which mentioned in two sections of 6.2.1 and 6.2.2, respectively.

6.2.1 IONIC CONDUCTIVITY

The EIS data for first three systems with only RS and iodide salts (LiI, NH₄I and NaI) show enhancement of ionic conductivity with the addition of iodide salts. Figure 6.1 demonstrates variation of the ionic conductivity at different salt ratio of 5 to 35 wt.% of LiI, and 5 to 45 wt.% of NH₄I and NaI salts in the first three systems in this study.

While comparing LiI, NH₄I and NaI based SPEs, RS-7 SPE (containing 35 wt.% LiI) showed the highest ionic conductivity. In the RS:LiI system, SPE could not be prepared by adding more than 35 wt.% LiI due to difficulties in casting and handling the films.

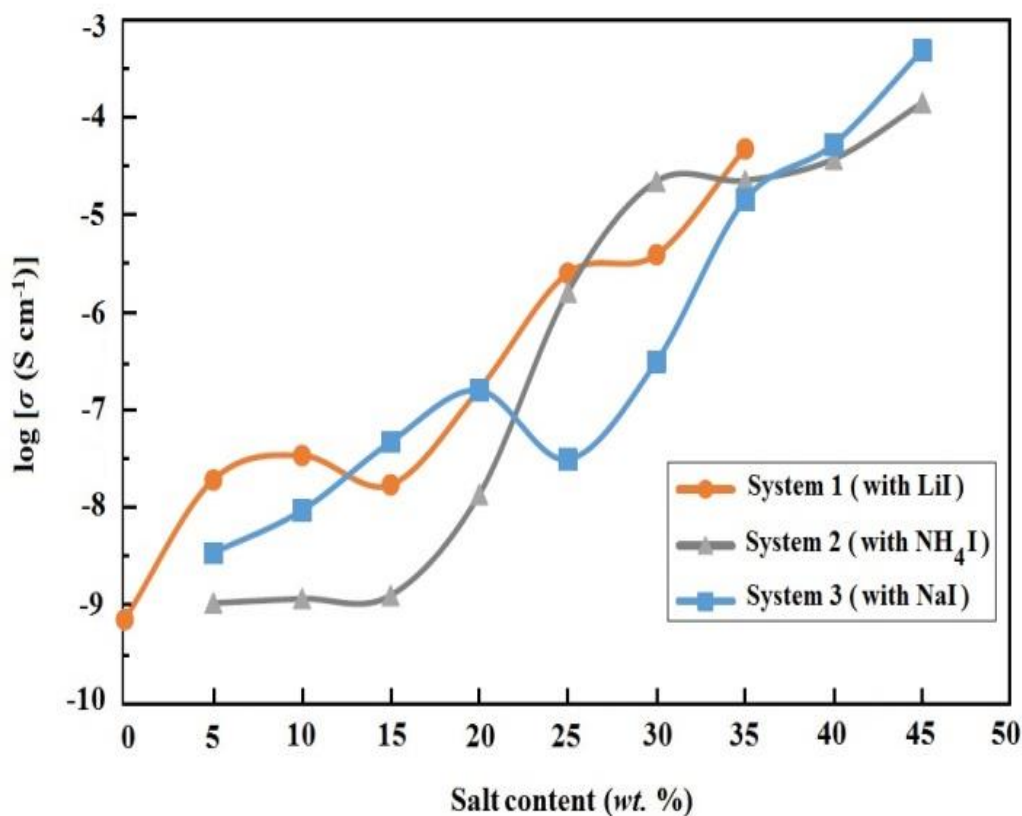


Figure 6.1: Ionic conductivity of RS: LiI, RS:NH₄I and RS:NaI systems at different salt contents

Further addition of other iodide salts showed an increasing trend in ionic conductivity. 45 wt.% NaI salt possesses the highest ionic conductivity compared to 45 wt.% of NH₄I salt (Khanmirzaei et al., 2015).

The electric resistivity of sodium (Na) is lower compared with lithium (Li). The electric resistivity of sodium and lithium are 47.7 and 92.8 (nΩ m), respectively, which can be the reason to increase the ionic conductivity in RS:NaI system compared with RS:LiI system (Serway, 1998).

The EIS data for ionic liquid based systems show ionic conductivity enhancement with the addition of MPII and HMII ionic liquids compared with the RS:LiI, RS:NH₄I and RS:NaI systems without ionic liquid.

Figure 6.2 shows the variation of ionic conductivity at different ionic liquid contents. The graph indicates that there is no significant ionic conductivity differences until 15 wt.% of MPII and HMII in both systems.

Consequently, according to Figure 6.2, after the addition of 20 wt.% of ionic liquid, there is a sharp increase of ionic conductivity with incorporation of HMII compared with MPII. This can be due to more plasticizing effect of HMII which increase the number of charge carriers due to the high self-dissociating and ion-transporting abilities of the ionic liquid (Jiang et al., 2006).

Among all five systems, RS:NaI:HMII exhibits highest ionic conductivity enhancement which in RNaH-4 SPE reaches to the highest ionic conductivity of 1.83×10^{-3} (S cm⁻¹) with 20 wt.% of HMII.

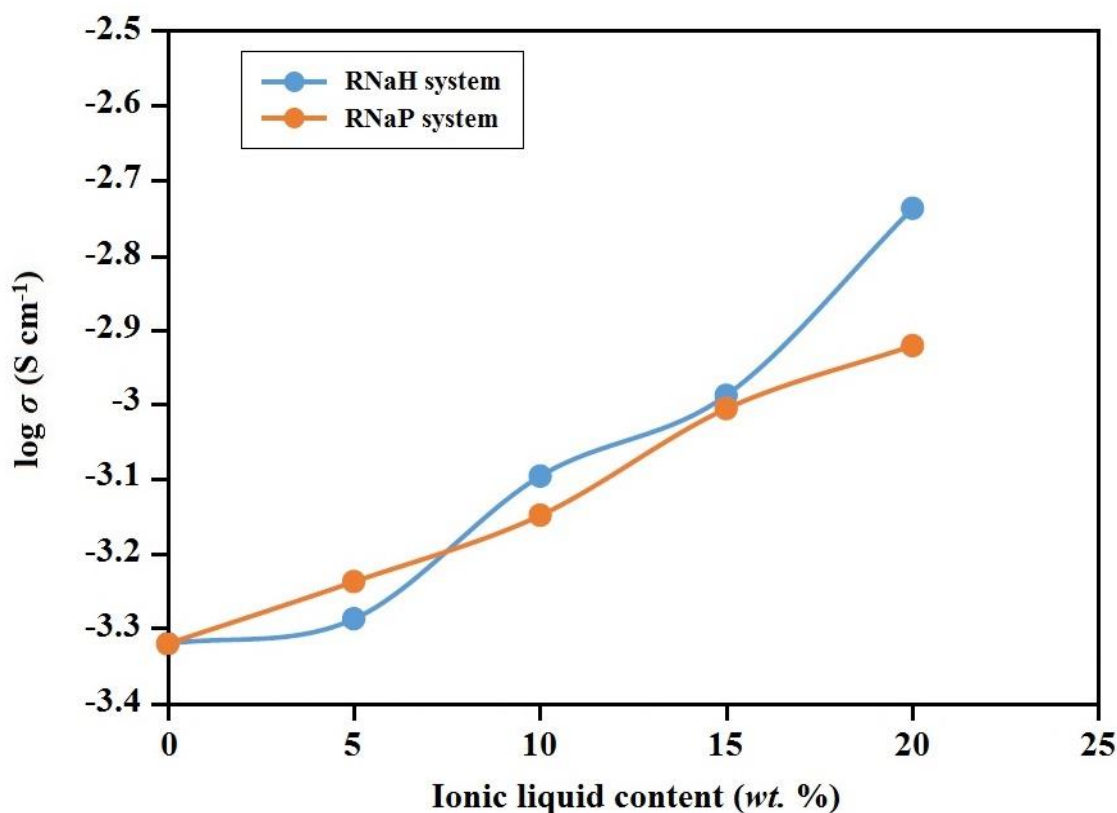


Figure 6.2: Ionic conductivity of RNaP and RNaH systems at different ionic liquid contents

6.2.2 TEMPERATURE DEPENDENT IONIC CONDUCTIVITY

The results for temperature dependent ionic conductivity study indicate that the ionic conductivity of all SPEs developed in this study, increases with increasing of temperature. This can be a further confirmation of no incorporation and existence of water in SPE samples. The results further show that activation energy decreases with an increase of ionic conductivity. The temperature-dependent results express that all five systems follow Arrhenius thermal activated model.

6.3 FTIR AND XRD STRUCTURAL CHARACTERIZATIONS

FTIR spectra in five systems in this work show confirmation of complexation between RS, iodide salts and ionic liquids. In all five systems, frequencies shift to another frequencies. The sequences of frequency shifts are different in some systems.

Furthermore, the shifting to lower frequencies in one system or higher frequency in another system like the shifting of frequency to lower in NH_4I based system and to higher in NaI based system may be due to more or less accumulation and aggregation of NaI salt (Liang et al., 2013; Tara-Lunga-Mihali et al., 2014).

The XRD patterns in all systems generally show more broadening after increase of iodide salts or ionic liquids. The system $\text{RS}:\text{NaI}$ shows more broadening compared to systems $\text{RS}:\text{LiI}$ and $\text{RS}:\text{NH}_4\text{I}$ which is result of more amorphous nature of $\text{RS}:\text{NaI}$ system according to the XRD patterns.

Consequently, the broadening in systems $\text{RS}:\text{NaI}:\text{MPII}$ and $\text{RS}:\text{NaI}:\text{HMII}$ including ionic liquid shows more broadening compared with first three systems without ionic liquid. This is due to existence of ionic liquid in SPEs after addition of ionic liquid, which can increase the ion mobility and flexibility.

6.4 TGA AND DSC THERMAL STUDIES

The TGA thermograms in all five systems show shifts in decomposition temperature (T_{dc}). The T_{dc} shifts to lower value in all five systems with the addition of iodide salt or ionic liquid.

Moreover, the DSC thermograms show the shift of glass transition temperature (T_g) in five systems. The T_g shifts by addition of LiI, NH_4I and NaI, but the shift in NH_4I and NaI based systems are larger than LiI based system. The reason can be expressed by molar mass of iodide salts, where the molar mass of LiI is 133.85 g/mol, for NH_4I is 144.94 g/mol and for NaI is 149.89 g/mol ($Mn(NaI) > Mn(NH_4I) > Mn(LiI)$). Thus, the molar mass of sodium iodide and ammonium iodide are very close to each other but for LiI there is big difference.

Consequently, this can be explained by Flory-Fox equation as equation given below (Bueche, 1956; Fox et al., 1950):

$$T_g = T_{g,\infty} - \frac{K}{M_n} \quad (6.1)$$

where $T_{g,\infty}$ is maximum glass transition temperature by theoretical infinite molecular mass, K is an empirical parameter related to the free volume of sample and M_n is molecular mass.

Thus, the Flory-Fox equation confirms that the LiI with lower molecular mass predicted to has lower glass transition temperature. In ionic liquid based systems the T_g value remains almost unchanged due to reason expressed in Chapter 5.

6.5 J-V CHARACTERISTICS

The J-V results in RS:NaI:MPH and RS:NaI:HMII systems shows significance enhancement of energy conversion efficiency compared with RNa-9 SPE without ionic

liquid. Figure 6.3 indicates that DSSC performance significantly improves in RNaP-3 and RNaP-4. Consequently, the current density in RNaP-3 is higher than RNaP-4 where open-circuit voltage and efficiency in RNaP-4 is higher than RNaP-3. The overall outcome of the results reveals that DSSC has higher performance fabricated with RNaP-4 SPE with 20 wt.% of HMII ionic liquid.

Figure 6.4 illustrates that DSSC performance is significantly higher in RNaH-4 compared with other SPEs in RS:NaI:HMII system and even among RS:NaI:MPII system. This maybe due to highest electron movement and mobility in RNaH-4, which increases the current density of the cell. This is due to higher plasticizing effect of HMII which results in higher flexibility of polymer backbone and facilitates ionic carriers' movement.

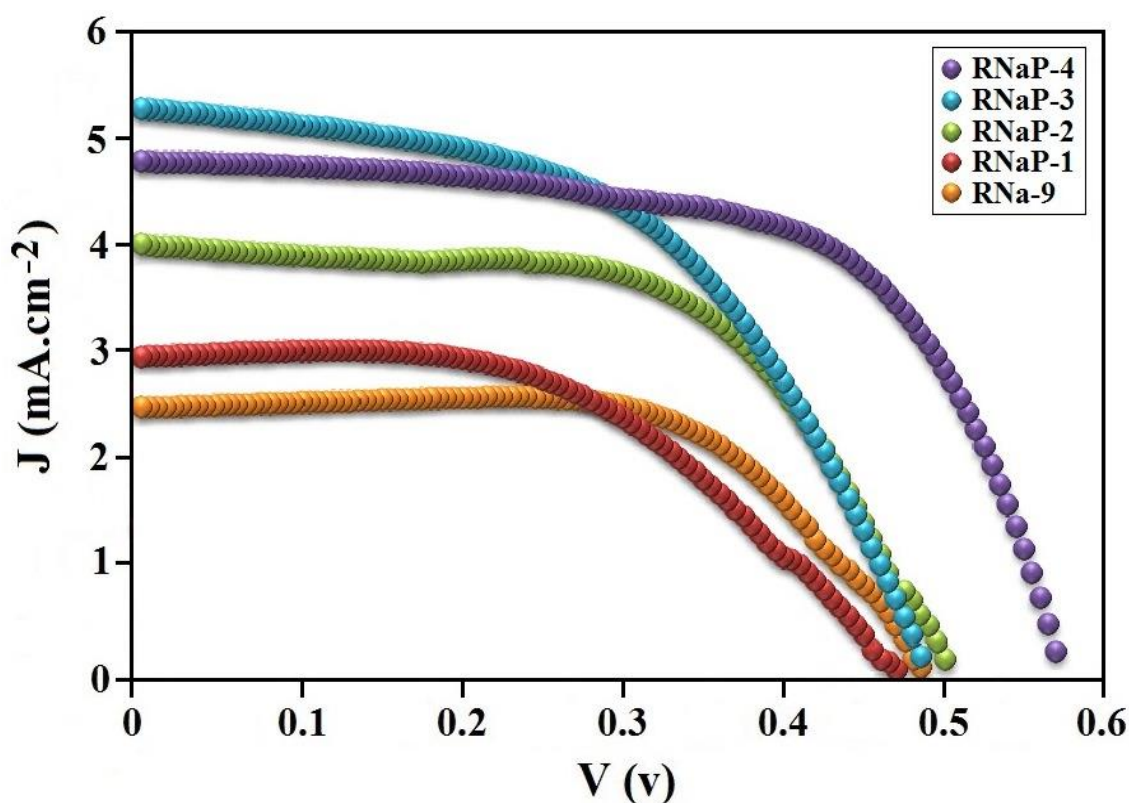


Figure 6.3: Photocurrent density versus cell potential (J-V) for DSSC fabricated using RNa-9, RNaP-1, RNaP-2, RNaP-3 and RNaP-4

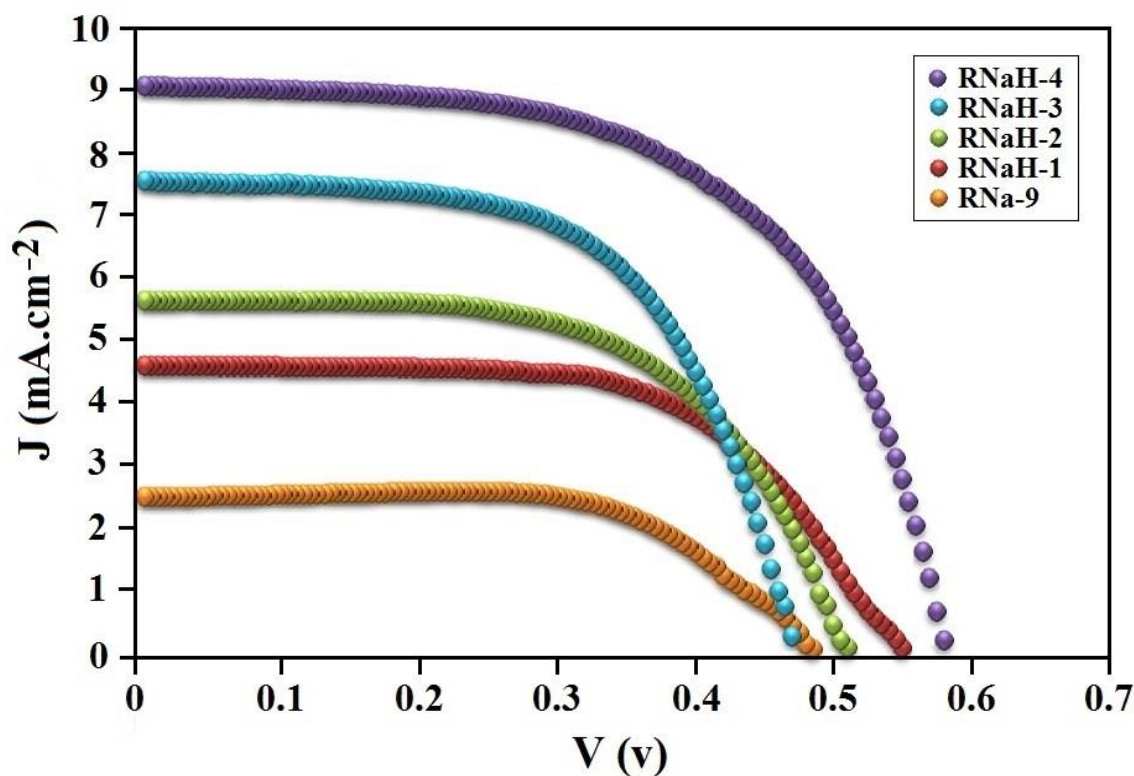


Figure 6.4: Photocurrent density versus cell potential (J-V) for DSSC fabricated using RNA-9, RNAH-1, RNAH-2, RNAH-3 and RNAH-4

The performance of fabricated DSSCs can further compared with comparison of energy conversion efficiencies. Figure 6.5 expresses the variation of efficiency at different MPII and HMII ionic liquid contents. The efficiency is significantly higher in HMII based systems compared with MPII based systems in all ionic liquid ratios. Especially, when the ionic liquid contents reach to 20 wt.% which means RNAH-4 and RNAH-4. Efficiency in RNAH-4 and RNAH-4 is 2.09 and 3.42 %, respectively. Therefore, efficiency in RNAH-4 is almost 1.6 times higher than RNAH-4. This is due to higher current density in HMII based SPEs which according to Equation (3.45) results in higher short-circuit current density and higher energy conversion efficiency.

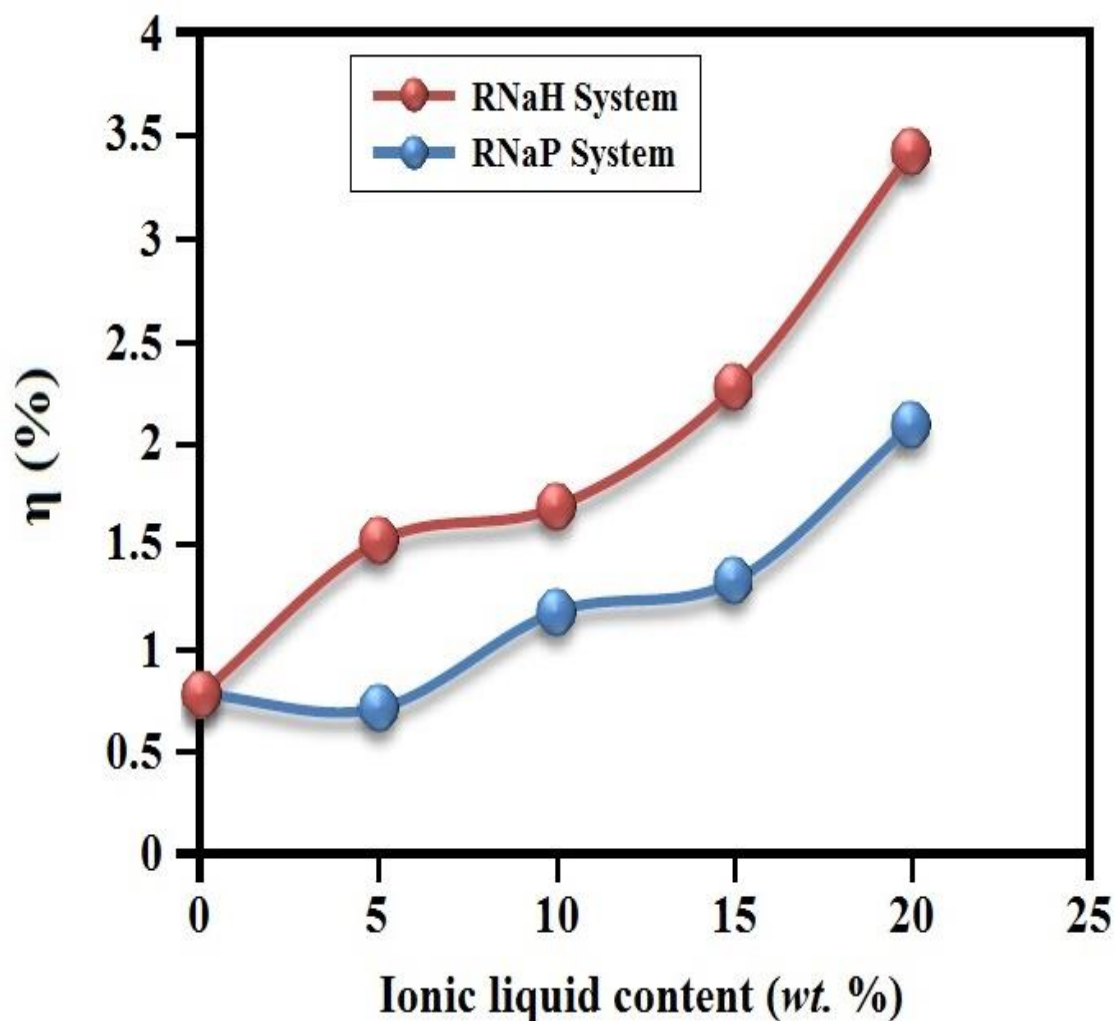


Figure 6.5: Variation of efficiency with MP11 and HM11 ionic liquid contents

Furthermore, compared to other works in literature, this work exhibits significant energy conversion efficiency enhancement of DSSC using biopolymer based polymer electrolyte after incorporation of ionic liquid. Among polymer electrolyte based DSSCs using biopolymers, Bandara et al., 2008, achieved energy conversion efficiency of 0.028 % using solid polymer electrolyte incorporating PEO, tetrapropylammonium iodide (Pr_4NI) and ethylene carbonate (EC) as plasticizer (PEO: Pr_4NI :EC). Singh P. K. et al., 2010, achieved efficiency of 0.73 % with solid polymer electrolyte with composition of chitosan, sodium iodide (NaI) and 1-ethyl-3-methylimidazolium thiocyanate (EMImSCN) ionic liquid (Chitosan:NaI:EMImSCN).

Singh R. et al., 2013, achieved 0.54 % using gel polymer electrolyte with composition of agarose and potassium iodide (KI) salt (Agarose:KI). Consequently, Singh R. et al., 2014, achieved efficiency of 0.63 % using solid polymer electrolyte with composition of Arrowroot Starch:KI. Table 9.1 further shows the comparison of efficiency of this work with the others work.

Table 6.1: Comparison of this work with other works on efficiency enhancement

Compositions	Conductivity, σ (S cm ⁻¹)	Efficiency, η (%)
PEO:Pr ₄ NI:EC (SPE)	$\sim 10^{-4}$	0.028
Chitosun:NaI:EMImSCN* (SPE)	$\sim 10^{-4}$	0.73
Agarose:KI (GPE)	$\sim 10^{-3}$	0.54
Arrowroot Starch:KI (SPE)	$\sim 10^{-4}$	0.63
RNaH-4 (this work) (SPE)	$\sim 10^{-3}$	3.42

* 1-ethyl 3-methyl imidazolium thiocyanate

6.6 SUMMARY

The differences between five solid polymer electrolytes were discussed in this chapter based on the results in Chapter 4 and Chapter 5. The EIS, structural, thermal and DSSC characterization results were compared for all systems. In conclusion, the RNaH-4 SPE with incorporation of 20 wt.% of HMII ionic liquid showed the highest ionic conductivity and energy conversion efficiency with the best DSSC performance among all the SPEs in this study. The conclusion of this study will be expressed in the following final chapter.

CHAPTER 7

CONCLUSION

The rice starch based solid polymer electrolytes (SPEs) incorporating LiI, NH₄I and NaI iodide salts, and 1-methyl-3-propylimidazolium iodide (MPII) and 1-hexyl-3-methylimidazolium iodide (HMII) ionic liquids were prepared in five systems using solution cast technique. The ionic conductivity of SPE samples were measure using EIS. The highest ionic conductivity of 4.68×10^{-5} (S cm⁻¹) was achieved in RS:LiI system with 35 wt.% of LiI (RS-7) with the lowest bulk resistance (R_b) of 96.0 Ω . In RS:NH₄I and RS:NaI systems, the highest ionic conductivity of 1.39×10^{-4} and 4.79×10^{-4} (S cm⁻¹), and the lowest R_b of 17.3 and 11.4 Ω were achieved, with 45 wt.% of NH₄I (RN-9) and NaI (RNa-9), respectively.

In ionic liquid incorporated systems, RS:NaI:MPII and RS:NaI:HMII systems, the highest ionic conductivity and lower R_b were achieved compared with the first three systems without ionic liquid. In RS:NaI:MPII system, the highest ionic conductivity and the lowest R_b of 1.20×10^{-3} (S cm⁻¹) and 5.37 Ω , respectively, were achieved with 20 wt.% of MPII ionic liquid (RNaP-4). Moreover, in RS:NaI:HMII system, the highest ionic conductivity and the lowest R_b of 1.83×10^{-3} (S cm⁻¹) and 2.66 Ω , respectively, were achieved with 20 wt.% of HMII (RNaH-4). Among all systems, RNaH-4 with 20 wt.% of HMII achieved the highest ionic conductivity. According to temperature-dependent studies, all five systems followed Arrhenius thermal activated model.

In structural characterizations, FTIR and XRD results confirmed in first three systems, complexation between rice starch and LiI, NH₄I and NaI occurred. In systems 4 and 5, FTIR and XRD results, confirmed complexation between rice starch, NaI, MPII and HMII occurred, as well.

FTIR spectra revealed that frequencies shifted to higher or lower frequencies after incorporation of LiI, NH₄I and NaI iodide salts, and MP11 and HM11 ionic liquids.

XRD patterns showed more broadening with less intense and amorphous nature after the addition of iodide salts and ionic liquids. More broadening occurred in RS:NaI:MP11 and RS:NaI:HM11 systems containing MP11 and HM11 ionic liquids.

In thermal studies, TGA and DSC characterization applied to SPEs. Thermal studies further confirmed complexation between rice starch and iodide salts and ionic liquids. According to TGA results, T_{dc} shifted to lower temperatures after addition of iodide salts and ionic liquids. In DSC studies, T_g shifted to lower temperatures after addition of LiI, NH₄I and NaI iodide salts and, MP11 and HM11 ionic liquids.

The composition of SPE with the highest achieved ionic conductivity in first three samples without ionic liquid, which is RNa-9 with 45 wt.% of NaI iodide salt, used in preparation of SPEs in systems 4 and 5 with MP11 and HM11 ionic liquids. Consequently, All SPEs in systems 4 and 5, and RNa-9 used for dye-sensitized solar cell (DSSC) fabrication. All the mentioned SPEs examined under Sun simulator in 100 mW/m² to obtain the J-V curves. DSSC based on RNa-9 (without ionic liquid) showed the lowest energy conversion efficiency of 0.78 %. In systems 4 and 5, almost in all SPEs the current density (J) increased with the addition of MP11 and HM11 ionic liquids. In system 4, RNaP-4 showed the highest efficiency of 2.09 %. Moreover, in system 5, RNaH-4 showed the highest energy conversion efficiency of 3.42 % with J_{sc}, V_{oc} and ff of 9.07 (mA cm⁻²), 0.58 (V) and 0.65. The highest open-circuit voltage of 0.58 V is also achieved in RNaH-4. Consequently, RNaH-4 achieved the highest efficiency among all the systems.

The ionic liquid based solid polymer electrolytes in RS:NaI:MPII and RS:NaI:HMII systems in this study can be good candidate to fabricate Dye-sensitized solar cells based on biodegradable environmentally friendly polymers like rice starch. This study can further studied using other biopolymers such as hydroxypropyl cellulose (HPC), agar and carrageenan for future works.

As future works, this work can be further studied to enhance the ionic conductivity of solid polymer electrolytes, and efficiency and performance of dye-sensitized solar cell. The solid polymer electrolytes in this work can be further enhanced using binary ionic liquid based systems such as MPII:HMII binary system. Consequently, the ionic conductivity can be enhanced with incorporation of fillers such as TiO_2 and carbon nanotubes (CNTs) and graphene oxides (GOs). Moreover, energy conversion efficiency and performance of solid polymer electrolyte based dye-sensitized solar cells in this work can be further enhanced using some other dyes such as sulfonate dyes, or use some additives of redox electrolyte to improve fill factor or open-circuit voltage of dye-sensitized solar cells such as 4-tert-butylpyridine into photo-anode electrode which can enhance the energy conversion efficiency.

REFERENCES

- Aoyagi, S., Izumi, H., Nakahara, S., Ochi, M., & Ogawa, H. (2008). Laser Microfabrication Of Long Thin Holes On Biodegradable Polymer In Vacuum For Preventing Cloginess And Its Application To Blood Collection. *Sensors And Actuators A: Physical*, 145–146(0), 464-472.
- Arbizzani, C., Gabrielli, G., & Mastragostino, M. (2011). Thermal Stability And Flammability Of Electrolytes For Lithium-Ion Batteries. *Journal Of Power Sources*, 196(10), 4801-4805.
- Armand, M. (1983). Polymer Solid Electrolytes - An Overview. *Solid State Ionics*, 9–10, Part 2(0), 745-754.
- Armand, M. (1986). Polymer Electrolytes. *Annual Review Of Materials Science*, 16(1), 245-261.
- Armand, M. (1994). The History Of Polymer Electrolytes. *Solid State Ionics*, 69(3–4), 309-319.
- Armand, M., Chabagno, J. M., & Duclot, M. J. (1979). *Fast Ion Transport In Solids* (P. Vashishta, J. N. Mundy & G. K. Shenoy Eds.). North-Holland, Amsterdam.
- Armentano, I., Dottori, M., Fortunati, E., Mattioli, S., & Kenny, J. M. (2010). Biodegradable Polymer Matrix Nanocomposites For Tissue Engineering: A Review. *Polymer Degradation And Stability*, 95(11), 2126-2146.
- Arvanitoyannis, I., Biliaderis, C. G., Ogawa, H., & Kawasaki, N. (1998). Biodegradable Films Made From Low-Density Polyethylene (Ldpe), Rice Starch And Potato Starch For Food Packaging Applications: Part 1. *Carbohydrate Polymers*, 36(2–3), 89-104.
- Bandara, T. M. W. J., Dissanayake, M. A. K. L., Ileperuma, O. A., Varapathan, K., Vignarooban, K., & Mellander, B. E. (2008). Polyethyleneoxide (Peo)-Based, Anion Conducting Solid Polymer Electrolyte For Pec Solar Cells. *Journal Of Solid State Electrochemistry*, 12(7-8), 913-917.
- Bandara, T. M. W. J., Dissanayake, M. A. K. L., Jayasundara, W. J. M. J. S. R., Albinsson, I., & Mellander, B. E. (2012). Efficiency Enhancement In Dye Sensitized Solar Cells Using Gel Polymer Electrolytes Based On A Tetrahexylammonium Iodide And Mgi2 Binary Iodide System. *Physical Chemistry Chemical Physics*, 14(24), 8620-8627.

- Bandara, T. M. W. J., & Mellander, B.-E. (2011). Evaluation Of Mobility, Diffusion Coefficient And Density Of Charge Carriers In Ionic Liquids And Novel Electrolytes Based On A New Model For Dielectric Response. In P. A. Kokorin (Ed.), *Ionic Liquids: Theory, Properties, New Approaches*: Intech.
- Baskaran, R., Selvasekarapandian, S., Hirankumar, G., & Bhuvaneshwari, M. S. (2004). Dielectric And Conductivity Relaxations In Pvac Based Polymer Electrolytes. *Ionics*, 10(1-2), 129-134.
- Biliaderis, C. G. (1998). Structures And Phase Transitions Of Starch Polymers. In H. W. Reginald (Ed.), *Polysaccharide Association Structures In Food* (Vol. 87). Usa: Marcel Dekker, Inc.
- Blythe, A. R. (1979). *Electrical Properties Of Polymers*. Uk: Cambridge University Press.
- Boley, A., Müller, W. R., & Haider, G. (2000). Biodegradable Polymers As Solid Substrate And Biofilm Carrier For Denitrification In Recirculated Aquaculture Systems. *Aquacultural Engineering*, 22(1-2), 75-85.
- Bottom, R. (2008). Thermogravimetric Analysis. In P. Gabbott (Ed.), *Principles And Applications Of Thermal Analysis*. Singapore: Blackwell Publishing.
- Bower, D. I. (2002). *An Introduction To Polymer Physics*. Uk: Cambridge University Press.
- Brady, J. E., & Senese, F. (2004). *Chemistry Matter And Its Changes By Brady & Senese* (4th Ed.): John Wiley & Sons.
- Brouillet, F., Bataille, B., & Cartilier, L. (2008). High-Amylose Sodium Carboxymethyl Starch Matrices For Oral, Sustained Drug-Release: Formulation Aspects And In Vitro Drug-Release Evaluation. *International Journal Of Pharmaceutics*, 356(1-2), 52-60.
- Bruce, P. G. (1997). *Solid State Electrochemistry*: Cambridge University Press.
- Bueche, F. (1956). Derivation Of The Wlf Equation For The Mobility Of Molecules In Molten Glasses. *The Journal Of Chemical Physics*, 24(2), 418-419.

- Calinescu, C., Mondovi, B., Federico, R., Ispas-Szabo, P., & Mateescu, M. A. (2012). Carboxymethyl Starch: Chitosan Monolithic Matrices Containing Diamine Oxidase And Catalase For Intestinal Delivery. *International Journal Of Pharmaceutics*, 428(1-2), 48-56.
- Cameron, G. G. (1988). Polymer Electrolyte Reviews 1. In J. R. M. A. C. A. Vincent (Ed.), *British Polymer Journal* (Vol. 20, Pp. 299-300): John Wiley & Sons, Ltd.
- Cho, M., Seo, H., Nam, J., Choi, H., Koo, J., & Lee, Y. (2007). High Ionic Conductivity And Mechanical Strength Of Solid Polymer Electrolytes Based On Nbr/Ionic Liquid And Its Application To An Electrochemical Actuator. *Sensors And Actuators B: Chemical*, 128(1), 70-74.
- Choi, N.-S., Koo, B., Yeon, J.-T., Lee, K. T., & Kim, D.-W. (2011). Effect Of A Novel Amphipathic Ionic Liquid On Lithium Deposition In Gel Polymer Electrolytes. *Electrochimica Acta*, 56(21), 7249-7255.
- Cole, M., Sheldon, M. H., Glasse, M. D., Latham, R. J., & Linford, R. G. (1989). Exafs And Thermal Studies On Zinc Polymeric Electrolytes. *Applied Physics A-Materials Science & Processing*, 49(3), 249-257.
- De Freitas, J. N., Benedetti, J. E., Freitas, F. S., Nogueira, A. F., & De Paoli, M. A. (2010). Polymer Electrolytes For Dye-Sensitized Solar Cells. In C. Sequeira; & D. Santos (Eds.), *Polymer Electrolytes: Fundamentals And Applications*. Uk: Woodhead Publishing.
- Dunsch, L. (1988). Electrochemical Science And Technology Of Polymers. In R. G. Linford (Ed.), *Acta Polymerica* (Vol. 1, Pp. 468-469): Akademie Verlag GmbH.
- Elliott, S. R. (1987). A.C. Conduction In Amorphous Chalcogenide And Pnictide Semiconductors. *Advances In Physics*, 36(2), 135-217.
- Fei, Z. F., Kuang, D. B., Zhao, D. B., Klein, C., Ang, W. H., Zakeeruddin, S. M., Dyson, P. J. (2006). A Supercooled Imidazolium Iodide Ionic Liquid As A Low-Viscosity Electrolyte For Dye-Sensitized Solar Cells. *Inorganic Chemistry*, 45(26), 10407-10409.
- Fonseca, C. P., Rosa, D. S., Gaboardi, F., & Neves, S. (2006). Development Of A Biodegradable Polymer Electrolyte For Rechargeable Batteries. *Journal Of Power Sources*, 155(2), 381-384.

- Fox, T. G., & Flory, P. J. (1950). Second-Order Transition Temperatures And Related Properties Of Polystyrene. I. Influence Of Molecular Weight. *Journal Of Applied Physics*, 21(6), 581-591.
- Gabbott, P. (2008). A Practical Introduction To Differential Scanning Calorimetry. In P. Gabbott (Ed.), *Principles And Applications Of Thermal Analysis*. Singapore: Blackwell Publishing.
- Grätzel, M. (2003). Dye-Sensitized Solar Cells. *Journal Of Photochemistry And Photobiology C: Photochemistry Reviews*, 4(2), 145-153.
- Gray, F. M. (1991). *Solid Polymer Electrolytes, Fundamentals And Technological Applications*. Usa: Vch Publishers.
- Gray, F. M. (1997). *Polymer Electrolytes*. Cambridge, Uk: Rsc Materials Monographs.
- Griffiths, P. R., & Haseth, J. A. D. (2007). *Fourier Transform Infrared Spectrometry*. Usa: John Wiley & Sons.
- Gunatillake, P., Mayadunne, R., & Adhikari, R. (2006). Recent Developments In Biodegradable Synthetic Polymers. In M. R. El-Gewely (Ed.), *Biotechnology Annual Review* (Vol. Volume 12, Pp. 301-347): Elsevier.
- Hagfeldt, A., Boschloo, G., Sun, L., Kloo, L., & Pettersson, H. (2010). Dye-Sensitized Solar Cells. *Chemical Reviews*, 110(11), 6595-6663.
- Hara, K., & Arakawa, H. (2005). Dye-Sensitized Solar Cells *Handbook Of Photovoltaic Science And Engineering* (Pp. 663-700): John Wiley & Sons, Ltd.
- Imasaka, K., Yoshida, M., Fukuzaki, H., Asano, M., Kumakura, M., Mashimo, T., . . . Nagai, T. (1992). New Biodegradable Polymers Of L-Lactic Acid And Aromatic Hydroxy Acids And Their Applications In Drug Delivery Systems. *International Journal Of Pharmaceutics*, 81(1), 31-38.
- Jankowski, T., & Rha, C. K. (1986). Retrogradation Of Starch In Cooked Wheat. *Starch - Stärke*, 38(1), 6-9.
- Jiang, J., Gao, D., Li, Z., & Su, G. (2006). Gel Polymer Electrolytes Prepared By In Situ Polymerization Of Vinyl Monomers In Room-Temperature Ionic Liquids. *Reactive And Functional Polymers*, 66(10), 1141-1148.

- Kaplan, M. L., Reitman, E. A., & Cava, R. J. (1989). Solid Polymer Electrolytes: Attempts To Improve Conductivity. *Polymer*, 30(3), 504-508.
- Kelly, C. A., & Meyer, G. J. (2001). Excited State Processes At Sensitized Nanocrystalline Thin Film Semiconductor Interfaces. *Coordination Chemistry Reviews*, 211, 295-315.
- Kent-Jones, D. W. (2014). Cereal Processing, *Britannica*.
- Khanmirzaei, M. H., & Ramesh, S. (2013). Ionic Transport And Ftir Properties Of Lithium Iodide Doped Biodegradable Rice Starch Based Polymer Electrolytes. *International Journal Of Electrochemical Science*, 8(7), 9977-9991.
- Khanmirzaei, M. H., & Ramesh, S. (2014a). Nanocomposite Polymer Electrolyte Based On Rice Starch/Ionic Liquid/Tio2 Nanoparticles For Solar Cell Application. *Measurement*, 58(0), 68-72.
- Khanmirzaei, M. H., & Ramesh, S. (2014b). Studies On Biodegradable Polymer Electrolyte Rice Starch (Rs) Complexed With Lithium Iodide. *Ionics*, 20(5), 691-695.
- Khanmirzaei, M. H., Ramesh, S., & Ramesh, K. (2015). Effect Of Different Iodide Salts On Ionic Conductivity And Structural And Thermal Behavior Of Rice-Starch-Based Polymer Electrolytes For Dye-Sensitized Solar Cell Application. *Ionics*, 21 (8) 2383-2391.
- Kim, C. T., Shih, F. F., Champagne, E. T., & Daigle, K. (1999). Effects Of Phosphorylating Salts And Temperature On The Preparation Of Rice Starch Phosphates By Extrusion. *Starch-Starke*, 51(8-9), 280-286.
- Kim, M., Jung, B., & Park, J.-H. (2012). Hydrogel Swelling As A Trigger To Release Biodegradable Polymer Microneedles In Skin. *Biomaterials*, 33(2), 668-678.
- Kiran Kumar, K., Ravi, M., Pavani, Y., Bhavani, S., Sharma, A. K., & Narasimha Rao, V. V. R. (2011). Investigations On The Effect Of Complexation Of Naf Salt With Polymer Blend (Peo/Pvp) Electrolytes On Ionic Conductivity And Optical Energy Band Gaps. *Physica B: Condensed Matter*, 406(9), 1706-1712.
- Kizil, R., Irudayaraj, J., & Seetharaman, K. (2002). Characterization Of Irradiated Starches By Using Ft-Raman And Ftir Spectroscopy. *Journal Of Agricultural And Food Chemistry*, 50(14), 3912-3918.

- Klassen, B., Aroca, R., Nazri, M., & Nazri, G. A. (1998). Raman Spectra And Transport Properties Of Lithium Perchlorate In Ethylene Carbonate Based Binary Solvent Systems For Lithium Batteries. *The Journal Of Physical Chemistry B*, 102(24), 4795-4801.
- Klein, C., Nazeeruddin, M. K., Di Censo, D., Liska, P., & Grätzel, M. (2004). Amphiphilic Ruthenium Sensitizers And Their Applications In Dye-Sensitized Solar Cells. *Inorganic Chemistry*, 43(14), 4216-4226.
- Kobayashi, N., Sunaga, S., & Hirohashi, R. (1992). Effect Of Additive Salts On Ion Conductivity Characteristics In Solid Polymer Electrolytes. *Polymer*, 33(14), 3044-3048.
- Kremer, F., & Schonhals, A. (2003). *Broadband Dielectric Spectroscopy*
- Kulp, K., Ponte, J. G., & D'apponia, B. L. (1981). Staling Of White Pan Bread: Fundamental Causes. *C R C Critical Reviews In Food Science And Nutrition*, 15(1), 1-48.
- Kumar, M., Tiwari, T., & Srivastava, N. (2012). Electrical Transport Behaviour Of Bio-Polymer Electrolyte System: Potato Starch+Ammonium Iodide. *Carbohydrate Polymers*, 88(1), 54-60.
- Kurc, B. (2014). Precipitated Silica As Filler For Polymer Electrolyte Based On Poly(Acrylonitrile)/Sulfolane. *Journal Of Solid State Electrochemistry*, 18(7), 2035-2046.
- Kurlansky, M. (2002). *Salt: A World History*. Usa: Penguin Books.
- Lakshmi, S., Katti, D. S., & Laurencin, C. T. (2003). Biodegradable Polyphosphazenes For Drug Delivery Applications. *Advanced Drug Delivery Reviews*, 55(4), 467-482.
- Leclerc, E., Furukawa, K. S., Miyata, F., Sakai, Y., Ushida, T., & Fujii, T. (2004). Fabrication Of Microstructures In Photosensitive Biodegradable Polymers For Tissue Engineering Applications. *Biomaterials*, 25(19), 4683-4690.
- Leclerc, E., Miyata, F., Furukawa, K. S., Ushida, T., Sakai, Y., & Fujii, T. (2004). Effect On Liver Cells Of Stepwise Microstructures Fabricated In A Photosensitive Biodegradable Polymer By Softlithography. *Materials Science And Engineering: C*, 24(3), 349-354.

- Lemieux, M., Gosselin, P., & Mateescu, M. A. (2009). Carboxymethyl High Amylose Starch As Excipient For Controlled Drug Release: Mechanistic Study And The Influence Of Degree Of Substitution. *International Journal Of Pharmaceutics*, 382(1–2), 172-182.
- Lenz, R. (1993). Biodegradable Polymers. In R. Langer & N. Peppas (Eds.), *Biopolymers I* (Vol. 107, Pp. 1-40): Springer Berlin Heidelberg.
- Li, M., Wang, L., & Du, T. (2014). Preparation Of Polymer Electrolytes Based On The Polymerized Imidazolium Ionic Liquid And Their Applications In Lithium Batteries. *Journal Of Applied Polymer Science*, 131(20).
- Liang, G., Zhong, Z., Qu, S., Wang, S., Liu, K., Wang, J., & Xu, J. (2013). Novel In Situ Crosslinked Polymer Electrolyte For Solid-State Dye-Sensitized Solar Cells. *Journal Of Materials Science*, 48(18), 6377-6385.
- Liew, C.-W., Ramesh, S., Ramesh, K., & Arof, A. K. (2012). Preparation And Characterization Of Lithium Ion Conducting Ionic Liquid-Based Biodegradable Corn Starch Polymer Electrolytes. *Journal Of Solid State Electrochemistry*, 16(5), 1869-1875.
- Lopes, L. V. S., Dragunski, D. C., Pawlicka, A., & Donoso, J. P. (2003). Nuclear Magnetic Resonance And Conductivity Study Of Starch Based Polymer Electrolytes. *Electrochimica Acta*, 48(14–16), 2021-2027.
- Lörcks, J. (1998). Properties And Applications Of Compostable Starch-Based Plastic Material. *Polymer Degradation And Stability*, 59(1–3), 245-249.
- Lu, Y., & Chen, S. C. (2004). Micro And Nano-Fabrication Of Biodegradable Polymers For Drug Delivery. *Advanced Drug Delivery Reviews*, 56(11), 1621-1633.
- Lvovich, V. F. (2012). *Impedance Spectroscopy*. Usa: John Wiley & Sons.
- Marcondes, R. F. M. S., D'agostini, P. S., Ferreira, J., Giroto, E. M., Pawlicka, A., & Dragunski, D. C. (2010). Amylopectin-Rich Starch Plasticized With Glycerol For Polymer Electrolyte Application. *Solid State Ionics*, 181(13–14), 586-591.
- Marcus, Y. (1987). Ion Solvation. *Angewandte Chemie*, 99(8), 826-826.
- Mattos, R. I., Tambelli, C. E., Donoso, J. P., & Pawlicka, A. (2007). Nmr Study Of Starch Based Polymer Gel Electrolytes: Humidity Effects. *Electrochimica Acta*, 53(4), 1461-1465.

- Middleton, J. C., & Tipton, A. J. (2000). Synthetic Biodegradable Polymers As Orthopedic Devices. *Biomaterials*, 21(23), 2335-2346.
- Mohamad, A. A., & Arof, A. K. (2007). Plasticized Alkaline Solid Polymer Electrolyte System. *Materials Letters*, 61(14-15), 3096-3099.
- Mott, N. F., & Davis, E. A. (1979). *Electronic Processes In Non-Crystalline Materials* (2nd Ed.). Oxford: Clarendon Press.
- Mutters, R. G., & Thompson, J. F. (2009). *Rice Quality Handbook*. University Of California: Anr Publisher.
- Nair, L. S., & Laurencin, C. T. (2007). Biodegradable Polymers As Biomaterials. *Progress In Polymer Science*, 32(8-9), 762-798.
- Nakazawa, F., Noguchi, S., Takahashi, J., & Takada, M. (1985). Retrogradation Of Gelatinized Potato Starch Studied By Differential Scanning Calorimetry. *Agricultural And Biological Chemistry*, 49(4), 953-957.
- Nei De Freitas, J., Longo, C., Nogueira, A. F., & De Paoli, M.-A. (2008). Solar Module Using Dye-Sensitized Solar Cells With A Polymer Electrolyte. *Solar Energy Materials And Solar Cells*, 92(9), 1110-1114.
- Nelson, J. (2003). *The Physics Of Solar Cells*. Uk: Imperial College Press.
- Ning, W., Xingxiang, Z., Haihui, L., & Benqiao, H. (2009). 1-Allyl-3-Methylimidazolium Chloride Plasticized-Corn Starch As Solid Biopolymer Electrolytes. *Carbohydrate Polymers*, 76(3), 482-484.
- Ning, W., Xingxiang, Z., Haihui, L., & Jianping, W. (2009). N, N-Dimethylacetamide/Lithium Chloride Plasticized Starch As Solid Biopolymer Electrolytes. *Carbohydrate Polymers*, 77(3), 607-611.
- Nishat, N., & Malik, A. Biodegradable Coordination Polymer: Polycondensation Of Glutaraldehyde And Starch In Complex Formation With Transition Metals Mn(Ii), Co(Ii), Ni(Ii), Cu(Ii) And Zn(Ii). *Arabian Journal Of Chemistry*(0).
- Nishimoto, A., Agehara, K., Furuya, N., Watanabe, T., & Watanabe, M. (1999). High Ionic Conductivity Of Polyether-Based Network Polymer Electrolytes With Hyperbranched Side Chains. *Macromolecules*, 32(5), 1541-1548.

- Nithya, S., Selvasekarapandian, S., Karthikeyan, S., & Vinoth Pandi, D. (2015). Effect Of Propylene Carbonate On The Ionic Conductivity Of Polyacrylonitrile-Based Solid Polymer Electrolytes. *Journal Of Applied Polymer Science*, 132(14), N/A-N/A.
- Oregan, B., & Gratzel, M. (1991). A Low-Cost, High-Efficiency Solar-Cell Based On Dye-Sensitized Colloidal Tio₂ Films. *Nature*, 353(6346), 737-740.
- Panlasigui, L. N., Thompson, L. U., Juliano, B. O., Perez, C. M., Yiu, S. H., & Greenberg, G. R. (1991). Rice Varieties With Similar Amylose Content Differ In Starch Digestibility And Glycemic Response In Humans. *The American Journal Of Clinical Nutrition*, 54(5), 871-877.
- Polo Fonseca, C., & Neves, S. (2006). Electrochemical Properties Of A Biodegradable Polymer Electrolyte Applied To A Rechargeable Lithium Battery. *Journal Of Power Sources*, 159(1), 712-716.
- Pretsch, E., Buhlmann, P., & Badertscher, M. (2009). *Structure Determination Of Organic Compounds : Tables Of Spectral Data*, (4th Ed.). Berlin: Springer.
- Pu, H., Chen, L., Li, X., Xie, F., Yu, L., & Li, L. (2011). An Oral Colon-Targeting Controlled Release System Based On Resistant Starch Acetate: Synthetization, Characterization, And Preparation Of Film-Coating Pellets. *Journal Of Agricultural And Food Chemistry*, 59(10), 5738-5745.
- Ramesh, S., Shanti, R., & Morris, E. (2012a). Exerted Influence Of Deep Eutectic Solvent Concentration In The Room Temperature Ionic Conductivity And Thermal Behavior Of Corn Starch Based Polymer Electrolytes. *Journal Of Molecular Liquids*, 166(0), 40-43.
- Ramesh, S., Shanti, R., & Morris, E. (2012b). Studies On The Plasticization Efficiency Of Deep Eutectic Solvent In Suppressing The Crystallinity Of Corn Starch Based Polymer Electrolytes. *Carbohydrate Polymers*, 87(1), 701-706.
- Ren, S., Zheng, T., Zhou, Q., Zhang, L., & Li, H. (2014). Preparation And Ionic Conductivity Of Composite Polymer Electrolytes Based On Hyperbranched Star Polymer. *Ionics*, 20(9), 1225-1234.
- Revedin, A., Aranguren, B., Becattini, R., Longo, L., Marconi, E., Lippi, M. M., . . . Svoboda, J. (2010). Thirty Thousand-Year-Old Evidence Of Plant Food Processing. *Proceedings Of The National Academy Of Sciences Of The United States Of America*, 107(44), 18815-18819.

- Rice, M. J., & Roth, W. L. (1972). Ionic Transport In Super Ionic Conductors: A Theoretical Model. *Journal Of Solid State Chemistry*, 4(2), 294-310.
- Ring, S. G. (1985). Some Studies On Starch Gelation. *Starch - Stärke*, 37(3), 80-83.
- Rodrigues, E. M. O. A. A. (2012). *Starch: From Food To Medicine*: Intech.
- Saboktakin, M. R., Tabatabaie, R. M., Maharramov, A., & Ramazanov, M. A. (2011). Synthesis And In Vitro Evaluation Of Carboxymethyl Starch–Chitosan Nanoparticles As Drug Delivery System To The Colon. *International Journal Of Biological Macromolecules*, 48(3), 381-385.
- Samutsri, W., & Suphantharika, M. (2012). Effect Of Salts On Pasting, Thermal, And Rheological Properties Of Rice Starch In The Presence Of Non-Ionic And Ionic Hydrocolloids. *Carbohydrate Polymers*, 87(2), 1559-1568.
- Schnabelrauch, M., Vogt, S., Larcher, Y., & Wilke, I. (2002). Biodegradable Polymer Networks Based On Oligolactide Macromers: Synthesis, Properties And Biomedical Applications. *Biomolecular Engineering*, 19(2–6), 295-298.
- Schultze, J. W. (1996). Electrochemistry Of Novel Materials. Edited By And In J. Lipkowski & P. N. Ross (Eds.), *Advanced Materials* (Vol. 3, Pp. 360-361): Wiley-Vch Verlag Gmbh.
- Selvasekarapandian, S., Baskaran, R., Kamishima, O., Kawamura, J., & Hattori, T. (2006). Laser Raman And Ftir Studies On Li+ Interaction In Pvac–LiclO4 Polymer Electrolytes. *Spectrochimica Acta Part A: Molecular And Biomolecular Spectroscopy*, 65(5), 1234-1240.
- Sen, G., & Pal, S. (2009). A Novel Polymeric Biomaterial Based On Carboxymethylstarch And Its Application In Controlled Drug Release. *Journal Of Applied Polymer Science*, 114(5), 2798-2805.
- Sequeira, C., & Santos, D. (2010). *Polymer Electrolytes: Fundamentals And Applications*: Woodhead Publishing.
- Serway, R. A. N. E. E. (1998). *Principles Of Physics* (4th Ed.). Uk: Saunders College Publication.

- Shaarawy, H. H., El-Rafie, S. M., Abd El-Ghaffar, A. M., & El-Rafie, M. H. (2009). Electrocatalytic Oxidation Of Rice Starch Using Mixed Oxidant Generated Via Titanium/Rhodium Thermally Activated Modified Electrode: Part (I). *Carbohydrate Polymers*, 75(2), 208-213.
- Singh, P. K., Bhattacharya, B., Nagarale, R. K., Kim, K.-W., & Rhee, H.-W. (2010). Synthesis, Characterization And Application Of Biopolymer-Ionic Liquid Composite Membranes. *Synthetic Metals*, 160(1-2), 139-142.
- Singh, R., Baghel, J., Shukla, S., Bhattacharya, B., Rhee, H.-W., & Singh, P. K. (2014). Detailed Electrical Measurements On Sago Starch Biopolymer Solid Electrolyte. *Phase Transitions*, 87(12), 1237-1245.
- Singh, R., Bhattacharya, B., Rhee, H.-W., & Singh, P. K. (2014). New Biodegradable Polymer Electrolyte For Dye Sensitized Solar Cell. *International Journal Of Electrochemical Science*, 9(5), 2620-2630.
- Singh, R., Jadhav, N. A., Majumder, S., Bhattacharya, B., & Singh, P. K. (2013). Novel Biopolymer Gel Electrolyte For Dye-Sensitized Solar Cell Application. *Carbohydrate Polymers*, 91(2), 682-685.
- Singh, V. K., Annu, A., Singh, U., Singh, P., Pandey, S. P., Bhattacharya, B., & Singh, P. K. (2013). Dye Sensitized Solar Cell Based On Poly(Vinyl Alcohol) Doped With Ammonium Iodide Solid Polymer Electrolyte. *Journal Of Optoelectronics And Advanced Materials*, 15(9-10), 927-931.
- Sinha Ray, S., & Bousmina, M. (2005). Biodegradable Polymers And Their Layered Silicate Nanocomposites: In Greening The 21st Century Materials World. *Progress In Materials Science*, 50(8), 962-1079.
- Skotheim, T. (1988). *Electroresponsive Molecular And Polymeric Systems* (T. Skotheim Ed. Vol. 1). New York: Marcel Dekker.
- Strange, M., Plackett, D., Kaasgaard, M., & Krebs, F. C. (2008). Biodegradable Polymer Solar Cells. *Solar Energy Materials And Solar Cells*, 92(7), 805-813.
- Su'ait, M. S., Ahmad, A., Hamzah, H., & Rahman, M. Y. A. (2011). Effect Of Lithium Salt Concentrations On Blended 49% Poly(Methyl Methacrylate) Grafted Natural Rubber And Poly(Methyl Methacrylate) Based Solid Polymer Electrolyte. *Electrochimica Acta*, 57(0), 123-131.

- Subba Reddy, C. V., Sharma, A. K., & Narasimha Rao, V. V. R. (2003). Conductivity And Discharge Characteristics Of Polyblend (Pvp + Pva + Kio₃) Electrolyte. *Journal Of Power Sources*, 114(2), 338-345.
- Sudhakar, Y. N., & Selvakumar, M. (2012). Lithium Perchlorate Doped Plasticized Chitosan And Starch Blend As Biodegradable Polymer Electrolyte For Supercapacitors. *Electrochimica Acta*, 78(0), 398-405.
- Takahashi, T. (1989). *High Conductivity Solid Ionic Conductors* (T. T Ed.). Singapore: World Scientific.
- Tara-Lunga-Mihali, M., Plesu, N., Macarie, L., Iliescu, S., & Ilia, G. (2014). Polyaniline Composite Designed For Solid Polymer Electrolyte. *Pure And Applied Chemistry*, 86(11), 1853-1860.
- Tegge, G. (1987). Starch: Properties And Potential. Ed. By T. Galliard. Volume 13 Of Critical Reports On Applied Chemistry. Published For The Society Of Chemical Industry By John Wily & Sons, Chichester 1987. Isbn 0-471-91326-X. 150 Pages, With Numerous Tables And Figures. Hardcover £ 31.00. *Starch - Stärke*, 39(10), 374-374.
- Tian, H., Tang, Z., Zhuang, X., Chen, X., & Jing, X. (2012). Biodegradable Synthetic Polymers: Preparation, Functionalization And Biomedical Application. *Progress In Polymer Science*, 37(2), 237-280.
- Tominaga, Y., Asai, S., Sumita, M., Panero, S., & Scrosati, B. (2005). A Novel Composite Polymer Electrolyte: Effect Of Mesoporous Sio₂ On Ionic Conduction In Poly(Ethylene Oxide)–Licf₃so₃ Complex. *Journal Of Power Sources*, 146(1–2), 402-406.
- Tripathi, B. P., & Shahi, V. K. (2011). Organic–Inorganic Nanocomposite Polymer Electrolyte Membranes For Fuel Cell Applications. *Progress In Polymer Science*, 36(7), 945-979.
- Ueki, T., & Watanabe, M. (2008). Macromolecules In Ionic Liquids: Progress, Challenges, And Opportunities. *Macromolecules*, 41(11), 3739-3749.
- Uma, T., Mahalingam, T., & Stimming, U. (2003). Mixed Phase Solid Polymer Electrolytes Based On Poly(Methylmethacrylate) Systems. *Materials Chemistry And Physics*, 82(2), 478-483.

- Van Soest, J. J. G., De Wit, D., Tournois, H., & Vliegthart, J. F. G. (1994). Retrogradation Of Potato Starch As Studied By Fourier Transform Infrared Spectroscopy. *Starch - Stärke*, 46(12), 453-457.
- Vincent, C. A. (1987). Polymer Electrolytes. *Progress In Solid State Chemistry*, 17(3), 145-261.
- Viturawong, Y., Achayuthakan, P., & Suphantharika, M. (2008). Gelatinization And Rheological Properties Of Rice Starch/Xanthan Mixtures: Effects Of Molecular Weight Of Xanthan And Different Salts. *Food Chemistry*, 111(1), 106-114.
- Volkov, A. A., & Prokhorov, A. S. (2003). Broadband Dielectric Spectroscopy Of Solids. *Radiophysics And Quantum Electronics*, 46(8-9), 657-665.
- Walden, P. (1914). Ueber Die Molekulargröße Und Elektrische Leitfähigkeit Einiger Geschmolzenen Salze. *Известия Российской Академии Наук. Серия Математическая*, 8(6), 405-422.
- Walker, A. J., & Bruce, N. C. (2004). Cofactor-Dependent Enzyme Catalysis In Functionalized Ionic Solvents. *Chemical Communications*(22), 2570-2571.
- Wang, M., Zhang, Q. L., Weng, Y. X., Lin, Y., & Xiao, X. R. (2006). Investigation Of Mechanisms Of Enhanced Open-Circuit Photovoltage Of Dye-Sensitized Solar Cells Based The Electrolyte Containing 1-Hexyl-3-Methylimidazolium Iodide. *Chinese Physics Letters*, 23(3), 724-727.
- Wang, X., Li, X., Chen, L., Xie, F., Yu, L., & Li, B. (2011). Preparation And Characterisation Of Octenyl Succinate Starch As A Delivery Carrier For Bioactive Food Components. *Food Chemistry*, 126(3), 1218-1225.
- Wang, Y.-J., Pan, Y., Wang, L., Pang, M.-J., & Chen, L. (2005). Conductivity Studies Of Plasticized PEO-Lithium Chlorate-Fic Filler Composite Polymer Electrolytes. *Materials Letters*, 59(24-25), 3021-3026.
- Wang, Y.-J., Pan, Y., Wang, L., Pang, M.-J., & Chen, L. (2006). Characterization Of (PEO)₄LiClO₄-Li_{1.3}Al_{0.3}Ti_{1.7}(PO₄)₃ Composite Polymer Electrolytes With Different Molecular Weights Of PEO. *Journal Of Applied Polymer Science*, 102(5), 4269-4275.
- Winzenburg, G., Schmidt, C., Fuchs, S., & Kissel, T. (2004). Biodegradable Polymers And Their Potential Use In Parenteral Veterinary Drug Delivery Systems. *Advanced Drug Delivery Reviews*, 56(10), 1453-1466.

- Wright, P. V. (1975). Electrical Conductivity In Ionic Complexes Of Poly(Ethylene Oxide). *British Polymer Journal*, 7(5), 319-327.
- Xu, L., & Yamamoto, A. (2012). Characteristics And Cytocompatibility Of Biodegradable Polymer Film On Magnesium By Spin Coating. *Colloids And Surfaces B: Biointerfaces*, 93(0), 67-74.
- Yamamoto, H., Isozumi, N., & Sugitani, T. (2005). A Concavity Property Of The Viscosity Growth Curve During Alkali Gelatinization Of Rice Starch. *Carbohydrate Polymers*, 62(4), 379-386.
- Zalewska, A., Duminska, J., Langwald, N., Syzdek, J., & Zawadzki, M. (2014). Preparation And Performance Of Gel Polymer Electrolytes Doped With Ionic Liquids And Surface-Modified Inorganic Fillers. *Electrochimica Acta*, 121, 337-344.
- Zhang, C., Zhu, L., Shao, K., Gu, M., & Liu, Q. (2013). Toward Underlying Reasons For Rice Starches Having Low Viscosity And High Amylose: Physiochemical And Structural Characteristics. *Journal Of The Science Of Food And Agriculture*, 93(7), 1543-1551.
- Zhu, Y. S., Wang, X. J., Hou, Y. Y., Gao, X. W., Liu, L. L., Wu, Y. P., & Shimizu, M. (2013). A New Single-Ion Polymer Electrolyte Based On Polyvinyl Alcohol For Lithium Ion Batteries. *Electrochimica Acta*, 87(0), 113-118.
- Zobel, H. F. (1988). Molecules To Granules: A Comprehensive Starch Review. *Starch - Stärke*, 40(2), 44-50.